NISTIR 6196-1

Sprinkler, Smoke & Heat Vent, Draft Curtain Interaction -- Large Scale Experiments and Model Development

Kevin B. McGrattan
Anthony Hamins
David Stroup

United States Department of Commerce
National Institute of Standards and Technology

NISTIR 6196-1

Sprinkler, Smoke & Heat Vent, Draft Curtain Interaction -- Large Scale Experiments and Model Development

Kevin B. McGrattan
Anthony Hamins
David Stroup

September 1998

U.S. Department of Commerce
William M. Daley, *Secretary*
Technology Administration
Gary R. Bachula, *Acting Under Secretary for Technology*
National Institute of Standards and Technology
Raymond G. Kammer, *Director*

Executive Summary

This study was the result of a coordinated public-private research effort to gain insight into the interaction of sprinklers, roof vents and draft curtains through fire experiments and numerical modeling. The work was conducted over a period of two years.

The International Fire Sprinkler, Smoke and Heat Vent, Draft Curtain Fire Test Project organized by the National Fire Protection Research Foundation (NFPRF) brought together a group of industrial sponsors to support and plan a series of large scale tests to study the interaction of sprinklers, roof vents and draft curtains of the type found in large warehouses, manufacturing facilities, and warehouse-like retail stores. A Technical Advisory Committee consisting of representatives from the sponsoring organizations, the National Institute of Standards and Technology (NIST), and other interested parties planned 39 large scale fire tests that were conducted in the Large Scale Fire Test Facility at Underwriters Laboratories (UL) in Northbrook, Illinois. The tests were designed to address relatively large, open-area buildings with flat ceilings, sprinkler systems, and roof venting with and without draft curtains. To simulate these conditions in the 37 m by 37 m by 15 m high (120 ft by 120 ft by 48 ft high) main test bay, the vents, draft curtains and sprinklers were installed on a 30 m by 30 m (100 ft by 100 ft) adjustable-height platform, 7.6 m (25 ft) off the floor. During the tests, smoke and hot gases filled the volume enclosed by the draft curtains, and the excess smoke flowed around the edges of the platform into a plenum space above. The smoke in the plenum spaced was continually exhausted through a smoke abatement system.

Funding for the large scale tests, although substantial, permitted only five high rack storage commodity fire tests to be conducted. In order to best prepare for these tests and to add to the information available for model development and verification, 34 easily conducted and controlled heptane spray burner tests were also performed. Recognizing that the resources in terms of funding and time were limited, the NFPRF Technical Advisory Committee reduced the number of parameters in this study by selecting one commodity, one rack configuration and ignition source, a single sprinkler system and one sprinkler discharge density, one commercial vent design, and one vent/draft curtain arrangement.

In parallel with the large scale fire tests, a program was conducted at NIST to develop a numerical field model, Industrial Fire Simulator (IFS), that incorporated the physical phenomena of the experiments. A series of bench scale experiments was conducted to develop necessary input data for the model. These experiments generated data describing the burning rate and flame spread behavior of the cartoned plastic commodity, thermal response parameters and spray pattern of the sprinkler, and the effect of the water spray on the burning commodity. Simulations were first performed for the heptane spray burner tests, where they were shown to be in good *quantitative* agreement in terms of both predicting sprinkler activation times and near-ceiling gas temperature rise. The sprinkler activation times were predicted to within about 15% of the experiments for the first ring, 25% for the second. The gas temperatures near the ceiling were predicted to within about 15%. Next, simulations were performed and compared with unsprinklered calorimetry burns of the cartoned plastic commodity. The heat release rates of the growing fires were predicted to within about 20%. Simulations of the 5 cartoned plastic commodity fire tests were then performed. The goal of these simulations was to be able to differentiate between those experiments that activated a large number of sprinklers, and those that activated a small number. This goal has been met. The model was also used to provide valuable insight into what occurred in the experiments, and also what would have occurred in the event of various changes of test parameters. There are plans to

continue the development and evaluation of the IFS model beyond publication of this report.

The overall goal of the testing and modeling program was to investigate the effect of roof vents and draft curtains on the time, number, and location of sprinkler activations; and also the effect of sprinklers and draft curtains on the activation time, number, and discharge rates of roof vents. Based on the experiments and model simulations for the chosen test hardware and configurations, the major findings in this study were:

- The tests and model simulations showed that when the fire was not ignited directly under a roof vent, venting had no significant effect on the sprinkler activation times, the number of activated sprinklers, the near-ceiling gas temperatures, or the quantity of combustibles consumed.
- The tests and model simulations showed that when the fire was ignited directly under a roof vent, automatic vent activation usually occurred at about the same time as the first sprinkler activation, but the average activation time of the first ring of sprinklers was delayed. The length of the delay depended on the difference in activation times between the vent and the first sprinkler.
- The tests and model simulations showed that when the fire was ignited directly under a roof vent that activated either before or at about the same time as the first sprinkler, the number of sprinkler activations decreased by as much as 50% compared to tests performed with the vent closed.
- The tests and model simulations showed that when draft curtains were installed, up to twice as many sprinklers activated compared to tests performed without curtains.
- In one rack storage test where the ignition of the fire took place near a draft curtain and the fuel array extended underneath the curtain, disruption of the sprinkler spray and delay in sprinkler operation caused by the draft curtain led to a fire that consumed more commodity compared to the other tests where the fires were ignited away from the draft curtains. This result was demonstrated by the model simulation, as well.
- The significant cooling effect of sprinkler sprays on the near-ceiling gas flow often prevented the automatic operation of vents. This conclusion is based on thermocouple measurements within the vent cavity, the presence of drips of solder on the fusible links recovered from unopened vents, and several tests where vents remote from the fire and the sprinkler spray activated. In one cartoned plastic commodity experiment, a vent did not open when the fire was ignited directly beneath it. The model simulations could not predict this phenomenon.
- Model simulations indicated that the cooling effect of sprinkler sprays reduced the total vent discharge rate from that assumed in design calculations for unsprinklered buildings.
- Model simulations showed how the activation times of the the first and second sprinklers had a substantial impact on the overall number of activations in the plastic commodity tests. In the simulation of one test, it was shown that a delay of approximately one minute in the activation of the second sprinkler led to the activation of four times as many sprinklers as in a simulation of a test with no delay. It had been suggested that these different outcomes were due to the presence of draft curtains in the tests with the sprinkler delay, but the simulations showed that the curtains had no effect because they were over 9 m (30 ft) away from the ignition point.

Contents

List of Figures

List of Tables

List of Abbreviations

FMRC	Factory Mutual Research Corporation
gpm	(U.S.) gallons per minute (1 gallon = 3.785412 L)
IIT	Illinois Institute of Technology
LIFT	Lateral Ignition and Flame Spread Test
NFPA	National Fire Protection Association
NFPRF	National Fire Protection Research Foundation
NIST	National Institute of Standards and Technology
RTI	Response Time Index
SP	Swedish National Testing and Research Institute
UL	Underwriters Laboratories

Acknowledgments

The authors would like to thank the following individuals and organizations for their assistance in this project: Frederick Mulhaupt and Douglas Brown at the National Fire Protection Research Foundation for providing us the opportunity to participate in the International Fire Sprinkler, Smoke and Heat Vent, Draft Curtain Fire Test Project; the members of the Technical Advisory Committee for their advice and expertise in reviewing the test data and the drafts of the final report; David Sheppard, William Carey, Daniel Steppan and Pravin Gandhi at Underwriters Laboratories and Joe Hankins at Factory Mutual for sharing their test data and their experience in commodity fire testing; Linda Blevins and Glenn Forney of NIST for their work in characterizing sprinkler sprays; Leonard Cooper and Jay McElroy of NIST for their efforts to characterize the thermal response properties of fusible vent links; Stephen DiGiovanni of the University of Maryland and Roy McLane of NIST for their work in characterizing the burning rates of the plastic commodity used in the tests; and David Evans, Daniel Madrzykowski and Kenneth Steckler of NIST for their assistance in assembling this report.

1 Introduction

There has been a long-standing debate in the fire protection community about the combined use of roof vents, draft curtains (curtain boards) and sprinklers. Numerous studies have been conducted over the past few decades, yet many questions remain about the interaction of these devices. As a result, a coordinated public-private research effort was organized. A group of industrial sponsors was brought together by the National Fire Protection Research Foundation (NFPRF) to support and plan a series of large scale experiments using both a heptane spray burner and cartoned polystyrene cups (Group A plastic) as fire sources. A Technical Advisory Committee (TAC) made up of representatives of the sponsoring organizations, the National Institute of Standards and Technology (NIST), and other invited participants was created by the NFPRF to guide the studies. The TAC selected a test facility and a sprinkler system, roof vent, draft curtain design for installation in the test facility in order to simulate fire protection systems found in warehouses, warehouse retail stores and manufacturing facilities. In all, 39 tests were specified by the TAC. Fire modeling and supporting laboratory experiments provided by NIST aided in the planning of large scale experiments and in the analysis of the data.

There were three objectives of the study. First, there was a need to understand how sprinklers, vents and draft curtains interact. Second, there was a need to develop a numerical model capable of predicting multiple sprinkler activations and the heat release rate from a burning fuel array both before and after sprinkler activation with sufficient accuracy to reliably differentiate between fire scenarios that would produce a large versus small number of sprinkler activations. Third, there was a desire to look beyond current building practices and generate experimental data, along with a numerical modeling capability, that could be used to evaluate proposed changes to codes and standards.

All 39 experiments planned by the TAC were conducted in the Large Scale Fire Test Facility at Underwriters Laboratories in Northbrook, Illinois. The experiments were divided into three series: an initial set of 22 heptane spray burner tests (Heptane Series I) [1], 5 cartoned plastic commodity tests (Plastic Series) [2], and 12 additional heptane spray burner tests (Heptane Series II) [2]. Many of the test parameters did not change throughout the entire project. The ceiling heights were set at either 7.6 m (25 ft) or 8.2 m (27 ft), the storage height was nominally 6.1 m (20 ft) in the cartoned plastic tests, the sprinkler system consisted of 0.64 in orifice upright sprinklers spaced 3 m (10 ft) apart delivering a 0.34 L/(s·m^2) (0.50 gpm/ft^2) discharge density, and the 1.2 m by 2.4 m (4 ft by 8 ft) vents used were of the same design, from the same manufacturer, and UL listed[1]. The parameters that did change were fire size, fire/ignition position, mode of vent operation, and draft curtain placement.

A large effort was made to develop numerical techniques that could be used to interpret and potentially supplement the physical experiments. This work is a major undertaking by NIST. The Large Eddy Simulation (LES) Fire Model [3, 4] is a computational fluid dynamics (CFD) code that solves the differential equations that govern the transport of smoke and hot gases from a fire. The model being developed and applied in this project is referred to as the Industrial Fire Simulator (IFS). A series of bench scale experiments was conducted by NIST to develop necessary input data for the model. These experiments generated data describing the burning rate and flame spread

[1]Throughout this report, measured quantities will be reported with units conforming to the modern metric system (SI) with traditional units in parentheses. The exception is where the units are essential to the description of the object, apparatus, *etc.*

behavior of the cartoned plastic commodity, thermal response parameters and spray pattern of the sprinkler, and the effect of the water spray on the burning commodity. During its development the performance of the IFS model was assessed by comparing its results to those of the heptane spray burner experiments and calorimetry burns of the cartoned plastic commodity. The IFS model was used in planning experiments and also in the analysis to supplement the results of the relatively small number of cartoned plastic commodity tests that were conducted.

2 Background

Roof vents (usually accompanied by draft curtains) and sprinklers are two hardware systems used in buildings to provide fire protection for rack storage of materials. While sprinklers are intended to suppress and control the fire, roof vents are intended to aid the fire fighters. According to NFPA 204M, Guide for Smoke and Heat Venting [5], Paragraph 1-1.2:

> ...large undivided floor areas present extremely difficult fire fighting problems, since the fire department must enter these areas in order to combat fires in central portions of the building. If the fire department is unable to enter because of the accumulation of heat and smoke, fire fighting efforts may be reduced to a futile application of hose streams to perimeter areas while fire consumes the interior. Windowless buildings also present similar fire fighting problems. One fire protection tool that may be a valuable asset for fire fighting operations in such buildings is smoke and heat venting.

The design practice for sprinklers is given in NFPA 231C, Standard for Rack Storage of Materials [6]. The design practice for roof vents and draft curtains is given in NFPA 204M. These are independent documents. There is no nationally recognized standard for the combined installation of sprinklers and roof vents. Indeed, NFPA 204M, Paragraph 6-1 states:

> A broadly accepted equivalent design basis for using both sprinklers and vents together for hazard control (*e.g.* property protection, life safety, water usage, obscuration, *etc.*) has not been universally recognized.

Even though the practice of installing vents in sprinklered buildings has been debated for decades, and in spite of several projects involving large scale tests and numerical modeling, there is still disagreement about how roof vents and draft curtains affect the time, number and location of sprinkler activations; and how sprinklers and draft curtains affect the activation time, number and discharge rates of roof vents. As a result, there is a great disparity among building codes as to the proper treatment of these fire protection devices. The issue is even more important today because of the popularity of large warehouse-type retail stores that combine the function of sales and storage. Typically these stores will contain merchandise stacked up to 6 m (20 ft), with ceilings as high as 9 m (30 ft), and in areas over 10,000 m^2 (100,000 ft^2).

As part of the planning for the experiments described in this report, past experiments and modeling efforts involving vents and draft curtains (with and without sprinklers) were considered:

Roof Ventilation Requirements for Industrial Plants (1954–1955) Armour Research Foundation (former name of IIT Research). Experimental and modeling study of unsprinklered, vented facilities [7].

Underwriters Laboratories Roof Vent Testing (1964) Sprinkler/vent study in a 60 by 60 by 16 ft space [8].

Thomas and Hinkley (1964) Experimental and modeling studies at the Fire Research Station, UK [9].

Portsmouth Fire Test (1966) Colt Industries (UK). Full scale fire tests in Victoria Barracks, Portsmouth [10].

Rack Storage and Rubber Tire Tests (late 1960's, early 1970's) Factory Mutual Research Corporation (FMRC). Experimental studies of sprinklered facility with perimeter venting [11].

FMRC Modeling Study (1974) 1:12.5 scale model of large test facility built with vents [12].

IIT Research (1982) Fire Venting of Sprinklered Buildings. Large scale experiments of sprinkler performance in a vented facility. Includes a literature review of work done up to that date [13].

Ghent Fire Tests (1989) Colt Industries and Fire Research Station (UK). Thirty-three large scale tests of vents and sprinklers in a 50 m by 20 m by 10 m facility with 40 roof vents [14].

SP Interaction between Sprinklers and Fire Vents (1992) Swedish National Testing and Research Institute (SP). A series of experiments involving one or two vents and a single sprinkler [15]. A summary of the research in Europe involving smoke and heat vents can be found in a technical report from SP [16].

International Seminar on Sprinklers and Vents (1992) Fire Research Station (UK). A discussion of past work in the area, particularly the experiments at Ghent. Tentative guidelines are put forward to address the problem.

Early work by Thomas and Hinkley [9] in the 1960's on the performance of roof vents led to the tentative recommendation that sprinklers should be operated before vents because the cooling of the hot upper layer gases by the opening of vents could delay sprinkler activation. This recommendation found its way into many codes of practice. Since that time, there have been several large scale experimental and numerical studies performed to explore this issue. Notable among these is the Ghent fire test project, which consisted of hexane fires in a 50 m by 20 m (164 ft by 66 ft) facility with 40 roof vents, each with an area of 1.64 m^2 (18 ft^2). It has been claimed by proponents of venting that these tests showed that venting does not appreciably affect the activation of the first sprinkler, but does significantly reduce both the number of sprinklers opening within 60 s of the first as well as the total number of sprinklers operating. However, in all the vented fires, enough sprinklers operated to wet the fire and its immediate surroundings [17]. Hinkley's modeling work [18] reached similar conclusions, and he states that "Venting is unlikely to delay the operation of sprinklers in a compartment of such a large area that the hot gases would not have reached the boundaries before sprinklers operate". He goes on to say that for smaller compartments, slowly growing fires, and/or when draft curtains are used to build up the smoke layer, the vents can cause a small delay in sprinkler operation, but that this is a "second order" effect compared to the rate of fire growth and operating characteristics of the sprinkler.

However, a position paper by N.E. Gustafsson of Industrial Mutual, Helsinki, interprets the results of the Ghent tests completely differently [19]. He argues that for the rapidly growing fires, a significant delay in sprinkler activation was caused by the presence of vents. Even though the delay was about 10 to 20 s in most cases, this allowed the fire to grow from 10.2 MW in the unvented case to as much as 14.2 MW in one of the vented cases. He also cites the inability of the sprinkler system to surround the fire in the vented cases.

Rack storage fire tests conducted at Factory Mutual in the late 1960's raised the issue of the possible detrimental effects of smoke and heat vents in sprinklered buildings [11]. These experiments have been analyzed by a number of researchers, and the conclusions have been criticized

based mainly on the fact that ventilation was from doors and eave line windows rather than roof vents, thus only the potential disadvantage of venting (higher oxygen content) was maintained. The series of fire tests conducted by IIT Research Institute in 1982 [13, 20] showed no increase in oxygen in the air supplying the fire. The issue was not addressed in the modeling studies, nor in the Ghent or SP experiments due to the use of prescribed burning rates.

The experiments performed by IIT Research Institute with both sprinklers and vents rated at 74°C (165°F) showed a slight reduction in water demand for vent areas considered "large", but no change in water demand for a more limited vent area. The report also notes measurable reductions in near-ceiling gas temperatures away from the fire. The study concluded that roof vents do not impair the performance of 74°C (165°F) standard response sprinklers, but they provide only marginal benefit. For 141°C (286°F) sprinklers in the presence of propane fires, the benefits of reduced water demand and near-ceiling gas temperatures were more pronounced.

Draft curtains are usually installed to aid roof vents by creating a deeper layer of smoke and hot gases than would otherwise be formed in large, open area buildings. Recent experiments at Factory Mutual [21] investigated the effect of draft curtains on a sprinkler system without roof vents. As part of a test program to evaluate the effectiveness of various sprinkler designs, two pairs of high rack storage cartoned plastic fire tests were conducted with and without draft curtains installed. First, two tests were performed without curtains. Then the tests were repeated after draft curtains had been installed. The fires were ignited near the intersection of two draft curtains. With the curtains installed, the fire opened more sprinklers and caused more damage to the fuel array, apparently due to the disruption of the sprinkler discharge pattern and the lack of prewetting of the commodity (FMRC Standard Plastic test commodity). The report concluded that "...the presence of draft curtains close to the fire origin will (1) result in the development of a more severe fire and (2) deleteriously affect sprinkler protection."

Most of the past work on sprinkler, vent, and draft curtain interaction has focussed on the effects of vents and draft curtains on a sprinkler system. There has been much less work examining the effects of sprinklers on vents. The work done at SP [15] includes experiments designed to measure the effects of a single sprinkler on the temperature and velocity of gases flowing through a 1 m by 2 m (3.3 ft by 6.6 ft) ceiling vent centered in a 7.5 m by 15 m by 6 m high (25 ft by 50 ft by 20 ft high) test space that was open on two sides. The fire source was a 1.5 MW propane burner, located 6 m from the center of the vent. A single sprinkler with a flow rate of either 80 or 100 L/min (21 or 26 gpm) was installed at various locations upstream and downstream of the vent. The conclusions drawn by SP were that when the sprinkler was installed upstream of the vent (*i.e.* between the fire and the vent), it had a "significant" impact on the discharge rate of the vent, with the impact greatest when it was near the vent and decreasing with distance from the vent. When the sprinkler was installed downstream of the vent, its influence on the vent discharge was regarded as "negligible". No attempt was made in the SP study to examine the effects of a sprinkler on the activation of a thermally-responsive automatic vent.

3 Heptane Spray Burner Tests, Series I

In January, 1997, a series of 22 heptane spray burner experiments was conducted at the Large Scale Fire Test Facility at Underwriters Laboratories (UL) in Northbrook, Illinois [1]. The objective of the experiments was to characterize the temperature and flow field for fire scenarios with a controlled heat release rate in the presence of sprinklers, draft curtains and a single vent. The results of the experiments were used to evaluate the predictive capability of the IFS model, and also to provide guidance as to the interaction of vents and draft curtains with sprinklers for planning the cartoned plastic commodity fires.

3.1 Description

A number of components of this first series of tests were carried over into the cartoned plastic commodity tests and the second series of heptane spray burner tests. The same test space was used for all the testing, the same vent and sprinkler type, the same sprinkler configuration, and almost the same ceiling height. Below is a description of the first series of heptane spray burner tests. Changes to these parameters in the subsequent test series will be discussed in the appropriate sections. The Report of Test from UL may be found in Ref. [1].

3.1.1 Test Facility

The Large Scale Fire Test Facility at UL contains a 37 m by 37 m (120 ft by 120 ft) main fire test cell, equipped with a 30.5 m by 30.5 m (100 ft by 100 ft) adjustable height ceiling. The height of the ceiling may be adjusted by four hydraulic rams up to a maximum height of 14.6 m (48 ft). A flexible design sprinkler piping system was available at the ceiling to permit any arrangement of sprinkler spacing with minimum pressure losses. The sprinklers were provided with water from a 757 kL (200,000 gal) water reservoir using two 190 L/s (3,000 gpm) water pumps rated at 1.03 kPa (150 psi). The water pumps were computer controlled to maintain a constant pressure on the sprinklers.

The exhaust flow rate in the test facility could be adjusted up to a maximum of 28 m^3/s (60,000 ft^3/min). Four 1.5 m (5 ft) diameter inlet ducts provided make up air and were located at the walls 3 m (10 ft) above the test floor to minimize any induced drafts during the tests. The combustion products from the fire test were exhausted through a regenerative smoke abatement system. During the heptane tests, the exhaust was maintained at a minimum operating rate of 11 m^3/s (24,000 ft^3/min).

3.1.2 Test Layout

The layout of the first series of heptane spray burner tests is shown in Fig. 1. One 1.2 m by 2.4 m (4 ft by 8 ft) vent was installed among 49 upright sprinklers on a 3 m by 3 m (10 ft by 10 ft) spacing. The ceiling was raised to a height of 7.6 m (25 ft) and instrumented with thermocouples and other measurement devices (see section on instrumentation). The ceiling was constructed of 0.6 m by 1.2 m by 1.6 cm (2 ft by 4 ft by 5/8 in) UL fire rated Armstrong Ceramaguard (Item

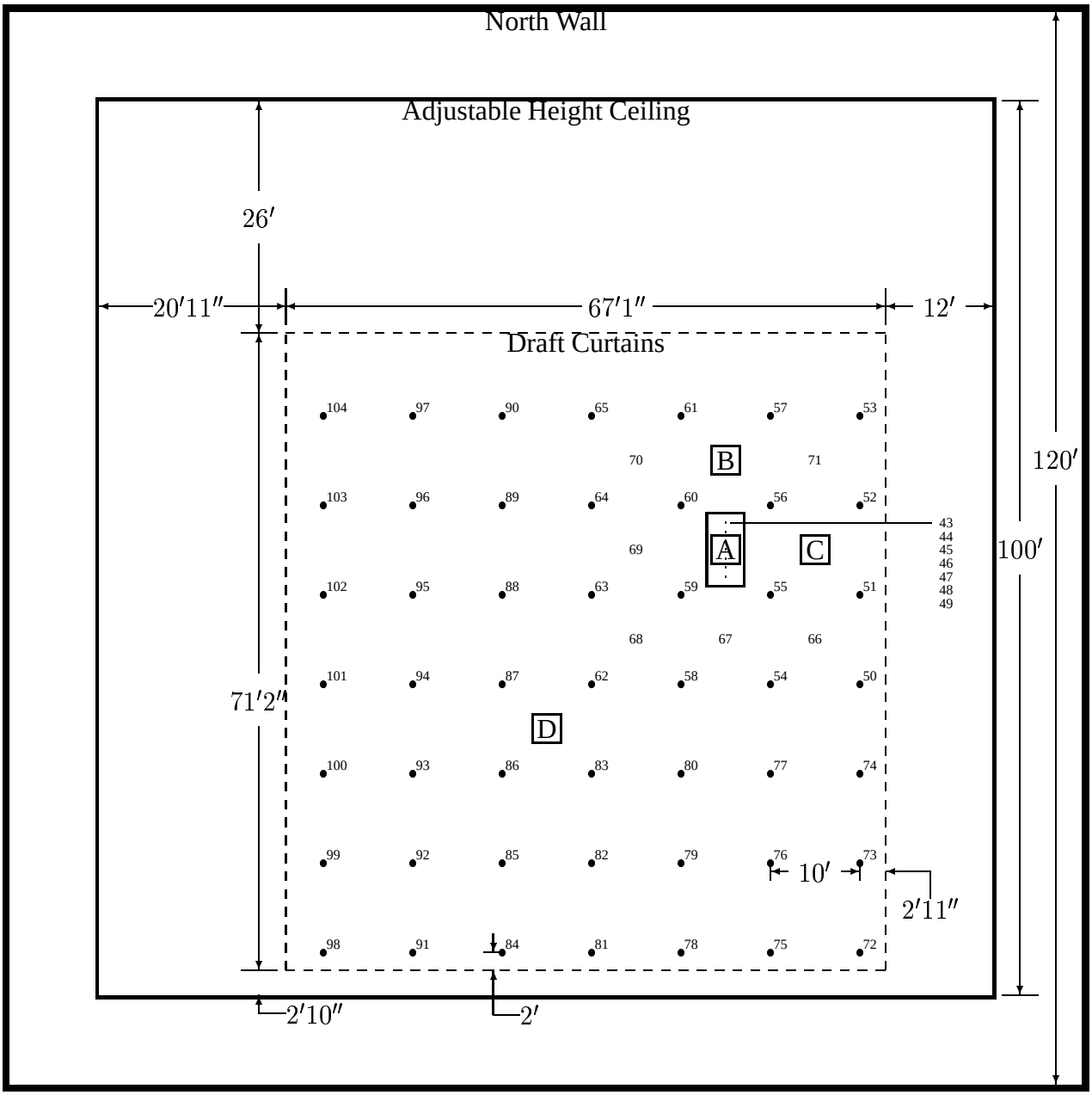

Figure 1: Plan view of heptane spray burner configuration, Series I. The sprinklers are indicated by the solid circles and are spaced 3 m (10 ft) apart. The number beside each sprinkler location indicates the channel number of the nearest thermocouple. The vent dimensions are 4 ft by 8 ft. The boxed letters A, B, C and D indicate burner positions. Corresponding to each burner position is a vertical array of thermocouples. Thermocouples 1–9 hang 7, 22, 36, 50, 64, 78, 92, 106 and 120 in from the ceiling, respectively, above Position A. Thermocouples 10 and 11 are positioned above and below the ceiling tile directly above Position B, followed by 12–20 that hang at the same levels below the ceiling as 1–9. The same pattern is followed at Positions C and D, with thermocouples 21–31 at C and 32–42 at D.

602B) ceiling tiles[2], suspended from 3.8 cm (1.5 in) wide steel angle brackets. The manufacturer reported the thermal properties of the material to be: specific heat 753 J/kg·K, thermal diffusivity 2.6×10^{-7} m^2/s, conductivity 0.0611 W/m·K, and density 313 kg/m^3.

Draft curtains 1.8 m (6 ft) deep were installed for 16 of the 22 tests, enclosing an area of about 450 m^2 (4,800 ft^2). The curtains were constructed of 1.4 m (54 in) wide sheets of 18 gauge sheet metal. The seams in the draft curtains were connected with aluminum tape.

3.1.3 Sprinkler Protection

The sprinklers used in both series of heptane spray burner tests plus the cartoned plastic commodity tests were Central ELO-231 (Extra Large Orifice) uprights. The orifice diameter of this sprinkler is reported by the manufacturer to be nominally 0.64 in, the reference actuation temperature is reported by the manufacturer to be 74°C (165°F). The RTI (Response Time Index) and C-factor (Conductivity factor) were reported by UL[3] to be 148 (m·s)$^{\frac{1}{2}}$ (268 (ft·s)$^{\frac{1}{2}}$) and 0.7 (m/s)$^{\frac{1}{2}}$ (1.3 (ft/s)$^{\frac{1}{2}}$), respectively [1]. When installed, the sprinkler deflector was located 8 cm (3 in) below the ceiling. The thermal element of the sprinkler was located 11 cm (4.25 in) below the ceiling. The sprinklers were installed with 3 m by 3 m (10 ft by 10 ft) spacing in a system designed to deliver a constant 0.34 L/(s·m^2) (0.50 gpm/ft^2) discharge density when supplied by a 131 kPa (19 psi) discharge pressure [4].

Branch lines were located 3 m (10 ft) apart. The branch lines were 2 in Schedule 40 pipe. The lines had a 6.032 cm (2.375 in) outer diameter and were mounted with a 22 cm (8.5 in) nominal clearance from the centerline of the pipe to the ceiling. The manifolds were mounted below the branch lines and were used to plumb the water to the branch lines. The manifolds were 6.4 cm (2.5 in) Schedule 40 pipe with an outer diameter of 7.303 cm (2.875 in). They were mounted with a 1.04 m (40.75 in) nominal clearance from the centerline of the pipe to the ceiling. Although not shown in Fig. 1, the branch lines ran from north to south. The branch lines and manifolds were filled with water during all tests.

3.1.4 Smoke and Heat Vent

A single UL listed double leaf fire vent with steel covers and steel curb was installed in the adjustable height ceiling in the position shown in Fig. 1. This vent was selected in collaboration with the NFPRF Technical Advisory Committee who sponsored the large scale tests. The vent is designed to open manually or automatically. The vent doors were recessed into the ceiling about 0.3 m (1 ft). A diagram of the vent used in shown in Fig. 2.

[2]The mention of particular manufacturer's products does not constitute endorsement by NIST, nor does it indicate that the products are necessarily those best suited for the intended purpose.

[3]The RTI and C-factor reported here are based on the equation governing the thermal activation of the fusible link of the sprinkler

$$\frac{dT_l}{dt} = \frac{\sqrt{u}}{\mathrm{RTI}}(T_g - T_l) - \frac{C}{\mathrm{RTI}}(T_l - T_m)$$

where T_l is the link temperature, T_g is the gas temperature in the neighborhood of the link, T_m is the temperature of the sprinkler mount, and u is the gas velocity.

[4]The flow rate from a sprinkler is proportional to the square root of the discharge pressure. The proportionality constant is often referred to as the K-factor, usually reported in units of gallons per minute divided by the square root of pounds per square inch. For the sprinkler used in these tests, the K-factor was approximately 11.4 gpm/(psi)$^{\frac{1}{2}}$.

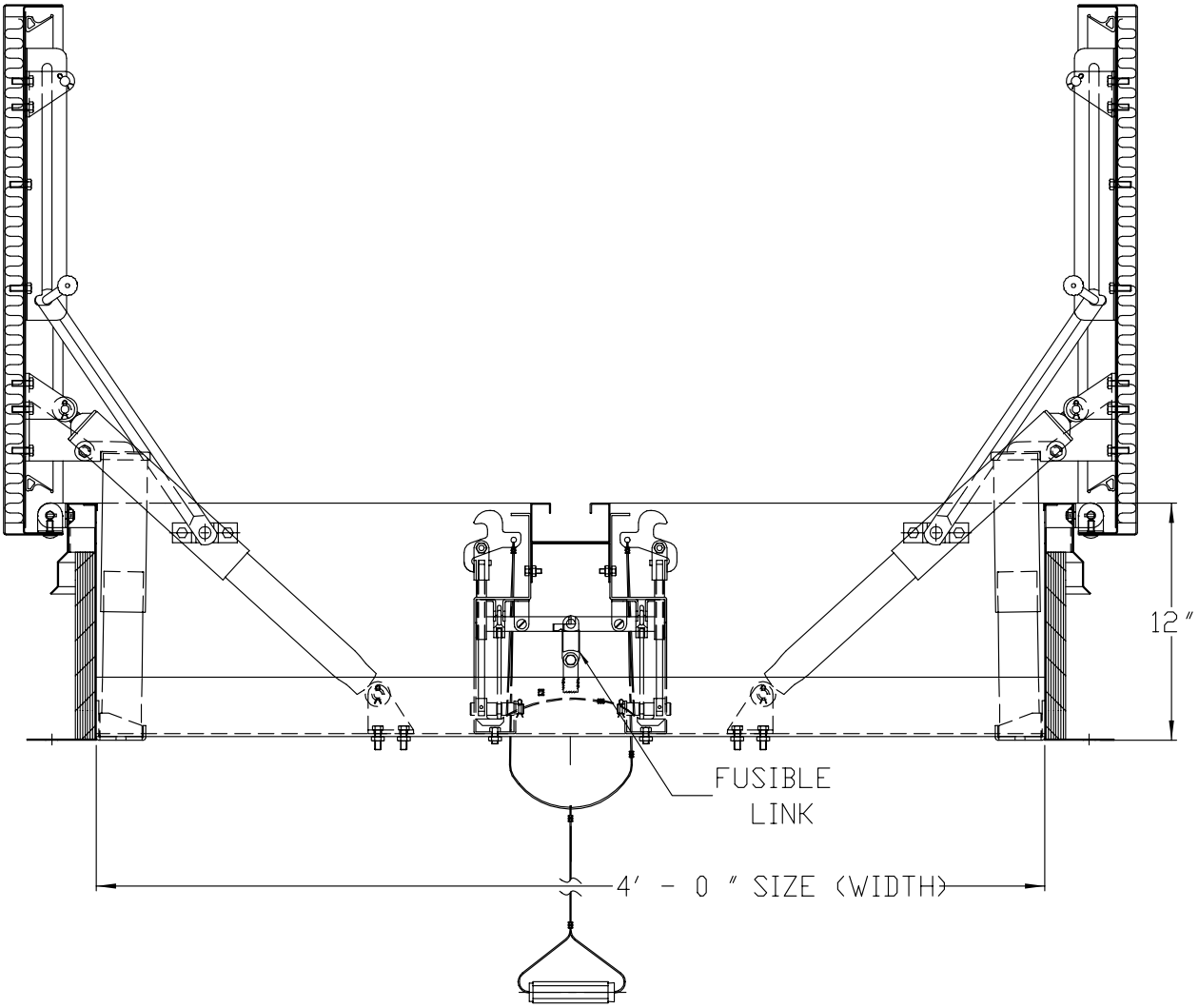

Figure 2: Diagram of the fire vent used in all the tests. Note that 12″=0.3048 m and 4′-0″=1.2192 m.

The vent could be operated manually or automatically. In cases where manual operation was performed, the opening times were chosen so that the vent would either be opened about 25 s prior to the first sprinkler activation, or 25 s after the first sprinkler activation. Preliminary calculations indicated that the first sprinkler in most cases would activate 60 to 70 s after ignition. In tests where automatic operation of the vents was desired, UL listed fusible links rated at either 74°C (165°F) or 100°C (212°F) were installed. In most tests, the 74°C link was used. To determine the thermal response properties of the fusible link, a plunge tunnel test was performed on a representative link assembly that consisted of a fusible link rated at 74°C bolted to a steel tab that was welded to a steel support bar. The link was spring-loaded with a force of 12.2 N (2.75 lbf). The link was instrumented with a thermocouple attached to the center of its rear surface. The tunnel air temperature was 134°C (273°F), the tunnel velocity was 2.5 m/s (8.2 ft/s), the ambient temperature was 25°C (77°F). When inserted into the tunnel perpendicular to the flow direction, the link reached 74°C after 34 s and remained at that temperature until it fused at 68 s. When parallel to the flow,

the link reached 74°C after 35 s and remained at this temperature until it fused at 63 s [22]. The interval between the time when the link reached its activation temperature and the time when it fused was significant, suggesting that a one parameter model of link activation may not suffice to fully characterize the thermal response of the link [23]. However, for the present study, an effective bulk RTI[5]. for the link assembly based on the fusing time was calculated to be between 167 and 180 $(\text{m}\cdot\text{s})^{\frac{1}{2}}$ (302 and 326 $(\text{ft}\cdot\text{s})^{\frac{1}{2}}$).

3.1.5 Heptane Spray Burner

The heptane spray burner consisted of a 1 m by 1 m (40 in by 40 in) square of 1/2 in pipe supported by four cement blocks 0.6 m (2 ft) off the floor (Fig. 3). Atomizing spray nozzles were used to provide a free spray of heptane that was then ignited. The number and locations of the atomizing nozzles used depended on the maximum heptane flow rate expected during a test. The two configurations used were nozzles in Positions A, B, C and G for fires less than or equal to 5 MW, and A, B, C, D, E, F and G for fires greater than 5 MW.

For all but one of the tests, the total heat release rate from the fire was manually ramped up following the curve[6]

$$\dot{Q} = \dot{Q}_0 \left(\frac{t}{\tau}\right)^2$$

where $\dot{Q}_0 = 10$ MW and $\tau = 75$ s ($\tau = 150$ s was used in Test I-16). The fire growth rate was intended to approximate the estimated growth rate of the cartoned plastic commodity burns conducted at FMRC [21]. The fire growth curve was followed until a specified fire size was reached or the first sprinkler activated. After either of these events, the fire size was maintained at that level until conditions reached roughly a steady state, *i.e.* the temperatures recorded near the ceilings remained steady and no more sprinkler activations occurred.

The flow of heptane to the burner was manually controlled using two float type flow meters. The two flow meters were connected in parallel. The first flow meter had a resolution of 0.02 gpm and a range of 0.68 L/min (0.18 gpm) to 9.1 L/min (2.4 gpm). The second flow meter had a resolution of 1.1 L/min (0.3 gpm) and a range of 0.91 L/min (0.24 gpm) to 11 L/min (3.0 gpm). The heat release rate from the burner was confirmed by placing it under the large product calorimeter at UL, ramping up the flow of heptane in the same manner as in the tests, and measuring the total and convective heat release rates. It was found that the convective heat release rate was 0.65 ± 0.02 of the total.

3.1.6 Instrumentation

The instrumentation for the tests consisted of thermocouples, gas analysis equipment, and pressure transducers. The locations of the instrumentation are referenced in the plan view of the facility

[5]The term "bulk RTI" indicates that the temperature of the object is assumed to be governed by the equation

$$\frac{dT_l}{dt} = \frac{\sqrt{u}}{\text{RTI}_b}(T_g - T_l)$$

where T_l is the temperature of the object and T_g is the temperature of the gas streaming past the object with speed u. This definition of RTI_b does not explicitly account for conductive losses from the object to surrounding objects, and should not be confused with the definition of RTI applied to fusible sprinkler links in this report.

[6]Because the flow rate of fuel was controlled manually, the growth curve for each test differed slightly.

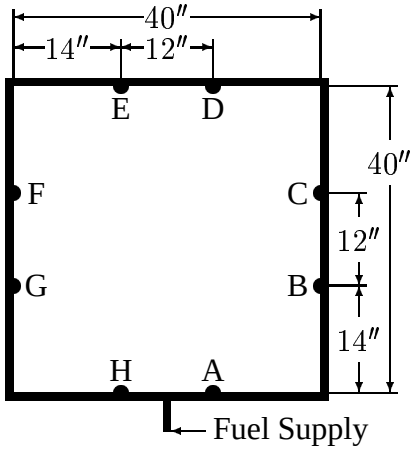

Figure 3: Plan view of heptane spray burner.

(Fig. 1).

Temperature measurements were recorded at 104 locations. Type K 0.0625 in diameter Inconel[7] sheathed thermocouples were positioned to measure (i) temperatures near the ceiling, (ii) temperatures of the ceiling jet, and (iii) temperatures near the vent. The thermocouples numbered 50–65 were positioned near the sprinklers, 10 cm (4 in) below the ceiling. These were intended to measure near-sprinkler gas temperatures as well as to detect sprinkler activation when wetted. Thermocouples 66–104 were placed 5 cm (2 in) below the ceiling. Thermocouples 43–49 ran down the centerline of the vent at the level of the ceiling, and were spaced 0.3 m (1 ft) apart. Thermocouples 1–42 were mounted on arrays hanging above each fire location. The positions are noted in the caption to Fig. 1.

Oxygen, carbon dioxide and carbon monoxide sampling probes were placed at the ground (5 cm (3 in) from the floor, 2 m (6 ft) from the burner), and at the vent (15 cm (6 in) below the ceiling, vent center). The oxygen concentrations were measured with paramagnetic analyzers with a resolution of 100 ppm. The carbon monoxide and carbon dioxide concentrations were measured with nondispersive infrared (NDIR) analyzers. The CO meters had a resolution of 10 ppm, the CO_2 meters 100 ppm.

One differential pressure was measured across the vent. The static pressure taps were mounted 0.15 m (6 in) above the top of the vent and 0.15 m below the ceiling. Both pressure taps were mounted at the center of the vent. The differential pressure was measured with a 0 to 133 Pa (0 to 1 Torr) differential pressure transducer.

All thermocouple, pressure transducer and gas species data were collected electronically at a 2 s scan rate.

[7]Inconel is a registered tradename of INCO Alloys, Inc., 3800-T Riverside Drive, P.O. Box 1958, Huntington, West Virginia, 25705-1771.

3.2 Results

The test results are summarized in Table 1. Sprinkler activation times for the 22 tests can be found in Figs. 4–11. Thermocouple temperatures are included in Appendix A, along with a comparison of the results of the experiments with those of the numerical model.

Heptane Spray Burner Test Series I						
Test No.	Burner Pos.	Vent Operation	First Sprinkler	No. of Sprinklers	Draft Curtains	Heat Release Rate MW @ s
I-1	B	Closed	1:05	11	Yes	4.4 @ 50
I-2	B	Manual (0:40)	1:06	12	Yes	4.4 @ 50
I-3	B	Manual (1:30)	1:04	12	Yes	4.4 @ 50
I-4	C	Closed	1:00	10	Yes	4.4 @ 50
I-5	C	Manual (0:40)	1:12	9	Yes	4.4 @ 50
I-6	C	Manual (1:30)	1:02	8	Yes	4.4 @ 50
I-7	C	74°C link (DNO)	1:10	10	Yes	4.4 @ 50
I-8	B	74°C link (9:26)	1:00	11	Yes	4.4 @ 50
I-9	D	74°C link (DNO)	1:10	12	Yes	4.4 @ 50
I-10	D	Manual (0:40)	1:12	13	Yes	4.4 @ 50
I-11	D	74°C link (4:48)	N/A	N/A	Yes	4.4 @ 50
I-12	A	Closed	1:08	14	Yes	4.4 @ 50
I-13	A	74°C link (1:04)	1:09	5	Yes	6.0 @ 60
I-14	A	Manual (0:40)	1:14	7	Yes	5.8 @ 60
I-15	A	Manual (1:30)	1:04	5	Yes	5.8 @ 60
I-16	A	74°C link (1:46)	1:46	4	Yes	5.0 @ 110
I-17	B	100°C link (DNO)	0:58	4	No	4.6 @ 50
I-18	C	100°C link (DNO)	0:58	4	No	3.7 @ 50
I-19	A	100°C link (10:00)	0:56	10	No	4.6 @ 50
I-20	A	74°C link (1:20)	0:54	4	No	4.2 @ 50
I-21	C	74°C link (7:00)	0:58	10	No	4.6 @ 50
I-22	D	100°C link (DNO)	1:00	6	No	4.6 @ 50

Table 1: Results of the heptane spray burner Series I. Note that DNO means "Did Not Open". Also note, the fires grew at a rate proportional to the square of the time until a certain flow rate of fuel was achieved at which time the flow rate was held steady. Thus, the "Heat Release Rate" was the size of the fire at the time when the fuel supply was levelled off.

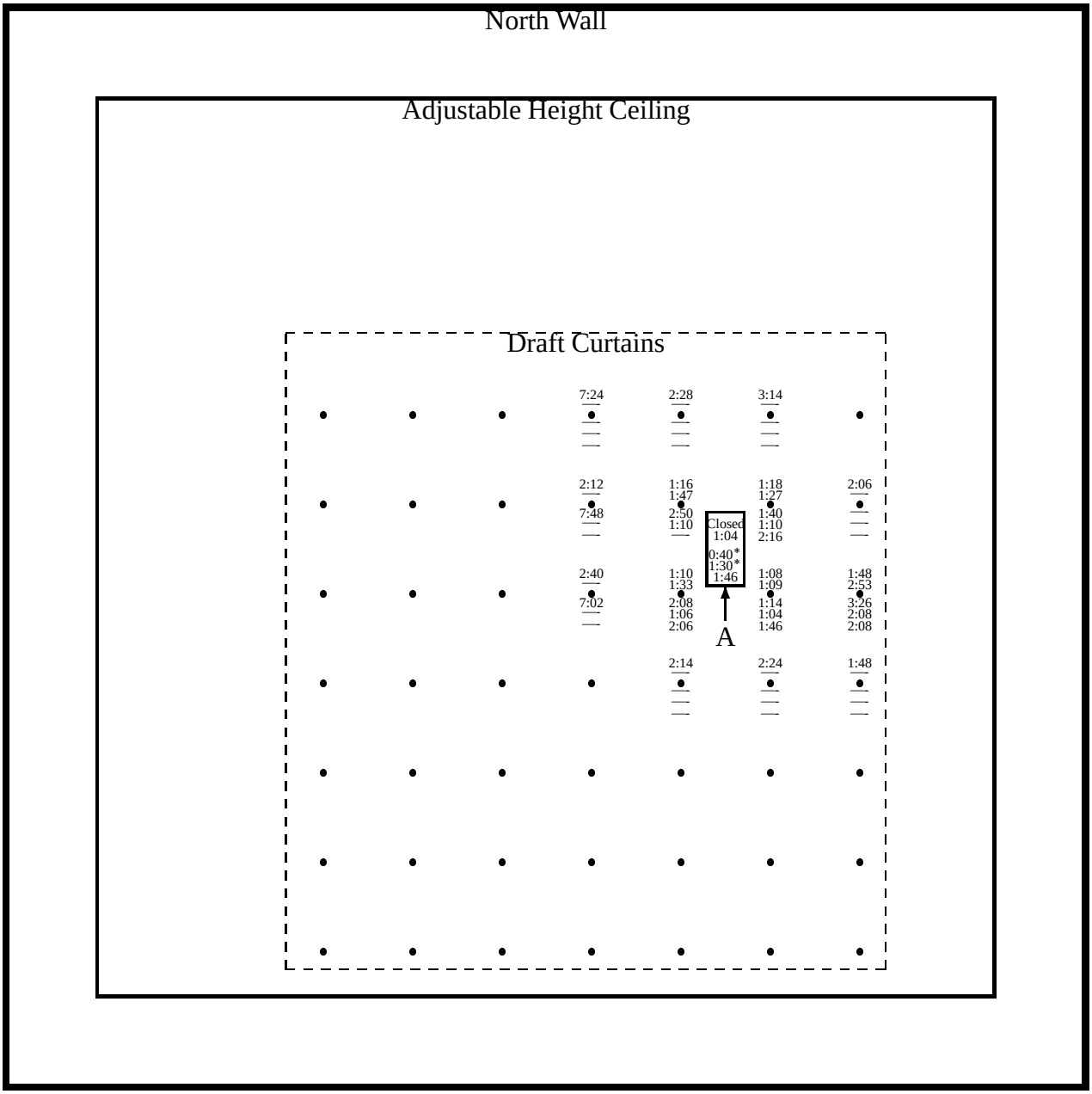

Figure 4: Plan view of Large Scale Fire Test Facility with the results of Heptane Series I curtained tests where the fires were at location A. The activations times are from Tests I-12, I-13, I-14, I-15 and I-16, respectively. Note that an asterisk beside a vent opening time indicates manual operation.

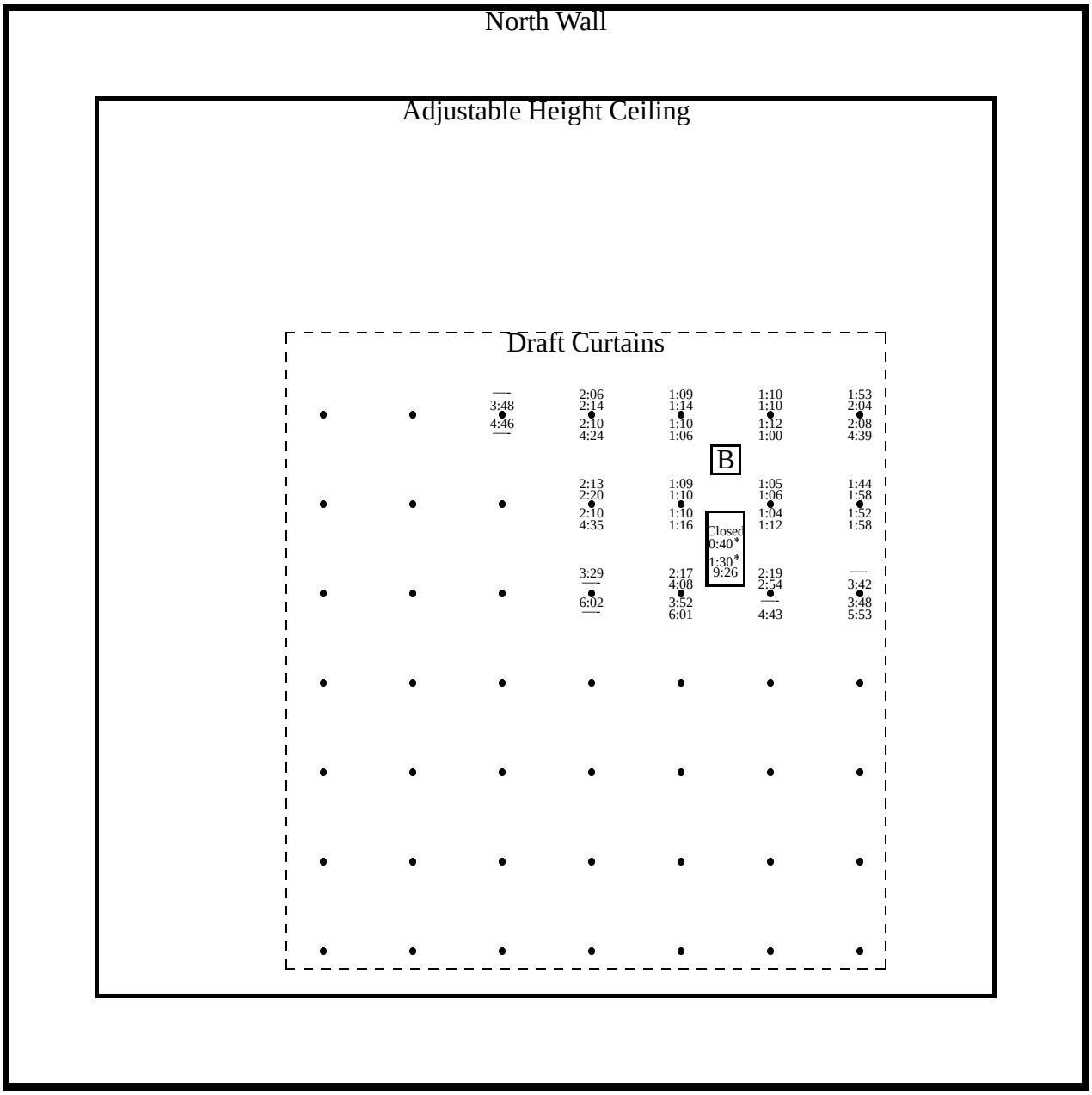

Figure 5: Plan view of heptane spray burner test (Series I) with the results of curtained tests where the fires were at location B. The activation times are from Tests I-1, I-2, I-3 and I-8, respectively. Note that an asterisk beside a vent opening time indicates manual operation.

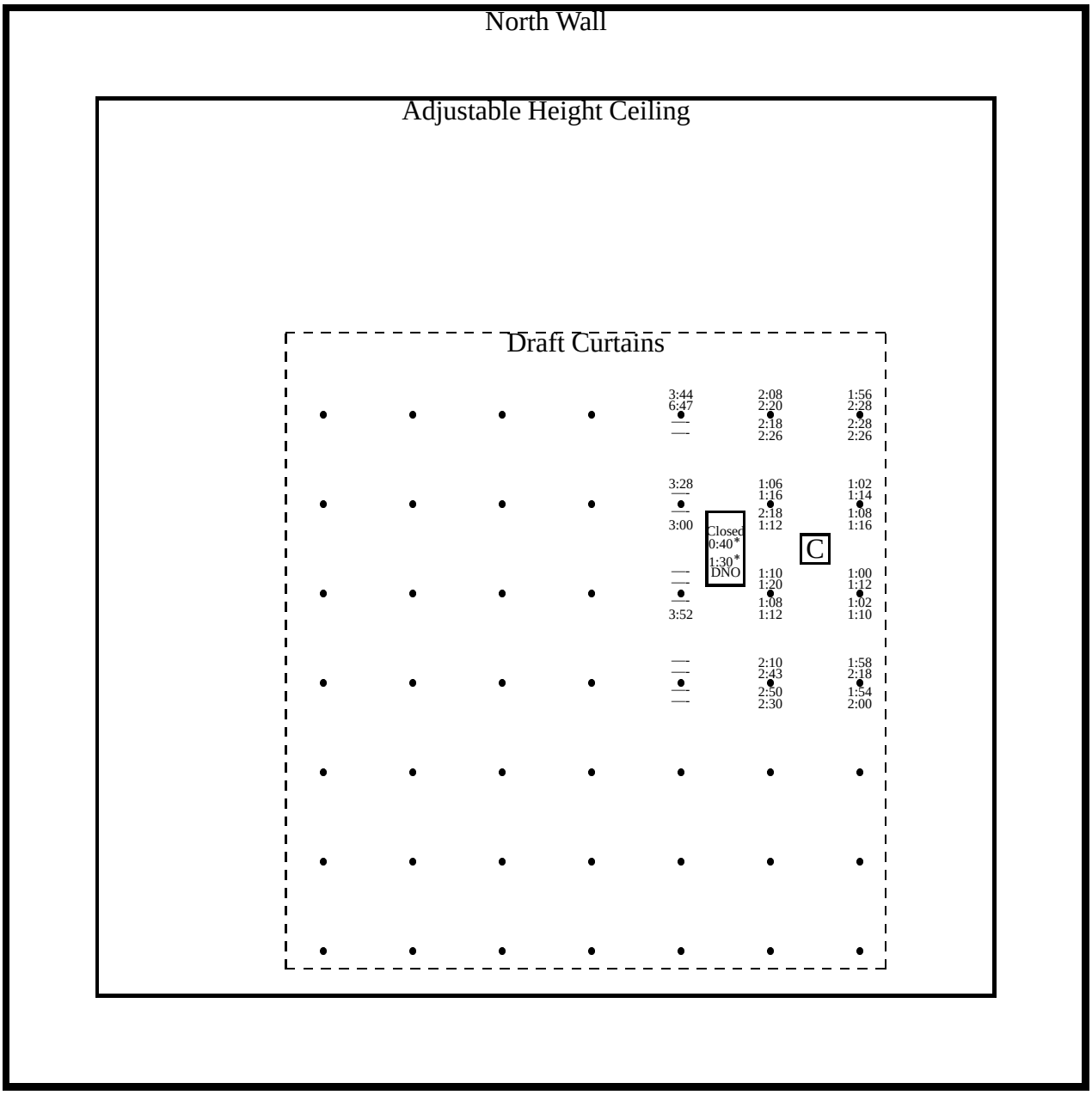

Figure 6: Plan view of heptane spray burner configuration with the results of curtained tests where the fires were at location C. The activation times are from Tests I-4, I-5, I-6 and I-7, respectively. Note that an asterisk beside a vent opening time indicates manual operation.

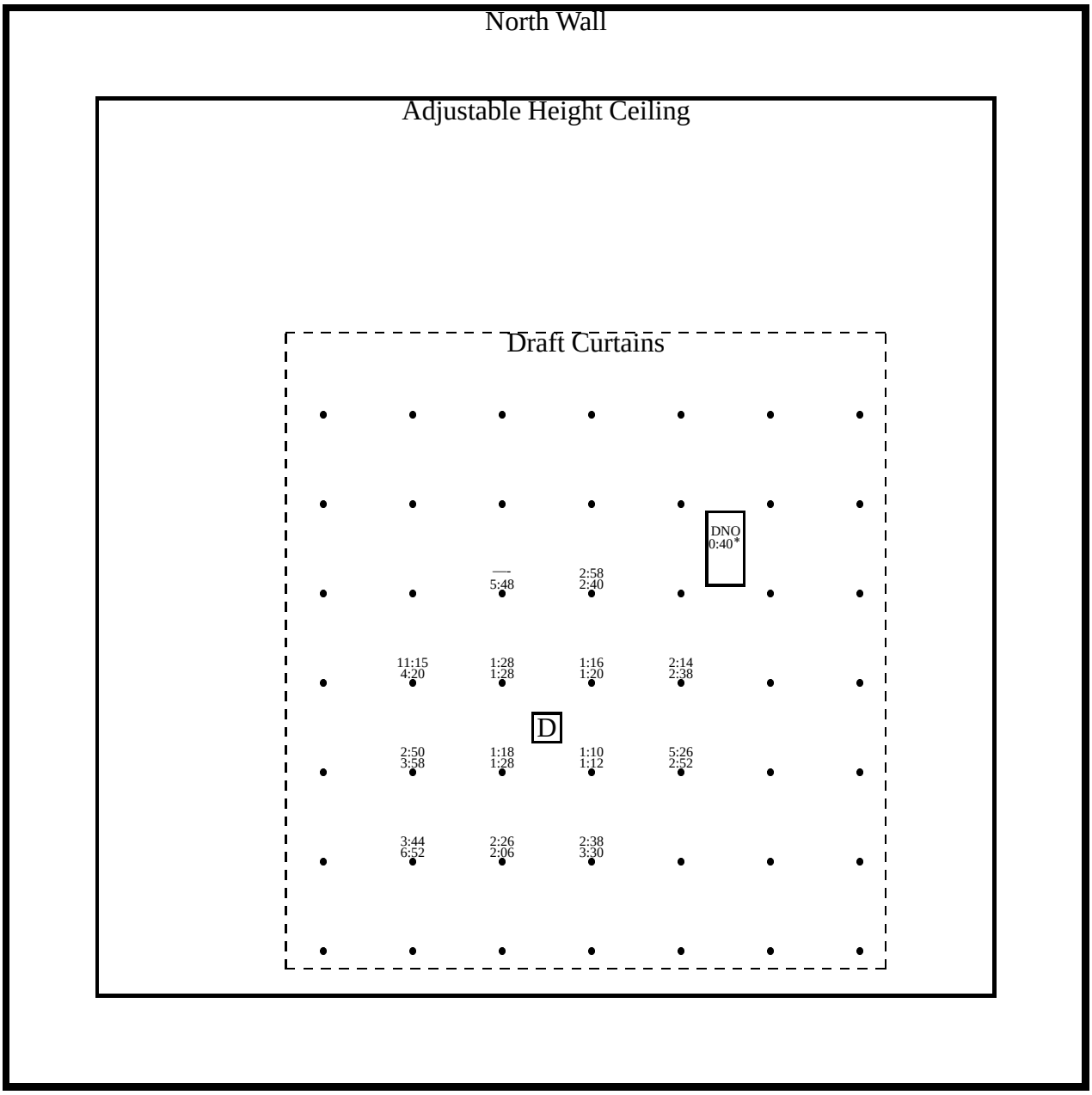

Figure 7: Plan view of heptane spray burner configuration with the results of curtained tests where the fires were at location D. The activation times are from Tests I-9 and I-10, respectively. Note that an asterisk beside a vent opening time indicates manual operation.

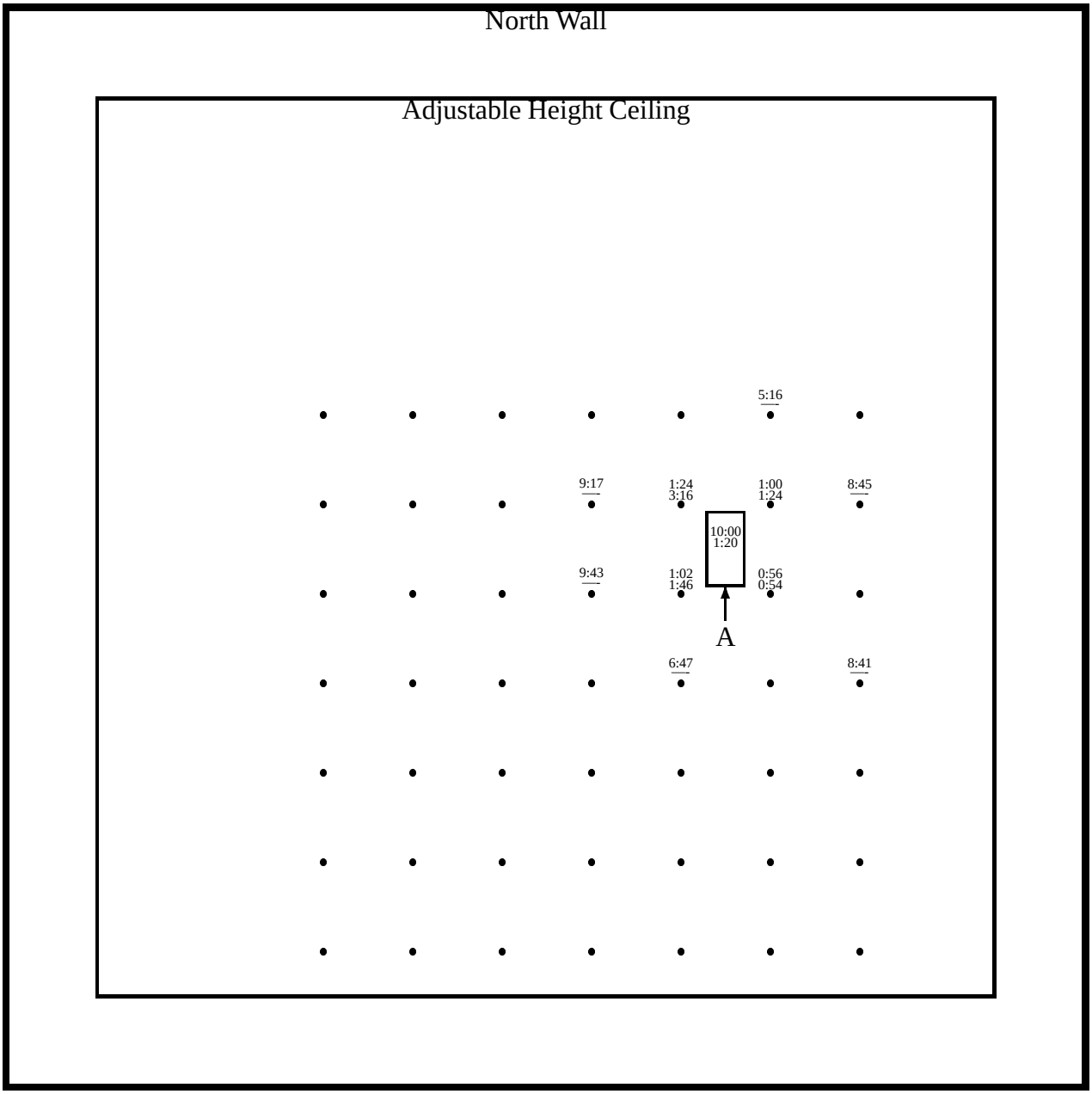

Figure 8: Plan view of heptane spray burner configuration with the results of uncurtained tests where the fires were at location A. The activation times are from Tests I-19 and I-20, respectively. Note that the vent opening time of 10:00 in Test I-19 is approximate because the electronic timing circuit malfunctioned.

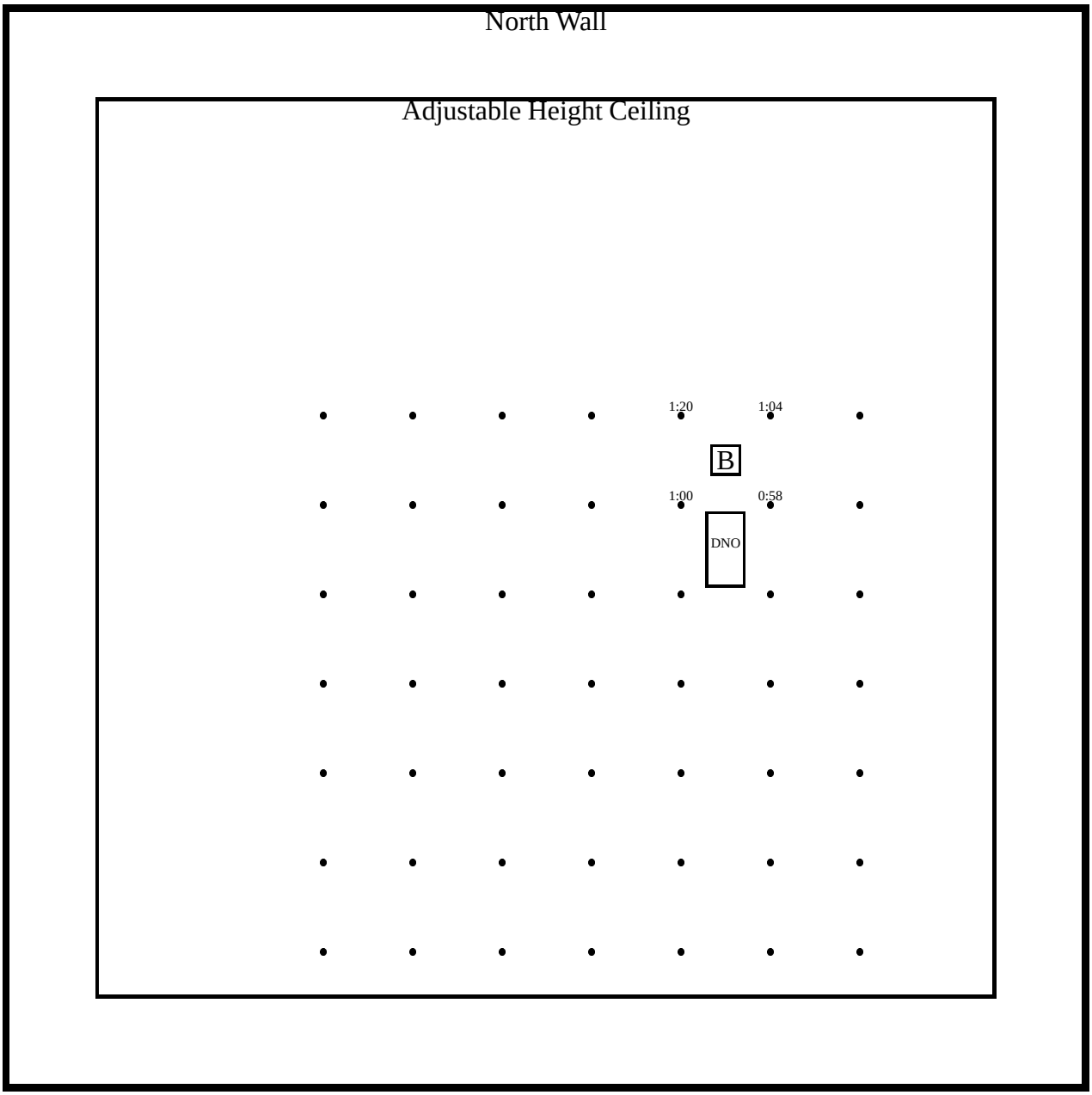

Figure 9: Plan view of heptane spray burner configuration with the results of uncurtained test (Test I-17) where the fire was at location B.

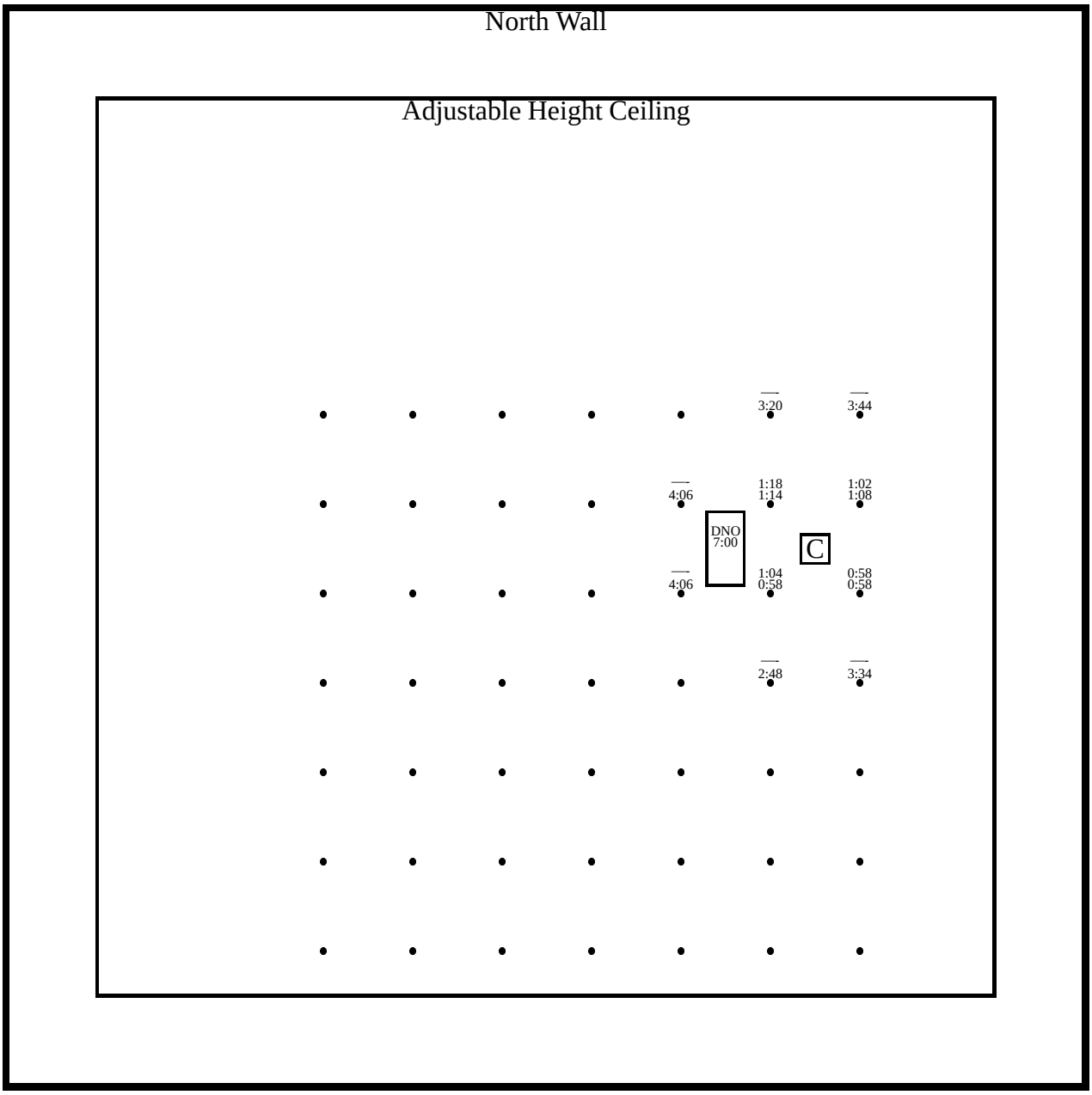

Figure 10: Plan view of heptane spray burner configuration with the results of uncurtained tests where the fires were at location C. The activation times are from Tests I-18 and I-21, respectively.

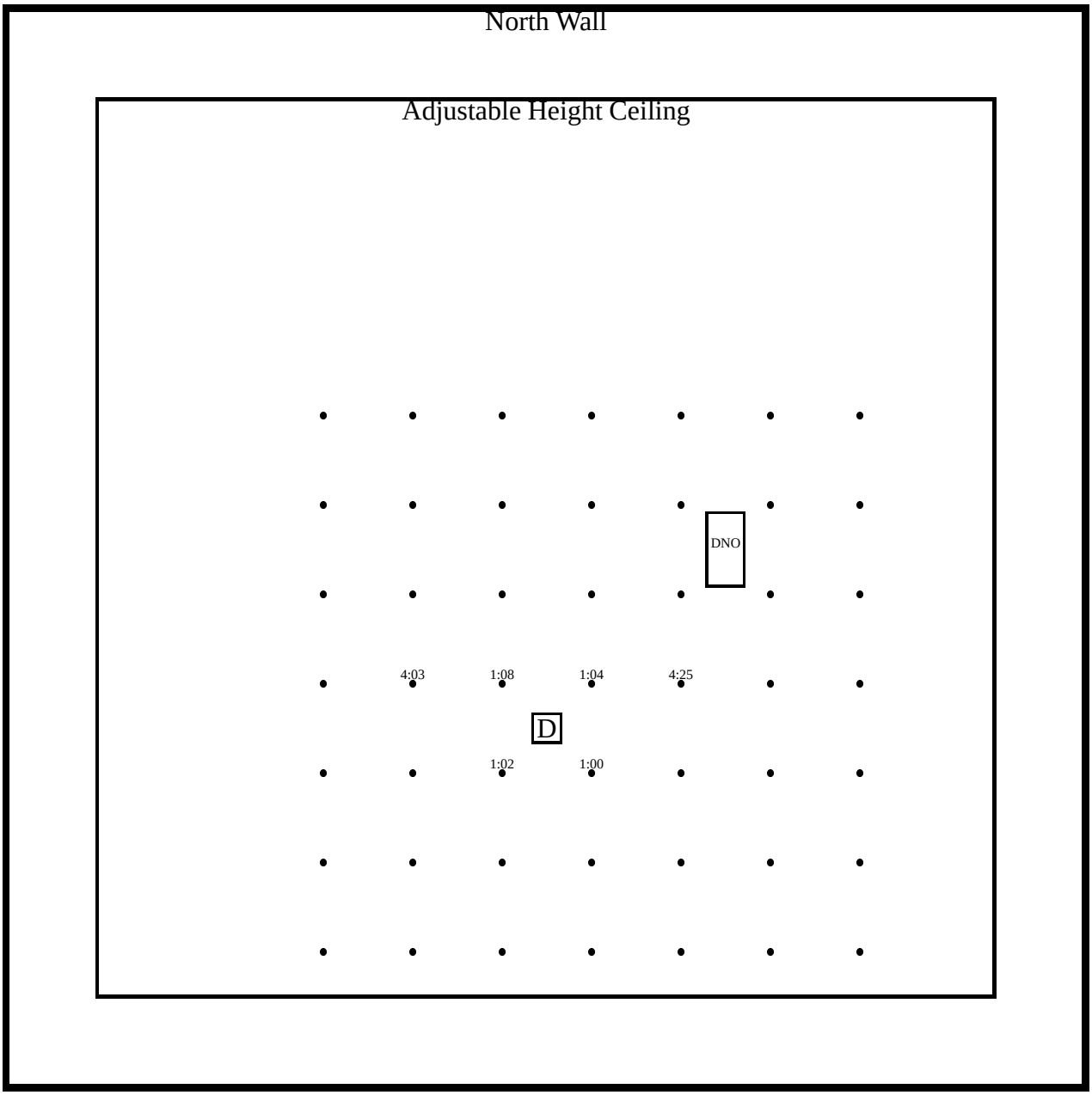

Figure 11: Plan view of heptane spray burner configuration with the results of uncurtained test (Test I-22) where the fire was at location D.

4 Heptane Spray Burner Tests, Series II

A series of additional heptane spray burner tests was performed during a three day period while the vents and draft curtains were installed for the cartoned plastic commodity tests. The objective was to generate larger fires than those of the first series of heptane burns, to provide more data in areas thought to be lacking in the previous tests, and to perform controlled tests in a vented, curtained area conforming to current model codes [24].

4.1 Description

Twelve tests were performed. The vent, draft curtain and burner positions are shown in Fig. 12. In each test the heptane spray burner was ramped up to 10 MW in 75 s following a t-squared curve. After 75 s the heat release rate was held constant. Draft curtains were installed at the ceiling for all of the tests. The same sheet metal curtains from the first series of heptane tests were installed to enclose an area 21 m by 23 m, 490 m^2 (70 ft by 76 ft, 5,320 ft^2) under the 8.2 m (27 ft) adjustable ceiling. The same type of vent used during the first heptane spray burner series was used again. The vents were designed to operate independently (as opposed to gang operation) at a temperature of 74°C (165°F), or manually. The area of the largest quadrant in Fig. 12 was selected to provide a larger vent to floor ratio (1:42) than called for by the Uniform Fire Code (1:50 for up to 20 ft of storage height and less then 6,000 ft^2 of curtained area) [24]. Only the vent in the northwest corner of the curtained area was instrumented, thus the fires were ignited at various locations in the northwest quarter of the curtained area.

During each 10 min test, the entire test facility was exhausted from the center of the 15 m (50 ft) high space (7.0 m (23 ft) above the adjustable ceiling) at the minimum operating rate of 11 m^3/s (24,000 ft^3/min).

Thermocouples were used to measure gas temperatures and "structural" steel temperatures. Two velocity probes were used to monitor the air flows, one in the instrumented vent, the other about 3 m (10 ft) to the south and 3 m to the east of the vent, 10 cm (4 in) below the ceiling. The velocities were measured with bi-directional probes connected to pressure transducers with a range of $\pm$133 Pa (1.0 mm Hg). A thermocouple array was placed 3 m (10 ft) to the south and 3 m to the east of the instrumented vent, as well as at a point 6 m (20 ft) south and 6 m east of the vent (Position D). A third thermocouple array was placed in front of the vent outside of the curtained area. Details about the thermocouple arrays may be found in Ref. [2]. A thermocouple was placed near each sprinkler to record temperatures and activation times. Electronic timing circuits were installed in the vents to determine when each opened.

Positioned near the fusible link installed within the vent cavity were three calibrated brass disks with different thermal responses, plus a 0.0625 in Inconel sheathed type K thermocouple. The bulk RTI[8] values of the disks were determined from plunge tests at UL [2]. The values were reported

[8]The term "bulk RTI" indicates that the temperature of the object is assumed to be governed by the equation

$$\frac{dT_l}{dt} = \frac{\sqrt{u}}{\mathrm{RTI}_b}(T_g - T_l)$$

where T_l is the temperature of the object and T_g is the temperature of the gas streaming past the object with speed u. This definition of RTI_b does not explicitly account for conductive losses from the object to surrounding objects, and should not be confused with the definition of RTI applied to fusible sprinkler links in this report.

to be 32, 164 and 287 $(m \cdot s)^{\frac{1}{2}}$ (58, 297 and 519 $(ft \cdot s)^{\frac{1}{2}}$) for the "fast", "medium" and "slow" disks, respectively [2]. The measurements of each ranged between -10% and +10% of the reported value.

4.2 Results

The results of the second series of heptane spray burner tests are summarized in Table 2. The sprinkler activation times can be found on the following pages, where the times of similar and repeated tests can be found on the same diagram to emphasize differences. The temperature histories of all 100 near-sprinkler thermocouples can be found in Appendix B. Note that the ambient temperature within the facility varied between 15°C and 20°C (59°F and 68°F) for all the tests.

Figures 19–21 show the temperatures recorded by the thermocouple and the calibrated brass disks within the vent located at the northwest corner of the curtained area. The brass disks were used as a means to assess the thermal environment of the vent cavity by providing a measure of temperature more indicative of that of the fusible link than the relatively fast-responding thermocouple. None of the disks could simulate the behavior of the fusible link exactly, however, because the fusing of the link involves the melting of solder.

Heptane Spray Burner Test Series II (10 MW Fires)							
Test No.	Burner Position	Vent Operation	Sprinklers Opened	First Activation	Last Activation	Avg. Peak Temp. °C	Avg. Peak Temp. °F
II-1	D	74°C link (DNO)	27	1:15	6:13	129.4	264.9
II-2	D	All Open at Start	28	1:05	5:53	128.8	263.8
II-3	A	74°C link (1:15)	12	1:08	4:00	101.8	215.2
II-4	B	74°C link (1:48)	16	1:03	5:54	108.8	227.8
II-5	D	74°C link (DNO)	28	1:10	7:07	130.0	266.0
II-6	D	All Open at Start	27	1:10	5:21	127.5	261.5
II-7	A	Closed	18	1:09	4:11	117.2	243.0
II-8	B	74°C link (1:12)	13	1:10	3:34	107.7	225.9
II-9	E	74°C link (DNO)	23	1:07	3:28	115.8	240.4
II-10	F	74°C link (3:20)	19+	1:14	3:01	108.4	227.1
II-11	C	74°C link (DNO)	23	1:02	3:56	123.4	254.1
II-12	C	All Open at Start	23	0:58	4:55	119.0	246.2

Table 2: Results of the heptane spray burner Series II. Note that all fires were ramped up to 10 MW in 75 s following a t-squared curve. Also, the plus sign appended to a value in the "Sprinklers Opened" column indicates that the area of sprinkler activation spread to the edge of the adjustable height ceiling, thus more activations might have occurred had the ceiling extended further.

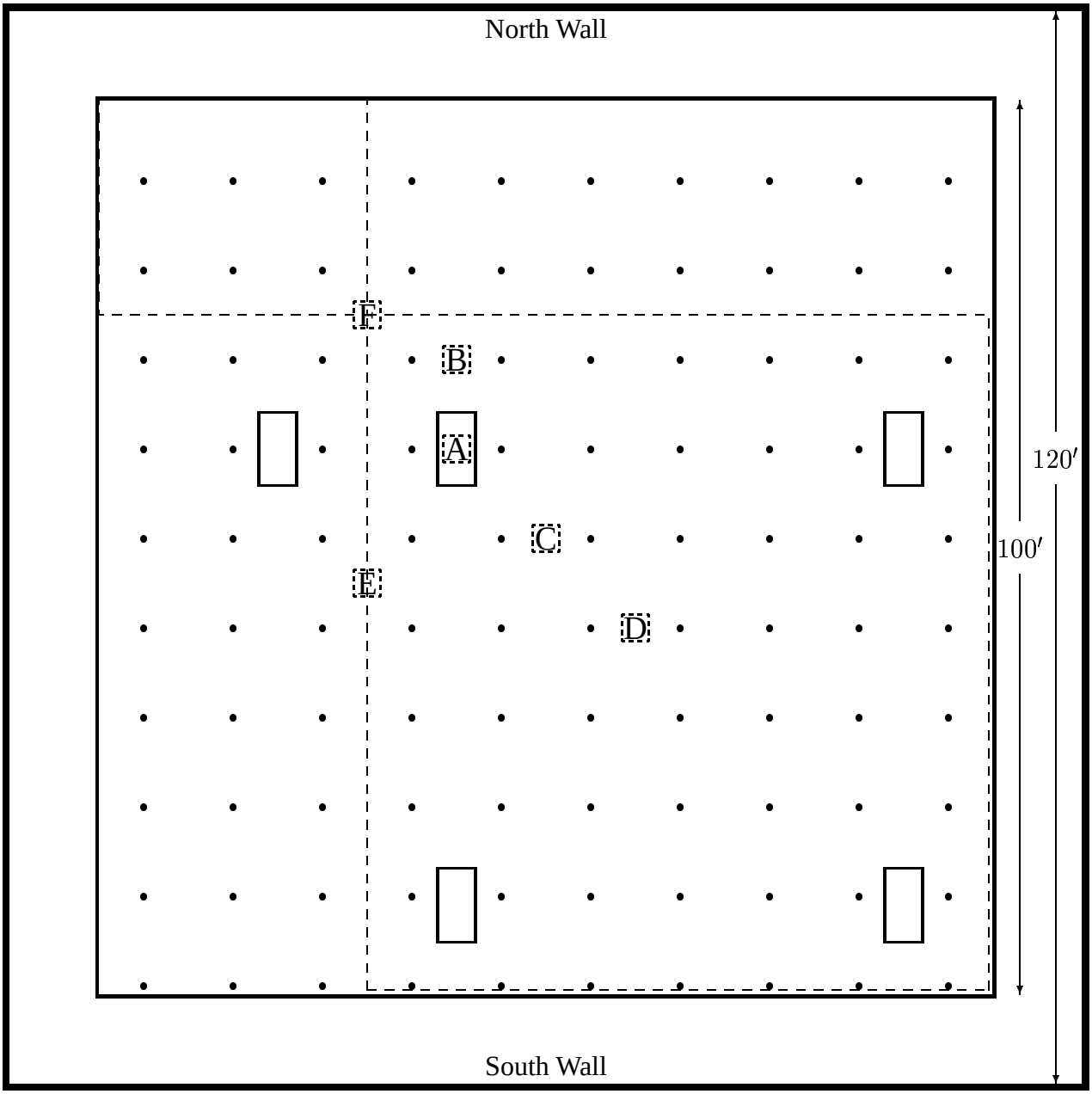

Figure 12: Plan view of large scale fire test facility with the burner, vent and draft curtain positions for the second series of heptane burner tests. The sprinklers are indicated by the solid circles and are spaced 10 ft apart. The branch lines run north to south. The vents are 4 ft by 8 ft.

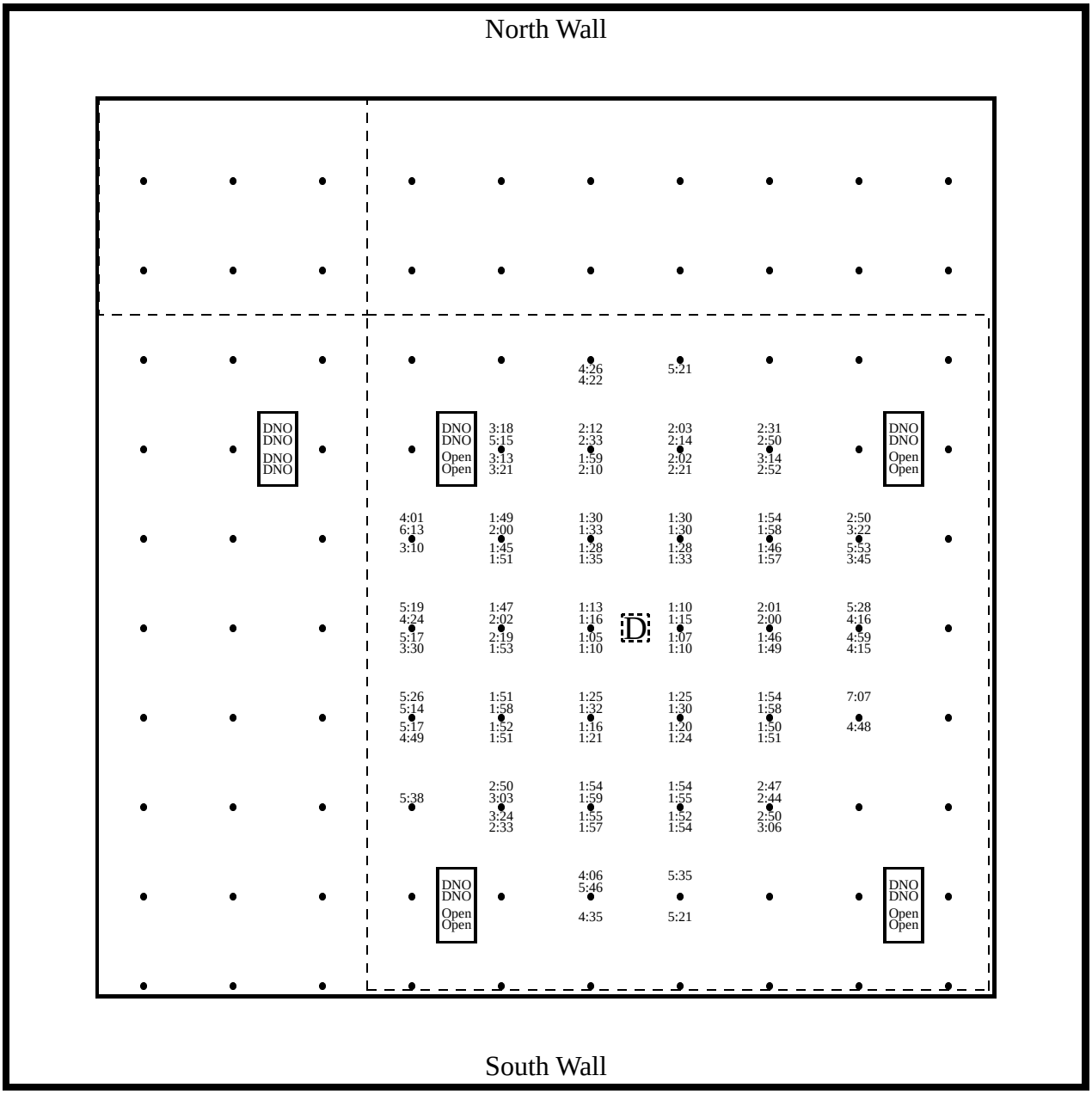

Figure 13: Plan view of large scale fire test facility with the sprinkler activation times of (from top to bottom) Tests II-5, II-1, II-2 and II-6 of the second heptane test series. Tests II-5 and 1 were performed with the vents controlled by fusible links. Tests II-2 and II-6 were performed with the vents open from the start.

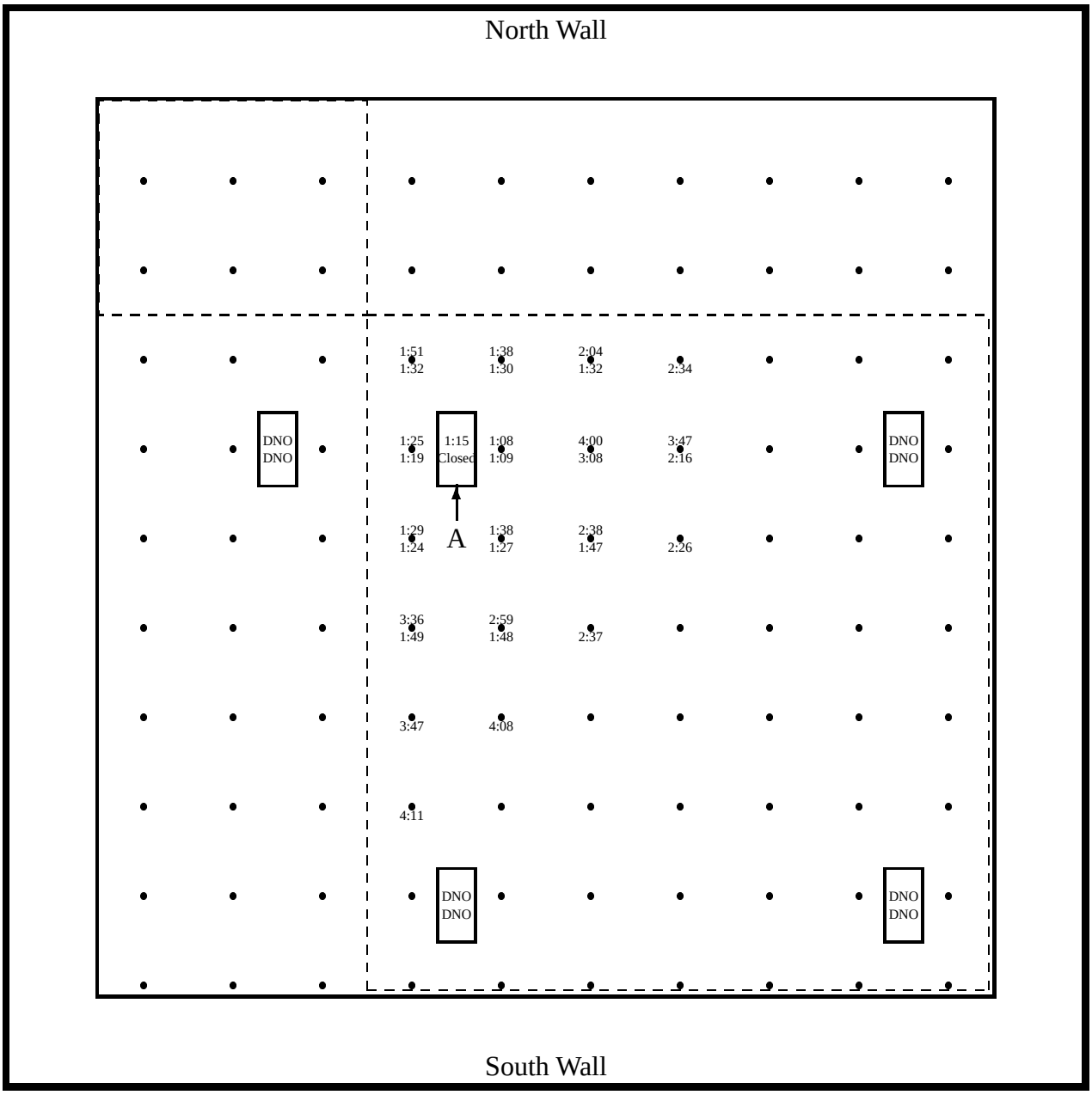

Figure 14: Plan view of large scale fire test facility with the sprinkler activation times for the second heptane test series where the burner was directly under the northwest vent in the curtained area (Position A). In Test II-3 (upper times), the vent link fused at 1:15, whereas in Test II-7 (lower times) the vent was held closed.

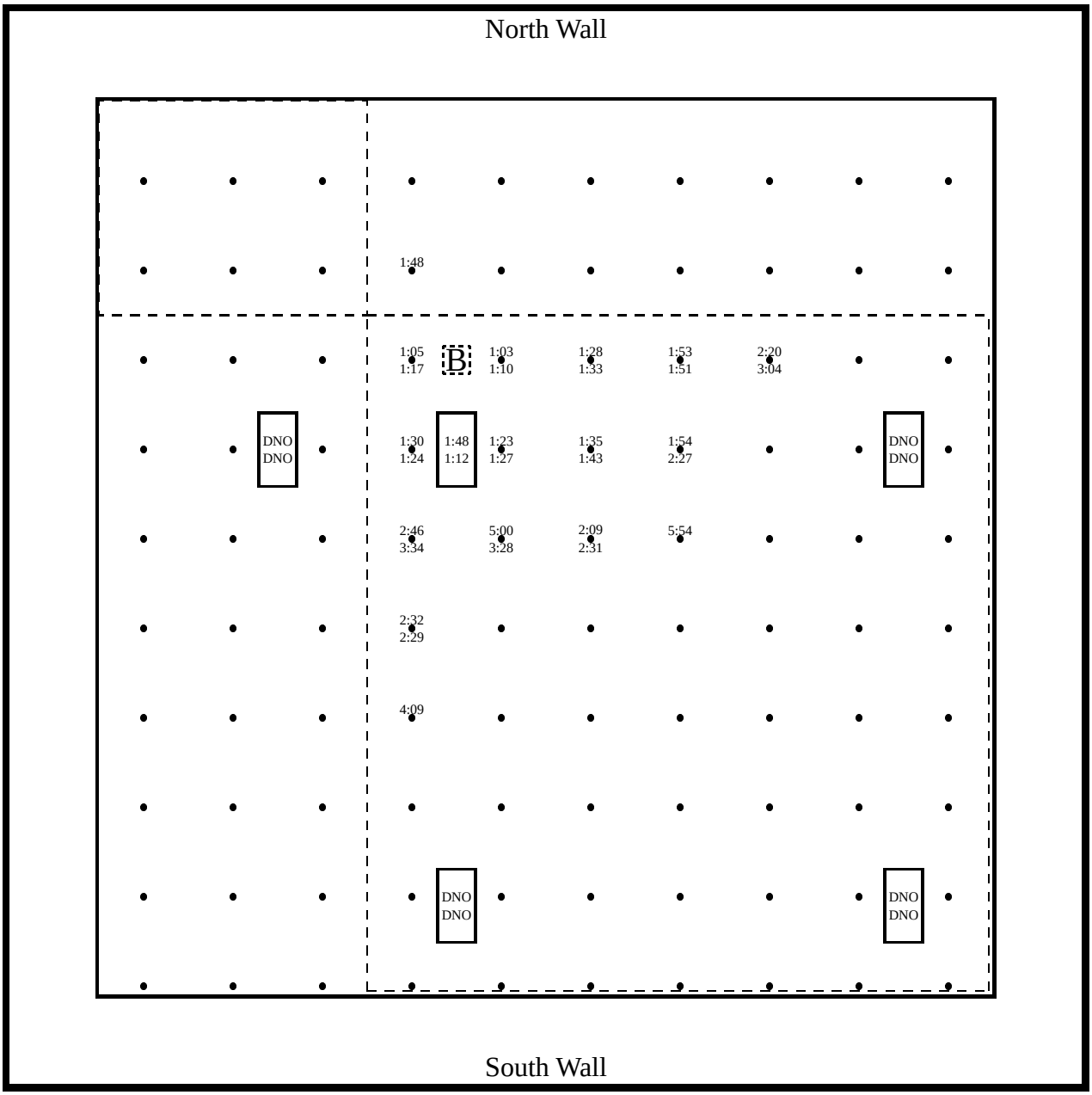

Figure 15: Plan view of large scale fire test facility with the sprinkler activation times for the second heptane test series where the burner was ten feet north of the northwest vent in the curtained area (Position B). In Test II-4 (upper times), the vent link fused at 1:48, whereas in Test II-8 (lower times), the vent link fused at 1:12.

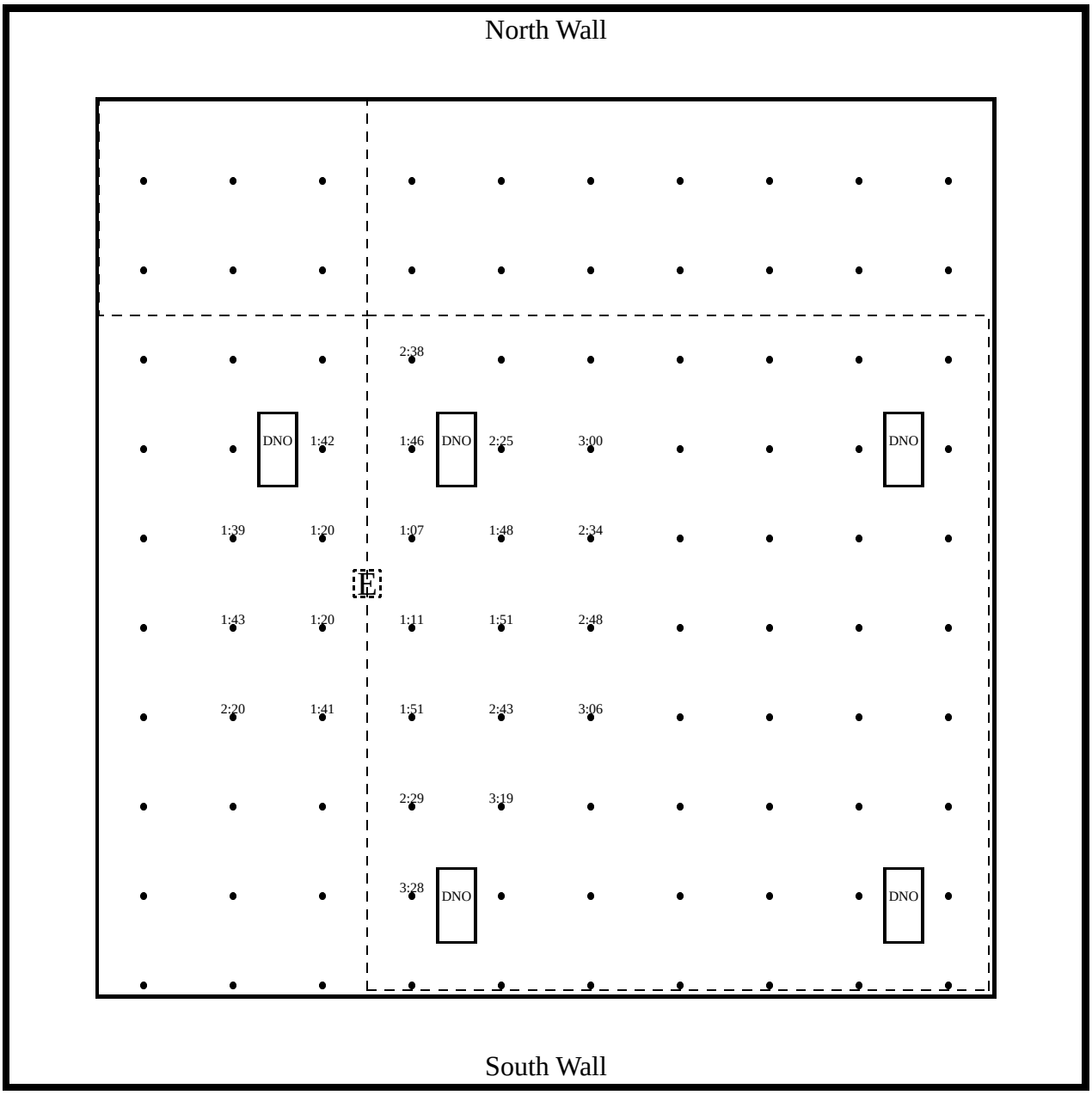

Figure 16: Plan view of large scale fire test facility with the sprinkler activation times for Test II-9 of the second heptane test series where the burner was under the north-south draft curtain (Position E).

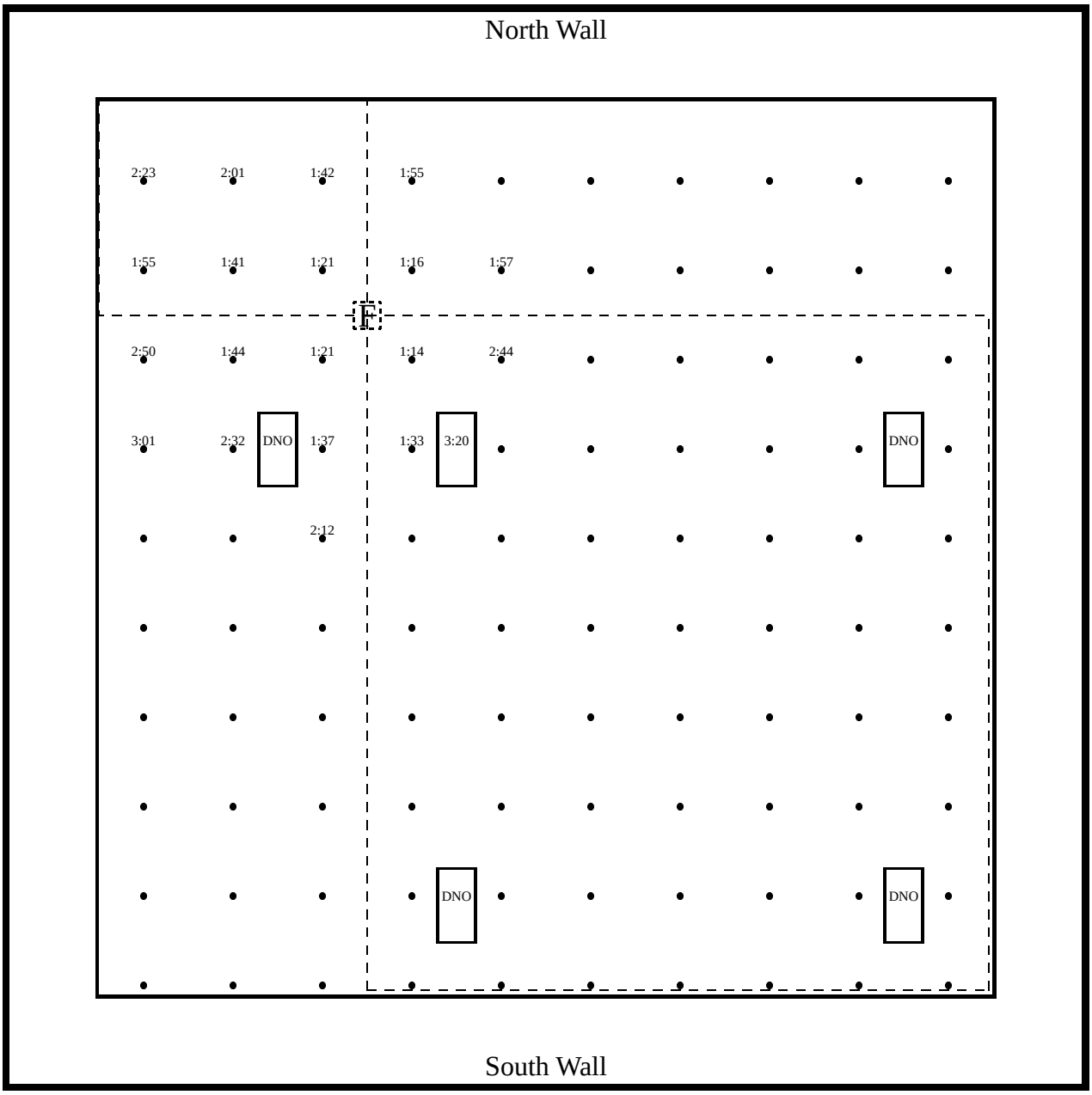

Figure 17: Plan view of large scale fire test facility with the sprinkler activation times for Test II-10 of the second heptane test series where the burner was under the intersection of the draft curtains (Position F).

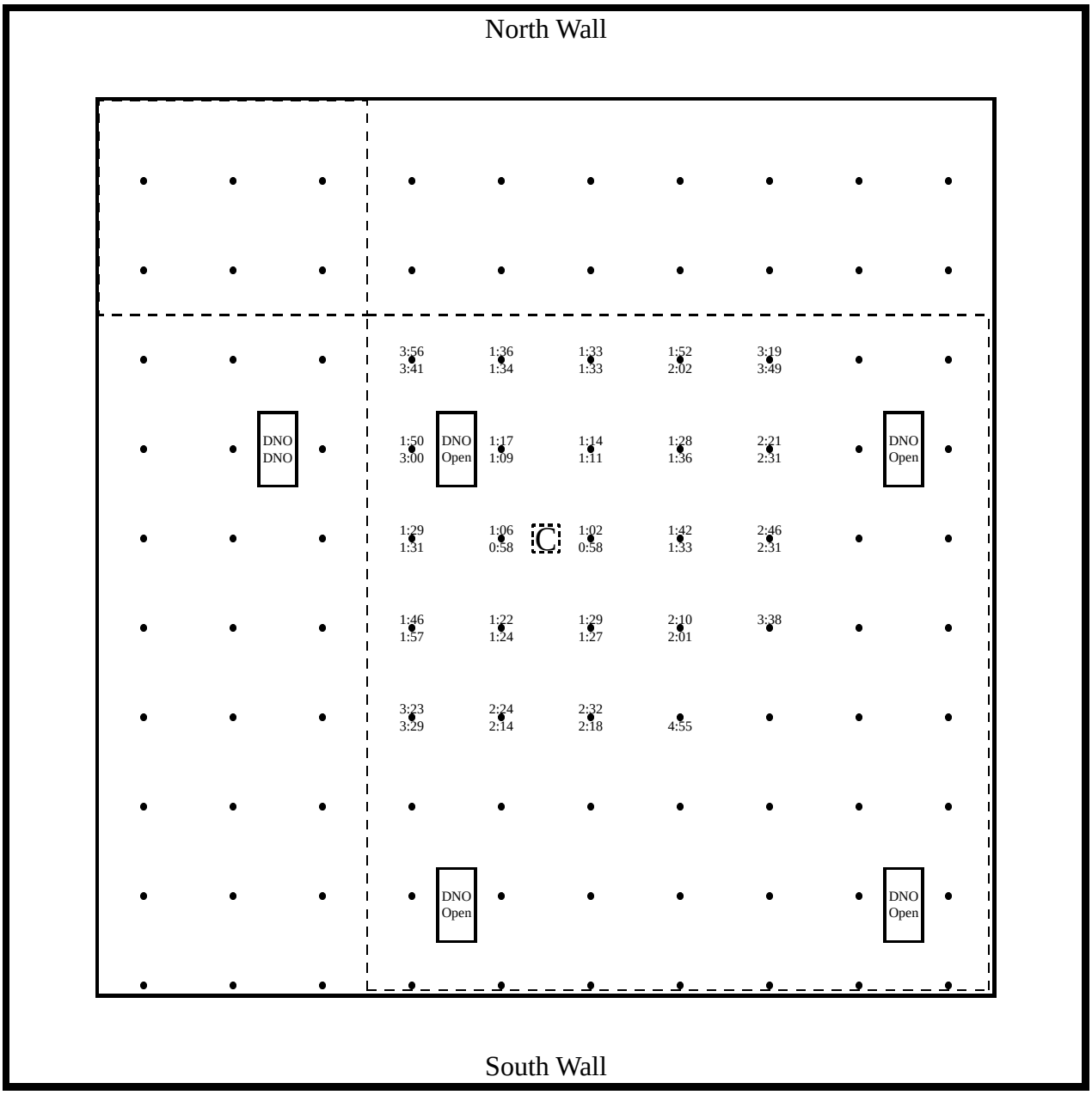

Figure 18: Plan view of large scale fire test facility with the sprinkler activation times for the second heptane series Tests II-11 and II-12 where the burner was at Position C.

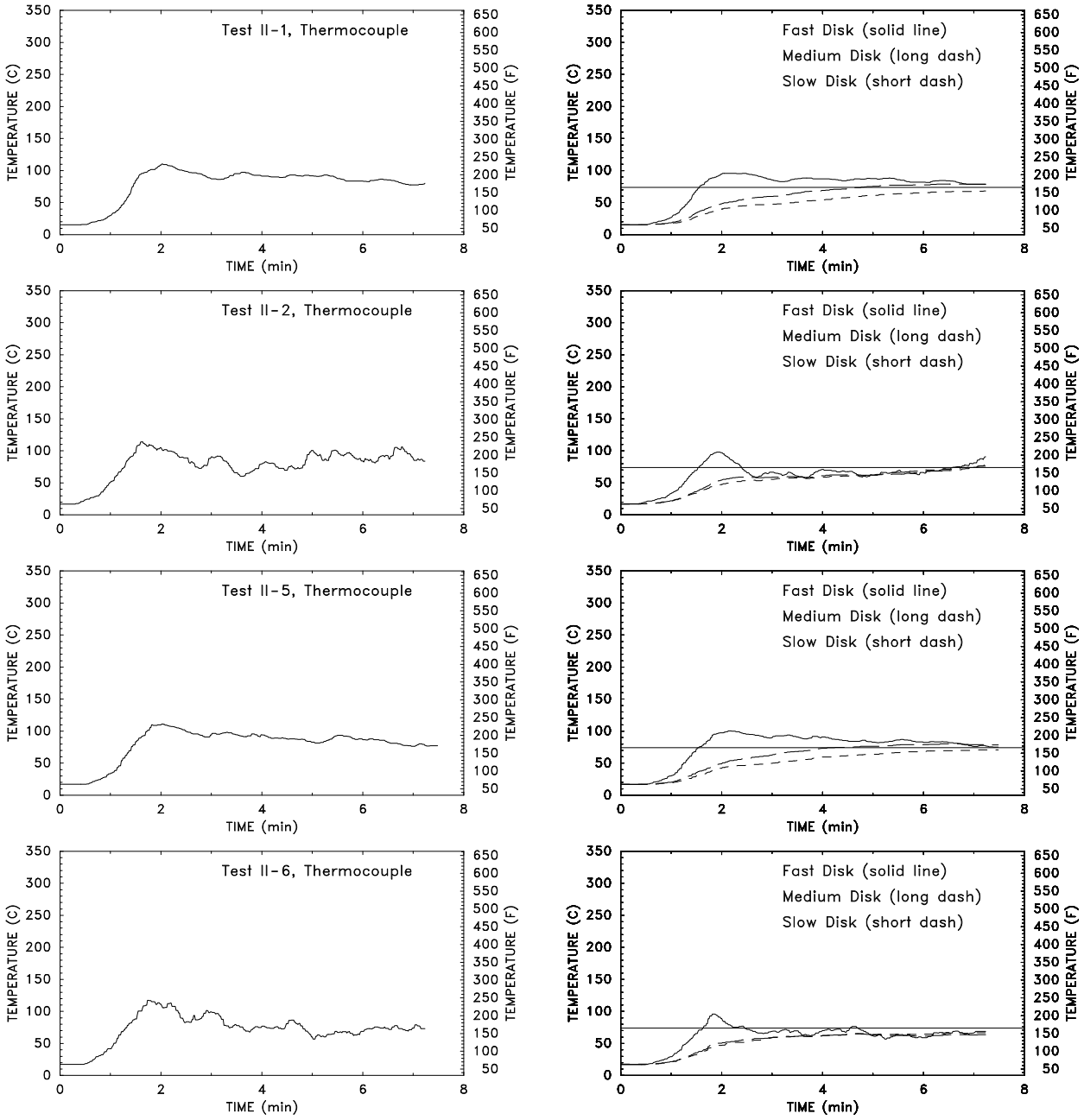

Figure 19: Northwest vent cavity temperatures for Tests II-1, II-2, II-5 and II-6 of the second heptane spray burner test series. The curves on the left display temperatures of the thermocouple near the fusible vent link. The curves on the right display temperatures of the brass disks. The straight horizontal lines indicate the link's activation temperature (74°C, 165°F). In each of the tests, the burner was located at Position D. In Test II-1 the vent did not open; in Test II-2 the vent was open from the start, in Test II-5 the vent did not open; in Test II-6 the vent was open from the start.

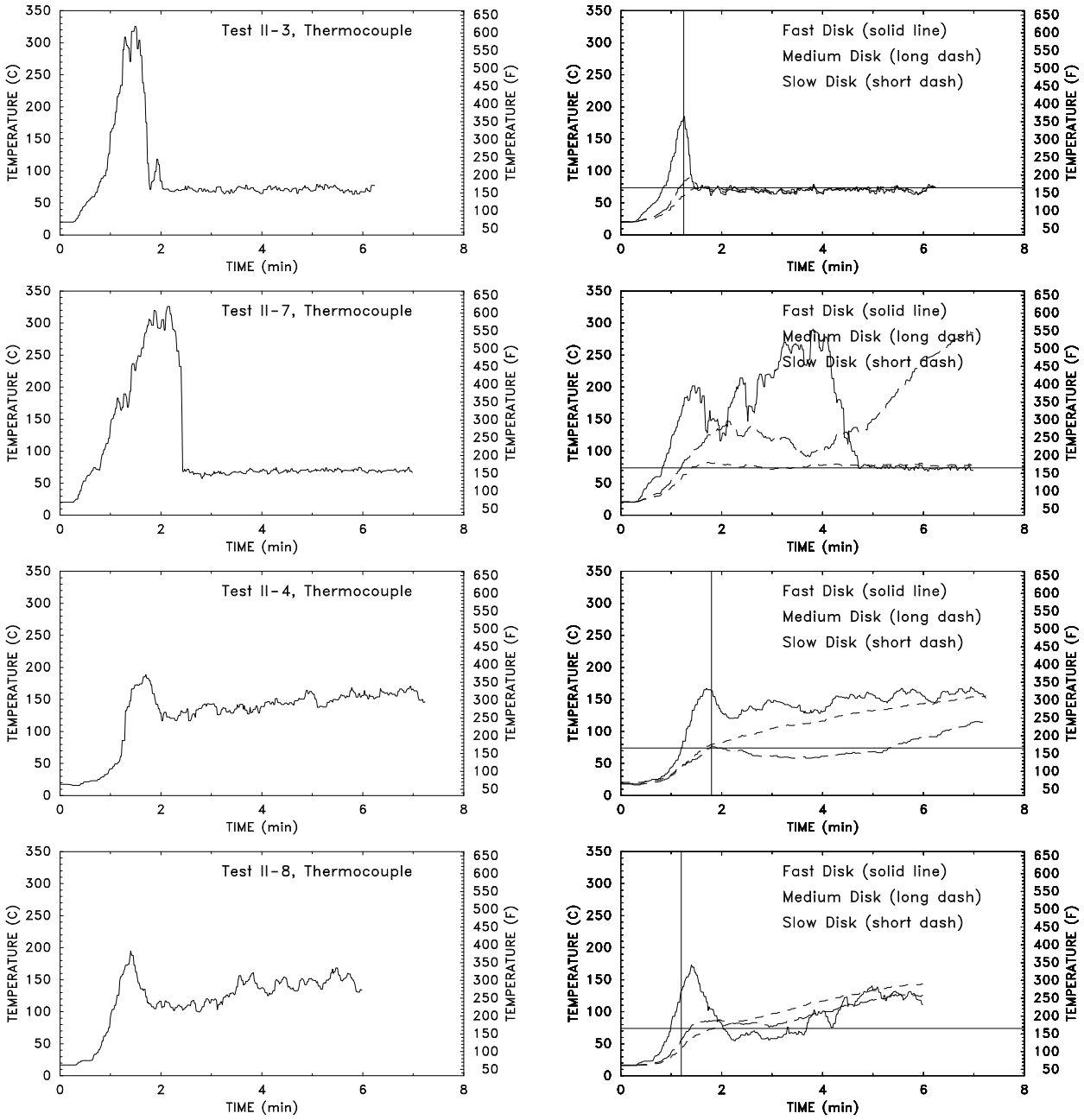

Figure 20: Northwest vent cavity temperatures for Tests II-3, II-4, II-7 and II-8 of the second heptane spray burner test series. The curves on the left display temperatures of the thermocouple near the fusible vent link. The curves on the right display temperatures of the brass disks. The straight horizontal lines indicate the link's activation temperature (74°C, 165°F), and the vertical lines indicate times of vent openings. In Test II-7 the vent was held closed.

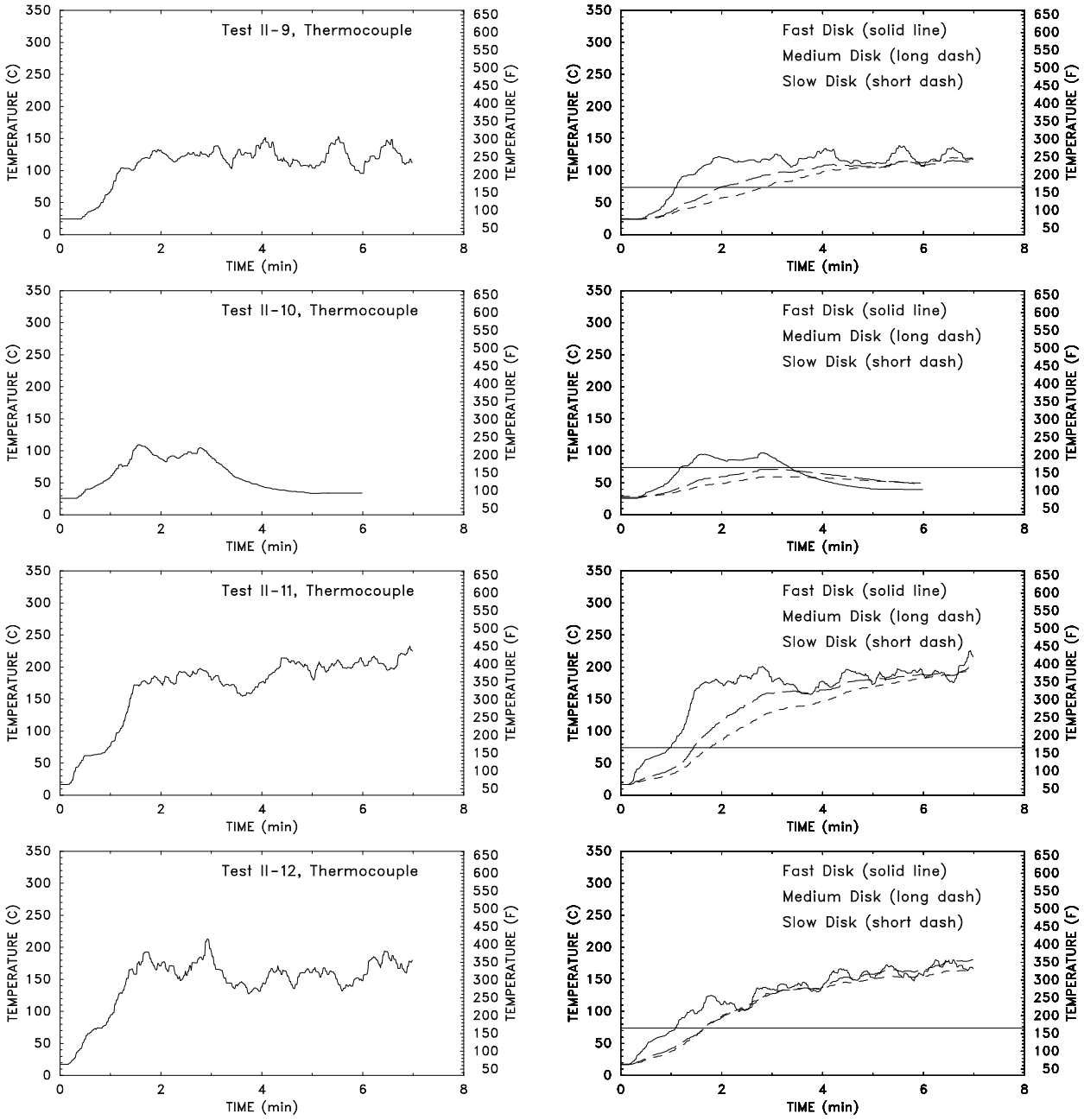

Figure 21: Northwest vent cavity temperatures for Tests II-9–12 of the second heptane spray burner test series. The curves on the left display temperatures of the thermocouple near the fusible vent link. The curves on the right display temperatures of the brass disks. The straight horizontal lines indicate the link's activation temperature (74°C, 165°F), and the vertical lines indicate times of vent openings. In Test II-9 the vent did not open; in Test II-10 the vent outside the draft curtains opened; in Test II-11 the vent did not open; in Test II-12 the vent was open from the start.

5 Cartoned Plastic Commodity Fire Tests

Following the analysis of the results of the first series of heptane spray burner tests, a series of high rack storage cartoned plastic commodity fire experiments was performed at the Large Scale Fire Test facility at UL, the same space that was used for the heptane burner tests described in Sections 3 and 4. In planning these experiments, the Technical Advisory Committee considered a number of factors, including the results of the heptane spray burner tests, numerical modeling, similar experiments performed by Factory Mutual, and current fire protection practices. In order to develop test specifications that represented a realistic situation, a number of documents were reviewed, including the 1994 edition of the Uniform Fire Code [24]; the 1991 edition of NFPA 231C, Standard for Rack Storage of Materials [6]; the 1991 edition of NFPA 204M, Guide for Smoke and Heat Venting [5]; and selected Factory Mutual data sheets [25, 26, 27]. In addition, an attempt was made to maintain consistency between these tests and the recent work completed by FMRC on "Extra Large Orifice" sprinklers for rack storage without vents [21, 28].

5.1 Description

Much of the description for the cartoned plastic commodity tests carries over from the heptane spray burner tests, including the test facility, sprinkler type, vent type and instrumentation. Differences are described below. The Report of Test from UL may be found in Ref. [2]. The UL report contains a complete description of the instrumentation and the measurements.

5.1.1 Fuel Package

The Factory Mutual Research Corporation (FMRC) Standard Plastic test commodity, a Cartoned Group A Unexpanded Plastic, served as the fuel for this test series [21]. This commodity has been used extensively for testing since 1971 [29]. The complete fuel package consists of a combination of the cartoned plastic commodity and Class II commodity.

The cartoned plastic commodity consists of rigid crystalline polystyrene cups (empty, 0.47 L (16 fl oz) size) packaged in compartmented, single-wall, corrugated paper cartons. The cups are arranged open end down in five layers, 25 per layer for a total of 125 per carton. Each carton, or box, is a cube 0.53 m (21 in) on a side. Eight boxes comprise a pallet load. Two-way, 1.06 m by 1.06 m by 0.13 m (42 in by 42 in by 5 in) slatted deck hardwood pallets support the loads. A pallet load weighs approximately 80 kg (170 lb), of which about 36% is plastic, 35% is wood and 29% is corrugated paper [21].

A Class II commodity was used in the target arrays. Typically, the commodity was located beyond the expected area of the fire spread. This commodity consists of double tri-wall corrugated paper cartons with five-sided steel stiffeners inserted for stability. The two cartons plus the liner form a single 1.06 m (42 in) cube having a combined nominal wall thickness of 2.5 cm (1 in). The single cube was supported on the same type of pallet supporting the cartoned plastic commodity.

5.1.2 Storage Method

A commodity storage height of 6 m (20 ft) with a ceiling height of 8.2 m (27 ft) represents one of the most severe arrangements allowable under NFPA 231C without requiring in-rack sprinklers.

Under the Uniform Fire Code, storage of the test commodity is required to be protected using sprinklers, vents and draft curtains when the size of the high piled storage area exceeds 230 m^2 (2,500 ft^2).

The test array (Fig. 22) was designed to create a challenging storage situation. Each storage array consisted of a main (ignition) double-row rack at the center, flanked on two sides by single row target racks. The rows were separated by 8 ft wide aisles. Each of the two rows of the main array consisted of four 2.4 m (8 ft) long bays; a 0.15 m (6 in) flue separated the rows. Longitudinal flues of 0.2 m (7.5 in) were used to separate the pallets within a row. The overall loaded area of the double-row rack measured approximately 2.3 m (7.5 ft) wide by 10 m (33 ft) long. The racks were divided vertically into 4 tiers; the overall loaded height was 5.8 m (19 ft). A similar configuration was used in a series of FMRC burns documented in Ref. [21].

The fire was ignited with 2 standard igniters which consisted of 8 cm (3 in) long by 8 cm diameter cylinders of rolled cotton material, each soaked in 120 mL (4 oz) of gasoline and enclosed in a polyethylene bag. The rolls were placed against the carton surfaces in the first tier, just above the pallet (Fig. 22). The igniters were lit with a flaming propane torch at the start of each test.

5.1.3 Sprinkler Protection

The sprinklers used in all of the tests were Central ELO-231 (Extra Large Orifice) uprights. The sprinklers, flow rates and activation temperatures were the same as in the first series of heptane spray burner tests. Even though UL listing and FM approval of this sprinkler with this type of storage arrangement are based on a minimum density requirement of 0.6 gpm/ft^2, the lower density of 0.5 gpm/ft^2 was used to allow for more challenging, but still controllable, fires and more sprinkler activations.

5.1.4 Test Layout

Draft curtains were installed at the ceiling for three of the five tests. The same sheet metal curtains from the heptane tests were installed to enclose an area 21 m by 23 m, 490 m^2 (70 ft by 76 ft, 5,320 ft^2) under the adjustable ceiling (Fig. 23). Five vents were installed in the adjustable ceiling, following the layout shown in Figure 23. This same type of vent was used during the first heptane spray burner series. The vents were designed to operate independently (as opposed to gang operation) at a temperature of 74°C (165°F), or manually. The area of the largest quadrant in Fig. 29 was selected to provide a larger vent to floor ratio (1:42) than called for by the Uniform Fire Code (1:50 for up to 20 ft of storage and less then 6,000 ft^2 of curtained area) [24]. Only the vent in the northwest corner of the curtained area was instrumented, thus the fires were ignited at various locations in the northwest quarter of the curtained area.

The layout of each of the five tests is shown on the following pages, along with the sprinkler activation times. In designing the layouts, there were several rules that were followed due to both the geometry of the test facility and a desire to maintain consistency from test to test: (1) the longer dimension of the 1.2 m by 2.4 m (4 by 8 ft) vents had to run north-south because of the arrangement of the structural elements in the adjustable ceiling; (2) the vents had to be placed between branch lines, which also run north-south; (3) the vents had to be placed between two sprinklers, roughly at the quarter points of the main test quadrant; (4) the draft curtains had to be placed between rows of sprinklers so as to maintain a 1.5 m (5 ft) spacing between the curtains and sprinklers; and (5)

Plan View

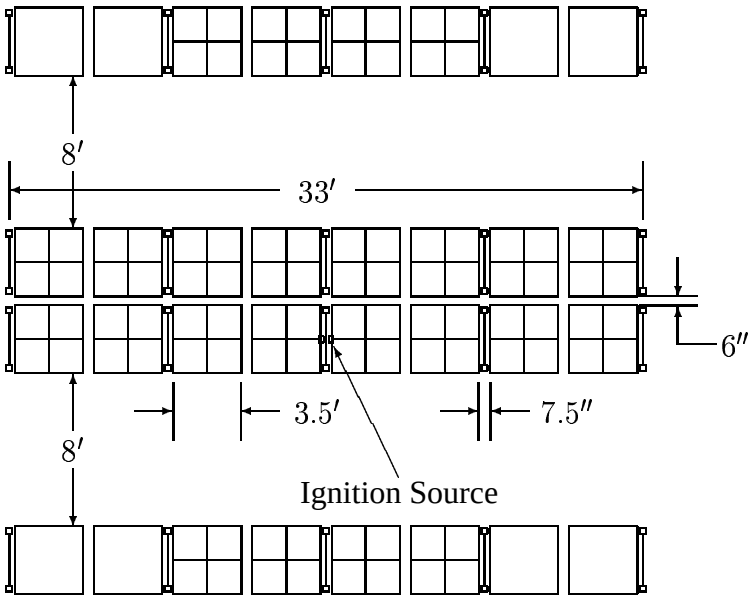

Side Elevation View

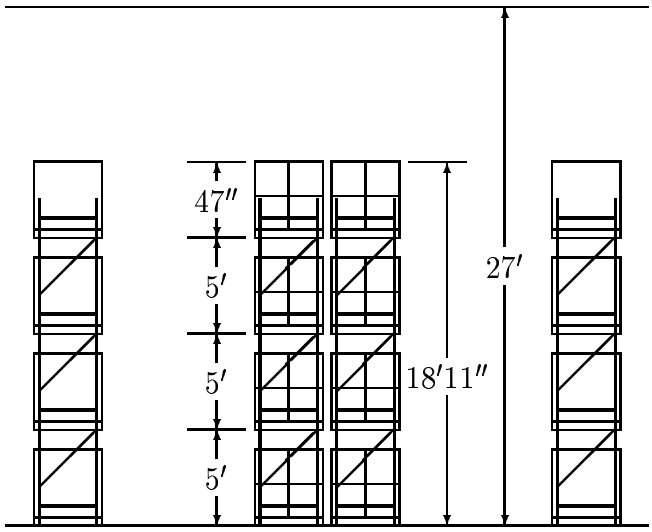

Figure 22: Configuration of the cartoned plastic commodity rack storage. Note that the pallets without perpendicular lines indicate Class II targets. The ignition location is indicated by two small rectangles in the center transverse flue of the Plan View.

the racks had to be arranged perpendicularly to the branch lines to eliminate "shadowing" effects. Three ignition locations were chosen: the first farthest from the vents, the second directly under a vent, and the third near the intersection of the draft curtains.

During each 30 min test, the entire test facility was exhausted from the center of the 15 m (50 ft) high space (7.5 m (25 ft) above the adjustable ceiling) at a rate of 28 m^3/s (60,000 ft^3/min), the maximum capacity.

5.1.5 Instrumentation

Visual observations of test events were recorded and assessments made of the amount of commodity consumed by the fire (fire damage). Photographic documentation included video tape and color slides. In addition, infrared video was used to record each test for analysis, and also to aid the fire fighters who extinguished the residual fire following each 30 min test.

Thermocouples were used to measure gas temperatures and "structural" steel temperatures. Two velocity probes were used to monitor the air flows, one in the instrumented vent, the other about 3 m (10 ft) to the south and 3 m to the east of the vent, 10 cm (4 in) below the ceiling. The velocities were measured with bi-directional probes connected to pressure transducers with a range of $\pm$133 Pa (1.0 mm Hg). A thermocouple array was placed 3 m (10 ft) to the south and 3 m to the east of the instrumented vent, as well as at a point 6 m (20 ft) south and 6 m east of the vent, above the ignition point for Test P-1. A third thermocouple array was placed in front of the vent outside of the curtained area. Details about the thermocouple arrays may be found in Ref. [2]. A thermocouple was placed near each sprinkler to record temperatures and activation times. Electronic timing circuits were installed in the vents to determine when each opened. In addition, a thermocouple and three calibrated brass disks were placed in one of the vent cavities to measure the air temperature and to simulate the thermal response of the fusible link. These same disks were installed during the second series of heptane spray burner tests.

Sprinkler water flow and pressure were continuously monitored. Oxygen, carbon monoxide and carbon dioxide concentrations were recorded near the ignition point. Three optical sensors consisting of a white light source separated from a photocell by 1 m were positioned 1 m above the adjustable ceiling, 1.8 m (6 ft) below the ceiling and 1.5 m (5 ft) above the floor at the location indicated in the plan views shown below.

5.2 Results

Five cartoned plastic commodity tests were conducted over the course of a month (October 1997). The results of the five tests are summarized in Table 3. In four of the tests, the vents were equipped with a fusible link, rated at 74°C (165°F). In one test (Test P-5) the vents were manually operated. Further details of each test can be found on the following pages.

Cartoned Plastic Commodity Test Series					
Test Number	P-1	P-2	P-3	P-4	P-5
Test Date	Sept. 30	Oct. 2	Oct. 16	Oct. 21	Oct. 28
Indoor Temperature (°C/°F)	20/68	18/65	19/67	17/63	18/64
Outdoor Temperature (°C/°F)	14/57	11/52	10/50	10/50	8/46
Relative Humidity (%)	51	51	48	30	43
Commodity Moisture Content (%)	9	9	8	6	8
Draft Curtains	No	No	Yes	Yes	Yes
Fire Pos. rel. to vent	20′E,20′S	Under	10′N	20′E,20′S	20′E,20′S
No. Vent Openings	0	1	1	0	4 (manual)
Vent Opening Time	DNO	6:04	4:11	DNO	1:14
First Sprinkler Activation	1:16	1:40	1:07	1:33	1:14
Last Sprinkler Activation	13:41	5:37	16:06	2:40	5:04
Activations in the 1st 6 min	4	23+	8	5	7
Total Sprinklers Activated	20	23+	19+	5	7
Estimated Boxes Consumed	117	127	184	103	81

Table 3: Results of the cartoned plastic commodity test series. Note that position of fire is in relation to the vent in the northwest corner of the curtained area. The vent that operated in Test P-2 was not the vent directly above the ignition source. The plus sign appended to a value in the "Activations in the 1st 6 min" or the "Total Sprinklers Activated" rows indicates that the area of sprinkler activation spread to the edge of the adjustable height ceiling, thus more activations might have occurred had the ceiling extended further.

5.2.1 Test P-1

The fire was ignited in a transverse flue, at the point where two boxes on the same pallet abut. The two ignitors were situated about 12 cm (5 in) off the floor. The flames reached the top of the third tier about 54 s after ignition; the fourth tier about 60 s. At this time, the flames could just be seen emerging from the array on the south face and entering the longitudinal flue separating the rows within the array. The first sprinkler activated 76 s after ignition, knocking the flames below the top of the fourth tier. The flames re-emerged from the longitudinal flue at about 1:53, followed by the second sprinkler activation at 2:14 on the opposite side of the ignition flue. The 58 s delay between the first and second sprinkler activation allowed the fire to spread more rapidly towards the east end of the array, ultimately opening up more sprinklers on the eastern side of the north-south line of symmetry. Although 20 sprinklers opened by about 15 min, only 4 had opened after 8 min. Examining the thermocouple data near each unactivated sprinkler, it appears that the near-ceiling temperatures outside of the first ring of sprinklers steadily grew following the first few activations, but eventually decreased following the 11 activations that occurred between 8 and 13 min.

By about 10 min after ignition the smoke layer throughout the test facility was at the height of the third tier. Up to this point in time, much more smoke was observed in the north aisle, reducing visibility to only a few meters. The south aisle remained relatively clear of smoke during the first 10 min.

The fire damage was limited to the bays surrounding the ignition point, both on the south and north side of the main array (Fig. 25). Most of the fire damage was found in the bay east of the ignition flue on tiers 1 through 3 due to the asymmetrical sprinkler activation pattern. The fourth tier was protected from fire damage by the sprinkler spray.

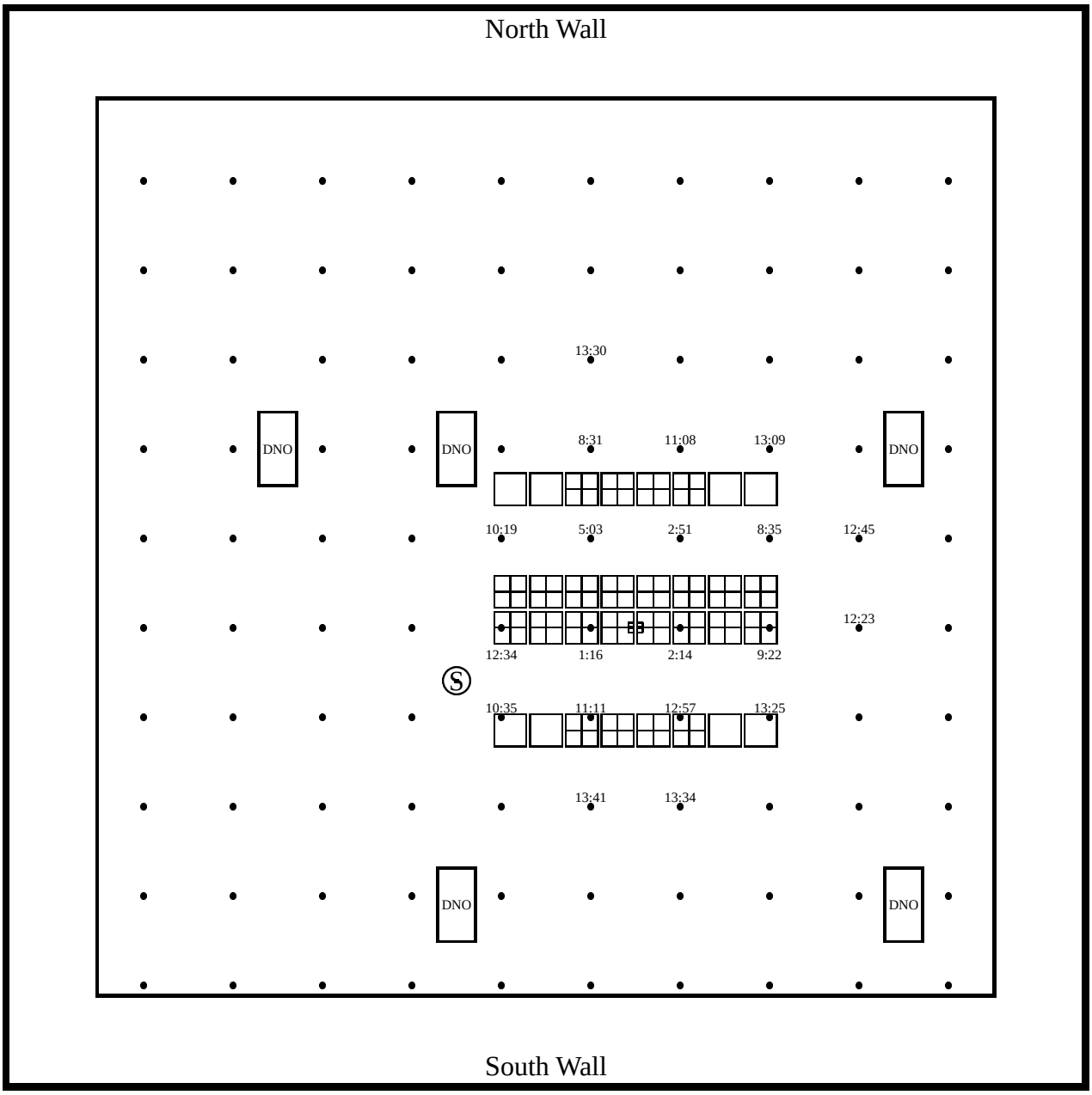

Figure 23: Plan view of Large Scale Fire Test Facility with the sprinkler activation times for Plastic Test P-1. The circled "S" denotes the location of the optical density meters or "smoke eyes".

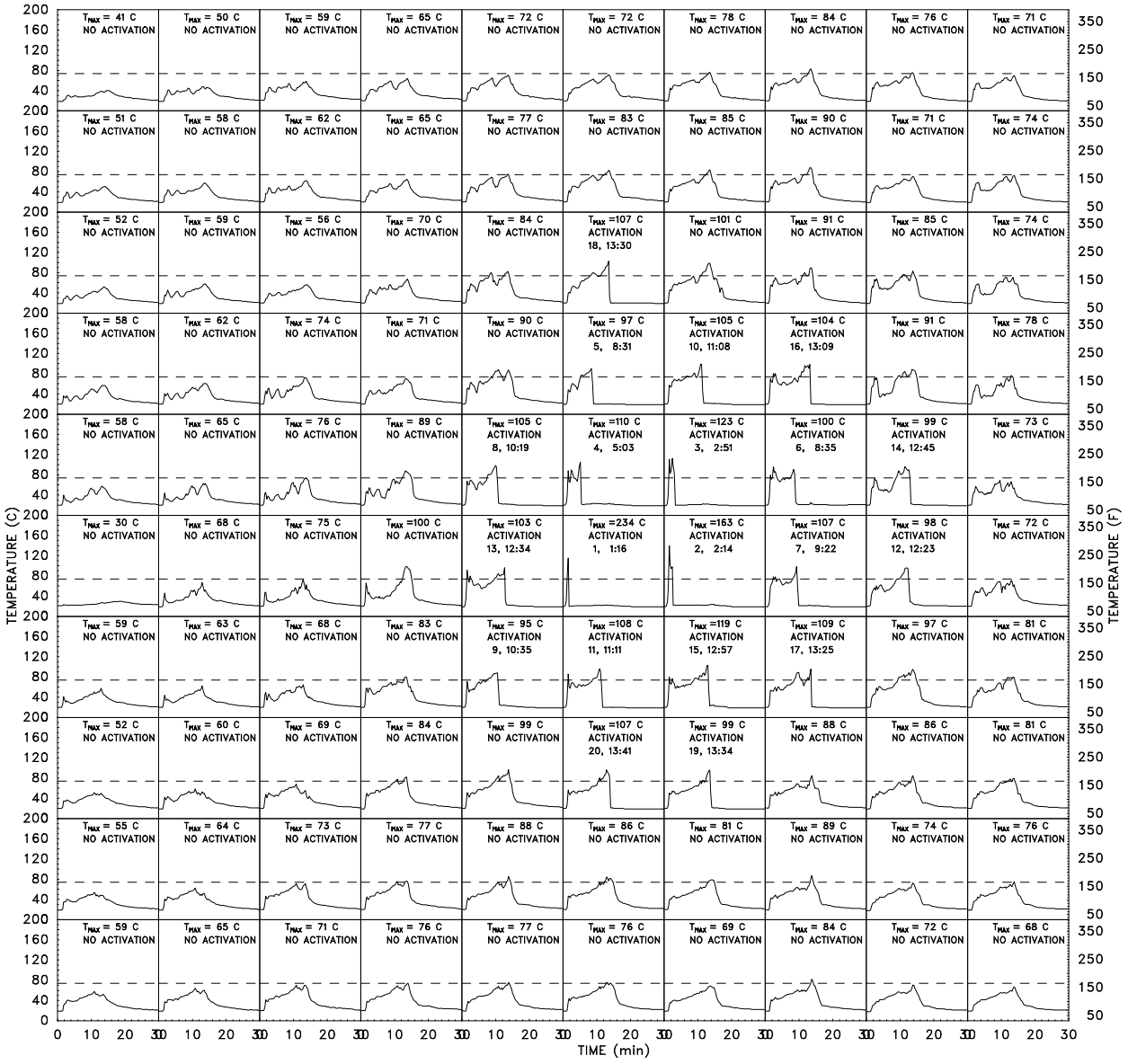

Figure 24: Temperature profiles from all 100 near-sprinkler thermocouples from Plastic Test P-1. The arrangement of the plots mimics that of Fig. 23.

View of Main Array from the South

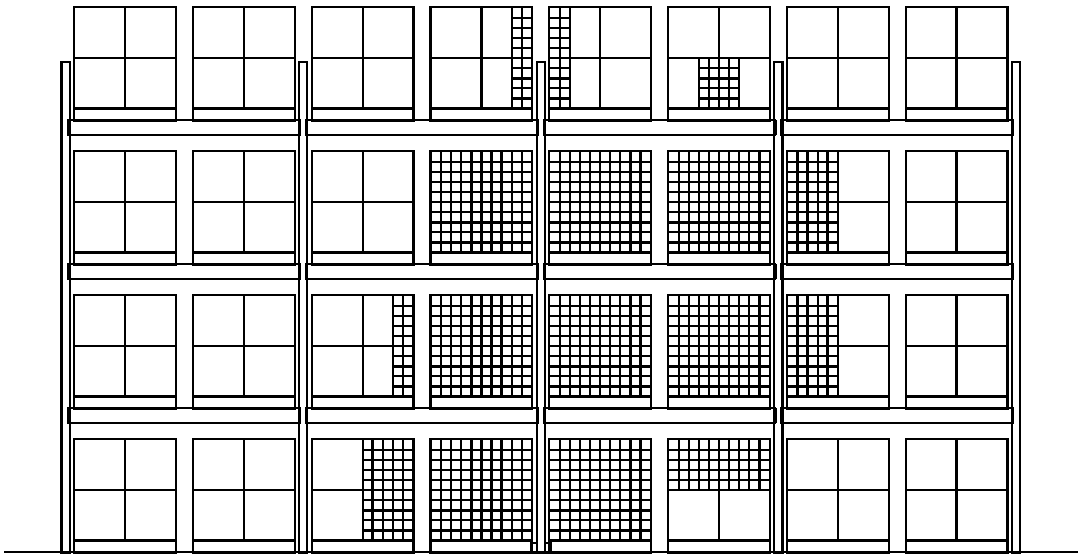

View of Main Array from the North

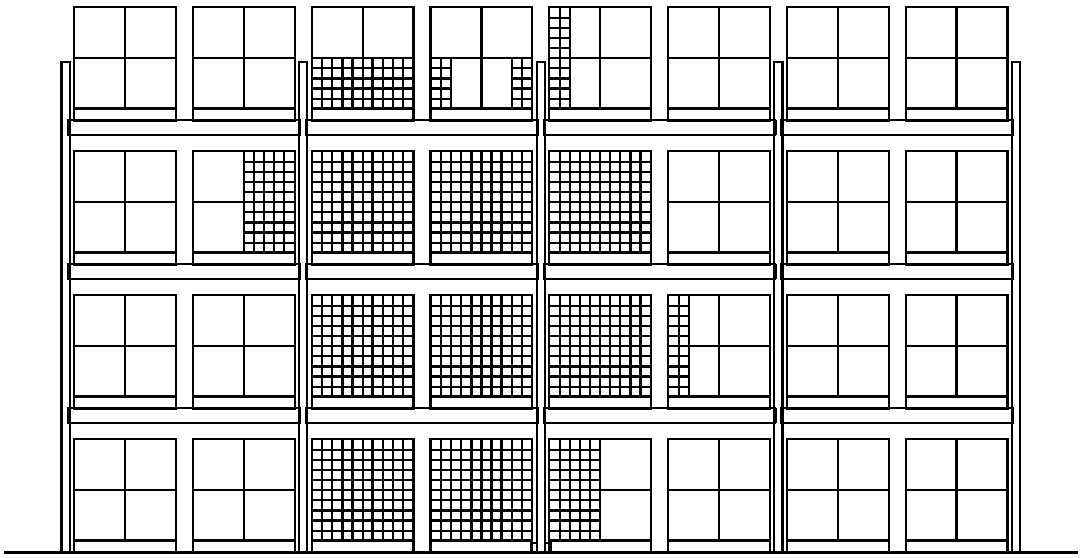

Figure 25: Fire damage from Plastic Test P-1.

5.2.2 Test P-2

Test P-2 was intended to present an extreme situation as far as venting is concerned. The ignition point was put directly under a vent. The objective was to see how vent activation soon after ignition could affect sprinkler response. In the experiment, flames reached the top of the central array at about 65 s and the vent cavity at about 70 s. The first sprinkler activated at 100 s, followed 8 s later by the sprinkler on the opposite side of the vent. The vent above the ignition point did not open at any time during the 30 min test. However, the vent 6 m (20 ft) to the west of the ignition point did open at 6:04. Unlike Test P-1, in Test P-2 all 23 sprinkler activations occurred within 6 min of ignition.

By about 10 min after ignition the smoke layer throughout the test facility was at the height of the third tier. Up to this point in time, there was no observable difference in the amount of smoke in the north and south aisles. The fire damage in Test P-2 was similar to that of Test P-1, with more damage observed in the fourth tier (Fig. 28).

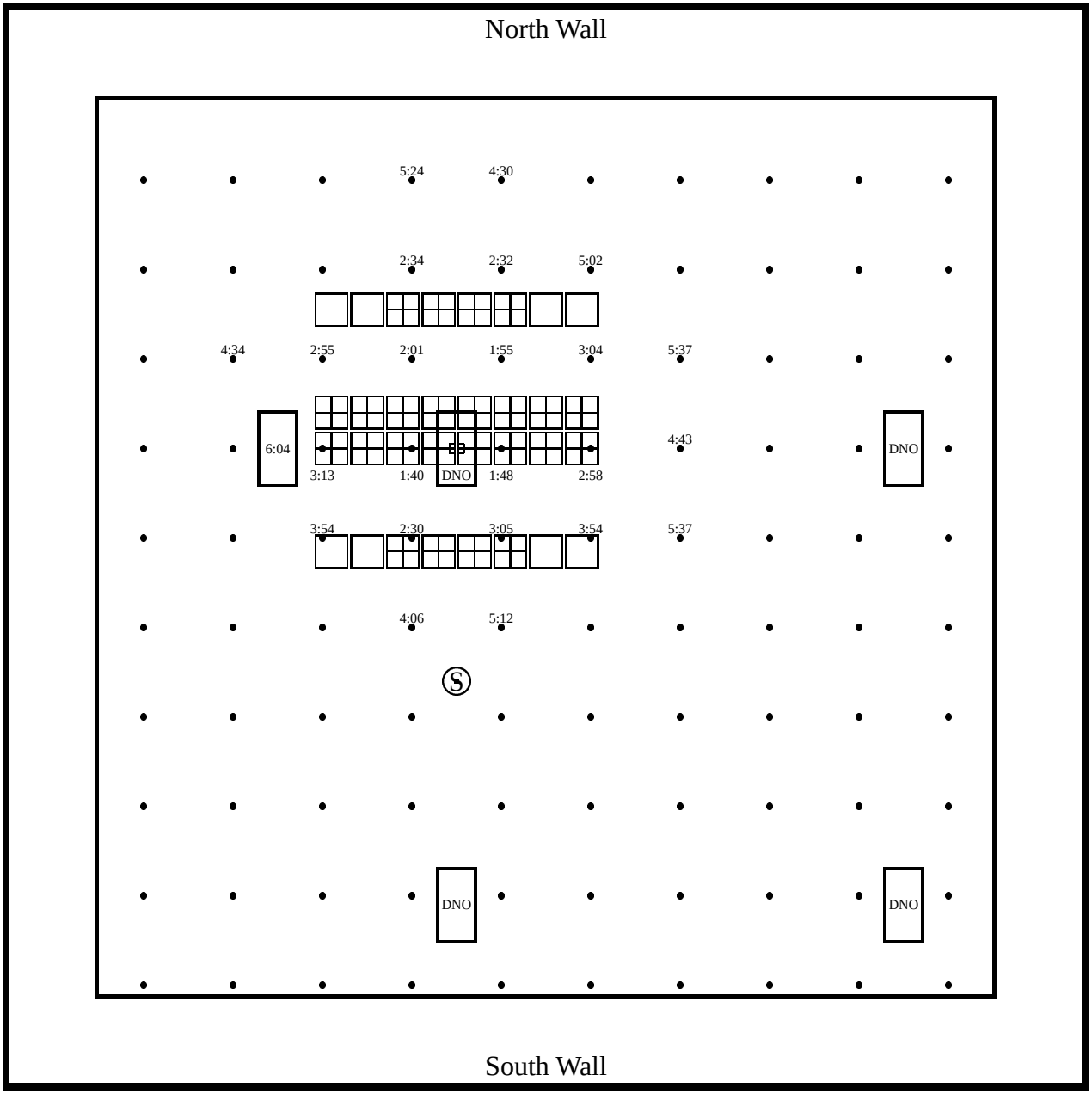

Figure 26: Plan view of Large Scale Fire Test Facility with the sprinkler activation times for Plastic Test P-2.

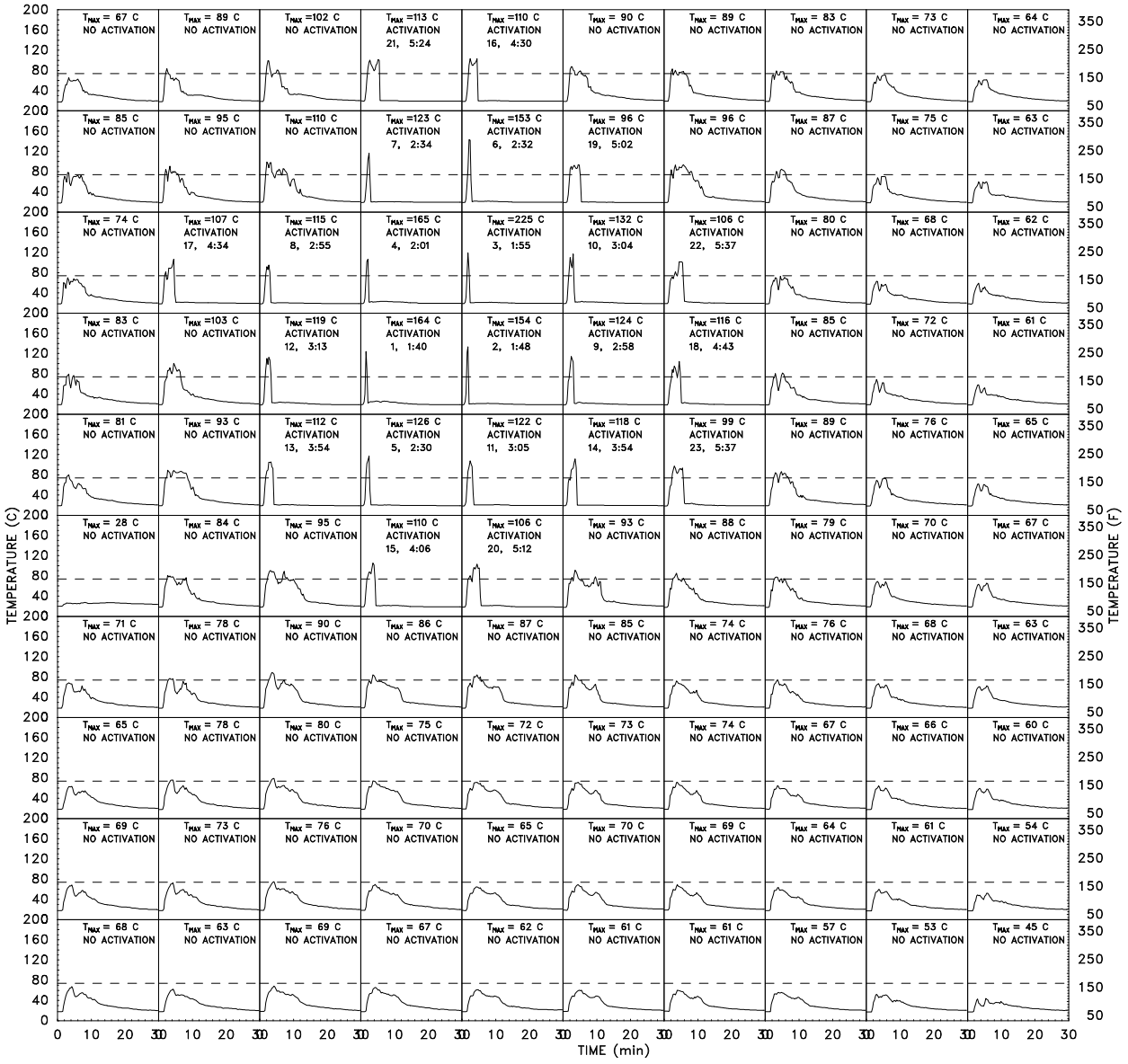

Figure 27: Temperature profiles from all 100 near-sprinkler thermocouples from Plastic Test P-2. The arrangement of the plots mimics that of Fig. 26.

View of Main Array from the South

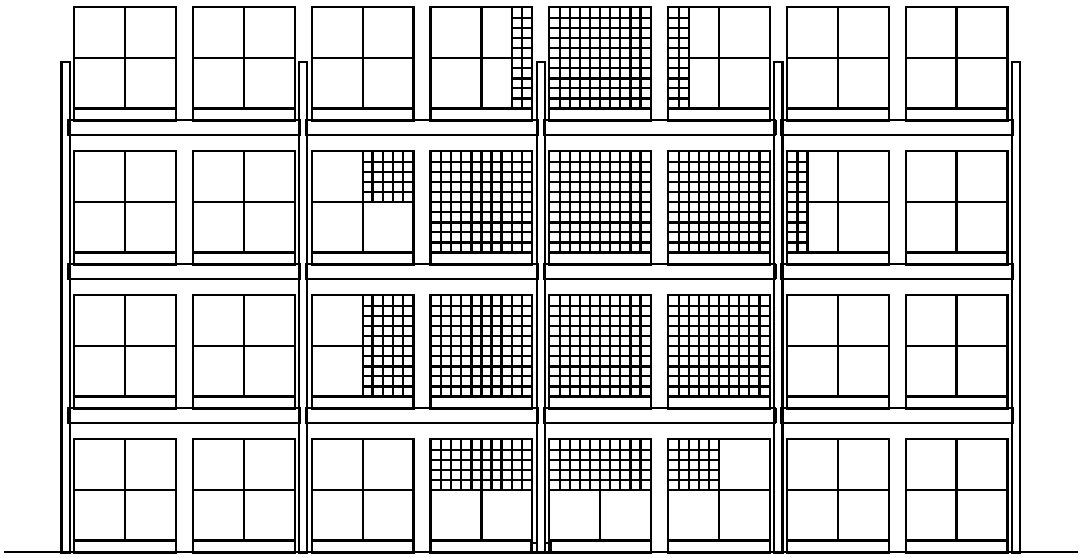

View of Main Array from the North

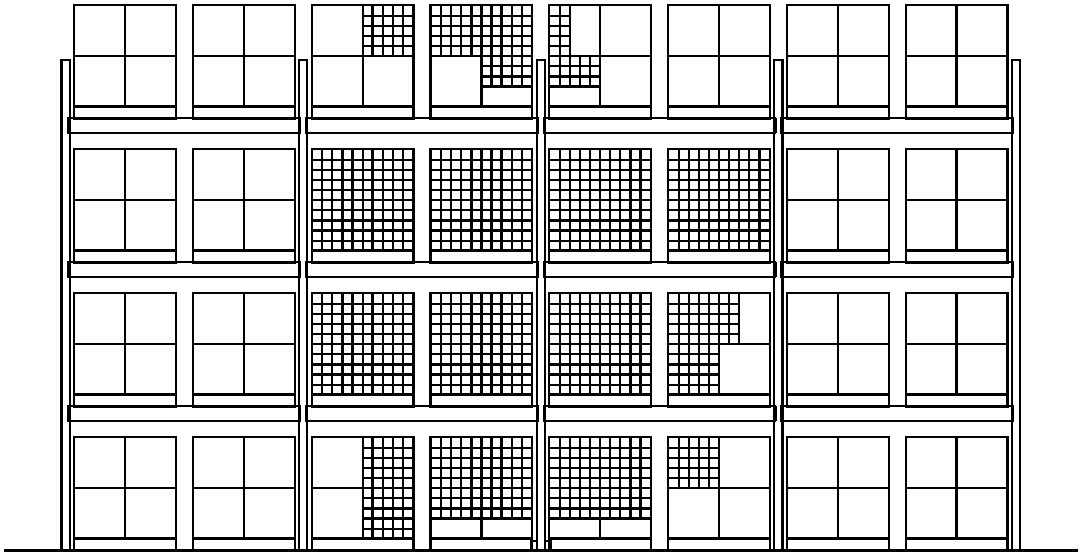

Figure 28: Fire damage from Plastic Test P-2.

5.2.3 Test P-3

Test P-3 was designed to be similar to a test performed during the high rack storage cartoned plastics series at Factory Mutual where the fire was ignited near the intersection of two draft curtains [21]. However, the test performed at Factory Mutual involved slatted wood shelving, a slightly different rack configuration, and different sprinkler spacing and flow rate.

The first sprinkler activation occurred after 67 s at the position closest to the curtain intersection, followed closely by the second at 72 s. The draft curtains channeled the smoke and hot gases towards the east and south, opening more sprinklers in these rows than would be expected if the curtains were not there. The vent did automatically activate at 4:11, but by that time the two sprinklers on each side of it had already activated.

The draft curtains did delay by 3 to 4 min the activation of the sprinklers to the north of the first two that activated, and blocked the water from wetting the north face of the center array. The fire was able to spread both to the north and to the west underneath the draft curtains, but activations within the adjacent quadrants were able to control the spread. The sprinkler activations went to the north edge of the adjustable height ceiling.

By about 10 min after ignition the smoke layer throughout the test facility was at the height of the third tier. Up to this point in time the north aisle remained relatively clear of smoke, the south aisle filled with smoke within the first 5 min. The fire damage from this fire was more extensive than that of Tests P-1 and P-2, going beyond the central two bays in tiers 2, 3 and 4 (Fig. 31).

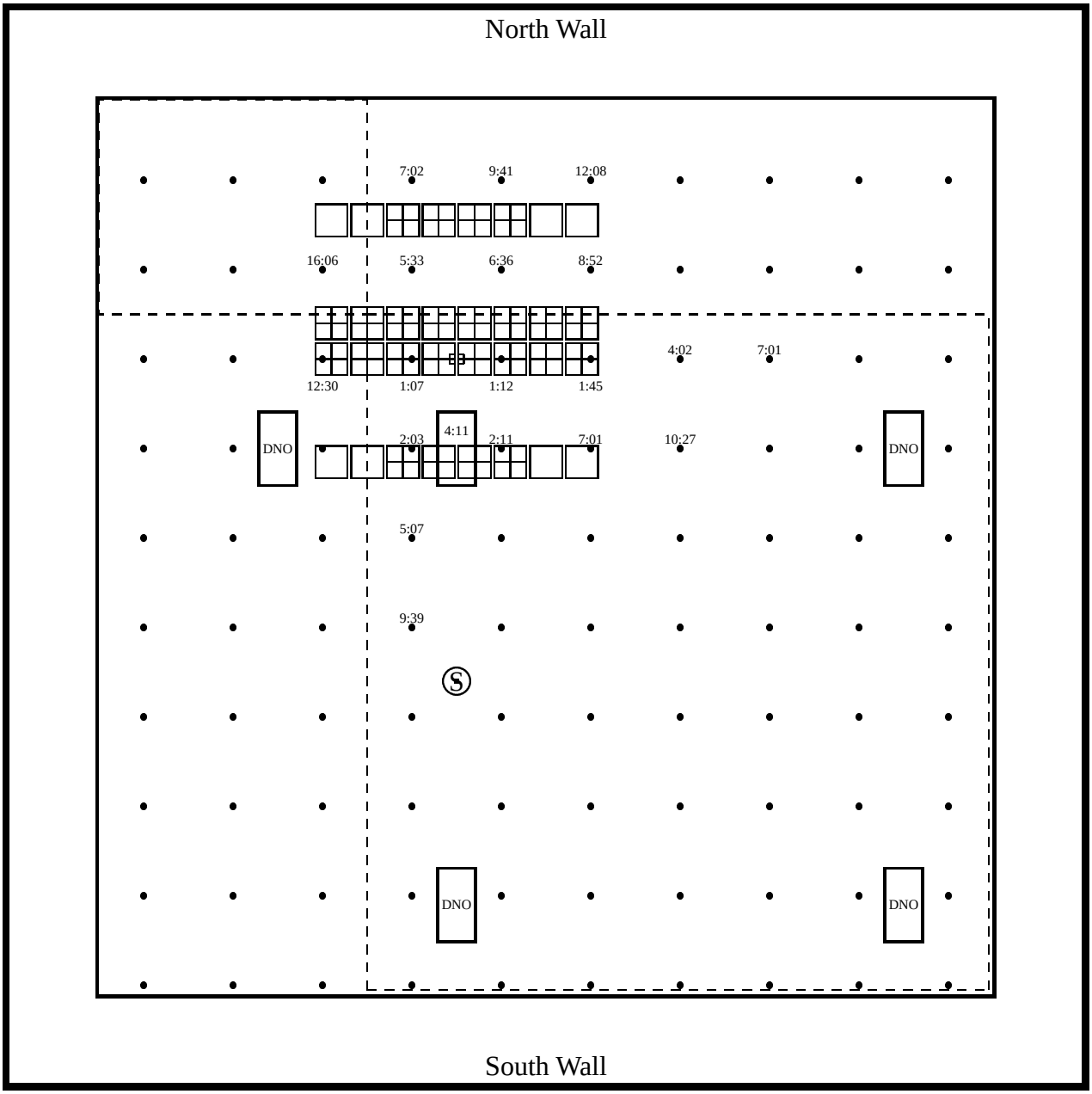

Figure 29: Plan view of Large Scale Fire Test Facility with the sprinkler activation times for Plastic Test P-3.

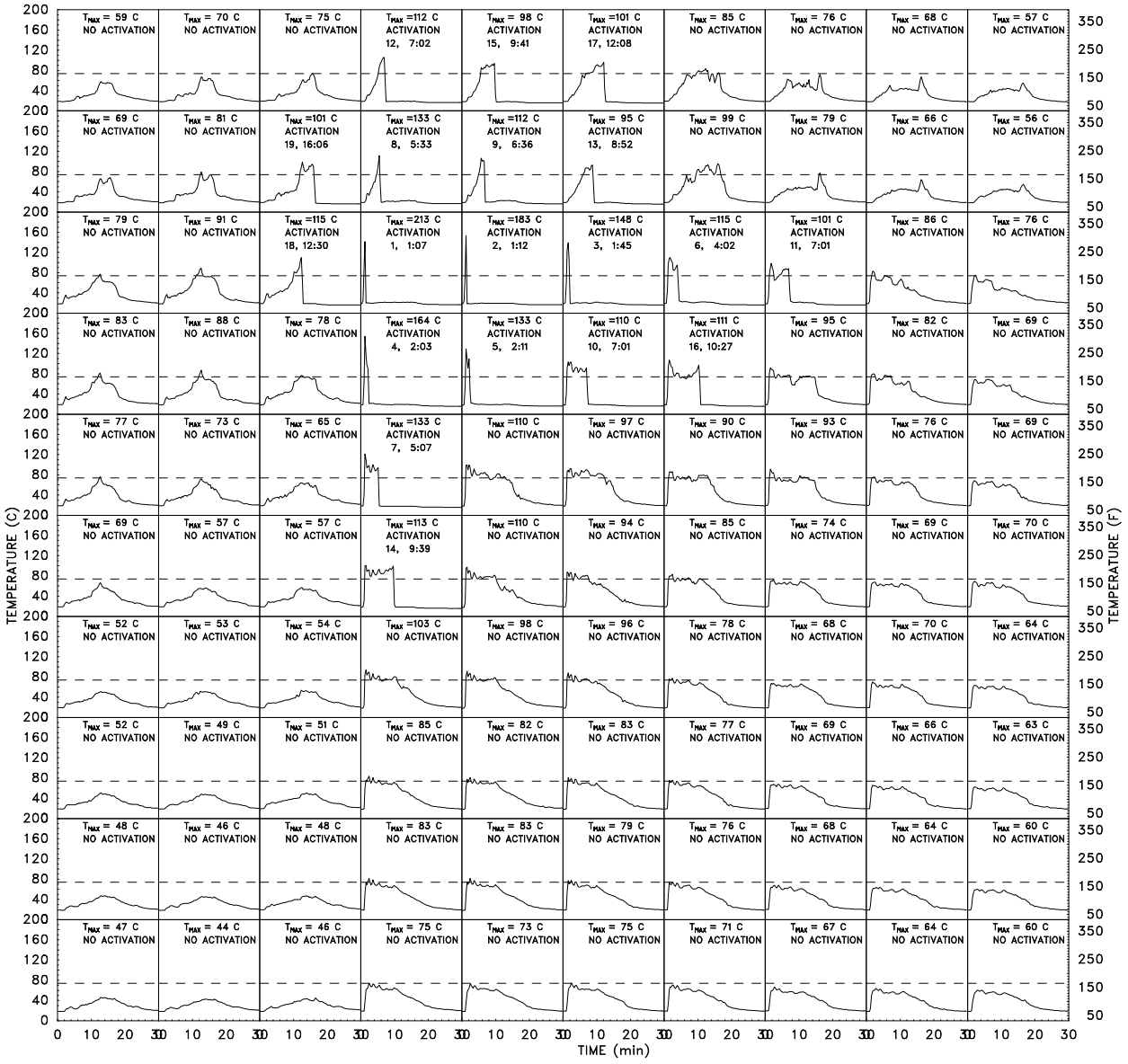

Figure 30: Temperature profiles from all 100 near-sprinkler thermocouples from Plastic Test P-3. The arrangement of the plots mimics that of Fig. 29.

View of Main Array from the South

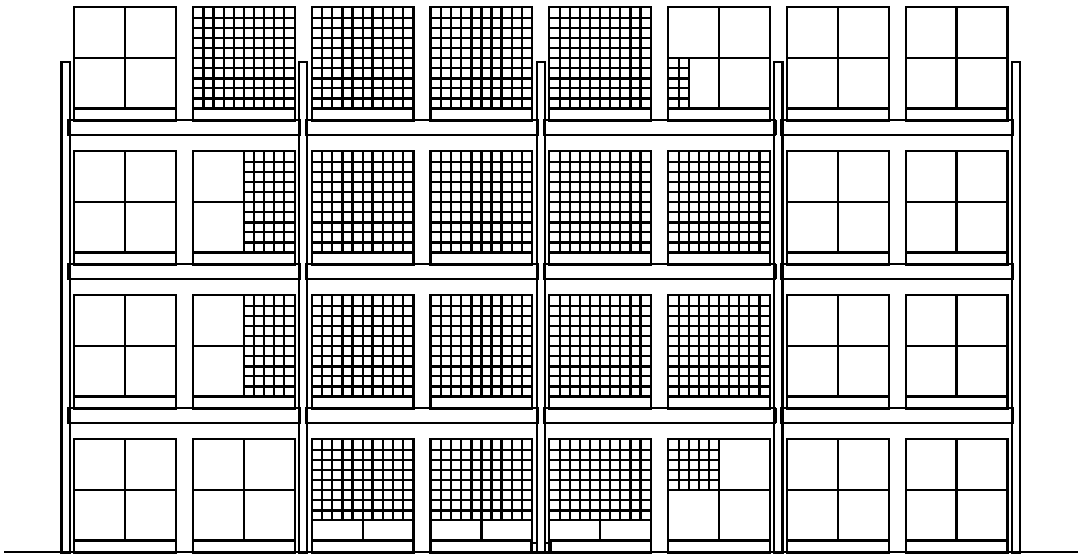

View of Main Array from the North

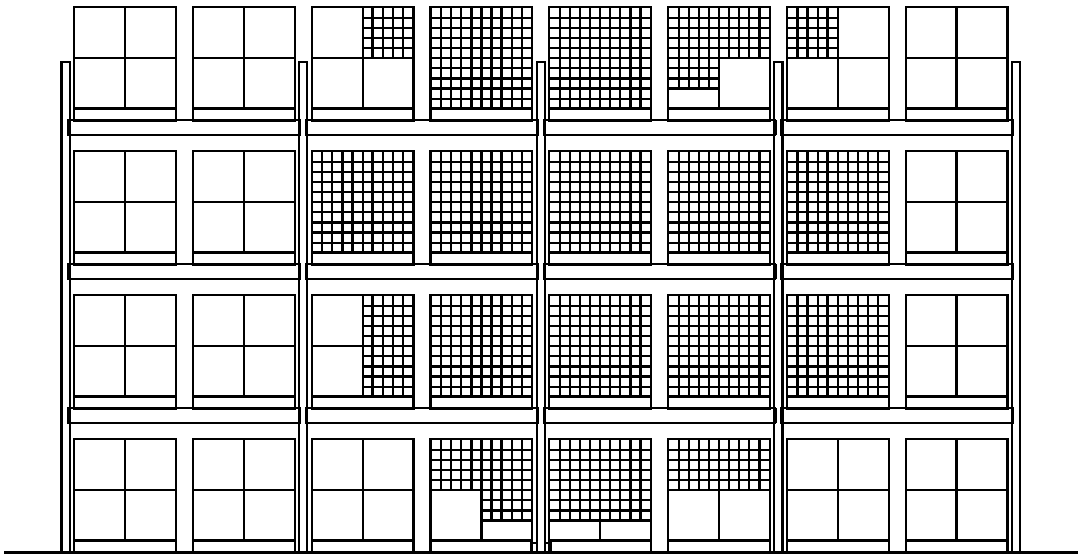

Figure 31: Fire damage from Plastic Test P-3.

5.2.4 Test P-4

Test P-4 was intended to be a replicate of Test P-1 with the only exception being the presence of the draft curtains. As in all the tests prior to this one, the flames emerged from the top tier after about 60 s. The first sprinkler opened after 93 s followed 1 s later by the second. This activation time was about 10 to 15 s longer than in previous tests under a flat ceiling, but it appeared to those observing the test that the quick succession of activations contained the fire to a volume roughly two pallet loads wide, three pallets high, and one pallet deep. The temperatures at all of the unactivated sprinklers decreased relatively quickly following the initial activations. There was no build-up of the fire following the first activation that was observed in Test P-1.

The smoke layer descended to the height of the third tier after about 15 min. Up to this point in time the south aisle was more heavily smoke logged than the north. The fire damage from this test was less extensive than that from the first three tests (Fig. 34).

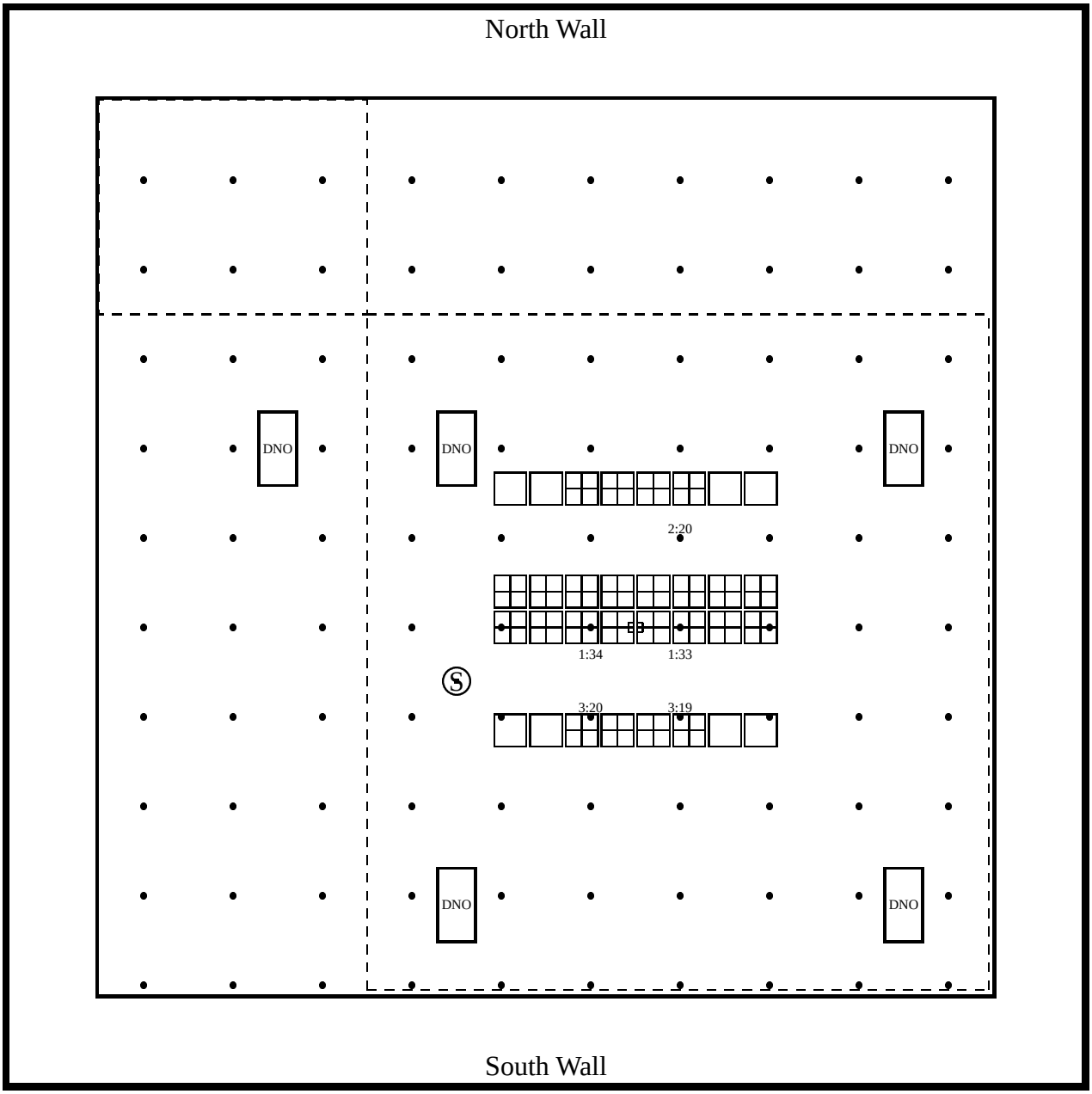

Figure 32: Plan view of Large Scale Fire Test Facility with the sprinkler activation times for Plastic Test P-4.

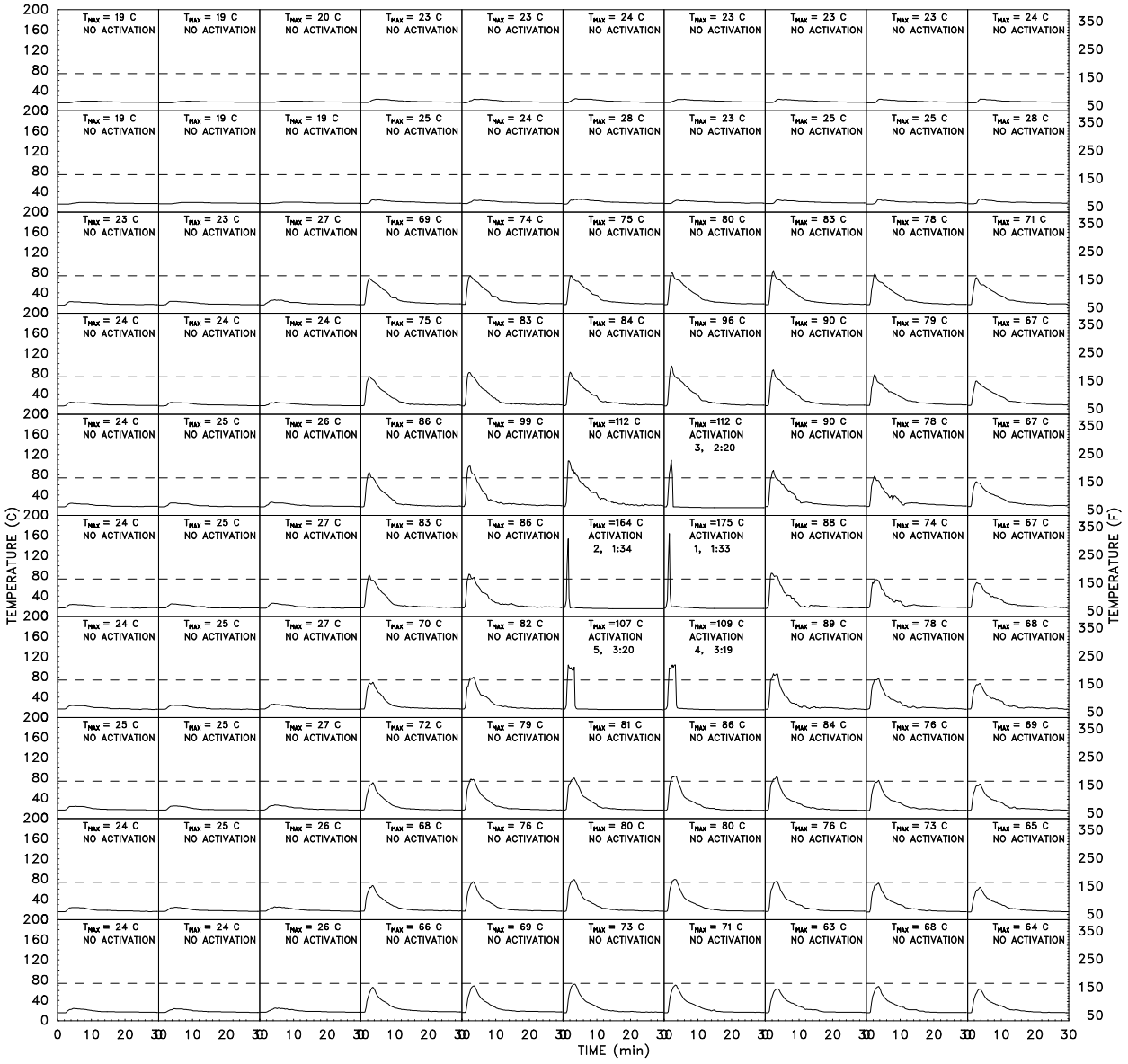

Figure 33: Temperature profiles from all 100 near-sprinkler thermocouples from Plastic Test P-4. The arrangement of the plots mimics that of Fig. 32.

View of Main Array from the South

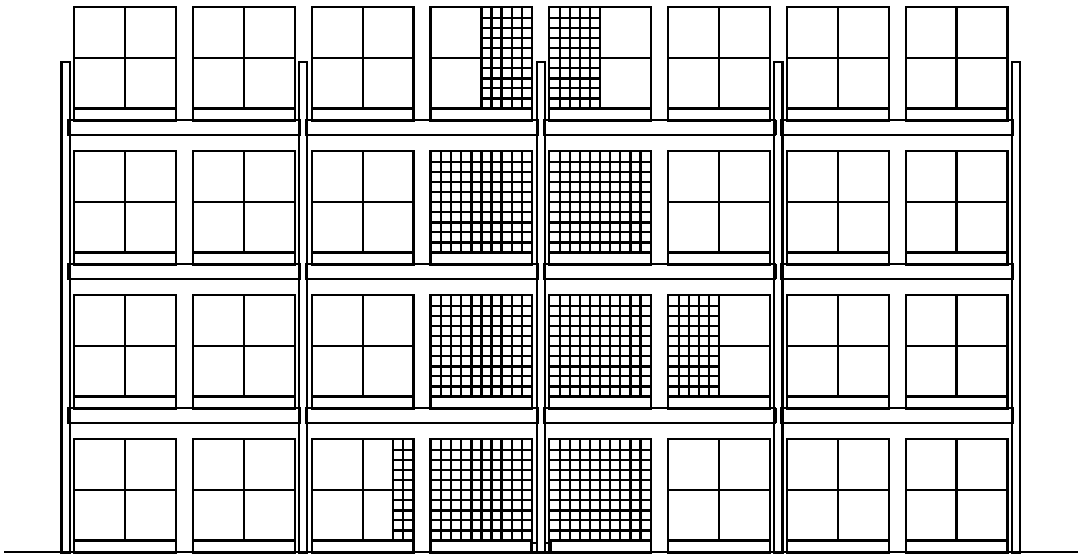

View of Main Array from the North

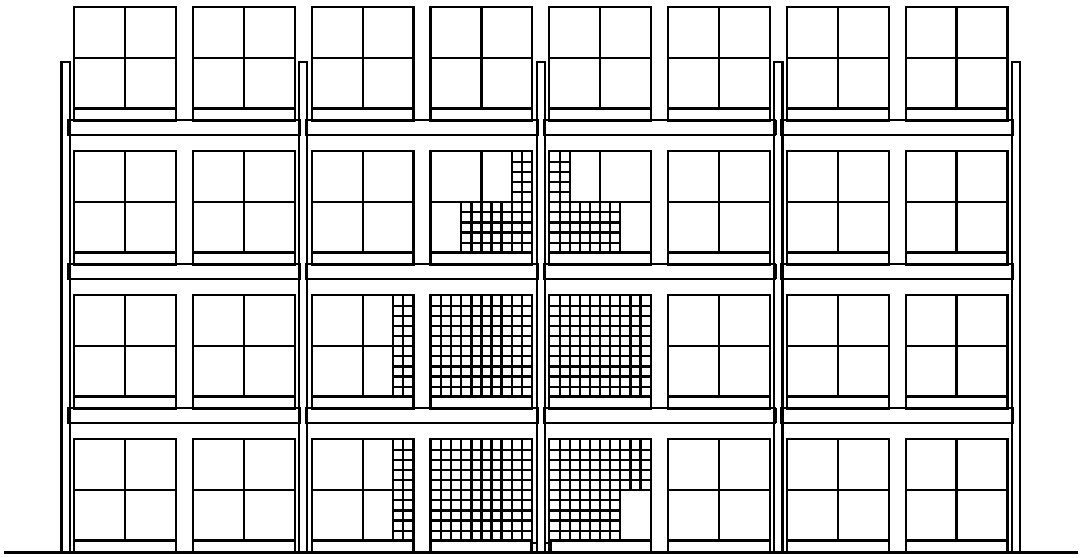

Figure 34: Fire damage from Plastic Test P-4.

5.2.5 Test P-5

Given the difference in sprinkler activity between Test P-1 (20 activations) and Test P-4 (5 activations), it was decided to repeat Test P-4, only now the vents were to be manually opened following the first sprinkler activation. It had become clear by this time in the project that the vents were unlikely to open when the fire was ignited more than about 4.6 m (15 ft) away.

The results of Test P-5 were similar to those of Test P-4. Again, the first two sprinklers opened within 1 s of each other, but about 20 s sooner than those in Test P-4. No change in test conditions could explain why the sprinklers activated sooner, thus it was attributed to the variability in the initial rate of heat release. Seven sprinklers opened in all, compared with 5 in Test P-4. The fire damage was slightly less extensive in this test than in Test P-4, possibly due to the earlier sprinkler activation.

The smoke layer descended to the height of the third tier after about 15 min. Up to this point in time the north aisle was more heavily smoke logged than the south. The fire damage from this test was similar to that of Test P-4.

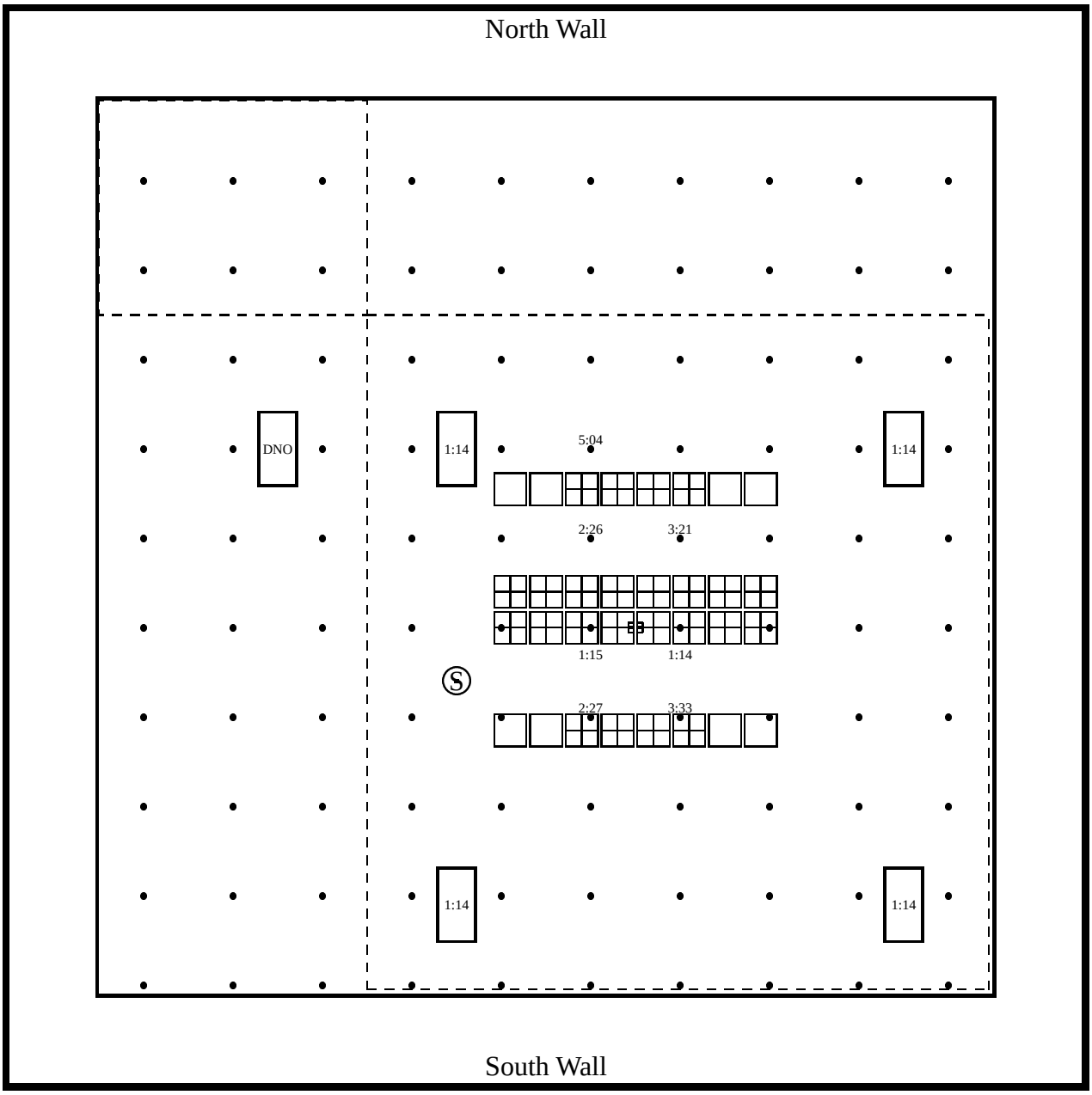

Figure 35: Plan view of Large Scale Fire Test Facility with the sprinkler activation times for Plastic Test P-5. The vents in the curtained area were opened manually following the first sprinkler activation.

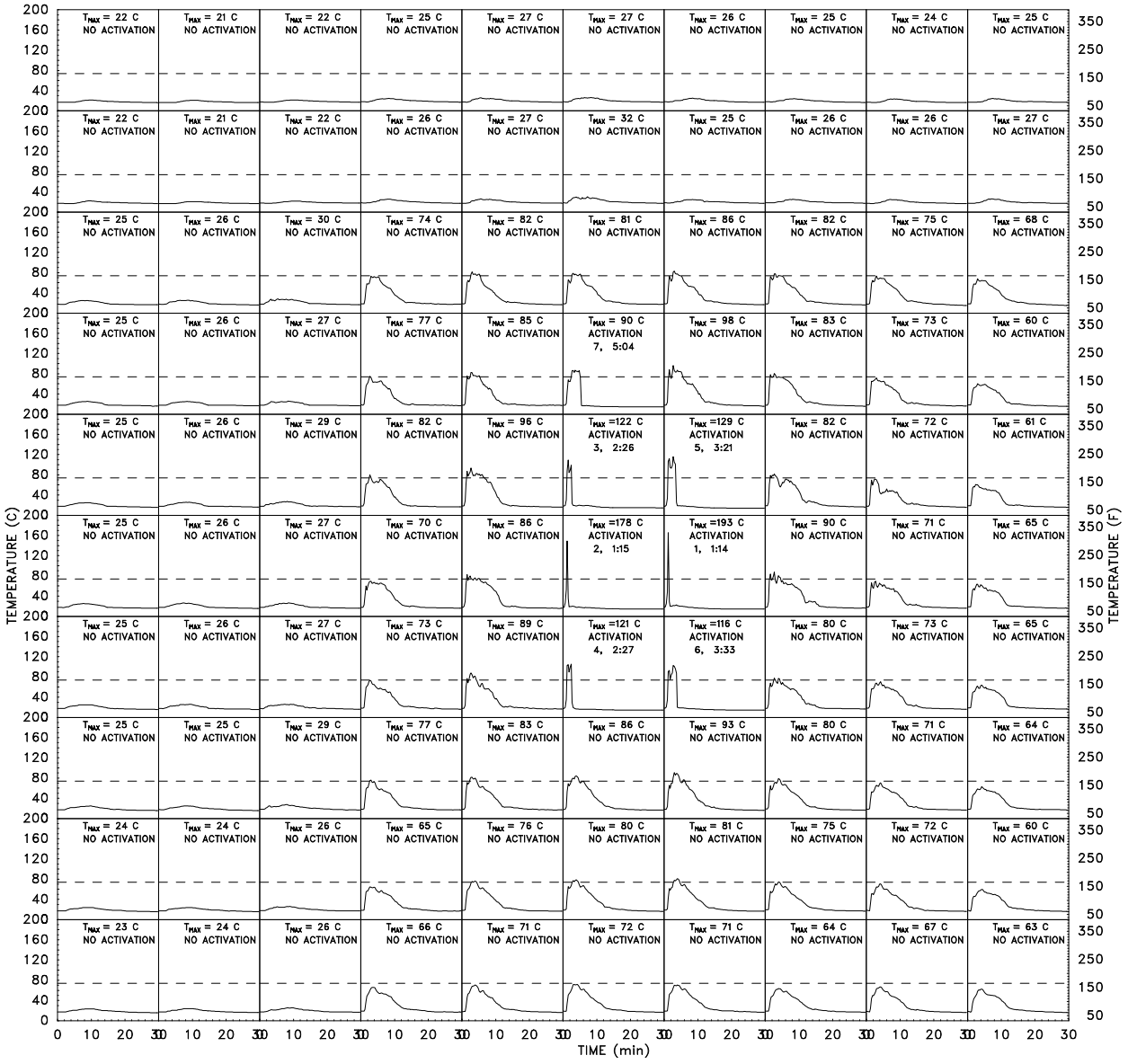

Figure 36: Temperature profiles from all 100 near-sprinkler thermocouples from Plastic Test P-5. The arrangement of the plots mimics that of Fig. 35.

View of Main Array from the South

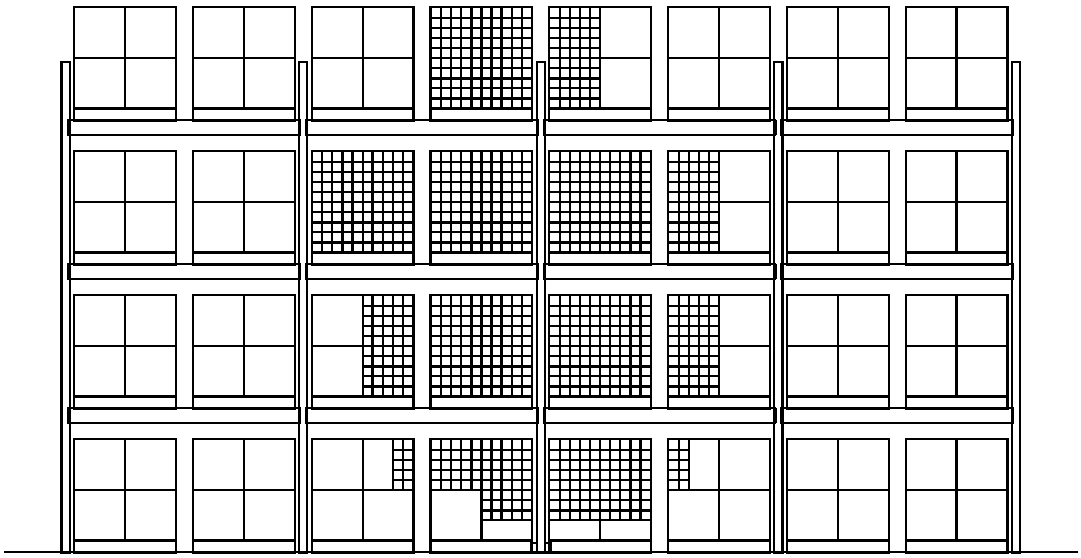

View of Main Array from the North

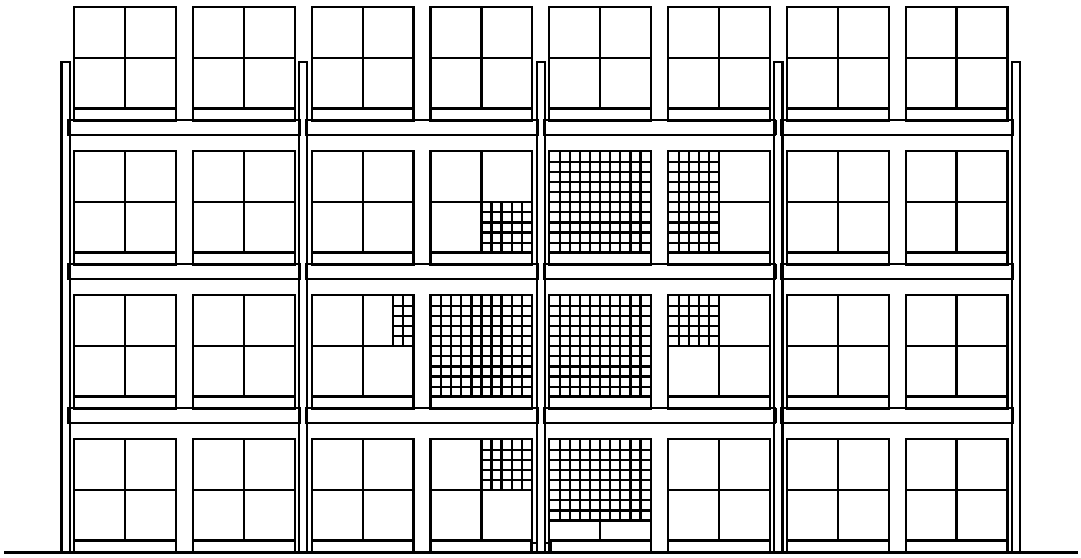

Figure 37: Fire damage from Plastic Test P-5.

5.2.6 Obscuration

Three optical sensors consisting of a white light source separated from a photocell by 1 m were positioned 1 m above the adjustable ceiling, 1.8 m (6 ft) below the ceiling and 1.5 m (5 ft) above the floor at the location indicated in the plan views of each test. The smoke eyes were not moved from test to test, even though the racks were. Figure 38 presents the data from all five tests. Because during every test, the exhaust fan above the plenum space was drawing smoke from the test space at a constant rate of 28 m^3/s (60,000 ft^3/min), the optical density data (averaged over time to eliminate local smoke logging effects) can be used as an indirect indicator of the relative size of the fire. Tests P-1, P-2 and P-3 were bigger fires than Tests P-4 and P-5 as indicated by the increased obscuration of the test facility and the amount of commodity consumed. Unfortunately, what the optical density data does not reveal is the effect of opening the smoke and heat vents because there is no way to separately account for the smoke flowing through the vents and the smoke flowing around the adjustable ceiling and up through the 3 m (10 ft) wide gap between the ceiling and the wall of the facility. In effect, all the tests were vented at the perimeter.

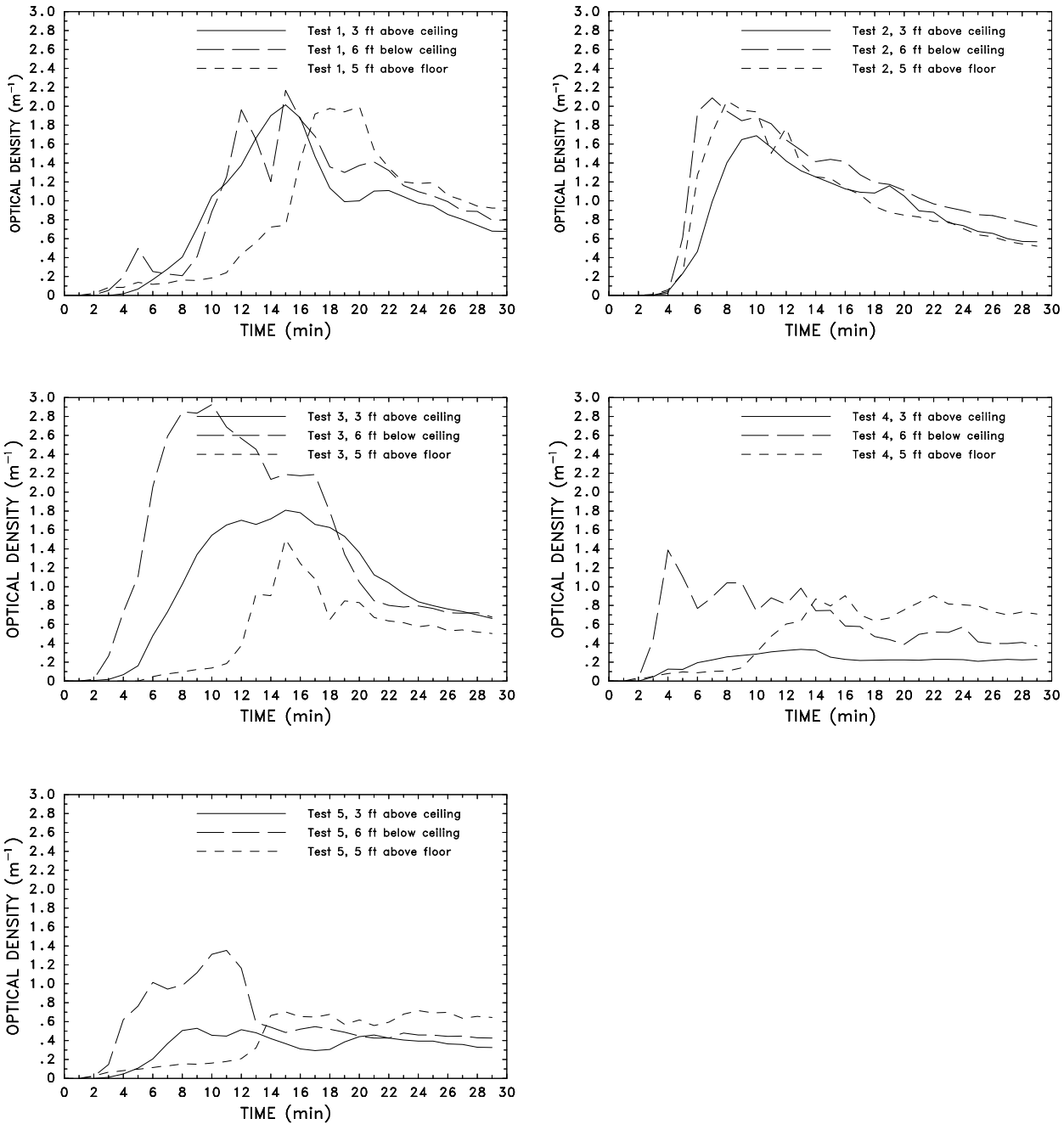

Figure 38: Local optical density measurements for the Plastic tests, averaged over a minute.

6 Discussion of Experimental Results

As in studies preceding this one, a series of large scale tests was used to gather information about the interaction of sprinklers, vents and draft curtains. In this study, engineering analysis using fire modeling techniques will provide additional insight into the behavior of these systems. To emphasize the contrast provided, it is instructive to pause here and discuss what can be determined from the large scale tests alone. Later, additional information from fire modeling will help bolster the confidence in these conclusions and provide additional insight.

Thus far the results of 39 full-scale fire experiments have been presented. In this section, these results will be discussed with an emphasis on how roof vents and draft curtains affect the time, number and location of sprinkler activations; and how sprinklers and draft curtains affect the time, number and discharge rates of roof vents. To facilitate the discussion, a summary of the 39 large scale experiments is presented in Table 4.

6.1 Effect of Vents and Draft Curtains on Sprinkler Activation Times

For all three series of tests, when the fire was not ignited directly underneath a vent, the activation times of the nearest sprinklers to the fire were not affected by the opening of vents either prior to or after the first sprinkler activation. When the fire was ignited 3 m (10 ft) from the vent center, the only discernible affect of the vent opening on sprinkler activation was for those sprinklers immediately downstream of the vent. For example, consider the sprinkler activation times for Tests I-4, I-5, I-6 and I-7 (Fig. 6). The two sprinklers to the west of the vent did not activate in Tests I-5 and I-6 when the vent was manually operated at 40 and 90 s. However, in Test I-7 when the vent did not open, both sprinklers activated, and in Test I-4 when the vent was held closed, one of the two sprinklers activated. Consider the peak gas temperatures near the two sprinklers in Tests I-4 and I-7 compared with those in Tests I-5 and I-6 (Figs. 88-91). Compared to the unopened tests, the temperatures were 25°C (45°F) lower when the vent was opened at 40 s, and 5°C (9°F) lower when the vent was opened at 90 s. When examining the temperatures and activation times for Tests I-1, I-2, I-3 and I-8 where the fire was in the B position (3 m (10 ft) to the north of the vent), the effect of opening the vent is not as clear because the shorter dimension of the vent is facing the fire.

In tests where the fire was ignited directly beneath a vent, vent openings prior to the activation of the nearest sprinklers had an effect on the sprinkler activation times. The earlier the vent opening, the more noticeable the effect. For example, in Tests I-12, I-13, I-14 and I-15 where the fire was positioned directly under the vent and the draft curtains were installed, the average sprinkler activation time of the nearest four sprinklers was 1:13 when the vent was held closed (Test I-12), 1:29 when the vent opened automatically at 1:04 (Test I-13), 1:58 when the vent was opened manually at 0:40 (Test I-14), and 1:08 when the vent was opened manually at 1:30 (Test I-15). This data suggests that the earlier the vent activation, the longer the delay in activation of the first ring of sprinklers.

Test I-16 was performed with a different fire growth curve, and cannot be directly compared with any other test. In that test, the first sprinkler activated at the same time that the vent opened (1:46), followed by the next two sprinklers at 2:06 and 2:08. One of the four sprinklers nearest the fire did not activate at all. The temperature near this sprinkler was 140°C (284°F) at the time of the vent opening, but it decreased to about 80°C (176°F) over the next few minutes. A similar effect

Summary of Sprinkler, Smoke&Heat Vent, Draft Curtain Project Experiments											
Test No.	Fire Location		Fire Size	Draft Curtains	Vent Operation	Sprinklers			Avg. Peak Temp.		# Boxes Consumed
	Pos.	Rel. to Vent	MW @ s			First	Last	Tot.	°C	°F	
I-12	A	0	4.4 @ 50	Yes	Closed	1:08	7:24	14	111.0	231.8	
I-13	A	0	6.0 @ 60	Yes	74°C link (1:04)	1:09	2:53	5	96.2	205.2	
I-14	A	0	5.8 @ 60	Yes	Manual (0:40)	1:14	7:48	7	95.2	203.4	
I-15	A	0	5.8 @ 60	Yes	Manual (1:30)	1:04	2:08	5	113.8	236.9	
I-16	A	0	5.0 @ 110	Yes	74°C link (1:46)	1:46	2:16	4	87.7	189.9	
I-19	A	0	4.6 @ 50	No	100°C link (10:00)	0:56	9:43	10	84.4	183.8	
I-20	A	0	4.2 @ 50	No	74°C link (1:20)	0:54	3:16	4	75.8	168.5	
II-3	A	0	10 @ 75	Yes	74°C link (1:15)	1:08	4:00	12	101.8	215.2	
II-7	A	0	10 @ 75	Yes	Closed	1:09	4:11	18	117.2	243.0	
P-2	A	0	Plastic	No	74°C link (DNO)	1:40	5:37	23	85.8	185.9	127
I-1	B	10′N	4.4 @ 50	Yes	Closed	1:05	3:29	11	110.9	231.6	
I-8	B	10′N	4.4 @ 50	Yes	74°C link (9:26)	1:00	6:01	11	99.7	211.4	
I-2	B	10′N	4.4 @ 50	Yes	Manual (0:40)	1:06	4:08	12	105.9	222.7	
I-3	B	10′N	4.4 @ 50	Yes	Manual (1:30)	1:04	6:02	12	109.2	228.5	
I-17	B	10′N	4.6 @ 50	No	100°C link (DNO)	0:58	1:20	4	81.2	178.1	
II-4	B	10′N	10 @ 75	Yes	74°C link (1:48)	1:03	5:54	16	108.8	227.8	
II-8	B	10′N	10 @ 75	Yes	74°C link (1:12)	1:10	3:34	13	107.7	225.9	
P-3	B	10′N	Plastic	Yes	74°C link (4:11)	1:07	16:06	19	90.5	194.9	184
I-4	C	10′E	4.4 @ 50	Yes	Closed	1:00	3:44	10	109.6	229.3	
I-7	C	10′E	4.4 @ 50	Yes	74°C link (DNO)	1:10	3:52	10	107.3	225.1	
I-5	C	10′E	4.4 @ 50	Yes	Manual (0:40)	1:12	6:47	9	98.9	210.0	
I-6	C	10′E	4.4 @ 50	Yes	Manual (1:30)	1:02	2:50	8	105.2	221.4	
I-18	C	10′E	3.7 @ 50	No	100°C link (DNO)	0:58	1:18	4	70.9	159.7	
I-21	C	10′E	4.6 @ 50	No	74°C link (7:00)	0:58	4:06	10	85.6	186.1	
II-11	C	10′E, 10′S	10 @ 75	Yes	74°C link (DNO)	1:02	3:56	23	123.4	254.1	
II-12	C	10′E, 10′S	10 @ 75	Yes	Manual (0:00)	0:58	4:55	23	119.0	246.2	
I-9	D	20′W, 20′S	4.4 @ 50	Yes	74°C link (DNO)	1:10	11:15	12	108.7	227.7	
I-10	D	20′W, 20′S	4.4 @ 50	Yes	Manual (0:40)	1:12	6:52	13	107.5	225.5	
I-11	D	20′W, 20′S	4.4 @ 50	Yes	74°C link (4:48)	N/A	N/A	N/A	184.9	364.9	
I-22	D	20′W, 20′S	4.6 @ 50	No	100°C link (DNO)	1:00	4:25	6	88.7	191.7	
II-1	D	20′E, 20′S	10 @ 75	Yes	74°C link (DNO)	1:15	6:13	27	129.4	264.9	
II-5	D	20′E, 20′S	10 @ 75	Yes	74°C link (DNO)	1:10	7:07	28	130.0	266.0	
II-2	D	20′E, 20′S	10 @ 75	Yes	Manual (0:00)	1:05	5:53	28	128.8	263.8	
II-6	D	20′E, 20′S	10 @ 75	Yes	Manual (0:00)	1:10	5:21	27	127.5	261.5	
P-1	D	20′E, 20′S	Plastic	No	74°C link (DNO)	1:16	13:41	20	93.8	200.8	117
P-4	D	20′E, 20′S	Plastic	Yes	74°C link (DNO)	1:33	2:40	5	82.6	180.7	103
P-5	D	20′E, 20′S	Plastic	Yes	Manual (1:14)	1:14	5:04	7	83.3	181.9	81
II-9	E	10′W, 15′S	10 @ 75	Yes	74°C link (DNO)	1:07	3:28	23	115.8	240.4	
II-10	F	10′W, 15′N	10 @ 75	Yes	74°C link (3:20)	1:14	3:01	19	108.4	227.1	

Table 4: Summary of the 39 Large Scale Experiments. Note that DNO means "Did Not Open". Test No. I-n refers to the first series of heptane spray burner tests, II-n the second series, and P-n the Plastic tests. The "Avg. Peak Temp." refers to the average of the maximum temperatures recorded at all the near-sprinkler thermocouples in the test area.

was seen in Test I-20 (Fig. 8). Following a vent opening at 1:20, one of the four sprinklers nearest the fire did not open until 3:16. The first sprinkler activation was at 0:54.

During the second series of heptane spray burner tests, two tests were performed with the burner directly under a vent (Fig. 14). In Test II-7, where the vent was held closed, the average activation times of the nearest two sprinklers was 1:14 and the nearest six 1:24. In Test II-3, where the vent opened automatically at 1:15, the average of the nearest two sprinklers was 1:17 and the nearest six 1:32.

Draft curtains also had an effect on sprinkler activation times. Given two sprinklers equidistant from a fire, the one nearer to a curtain showed a tendency to activate sooner. For example, in tests where the fire was placed at Position B in the first series of heptane tests, activation at sprinkler 52 (1 m from east curtain, 6 m from north curtain) occurred about 20 s on average before activation at sprinkler 64 (10 m from east curtain, 6 m from north curtain). The Position B experiments with curtains (Tests I-1, I-2, I-3, I-8) also showed activation at sprinkler 90 in Tests I-2 and I-3. This sprinkler was over 7.6 m (25 ft) from the burner, the farthest distance of any activation in the test series. Based on an examination of thermocouple data, activation at this sprinkler was believed to be due to the channeling of the smoke and hot gases by the north draft curtain.

6.2 Effect of Vents and Draft Curtains on Number of Sprinkler Activations

In general, draft curtains increased the number of sprinkler activations. Inspection of Table 4 indicates that in Tests I-1 and I-8 there were 11 activations when the draft curtains were installed and the vent was closed, and in Test I-17 there were 4 activations when the curtains were not installed and the vent was closed. Tests I-4 and I-7 both had 10 activations with the curtains installed and the vent closed, Tests I-18 and I-21 had 4 and 10 activations with the curtains removed. Tests I-9 and I-10 had 12 and 13 activations with curtains installed, Test I-22 had 6 activations with the curtains removed. This data indicates that in tests performed with draft curtains where the fire was not directly beneath a vent, there were up to twice as many sprinkler activations compared to tests performed without draft curtains.

The reason for the increased number of activations is that draft curtains lead to an increase of the near-ceiling gas temperatures. Consider, for example, the peak gas temperatures near the second ring sprinklers in Test I-1 (Fig. 85) compared to those of Test I-17 (Fig. 101). The temperatures were between 20°C and 30°C (36°F and 54°F) lower in Test I-17. Similar differences can be seen when comparing temperatures in Tests I-1 through I-16 with those in Tests I-17 through I-22. The difference between temperatures in the curtained and uncurtained tests can be explained by considering a fire plume impinging on a well-developed, 1.8 m (6 ft) deep smoke layer as opposed to a thinner layer. In the latter case, the plume can entrain more cool air before it reaches the ceiling layer, and therefore the smoke is cooler by the time it reaches the ceiling. Plus, the deeper smoke layer formed by the draft curtains insulates the sprinklers from cooler air below the layer, leading to more activations.

What effect did the vents have on the number of activations? When the fire was ignited directly under a vent (Position A), the number of activations was reduced. Consider Test I-12 versus Tests I-13, I-14, I-15 and I-16. The number of activations was roughly halved due to the opening of the vent directly above the fire. Tests II-3 and II-7 show the number of activations reduced from 18 to 12. However, when the fire was not ignited under a vent, there was either a small decrease or no decrease at all in the number of sprinkler activations. Tests I-1 and I-8 compared with Tests

I-2 and I-3 showed no reduction in the number of activations when the fire was ignited 3 m (10 ft) north of the vent. Tests I-4 and I-7 compared to Tests I-5 and I-6 showed a reduction of 1 and 2 sprinklers from 10. Tests II-11 and II-12 showed no reduction at all. Tests I-9 and I-10, as well as Tests II-1, II-5, II-2 and II-6 showed no reduction either. Thus, unless the ignition took place under or very near a vent, there was no evidence in this data set that venting reduced the number of sprinkler activations.

To see why vents had little effect on the number of sprinkler activations, consider the average peak temperatures in the curtained area in Tests II-1, II-2, II-5, II-6, II-11 and II-12. In Tests II-1 and II-5 where the fire was located at Position D and no vents operated, the average peak temperatures were 129.4°C and 130.0°C, respectively. In Tests II-2 and II-6 where the fires were at Position D but all the vents were opened at the start of the tests, the average peak temperatures were 128.8°C and 127.5°C, respectively. Similarly, in Test II-11 where the fire was at Position C and the vent did not operate, the average peak temperature was 123.4°C, whereas in Test II-12, where all the vents were opened at the start, the temperature was 119.0°C.

6.3 Effect of Vents and Draft Curtains on Sprinkler Discharge Pattern

In the cartoned plastic commodity Test P-3, the draft curtain to the north of the ignition point delayed the operation of sprinklers further north and blocked the spray of sprinklers on either side of it. In this test, the fuel array extended beneath the north and west curtains. The fire spread to the north side of the main array because the commodity there was unwetted due to a delay in sprinkler activation on the north side of the curtain and blockage of the sprinkler spray from the south side. The results of Test P-3 reinforced evidence provided by two similar[9] tests performed by Factory Mutual [21]. In the FMRC tests, the fires spread underneath the curtains, resulting in the development of a more severe fire, a greater number of sprinkler operations, an atypical sprinkler opening pattern, distorted sprinkler discharge patterns which affected prewetting of commodity, and more smoke production. Although the fire damage and number of sprinkler activations in Test P-3 were not as great as that seen in the tests performed at FMRC, the fire damage was substantially higher in this test than in any other test performed in the series, even though the first two sprinkler activations were relatively early (67 and 72 s). This early activation was most likely due to the close proximity of the fire to the intersection of the draft curtains. However, the early jump on the fire did not lead to a rapid decrease in temperatures or sprinkler activations as was the case in Tests P-4 and P-5, the other two tests performed with draft curtains installed. Instead, the fire spread to the unprotected north face of the central array; and even though it was eventually controlled by sprinklers on the north side of the east-west curtain, it ultimately consumed approximately 184 boxes, nearly twice as much as Tests P-4 and P-5. A vent did automatically activate at 4:11, but by that time the two sprinklers on each side of it had already activated. Based on an examination of the the sprinkler activation pattern and the thermocouple data, the opening of the vent had no influence on the test results.

[9]The tests performed at FMRC involved slatted wood shelving, a slightly different rack configuration, and different sprinkler spacing and flow rate.

6.4 Effect of Sprinklers on the Number and Time of Vent Activations

Based on the test data collected in this study, it is difficult to assess how, in general, sprinklers affect the activation of vents because (1) there is little information about how the vents would have operated in an unsprinklered facility because only one test was performed without sprinklers, and (2) only one vent design was used in the test program. However, it appears from the data below that the sprinkler spray influenced the thermal response characteristics of this particular vent, and it is believed that sprinklers could have a similar influence on similar vent designs.

In the one unsprinklered test of the study (Test I-11), the vent opened at 4:48. The heptane spray burner was 8.6 m (28 ft) from the vent center. Six other tests were performed with the fire at this distance from the vent when the vent was equipped with a fusible link, and in none of these tests did the vent open. In the unsprinklered Test I-11, the temperature near the vent was about 170°C (338°F), whereas in Test I-10, with the fire at the same location, the temperature near the vent was about 90°C (194°F) after the sprinklers had activated around the fire (Figs. 94 and 95). Examination of the near-ceiling temperatures from all the tests indicates that sprinklers of this type have a significant cooling effect, and this will certainly have an effect on thermally-responsive, independently-controlled vents.

To better understand the thermal environment in the vicinity of the vent's fusible link, a thermocouple and three calibrated brass disks were placed near the link of the vent located at the northwest corner of the curtained area during the cartoned plastic and the second series of heptane spray burner tests (see Section 4.1 for a description of the instrumentation). Figures 19–21 show the temperatures recorded by the thermocouple and the brass disks within the vent cavity during the heptane tests. In Tests II-3 and II-4, when the vent opened automatically, the temperature of the "medium" and "slow" disks rose above the rated temperature of the link (74°C, 165°F) at about the same time that the vent opened. In Test II-8, the vent opened about 10 s before the "medium" disk temperature reached 74°C, and 30 s before the "slow" disk temperature reached 74°C. In Tests II-9 and II-11, where the vent did not open, the temperatures recorded by the "medium" and "slow" disks were comparable to those recorded by the disks in Tests II-3, II-4 and II-8.

In Plastic Test P-2, the fire was ignited directly under a vent. In the experiment, flames reached the top of the central array at about 65 s and the vent cavity at about 70 s. The first sprinkler activated at 100 s. The vent did not open at any time during the 30 min test even though another vent 6 m (20 ft) to the west of the unopened vent opened at 6:04. The temperature history of the brass disks within the cavity of the unopened vent is given by Fig. 39. After the test, the fusible link was examined, and it was observed that the solder holding the two strips of metal together had begun to melt. This observation had been made when examining the links after several of the heptane spray burner tests, as well.

This data, along with the plunge tunnel measurements reported in Section 3.1.4, suggests that the fusible link reached its activation temperature before or at about the same time as the the first sprinkler activated, but the link did not fuse. It is not clear whether the link did not fuse because it was cooled directly by water drawn upwards into the vent cavity, or whether the sprinkler spray simply cooled the rising smoke plume enough to prevent the link from fusing. In any event, this phenomenon deserves further study.

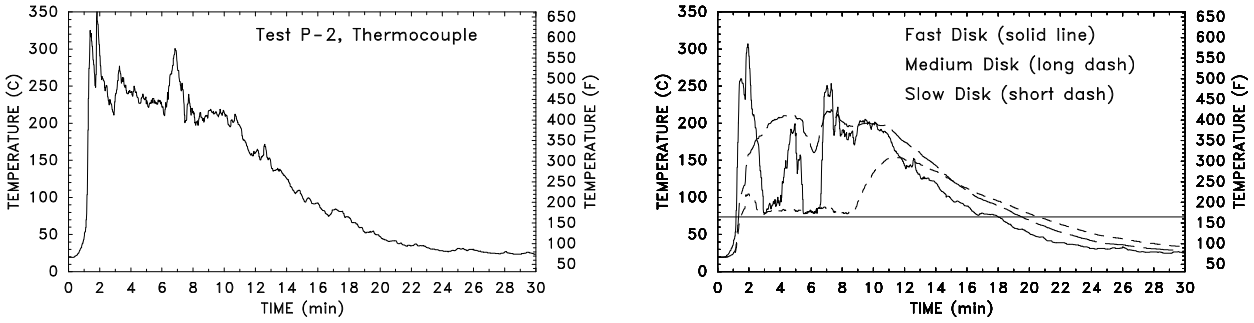

Figure 39: Temperatures inside the instrumented vent cavity during Plastic Test P-2. The curve on the left displays the temperature of the thermocouple near the fusible link. The curve on the right displays the temperature of the brass disks. The horizontal line on the left plot indicates the rated temperature of the fusible link.

6.5 Effect of Sprinklers on the Discharge Rate of Vents

The cooling of the near-ceiling gases due to the operation of sprinklers will affect the rate of discharge through a vent. To measure the flow of gases through a vent, a velocity probe and thermocouples were positioned in the vent nearest the fire location in the second series of heptane burner tests and the cartoned plastic commodity tests. Unfortunately, the velocity data was deemed unreliable, thus there was no means to directly measure the discharge rate. The numerical model to be described in the next section will be used to examine the effect of sprinklers on the discharge rate of vents.

An indirect effect of sprinklers on vent performance is that sprinkler sprays entrain smoke and hot gases, cool them, and transport them towards the floor. No measurements were made during the tests to quantify this phenomenon, but visual observations were made to determine what areas of the test space filled with smoke during the first 5 or 10 minutes of the cartoned plastic commodity tests. In Test P-1, earlier and more frequent sprinkler activation occurred to the north of the ignition point, leading to heavier observed smoke logging in the north aisle. In Test P-2 it was less obvious which aisle was more heavily smoke logged. In Test P-3, the south aisle was more smoke logged because sprinklers to the north of the ignition point were delayed by the draft curtains. The curtains also blocked the smoke from the north aisle, at least initially. In Test P-4, the south aisle was more heavily smoke logged; in Test P-5, the north aisle. The sprinkler activation pattern in Tests P-4 and P-5 was consistent with these observations.

7 Numerical Modeling

The numerical model used to simulate the physical experiments is based on techniques common to the computational fluid dynamics (CFD) community. Often these types of models are referred to as "field models" by the fire research community, to distinguish them from "zone models". The basic idea behind most CFD models is to divide the space of interest into small control volumes or computational cells, and in each cell compute the density, velocity, temperature, pressure and species concentration based on conservation laws of mass, momentum and energy. The accuracy of the results often depends on the number of cells used to discretize the volume of interest. The technique being applied in this project is referred to as large eddy simulation (LES). The idea behind this approach is to divide the test space into as many cells as possible (in this case, hundreds of thousands to over a million) to resolve as much of the convective motion of the gases (air, smoke) as possible. In this way, much of the mixing of the hot gases from the fire with the cool surrounding air can be captured directly, reducing the dependence on empirical entrainment or turbulence parameters that are often subject to much debate and uncertainty.

7.1 Model Description

The heart of the numerical model is an algorithm that solves the set of partial differential equations describing the transport of smoke and hot gases from the fire and its subsequent mixing with the surrounding air. This is often referred to as the hydrodynamic model. The driving forces, like the fire and the sprinkler spray, are represented by source terms in the governing equations. The physical boundaries and their properties provide the boundary conditions for the equations. In the sections to follow, the major equations and the assumptions behind them are put forward.

7.1.1 Hydrodynamics

Consider a thermally expandable ideal gas driven by a prescribed heat source. The equations of motion governing the fluid flow are written in a form suitable for low Mach number applications [30]. Sometimes, this form of the equations is referred to as "weakly compressible". The most important feature of these equations is that in the energy conservation equation and the equation of state the spatially and temporally varying pressure is replaced by an average pressure p_0 that depends only on time. This is done to filter out acoustic waves. The efficiency of the numerical solution of the equations is dramatically increased by this approximation.

In the equations to follow, all symbols have their usual fluid dynamical meaning: ρ is the density, $\mathbf{u}$ the velocity vector, $\boldsymbol{\omega} = \nabla \times \mathbf{u}$ the vorticity, p the pressure, $\mathbf{g}$ the gravity vector, c_p the constant-pressure specific heat, T the temperature, k the thermal conductivity, t the time, $\dot{q}'''$ the prescribed volumetric heat release rate, $\mathcal{R}$ the gas constant equal to the difference of the specific heats $\mathcal{R} = c_p - c_v$, $\mathcal{F}$ the external force term (in this case the sprinkler spray), and $\boldsymbol{\sigma}$ the standard stress tensor for compressible fluids.

Conservation of Mass

$$\frac{\partial \rho}{\partial t} + \nabla \cdot \rho \mathbf{u} = 0 \tag{1}$$

Conservation of Momentum

$$\rho\left(\frac{\partial \mathbf{u}}{\partial t}+(\mathbf{u}\cdot\nabla)\mathbf{u}\right)+\nabla p-\rho\mathbf{g}=\mathcal{F}+\nabla\cdot\boldsymbol{\sigma} \tag{2}$$

Conservation of Energy

$$\rho c_p\left(\frac{\partial T}{\partial t}+\mathbf{u}\cdot\nabla T\right)-\frac{dp_0}{dt}=\dot{q}'''+\nabla\cdot k\nabla T \tag{3}$$

Equation of State

$$p_0(t)=\rho\mathcal{R}T \tag{4}$$

The divergence of the flow $\nabla\cdot\mathbf{u}$ is a very important quantity in the analysis to follow, and it is readily found by combining Eqs. (1) and (3), using the equation of state (4)

$$p_0\,\nabla\cdot\mathbf{u}+\frac{1}{\gamma}\frac{dp_0}{dt}=\frac{\gamma-1}{\gamma}\left(\dot{q}+\nabla\cdot k\nabla T\right) \tag{5}$$

where $\gamma=c_p/c_v$. Integrating Eq. (5) over the entire domain Ω yields a consistency condition for the background pressure $p_0(t)$

$$p_0\int_{\partial\Omega}\mathbf{u}\cdot d\mathbf{S}+\frac{V}{\gamma}\frac{dp_0}{dt}=\frac{\gamma-1}{\gamma}\left(\int_\Omega \dot{q}\,dV+\int_{\partial\Omega}k\nabla T\cdot d\mathbf{S}\right) \tag{6}$$

where V is the volume of the enclosure. The background pressure can be expressed in terms of a background temperature $T_0(t)$ and density $\rho_0(t)$

$$p_0=\mathcal{R}\rho_0 T_0 \tag{7}$$

These spatially averaged quantities play the same role that ambient conditions do in the Boussinesq approximation. Perturbations to each are represented by the relations

$$T=T_0(t)(1+\tilde{T})\quad;\quad \rho=\rho_0(t)(1+\tilde{\rho}) \tag{8}$$

The perturbation values are thus simply related

$$(1+\tilde{T})(1+\tilde{\rho})=1 \tag{9}$$

Defining T_0 and ρ_0 through the adiabatic process

$$\frac{\rho_0}{\rho_\infty}=\left(\frac{p_0}{p_\infty}\right)^{1/\gamma} \tag{10}$$

allows the energy equation to be expressed in terms of the perturbation temperature $\tilde{T}$ and the divergence

$$\frac{\partial\tilde{T}}{\partial t}+\mathbf{u}\cdot\nabla\tilde{T}=(1+\tilde{T})\left[\nabla\cdot\mathbf{u}+\frac{1}{\gamma p_0}\frac{dp_0}{dt}\right] \tag{11}$$

The background pressure is found from Eq. (6).

Walls and other solid surfaces that form the boundary of the flow domain are heated by the surrounding gases. Heat is conducted into the solid according to the equation

$$\rho_s \, c_s \, \frac{\partial T_s}{\partial t} = \frac{\partial}{\partial n} k_s \frac{\partial T_s}{\partial n} \tag{12}$$

where ρ_s is the density of the solid, c_s the specific heat, T_s the temperature, k_s the conductivity, and n the normal direction coordinate. Heat is transferred to solids by convection and thermal radiation. More detail on these processes is included below.

The pressure is composed of three components, the background $p_0(t)$, the hydrostatic, and a perturbation to the hydrostatic $\tilde{p}$

$$p(\mathbf{x}, t) = p_0(t) - \rho_0(t) g z + \tilde{p}(\mathbf{x}, t) \tag{13}$$

where $\mathbf{x}$ is the position vector (x, y, z) and z is the vertical coordinate. Subtracting off the hydrostatic pressure gradient from the momentum equation (2), and then dividing by the density yields

$$\frac{\partial \mathbf{u}}{\partial t} + \frac{1}{2} \nabla |\mathbf{u}|^2 - \mathbf{u} \times \boldsymbol{\omega} + \frac{1}{\rho} \nabla \tilde{p} - \frac{\rho - \rho_0}{\rho} \mathbf{g} = \frac{1}{\rho} \nabla \cdot \boldsymbol{\sigma} \tag{14}$$

Note the use of the vector identity: $(\mathbf{u} \cdot \nabla)\mathbf{u} = |\mathbf{u}|^2/2 - \mathbf{u} \times \boldsymbol{\omega}$. To simplify this equation further, the density in the pressure term is assumed ambient, and then the term $|\mathbf{u}|^2/2$ is combined with the perturbation pressure $\tilde{p}/\rho_0$ and written as a total pressure, $\mathcal{H}$. This approximation assumes that the buoyancy generated vorticity dominates the baroclinic contribution caused by the non-alignment of perturbation pressure and density gradients. This is not a good approximation at the small scales where the actual combustion heat release takes place. However, at the resolvable scales this is nothing more than the assumption that these are buoyancy dominated flows.

There are numerous ways of handling the viscous terms in the momentum equation – the simplest is to simply prescribe a constant viscous coefficient in cases where the grid resolution is fine enough to capture the mixing processes at all relevant scales. More often one is forced due to lack of adequate grid resolution to use a sub-grid scale model. For the problem of smoke movement in a warehouse, the latter condition applies. The treatment of sub-grid scale mixing follows very closely the analysis of Smagorinsky [31]. The stress tensor $\boldsymbol{\sigma}$ in Eq. (14) is replaced by the Reynolds stress tensor $\boldsymbol{\tau}$ whose components are written in the form

$$\tau_{ij} = 2 \, \rho \, (C_s \, \Delta)^2 \, |S| \, S_{ij} \quad ; \quad S_{ij} = \frac{1}{2} \left(\frac{\partial u_i}{\partial x_j} + \frac{\partial u_j}{\partial x_i} \right) \tag{15}$$

where C_s is taken as 0.21, $\Delta = (\delta x \, \delta y \, \delta z)^{\frac{1}{3}}$, δx, δy and δz are the grid cell dimensions, and $|S| = \sqrt{2 S_{ij} S_{ij}}$. There have been numerous refinements of the original Smagorinsky model [32, 33, 34], but it is difficult to assess the improvements offered by these newer schemes for the problem of smoke movement. There are two reasons for this. First, the structure of the fire plume is so dominated by the large scale, resolvable eddies that even a constant eddy viscosity gives results almost identical with those obtained with the Smagorinsky scheme [4]. Second, the lack of precision in most large scale fire data makes it difficult to sort out the subtleties associated with these models. For the time being, the Smagorinsky model with the given C_s produces satisfactory results for most large scale applications where boundary layers are not important or are not resolvable.

To obtain the pressure perturbation, we take the divergence of the momentum equation

$$\frac{\partial \mathbf{u}}{\partial t} + \mathbf{F} + \nabla \mathcal{H} = 0 \tag{16}$$

where all the convective and diffusive terms have been incorporated in the term $\mathbf{F}$. The resulting equation for the total pressure $\mathcal{H}$ is an elliptic partial differential equation

$$\nabla^2 \mathcal{H} = -\frac{\partial (\nabla \cdot \mathbf{u})}{\partial t} - \nabla \cdot \mathbf{F} \tag{17}$$

The linear algebraic system arising from the discretization of Eq. (17) has constant coefficients and can be solved to machine accuracy by a fast, direct (*i.e.* non-iterative) method that utilizes fast Fourier transforms. No-flux boundary conditions are specified by asserting that

$$\frac{\partial \mathcal{H}}{\partial n} = -F_n \tag{18}$$

at solid walls, where F_n is the normal component of $\mathbf{F}$ at the wall. This equation asserts that the normal component of velocity at the wall does not change with time, and indeed remains zero assuming the flow velocity is initially zero. At open external boundaries it is assumed that the perturbation pressure is zero, a reasonable assumption as long as the fire is well within the numerical domain.

Direct Poisson solvers are most efficient if the domain is a rectangular region, although other geometries such as cylinders and spheres can be handled almost as easily. For these solvers, the no-flux condition (18) is simple to prescribe at external boundaries. However, many practical problems involve more complicated geometries. For building fires, doors and windows within multi-room enclosures are very important features of the simulations. These elements may be included in the overall domain as masked grid cells, but the no-flux condition (18) cannot be directly prescribed at the boundaries of these blocked cells due to consistency issues. However, it is possible to exploit the relatively small changes in the pressure from one time step to the next to enforce the no-flux condition. At the start of a time step, the components of the convection/diffusion term $\mathbf{F}$ are computed at all cell faces that do not correspond to walls. Then, at those cell faces that do, set

$$F_n = -\frac{\partial \mathcal{H}^*}{\partial n} + \beta u_n \tag{19}$$

where F_n is the normal component of $\mathbf{F}$ at the wall, and β is a relaxation factor empirically determined to be about 0.8 divided by the time step. The asterisk indicates the most recent value of the pressure. Obviously, the pressure at this particular time step is not known until the Poisson equation is solved. Equation (19) asserts that following the solution of the Poisson equation for the pressure, the normal component of velocity u_n will be driven closer to zero according to

$$\frac{\partial u_n}{\partial t} \approx -\beta u_n \tag{20}$$

This is approximate because the true value of the velocity time derivative depends on the solution of the pressure equation, but since the most recent estimate of pressure is used, the approximation is very good. Also, even though there are small errors in normal velocity at solid surfaces, the

divergence of each blocked cell remains exactly zero for the duration of the calculation, and the consistency condition (6) ensures global mass conservation. In other words, the total flux into a given obstacle is always identically zero, and the error in normal velocity is usually at least 3 or 4 orders of magnitude smaller than the characteristic flow velocity. When implemented as part of a predictor-corrector updating scheme, the no-flux condition at solid surfaces is well maintained.

7.1.2 The Fire

The fire is represented by a large number of Lagrangian elements (particles that move with the flow) that release heat as they are transported by the thermally-induced motion. Since the fluid motion determines where the heat is actually released, and the heat release determines the motion, the large scale features of the coupling between the fire and the smoke transport are retained. The heat release rate per unit mass of burning fuel is determined from experiment. The spread of the fire through the fuel array is predicted by the calculation. Smoke is simulated by tracking the convected elements after the fuel burnout is completed. A specified percentage of the fuel consumed is assumed to be converted to smoke particulate. Thus, a knowledge of the spatial distribution of the Lagrangian elements is equivalent to a specification of the smoke particulate density at any instant of time. This "thermal element" model, which represents the combustion heat release as a large number of point sources convected by the resolvable flow field, is in fact a simple combustion model in its own right. It is consistent with more detailed combustion theories currently in use, and it permits the use of experimental data from fire experiments in a way that does not violate the consequences of those theories. A more detailed discussion of this model can be found in Ref. [35].

The volumetric heat release rate term in the energy conservation equation (3) is essentially the sum of the heat released from the thermal elements that represent the fire. Thermal elements originate at solid (burning) surfaces. In the case of boxed polystyrene cups, the cardboard box heats up due to both convective and radiative heat transfer from the surrounding gas. When the surface heats up to its measured ignition temperature, thermal elements are ejected from the surface and burned at a prescribed rate (an input heat release rate per unit area). The surface is assumed to be thermally-thin. This assumption is technically not correct, but a more detailed treatment of the heat transfer properties of cardboard would complicate an already complicated situation. As with all the assumptions made in the model, future refinements will be made if warranted. The assumed thermally-thin cardboard heats up according to its given density ρ_s, specific heat c_s and characteristic thickness δ

$$\frac{dT_s}{dt} = \frac{\dot{q}_c'' + \dot{q}_r'' - \dot{q}_e''}{\rho_s c_s \delta} \tag{21}$$

where $\dot{q}_c''$, $\dot{q}_r''$ and $\dot{q}_e''$ represent heat fluxes due to convection, radiative absorption, and radiative emission. The individual values of the parameters ρ_s, c_s and δ are not relevant here; rather it is their product that is determined experimentally, and this product is referred to as the lumped thermal capacitance of the fuel. For a vertical cardboard sample of the cartoned plastic commodity used in the tests, $\rho_s c_s \delta$ was determined from the LIFT (Lateral Ignition and Flame spread Test) apparatus at NIST to be 1.5 ± 0.4 kJ/m^2·K [36]. Note that the data analysis was based on a thermally-thin assumption, following the method outlined by Ohlemiller [37]. The ignition temperature of the sample was determined to be (370°C, 700°F).

The convective heat flux to the surface $\dot{q}_c''$ is estimated from a correlation of the form

$$\dot{q}_c'' = C\,\Delta T^{\frac{1}{3}}\,\Delta T \quad \text{W/m}^2 \tag{22}$$

where ΔT is the difference between the wall and gas temperature, and C is an empirical constant of value 1.43 for a horizontal surface and 0.95 for a vertical surface [38].

The radiative heat flux to the surface, $\dot{q}_r''$, is calculated based on the assumption that a prescribed fraction of the heat released from a thermal element is radiated away, and this energy is absorbed by the surrounding surfaces without attenuation by the surrounding gas. Usually, the fraction of energy radiated away from the fire is obtained by comparing the total heat release rate with the convective heat release rate. For a given point $\mathbf{x}_s$ on a wall or surface, the radiative flux is given as

$$\dot{q}_r'' = \sum_{i=1} \cos(\phi_i) \frac{\chi_r\,\dot{q}_i}{4\pi\,|\mathbf{x}_i - \mathbf{x}_s|^2} \tag{23}$$

where $\mathbf{x}_i$ is the position of the ith thermal element, χ_r is the fraction of the heat release rate of the ith element, $\dot{q}_i$, converted into radiative energy, and ϕ_i is the angle formed by the normal to the surface and the vector $\mathbf{x}_p - \mathbf{x}_s$. Since there are hundreds of thousands of thermal elements in a typical calculation, the above summation is made over a sampling of the elements.

As the cardboard heats up, energy is lost to radiation according to

$$\dot{q}_e'' = \sigma\epsilon\,(T_s^4 - T_\infty^4) \tag{24}$$

where σ is the Stefan-Boltzmann constant $\sigma = 5.67 \times 10^{-8}$ W/m^2/K^4, and ϵ is the emissivity of the surface. In this case, the emissivity was assumed to be 0.8.

Once the cardboard reaches its ignition temperature, Lagrangian particles representing pyrolyzed fuel are ejected at a rate of $\dot{n}''$ particles per unit time per unit area (about 1,000 particles/m^2·s) with a small normal velocity (≈0.20 m/s) into the flow domain. The heat release rate for the fire at a given time t is then expressed by summing over all of the thermal elements in the flow field

$$\dot{q}(t) = \sum \frac{\dot{q}''}{\dot{n}''}\,\frac{1}{\tau} \qquad (t - t_0 < \tau) \tag{25}$$

where the $\dot{q}''$ is a prescribed rate of heat release per unit area, τ is a characteristic element burn-out time, and t_0 is the time that a given particle leaves a solid surface. The heat release rate per unit area $\dot{q}''$ is determined from small scale cone calorimeter measurements [39]. Figure 40 displays the heat release rate per unit area for a small sample compartment consisting of a single polystyrene cup surrounded by cardboard [40]. The burn-out time is obtained from the plume correlation of Baum and McCaffrey [41]. In the flame region, the vertical centerline velocity is given as $w = 2.18\sqrt{gz}$ for $0 < z < 1.32\,D^*$, where $D^* = (\dot{Q}/c_p\rho_\infty T_\infty\sqrt{g})^{2/5}$ is the characteristic diameter of a fire whose total heat release rate is $\dot{Q}$. The burn-out time is the time it takes a thermal element to reach the top of the flame region

$$\tau \approx \int_0^{1.32\,D^*} \frac{dz}{2.18\,\sqrt{gz}} = \frac{2}{2.18}\sqrt{\frac{1.32\,D^*}{g}} \tag{26}$$

and is usually a few tenths of a second.

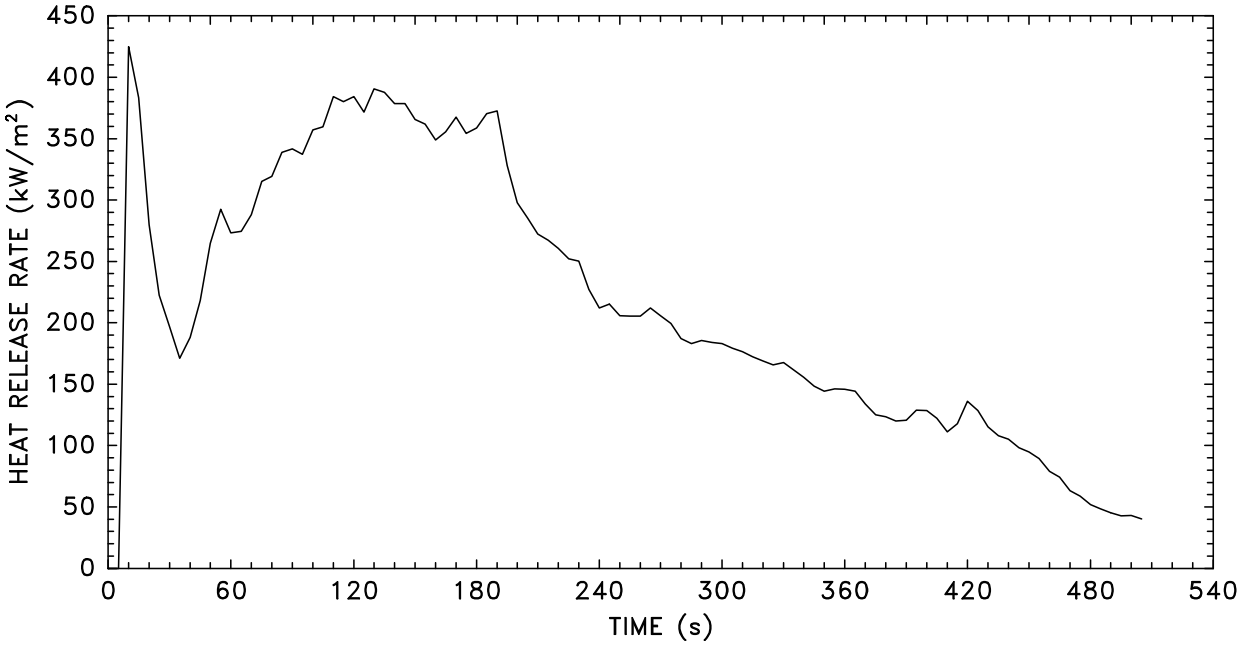

Figure 40: Heat release rate per unit area of the FMRC Standard Plastic test commodity obtained from a cone calorimeter measurement. The cone was in a vertical configuration, and the peak radiative flux on the object was 75 kW/m^2.

Oxygen transport and consumption is included in the calculation, and the burn-out time of any thermal element will vary based on the concentration of oxygen in the gas surrounding it. It is assumed that 1 kg of oxygen is consumed for every 13,100 kJ of energy released. When the oxygen mass fraction Y_{O_2} falls to a certain prescribed lower limit (about 12%), combustion is assumed to stop, and the unburned fuel associated with the thermal elements remains unburned until more oxygen can be found.

Another useful input parameter associated with the given solid fuel is the total amount of potential energy contained within a unit volume of the unburned fuel. The computational cell representing a piece of the fuel will disappear once the energy contained within that volume is consumed. This parameter is referred to as the Energy Per Unit Volume, and is expressed in units of kJ/m^3. If prescribed, this parameter permits fire spread through the solid fuel, as in the combustion of a boxed commodity or a crib.

7.1.3 Sprinkler Activation

The temperature of the sensing element of an automatic sprinkler is estimated from the differential equation presented by Heskestad and Bill [42, 43]

$$\frac{dT_l}{dt} = \frac{\sqrt{u}}{\mathrm{RTI}}(T_g - T_l) - \frac{C}{\mathrm{RTI}}(T_l - T_m) \tag{27}$$

where T_l is the link temperature, T_g is the gas temperature in the neighborhood of the link, T_m is the temperature of the sprinkler mount, and u is the gas velocity. The thermal sensitivity of

the detector is indicated by the value of RTI[10]. The heat lost to the mount due to conduction is characterized by the "C-factor", C. A heated wind tunnel (plunge test) is used to determine both of these parameters by creating an environment in which the air velocity and temperature, plus the mount temperature, are held at constant values. The C-factor is measured first. There are two methods of performing the tests [44], both of which are designed to pinpoint combinations of air temperature and velocity at which an energy balance is established for the heat gained and lost by the sensing element. For these combinations of air temperature and velocity, the right hand side of Eq. (27) is zero, and consequently

$$C = \left(\frac{T_g - T_m}{T_{l,act} - T_m} - 1 \right) \sqrt{u} \tag{28}$$

Following the determination of the C-factor, the RTI is determined from the solution of Eq. (27) (assuming the values of T_g, T_m, and u are constant)

$$T_l(t) = T_m + \frac{T_g - T_m}{1 + C/\sqrt{u}} \left[1 - \exp\left(\frac{-(1 + C/\sqrt{u})\sqrt{u}}{\text{RTI}}\, t \right) \right] \tag{29}$$

The formula for the RTI is given by

$$\text{RTI} = \frac{-t_{act}\,(1 + C/\sqrt{u})\,\sqrt{u}}{\ln\left(1 - \frac{(T_{l,act} - T_m)(1 + C/\sqrt{u})}{T_g - T_m}\right)} \tag{30}$$

where $T_{l,act}$ is the mean liquid bath operating temperature of the sprinkler, and t_{act} is the activation time following the introduction of the sprinkler into the heated wind tunnel.

7.1.4 Sprinkler Droplet Size Distribution

Once a sprinkler has activated, the sizes, temperatures and trajectories of a representative sample of the water droplets are computed. The initial conditions are deduced from measurements of droplet sizes and density patterns of sprays not subjected to a fire plume. Note that tracking every droplet is prohibitively expensive, and unnecessary. The sampling of droplets has been referred to as the "superdrop" concept [45]. It is directly analogous to the thermal element concept discussed above, and indeed tracking water droplets does not introduce any new machinery into the numerical code. In the calculations that will be discussed below, typically five to ten thousand droplets from each active sprinkler interact with the gas at any given time. This number of droplets ensures that a sufficient distribution of the water is obtained.

In order to compute the droplet trajectories, the initial size and velocity of each droplet must be prescribed. This is done in terms of random distributions. The initial droplet size distribution of the sprinkler spray is expressed in terms of its Cumulative Volume Fraction (CVF), a function that relates the fraction of the water volume transported by droplets less than a given diameter. Typically, this function is represented very well by a combination of log-normal and Rosin-Rammler

[10]Often the thermal response of a sprinkler is characterized by a single parameter, also called the Response Time Index or RTI. This parameter lumps together the RTI as used in Eq. 27 and the C-factor. When reporting an RTI, it should be made clear what form of the governing equation is being solved. In this report, when only an RTI value is used to characterize the thermal response of an object, it is referred to an a "bulk" RTI.

distributions [46]

$$F(d) = \begin{cases} \frac{1}{\sqrt{2\pi}} \int_0^d \frac{1}{\sigma\,\delta}\, e^{-\frac{[\ln(\delta/d_m)]^2}{2\sigma^2}}\, d\delta & (d \le d_m) \\ 1 - e^{-0.693\left(\frac{d}{d_m}\right)^\gamma} & (d_m < d) \end{cases} \tag{31}$$

where d_m is the median droplet diameter (*i.e.* half the mass is carried by droplets d_m or smaller in diameter), and γ and σ are empirical constants equal to about 2.4 and 0.58, respectively. The median diameter varies from sprinkler to sprinkler, and it also varies with the pressure applied. It appears that γ is less sensitive to changes in sprinkler design and operating conditions.

In the numerical algorithm, the size of the sprinkler droplets are chosen to mimic the Rosin-Rammler/log-normal distribution. A Probability Density Function (PDF) for the droplet diameter is defined

$$f(d) = \frac{F'(d)}{d^3} \Bigg/ \int_0^\infty \frac{F'(\delta)}{\delta^3}\, d\delta \tag{32}$$

Note that $F'(d)$ denotes the first derivative of the function $F(d)$. Droplet diameters are randomly selected by equating the Cumulative Number Fraction of the droplet distribution with a uniformly distributed random variable U

$$U(d) = \int_0^d f(\delta)\, d\delta \tag{33}$$

Figure 41 displays typical Cumulative Volume Fraction and Cumulative Number Fraction functions. Of course, every droplet from a given sprinkler is not tracked. Instead, a sampled set of the droplets is tracked. Typically, 1,000 particles per sprinkler per second are released. The total number of droplets represented by each computed droplet is given by $\dot{m}_w/(\dot{n}\,\overline{m_d})$, where $\dot{m}_w$ is the mass flow rate of water from a single sprinkler, $\dot{n}$ is the number of droplets tracked per sprinkler per second, and $\overline{m_d}$ is the average mass of a droplet. The average mass of a droplet can be expressed in terms of the PDF

$$\overline{m_d} = \frac{4}{3}\pi\,\rho_w \int_0^\infty f(\delta) \left(\frac{\delta}{2}\right)^3 d\delta \tag{34}$$

where ρ_w is the density of water.

7.1.5 Sprinkler Spray Dynamics

The influence of the water spray is introduced into the governing equations of fluid motion through the force term $\mathcal{F}$ in Eq. (2). This term represents the momentum transferred from the water droplets to the gas, and it is computed by summing the force from each droplet in a control volume

$$\mathcal{F} = \frac{1}{2} \frac{\sum \rho c_d A_d (\mathbf{u}_d - \mathbf{u}_g)|\mathbf{u}_d - \mathbf{u}_g|}{V_{cv}} \tag{35}$$

where c_d is a drag coefficient, A_d is an effective cross sectional area of the particle, $\mathbf{u}_g$ is the velocity of the surrounding gas, $\mathbf{u}_d$ is the velocity of the droplet, and V_{cv} is the volume of the control volume. The trajectory of an individual droplet is governed by the equation

$$\frac{d}{dt}(m_d \mathbf{u}_d) = m_d\,\mathbf{g} - \frac{1}{2}\rho\, c_d\, A_d\, (\mathbf{u}_g - \mathbf{u}_d)|\mathbf{u}_g - \mathbf{u}_d| \tag{36}$$

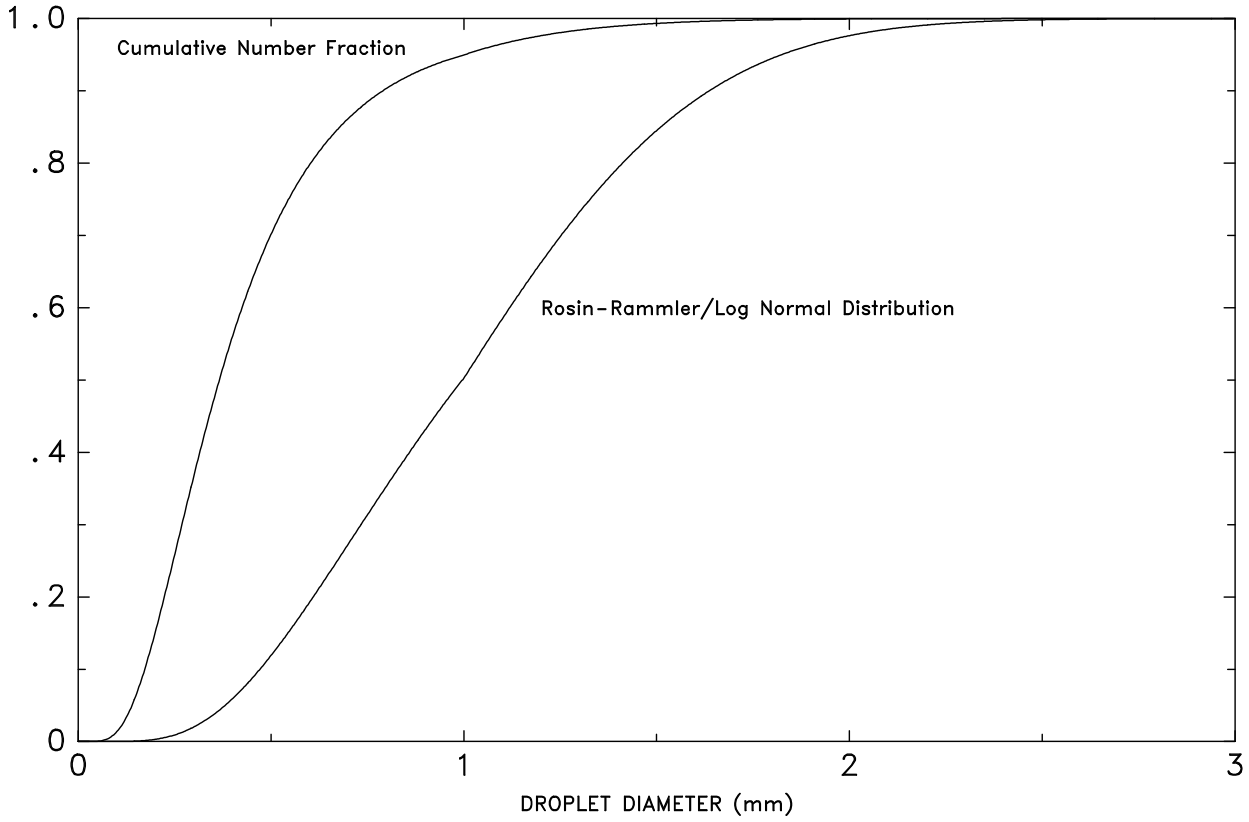

Figure 41: Cumulative Volume Fraction and Cumulative Number Fraction functions of the droplet size distribution from a typical industrial fire sprinkler. The median diameter d_m is 1 mm, $\sigma = 0.58$ and $\gamma = 2.43$.

where m_d is the mass of the droplet. The initial droplet velocity and direction are estimated from measurements of the water flux near the floor through a trial and error sequence of calculations. Typically, the initial direction is chosen randomly from a range of angles from the vertical through which the droplet exits the sprinkler deflector.

The sprinkler spray droplet temperature T_d and radius r_d are governed by the following equations

$$\frac{dT_d}{dt} = \begin{cases} \frac{3\,h_d}{c_w\,r_d\,\rho_d}(T_g - T_d) & T_d < T_v \\ 0 & T_d = T_v \end{cases} \tag{37}$$

$$\frac{dr_d}{dt} = \begin{cases} 0 & T_d < T_v \\ -\frac{h_d}{h_v\,\rho_d}(T_g - T_d) & T_d = T_v \end{cases} \tag{38}$$

where c_w is the specific heat of water, ρ_d is the density of the droplet, T_g is the gas temperature, T_v is the vaporization temperature of water (100°C), h_v is the heat of vaporization of water, h_d is the heat transfer coefficient between air and the water droplet, given by

$$h_d = \frac{\mathrm{Nu}\,k_a}{2r_d}$$

Nu is the Nusselt number given by

$$\mathrm{Nu} = 2 + 0.6\ \mathrm{Re}^{\frac{1}{2}}\ \mathrm{Pr}^{\frac{1}{3}}$$

The Reynolds number is based on the velocity of the droplet, its diameter and the viscosity of air at ambient temperature. The Prandtl number is about 0.7, and k_a is the thermal conductivity of air. The change in gas temperature due to the presence of the water droplets is given by

$$\frac{dT_g}{dt} = \sum \left(\frac{m_w}{m_a}\right) \left(\frac{c_w}{c_p}\right) \frac{3\,h_d}{c_w\,r_d\,\rho_d}(T_d - T_g) \tag{39}$$

where m_w and m_a denote the mass of water and air in the control volume over which the summation is being performed.

7.1.6 Sprinkler Spray Interaction with Burning Commodity

When a water droplet hits a solid horizontal surface, it is assigned a random horizontal direction and moves at a fixed velocity until it reaches the edge, at which point it drops straight down at a constant speed. This terminal velocity was determined by injecting a colored dye into a stream of water that cascaded down the side of a carton. It was roughly 0.55 m/s. Both the heating of unburned surfaces and the heat release rates from burning surfaces are affected by the droplets. The heat transfer coefficient between the surface and the water film is calculated based on an empirical correlation for forced flow past a flat plate [47]

$$\mathrm{Nu} = \frac{h_L\,L}{k_w} = 0.664\,\mathrm{Re}^{\frac{1}{2}}\,\mathrm{Pr}^{\frac{1}{3}} \approx 450 \quad \text{for water flowing at 0.55 m/s} \tag{40}$$

The characteristic length L is assumed to be the size of the fuel package. For computational convenience, the water continues to be tracked in the form of droplets, but the heat transfer coefficient between the water droplets and their surroundings is written in terms of an equivalent heat transfer coefficient between the thin film of water and the surface. By doing this, the same thermodynamic formulae may be applied to the droplet whether it is airborne or not. This is a numerical convenience because the transport of water is much easier to describe in terms of Lagrangian droplets rather than sheets of liquid. If the water formed a thin sheet, its temperature T_w would be governed by

$$\frac{dT_w}{dt} = \frac{h_L\,(T_s - T_w)}{c_w\,m''_w} \tag{41}$$

On the other hand, as a droplet the water temperature T_d would be governed by

$$\frac{dT_d}{dt} = \frac{3\,h_d}{c_w\,r_d\,\rho_d}(T_g - T_d) \tag{42}$$

Equating dT_w/dt with dT_d/dt and taking $T_g = T_s$, an effective heat transfer coefficient is derived

$$h_d = \frac{h_L\,r_d\,\rho_d}{m''_w} \tag{43}$$

Here, r_d is an arbitrarily chosen droplet radius, and m''_w is the mass of water per unit area.

7.1.7 Extinguishment

Extinguishment of the fire is the single most difficult component of the numerical model. To date, most of the work in this area has been performed at Factory Mutual. An important paper on the subject is by Yu *et al.* [48]. Their analysis yields an expression for the total heat release rate from a rack storage fire after sprinkler activation

$$\dot{Q} = \dot{Q}_0 \, e^{-k(t-t_0)} \tag{44}$$

where $\dot{Q}_0$ is the total heat release rate at the time of application t_0, and k is a fuel-dependent constant that for the FMRC Standard Plastic test commodity is given as

$$k = 0.176 \, \dot{m}''_w - 0.0131 \quad \mathrm{s}^{-1} \tag{45}$$

The quantity $\dot{m}''_w$ is the flow rate of water impinging on the box tops, divided by the area of exposed surface (top and sides). It is expressed in units of kg/m^2/s.

Unfortunately, this analysis is based on global water fluxes and burning rates. The numerical model requires more detail about the burning rate as a function of the local water flux. Until better models can be developed, the present extinguishment model consists of an empirical rule that decreases the local heat release rate as more water is applied

$$\dot{q}'' = \left(1 - \left(\frac{m''_w}{m''_{w_0}} \right)^2 \right) \; \dot{q}''_0 \tag{46}$$

The critical water density m''_{w_0} is estimated from small scale calorimeter burns of the commodity.

7.1.8 Numerical Methodology

In summary, the equations that are solved numerically are the energy equation (11), the momentum equation (14), and a Poisson equation for the total pressure (17). The background pressure, temperature and density are found from Eqs. (6), (7) and (10). Each of the conservation equations emphasize the importance of the divergence and vorticity fields, as well as the close relationship between the thermally expandable fluid equations [30] and the Boussinesq equations for which the authors have developed highly efficient solution procedures [49, 3]. These are applied directly to the equations presented here with minor modifications and no loss in performance. The only changes from earlier methodology are a return to a uniform rectangular grid with blocks of cells masked to simulate internal boundaries; and the use of a second order Runge-Kutta scheme to advance the velocity and temperature fields in time. The speed and accuracy of this technique enable calculations on current generation workstations that involve over a million computational cells, yielding the spatial range of two orders of magnitude for a three-dimensional calculation.

Table 5 provides a summary of the input parameters required to perform the simulations of the experiments. As an example, Figs. 42 and 43 show a photograph of Plastic Test P-5 and the corresponding numerical simulation. The geometry of the simulation consists of the individual pallet loads of the cartoned plastic commodity, the vents and draft curtains. The wooden pallets are accounted for by modifying the burning characteristics of the bottom of the simulated boxes. The supporting racks are not included in the calculation.

Input Parameters for an Industrial Fire Simulation		
Category	Parameter	Value
Building	Facility	UL Large Scale Fire Test Facility
	Region of Simulation	Below adjustable ceiling + 1 m above
	Simulation Dimensions	30.5 m × 30.5 m × 8.2 m (100 ft × 100 ft × 27 ft)
Numerical	Grid Dimensions	144 × 144 × 40
	Cell Size	0.21 m × 0.21 m × 0.21 m (8 in × 8 in × 8 in)
	Lateral Boundary Conditions	Ambient Pressure
	Ceiling Boundary Conditions	Thermally Thick
	Floor Boundary Conditions	Adiabatic
Ceiling	Product Name	Armstrong Ceramaguard (Item 602B)
	Specific Heat, c_s (Eq. 12)	753 J/kg·K
	Conductivity, k_s (Eq. 12)	0.0611 W/m·K
	Density, ρ_s (Eq. 12)	313 kg/m^3
Fuel	Type	Racked cartoned plastic commodity
	Boxes + Pallet Dimensions	1.1 m × 1.1 m × 1.2 m (42 in × 42 in × 47 in)
	Ignition Temperature	370°C
	Lumped Thermal Capacitance, $\rho_s c_s \delta$ (Eq. 21)	1.5 kJ/(m^2·K)
	Heat Release Rate Per Unit Area, $\dot{q}''$ (Eq. 25)	500 kW/m^2
	Energy Content Per Unit Volume	500 MJ/m^3
	Radiative Fraction, χ_r (Eq. 23)	0.50
	Emissivity, ϵ (Eq. 24)	0.8
	Critical Water Density, m''_{w_0} (Eq. 46)	0.125 kg/m^2
Ignitor	Peak Heat Release Rate	25 kW
Sprinkler	Response Time Index, RTI (Eq. 27)	148 (m·s)$^{\frac{1}{2}}$ (268 (ft·s)$^{\frac{1}{2}}$)
	C-factor (Eq. (27))	0.7 (m/s)$^{\frac{1}{2}}$ (2.3 (ft/s)$^{\frac{1}{2}}$)
	Activation Temperature, $T_{l,act}$ (Eq. 28)	74°C (165°F)
	Flow Rate	189 l/min (50 gpm)
	Spray Angle, (Eq. 36)	5° – 80°
	Initial Droplet Velocity, (Eq. 36)	8 m/s (26 ft/s)
	Median Droplet Diameter, d_m (Eq. 31)	1 mm (0.04 in)
	Sprinkler Spacing	3 m × 3 m (10 ft × 10 ft)
	Distance below ceiling	8 cm (3 in)
Vent	Dimensions	1.2 m × 2.4 m (4 ft × 8 ft)
	Bulk Response Time Index, RTI	175 (m·s)$^{\frac{1}{2}}$ (317 (ft·s)$^{\frac{1}{2}}$)
	Activation Temperature	74°C (165°F)

Table 5: Input parameters used for the cartoned plastic fire simulations. Note that the grid dimensions varied from case to case, but the cell size did not. The dimensions listed above represent the largest calculations performed.

Figure 42: Photograph of Plastic Test P-5.

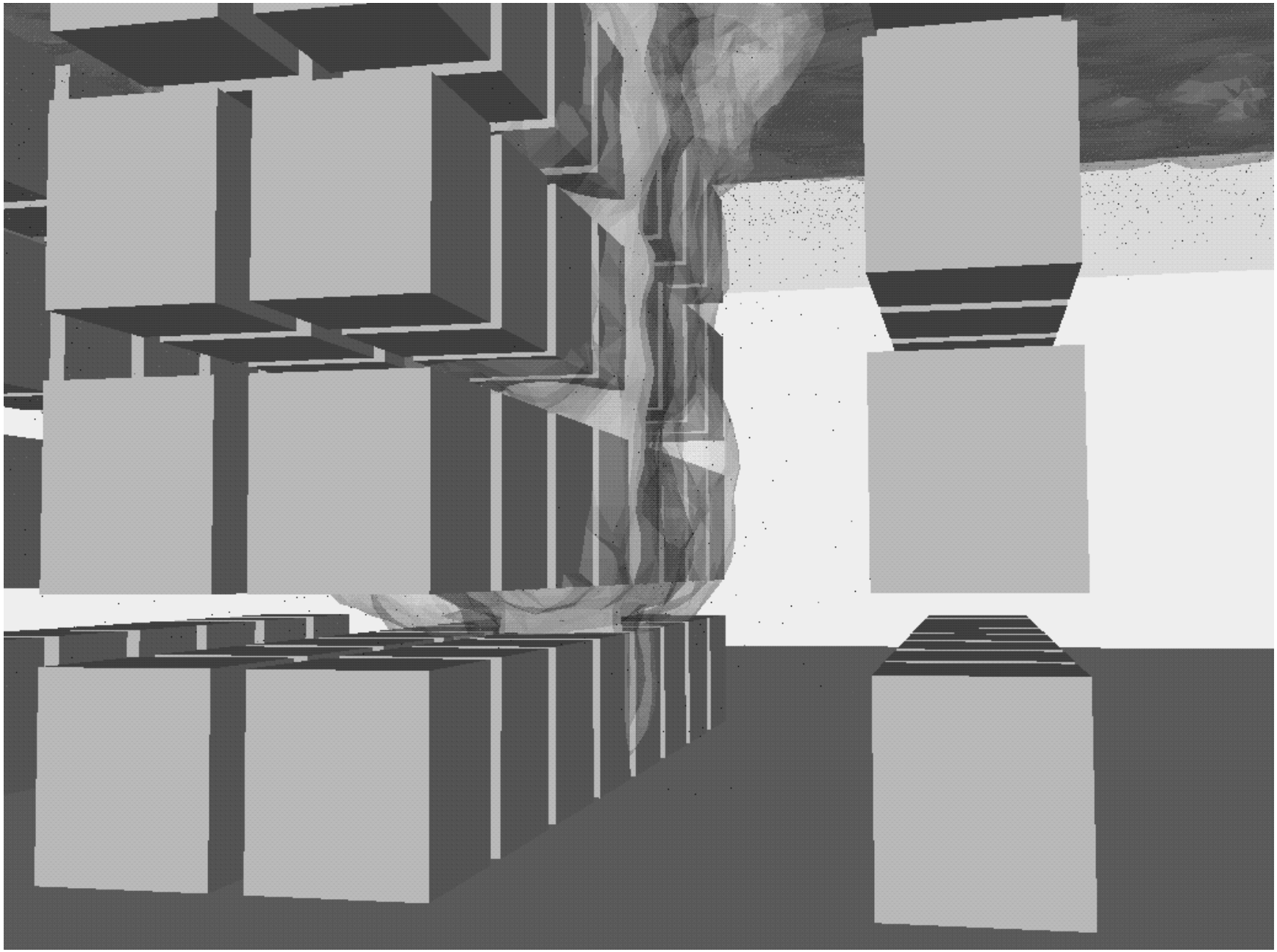

Figure 43: Numerical simulation of Plastic Test P-5.

7.2 Model Results

The first series of heptane spray burner tests provided a rich set of data with which to validate the hydrodynamics and sprinkler spray algorithm of the model. Then, the flame spread and fire growth algorithms were used to predict the results of the calorimetry burns conducted at UL. The empirical extinction algorithm (Eq. 46) was checked against commodity classification data reported in Ref. [48]. Finally, the model, as developed and verified, was used in the analysis of the cartoned plastic commodity fires to verify that certain phenomena observed during the tests were not anomalies, and also to explore various "what ifs" that could not be studied experimentally.

7.2.1 Heptane Spray Burner Test Series I

Numerical simulations of the first series of heptane spray burner experiments were performed to check the accuracy of the hydrodynamic and sprinkler spray models. For Tests I-1–16 in which the draft curtains were installed, the computational domain extended from the floor to a height 2 m (7 ft) above the ceiling, and encompassed the area enclosed by the draft curtains. For Tests I-17–22, the domain was extended beyond where the draft curtains were in the previous tests to account for the extra ceiling area. The numerical grid in all cases consisted of 186,624 cells, with dimensions 72 by 72 by 36, with the grid cells stretched in the vertical direction to cluster more cells near the ceiling. The width of each cell was about 0.3 m (1 ft), the height varied from about 0.15 m to 0.45 m (0.5 ft to 1.5 ft). Calculations performed with denser grids did not change the results significantly.

Heat losses to the ceiling were computed by solving a one-dimensional heat conduction equation for the internal temperature of the insulating tile. Because this is an insulating material, the heat losses to the ceiling were not significant compared with the energy absorbed by the sprinkler sprays. Over the fire the energy lost to the ceiling was on the order of 2 to 4 kW/m^2, and it dropped off rapidly in the radial direction.

The convective heat release rate for the heptane spray burner was measured using the large hood at UL. For the sizes of fires used in the tests, about 65% of the total heat release rate was convective. This was the number used by the model to define the heat output of the fire. The radiative energy did not play a role in the numerical simulation of a single gas burner. The calculations of the cartoned plastic commodity fires discussed in the following sections did not neglect radiation heat transfer because it was an important component of the flame spread algorithm.

The most obvious check of the numerical model is how well it predicted sprinkler activation times. Examination of the activation times of nearby sprinklers was also important, especially in cases where several sprinklers were at equal distances from the fire and, in theory, should have activated at the same time. Table 6 presents a summary of the numerical simulations, comparing the number and time of sprinkler activations and the average peak temperatures near the fire. Appendix A.1 contains the complete sprinkler activation history for all 22 tests, both experimental and numerical. Appendix A.2 contains thermocouple data at sprinklers near the fire, along with the numerical predictions.

In most of the tests, the numerical model predicted the activation of the first four sprinklers surrounding the fire to within about 5 or 10 s. For the next ring of sprinklers, the model underpredicted the activation times by 15 to 30 s, on average. This difference probably was due to the uncertainty in the droplet size distribution. Work is still underway to more accurately measure the

Heptane Spray Burner Test Series I Simulations										
Test No.	Burner Pos.	Vent Operation	Avg. Act. Time First Row		No. of Sprinklers		Avg. Peak Temp. (C)		Draft Curtains	Heat Release Rate MW @ s
			Exp.	Sim.	Exp.	Sim	Exp.	Sim.		
I-1	B	Closed	1:09	1:08	11	12	137	148	Yes	4.4 @ 50
I-2	B	Manual (0:40)	1:10	1:12	12	9	134	137	Yes	4.4 @ 50
I-3	B	Manual (1:30)	1:09	1:12	12	10	138	141	Yes	4.4 @ 50
I-4	C	Closed	1:05	1:09	10	10	136	142	Yes	4.4 @ 50
I-5	C	Manual (0:40)	1:16	1:10	9	8	125	132	Yes	4.4 @ 50
I-6	C	Manual (1:30)	1:24	1:13	8	8	137	134	Yes	4.4 @ 50
I-7	C	74°C link (DNO)	1:13	1:09	10	10	133	142	Yes	4.4 @ 50
I-8	B	74°C link (9:26)	1:09	1:09	11	12	125	148	Yes	4.4 @ 50
I-9	D	74°C link (DNO)	1:18	1:12	12	12	134	143	Yes	4.4 @ 50
I-10	D	Manual (0:40)	1:22	1:16	13	12	133	136	Yes	4.4 @ 50
I-11	D	74°C link (4:48)	N/A	N/A	N/A	N/A	196	152	Yes	4.4 @ 50
I-12	A	Closed	1:13	1:22	14	12	138	148	Yes	4.4 @ 50
I-13	A	74°C link (1:04)	1:29	1:48	5	4	119	114	Yes	6.0 @ 60
I-14	A	Manual (0:40)	1:58	2:14	7	4	116	108	Yes	5.8 @ 60
I-15	A	Manual (1:30)	1:08	1:19	5	4	143	153	Yes	5.8 @ 60
I-16	A	74°C link (1:46)	2:03	2:56	4	4	110	106	Yes	5.0 @ 110
I-17	B	100°C link (DNO)	1:06	1:01	4	10	105	122	No	4.6 @ 50
I-18	C	100°C link (DNO)	1:06	1:05	4	9	98	113	No	3.7 @ 50
I-19	A	100°C link (10:00)	1:06	1:15	10	12	110	127	No	4.6 @ 50
I-20	A	74°C link (1:20)	1:50	1:25	4	4	104	117	No	4.2 @ 50
I-21	C	74°C link (7:00)	1:05	1:03	10	10	119	125	No	4.6 @ 50
I-22	D	100°C link (DNO)	1:04	1:00	6	12	115	131	No	4.6 @ 50

Table 6: Results of the heptane spray burner Series I simulations. Note that "Avg. Peak Temp." in this table refers to the average peak temperature of the nearest 16 sprinkler-mounted thermocouples. The "Avg. Act. Time First Row" is the average activation time of the nearest 4 sprinklers.

droplet size distribution. A sensitivity analysis was performed to determine what parameters had the most impact on the results of the calculations, and droplet size was shown to be one of the more important. The reason for this is because the heat transfer between the hot gases and the droplet is directly proportional to the surface area of the droplet. Thus doubling the size of the droplets reduces the number of droplets by a factor of 8 and reduces the heat transferred from the gas by a factor of 4.

7.2.2 Fire Growth Validation

Experimental burns of the cartoned plastic commodity were performed at UL. Two, three and four tier configurations were tested. The ignition method was the same as the large scale commodity burns. Figure 44 plots the total[11] heat release rates versus time for the three experiments up to the point where water was applied. Figure 45 shows the convective[12] heat release rates for the same experiments compared with those computed in the numerical model. Figure 46 shows what one of these calculations looks like. For the period of time before water application, the simulation heat release rate is within 20% of the experiment.

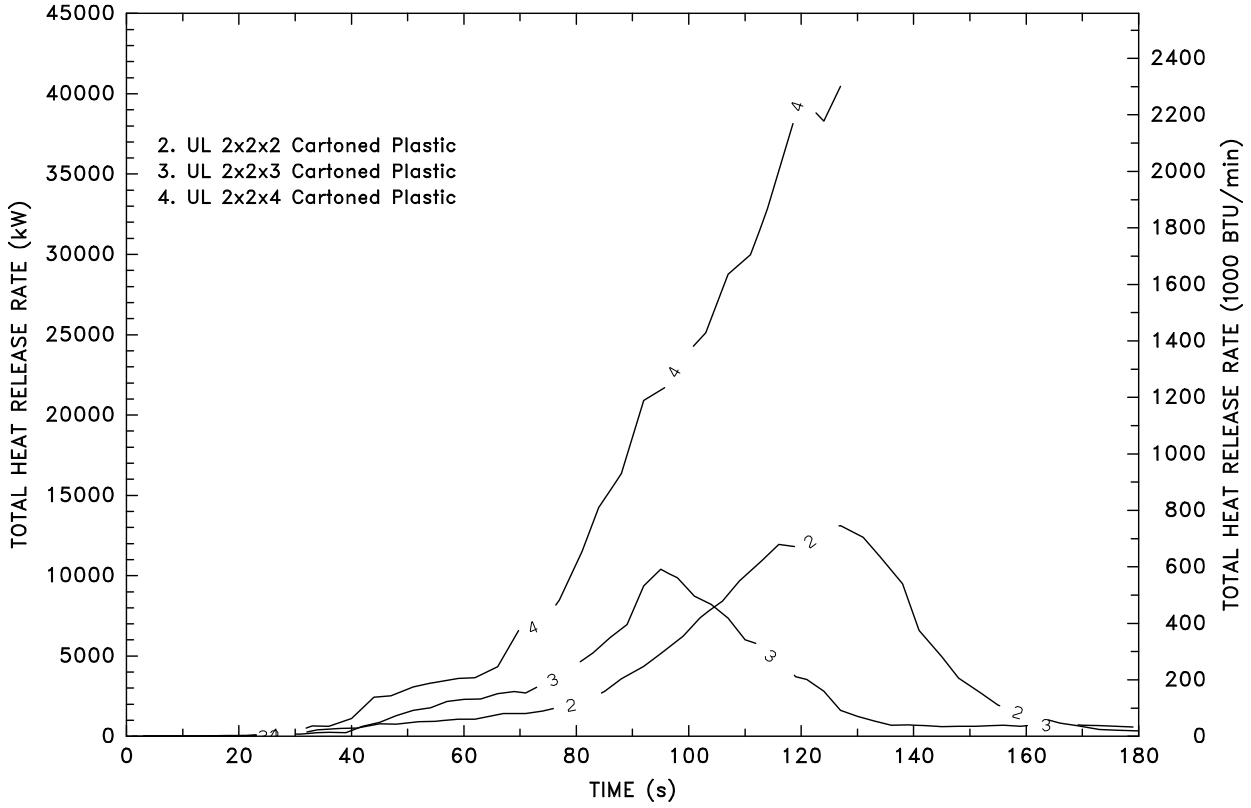

Figure 44: Total heat release rates for the two, three and four tier cartoned plastic commodity calorimetry burns. Water was applied to the fire at 130 s in the two tier test, and at 95 s in the three tier test.

[11] Based on oxygen consumption calorimetry.

[12] Based on measurement of the temperature and velocity of the exhaust gases through the hood.

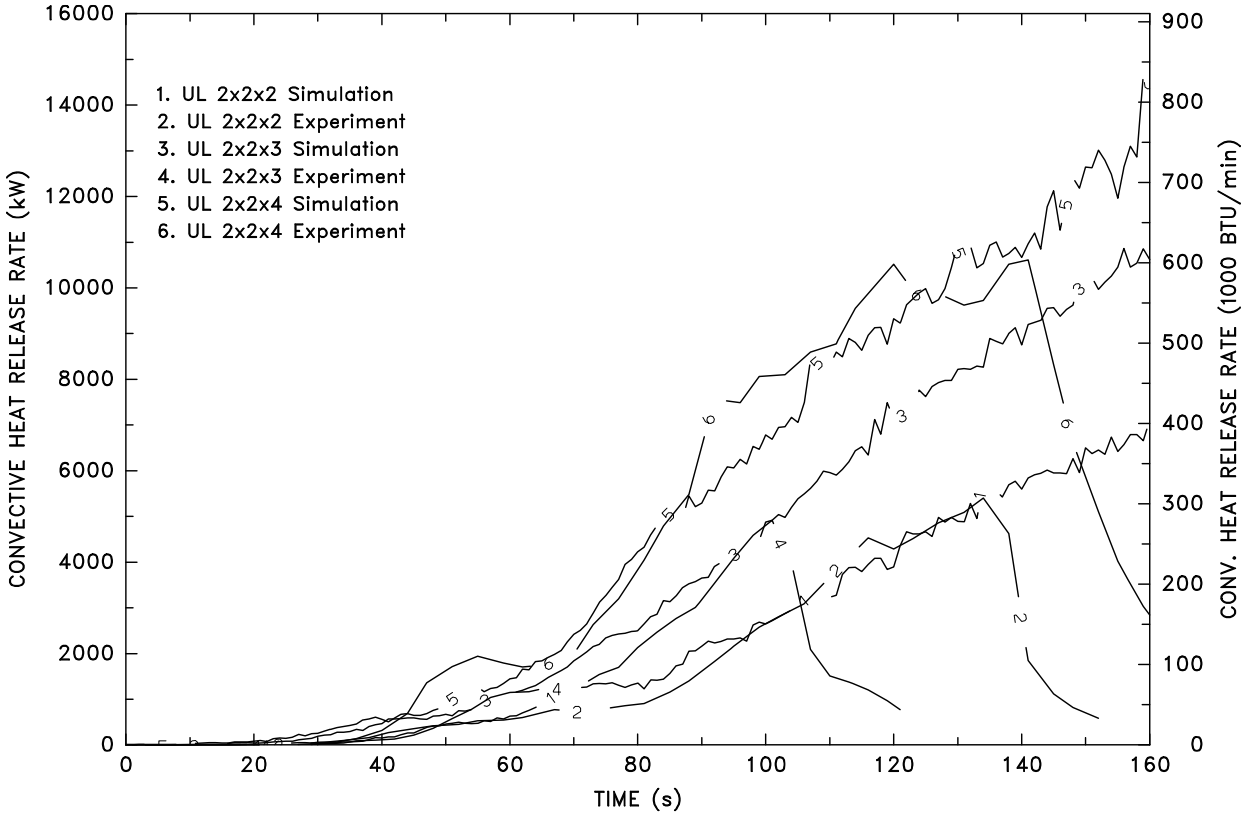

Figure 45: Comparison of experimental and simulated convective heat release rates for the two, three and four tier cartoned plastic calorimetry burns. Water was applied to the fire at 130 s in the two tier test, and 95 s in the three tier test. The simulations were performed with no water application.

Similar calorimetry experiments have been performed at Factory Mutual. There are two differences between the tests performed at FM and those at UL. The first is that the first pallet in the FM tests is raised 23 cm (9 in) off the floor whereas the first tier at UL is on the floor. Second, the FM burns are centrally ignited with four half-ignitors arranged in a pinwheel pattern at the intersection of the four pallets, whereas the UL burns are ignited in the center of one of the lateral flues with two half-ignitors, one on each side of the flue. As a result, the fire growth with the FM configuration is more rapid because of the fire has access to more fresh air from all four flues and from beneath. Figures 47 and 48 present the results of the FM burns, compared with the corresponding simulations.

The fire growth of the 2, 3 and 4 tier UL burns was also measured by taping bare-bead thermocouples to the sides of the boxes in order to determine at what time the fire had reached that particular place. Small scale experiments in the LIFT apparatus at NIST indicated a piloted ignition temperature for the cardboard to be about 370°C (700°F) [36, 37]. Using this temperature as an indicator of ignition, the simulation and experiment could be compared. Tables 7 and 8 give the locations and ignition times for the 2 and 4 tier experiments and simulations. The comparison between the two sets of data shows some large differences in ignition times, especially for locations outside of the ignition flue and far from the ignition point. This is to be expected, given the

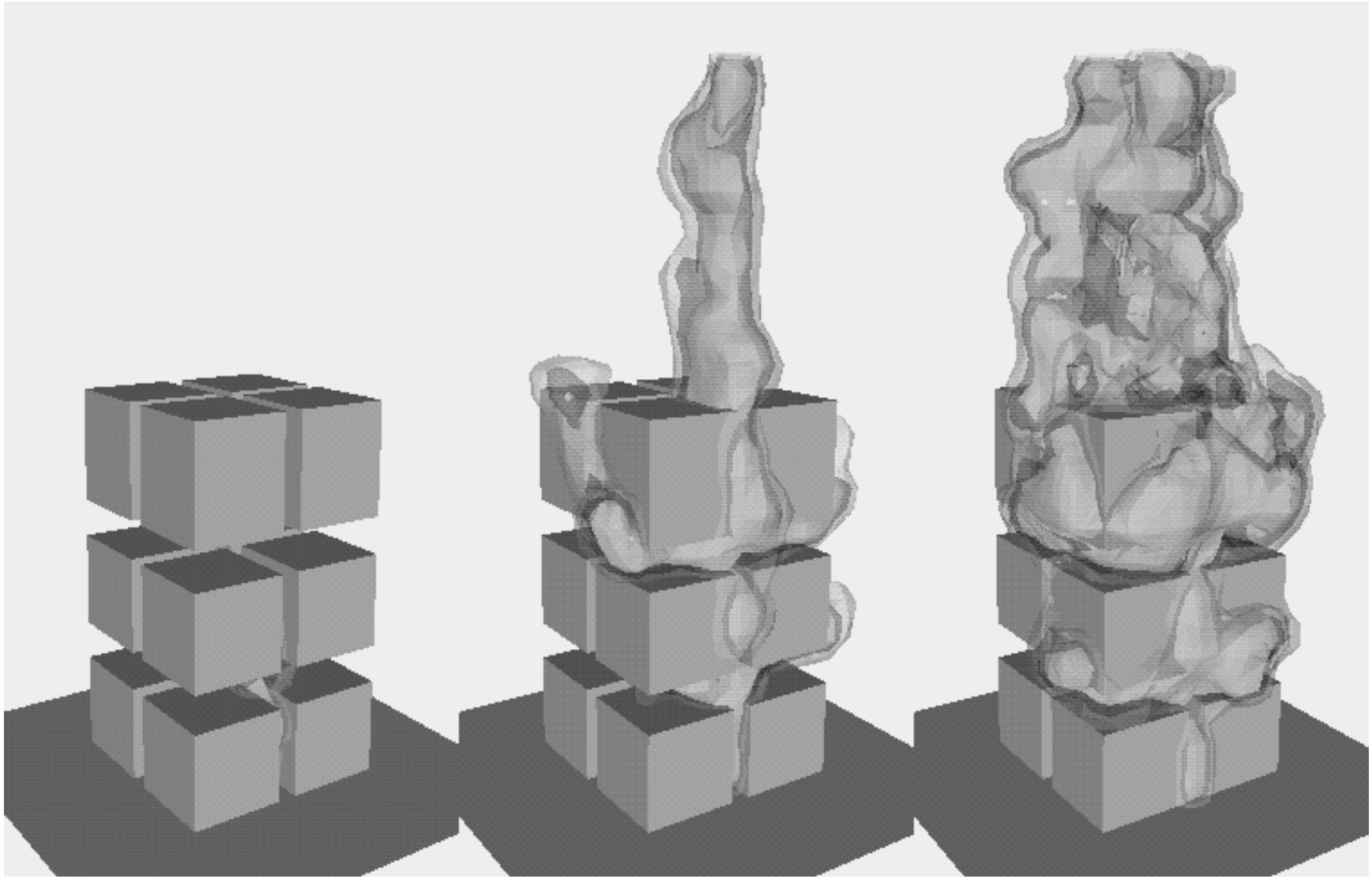

Figure 46: Simulation of three tier calorimetry burn at 30, 60 and 90 s following ignition.

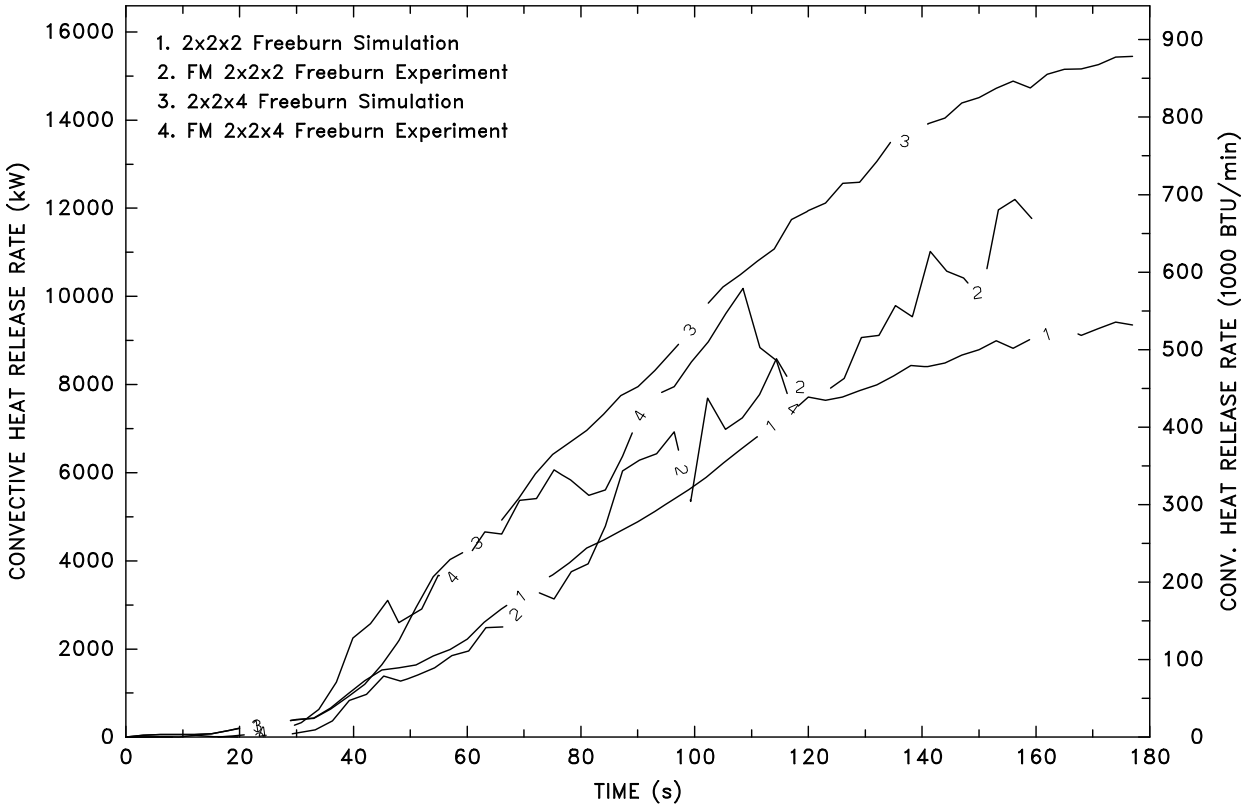

Figure 47: Comparison of experimental and simulated heat release rates for the $2 \times 2 \times 2$ and $2 \times 2 \times 4$ cartoned plastic calorimetry burns conducted at Factory Mutual. The ignition point was centrally located and the first tier pallet was raised 23 cm (9 in) off the ground. The actual experiments were extinguished with a large amount of water. The simulations did not include a water spray.

simplistic combustion sub-models. Nevertheless, the agreement with the heat release rate data is encouraging. It provides validation for the methodology for at least a few minutes of simulation, during which time most of the important interactions are taking place. The model in its present form can be used to analyze the cartoned plastic commodity experiments for the first few minutes. For longer times, a better characterization of the burning and extinguishment processes need to be developed and incorporated into the model.

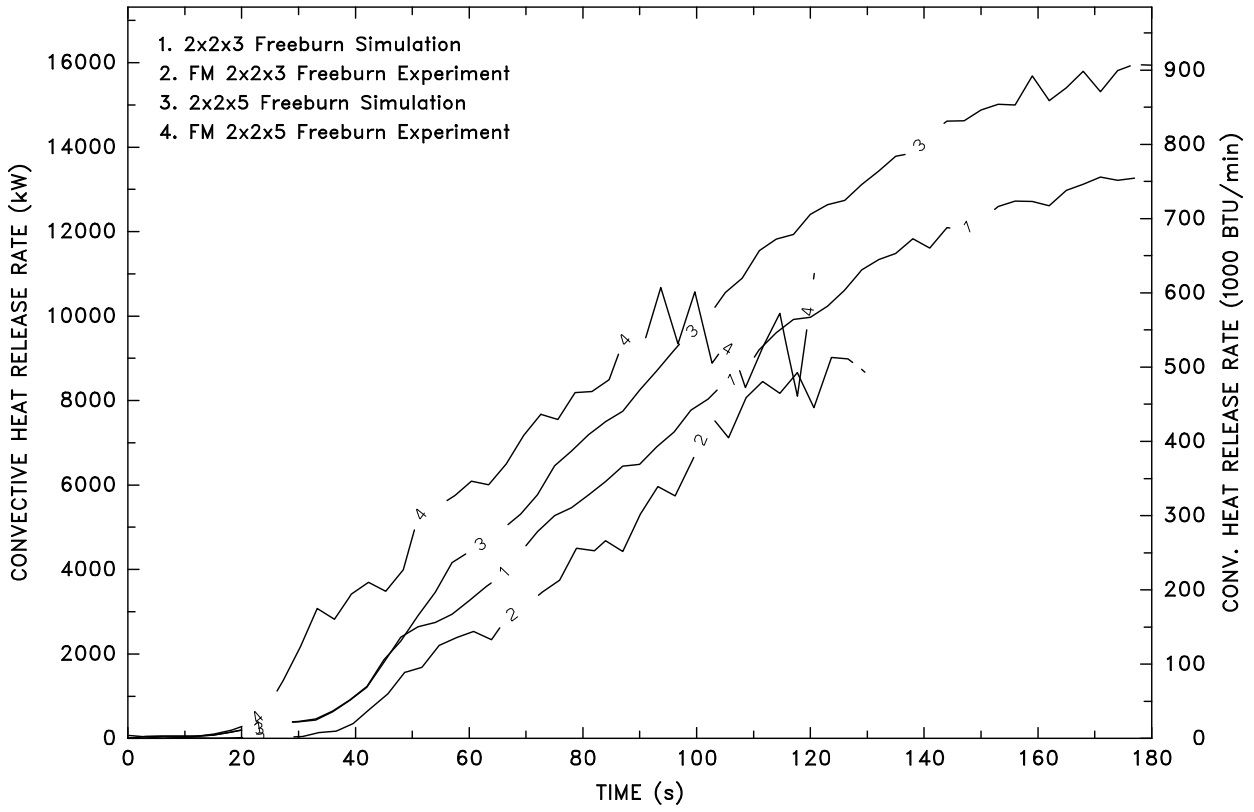

Figure 48: Comparison of experimental and simulated heat release rates for the $2 \times 2 \times 3$ and $2 \times 2 \times 5$ cartoned plastic calorimetry burns conducted at Factory Mutual. The ignition point was centrally located and the first tier pallet was raised 23 cm (9 in) off the ground. The actual experiments were extinguished with a large amount of water. The simulations did not include a water spray.

Two Tier Cartoned Plastic Calorimetry Burn					
TC coordinates (m)			Ignition Times (s)		
x	y	z	Exp.	Sim.	Diff.
-0.69	0.08	2.27	69	69	0
-0.76	0.08	1.19	99	80	-19
-0.69	0.08	1.12	93	71	-22
-0.76	0.00	2.64	82	78	-4
-0.76	0.00	1.12	100	86	-14
-0.46	0.08	1.19	72	68	-4
-0.28	0.08	1.19	60	55	-5
-0.08	0.08	1.19	53	50	-3
0.08	0.08	1.19	60	50	-10
0.28	0.08	1.19	72	68	-4
0.46	0.08	1.19	84	75	-9
0.27	0.00	1.12	58	57	-1
-0.46	0.00	2.11	50	56	+6
-0.08	0.00	2.11	38	45	+7
0.08	0.00	2.11	47	45	-2
0.46	0.00	2.11	67	67	0
-0.46	0.00	2.64	48	59	+11
-0.28	0.00	2.64	39	49	+10
-0.08	0.00	2.64	38	49	+11
0.08	0.00	2.64	48	49	+1
0.28	0.00	2.64	55	58	+3
0.46	0.00	2.64	62	69	+7

Table 7: Location of thermocouples relative to the ignition point and the ignition times of the experiment and the numerical simulation for the two tier high cartoned plastic commodity burn. The x coordinate indicates the distance along the ignition flue, with the negative direction being towards the center of the array, the y coordinate indicates the distance down the non-ignition flue, and the z coordinate indicates the height off the floor. All dimensions are in meters.

Three Tier Cartoned Plastic Calorimetry Burn					
TC coordinates (m)			Ignition Times (s)		
x	y	z	Exp.	Sim.	Diff.
-1.50	0.00	4.95	86	89	+3
-0.95	0.00	4.95	72	74	+2
-0.69	0.80	4.95	78	90	+12
-0.69	0.27	4.95	69	69	0
-0.27	0.00	4.95	42	56	+14
0.00	0.00	5.25	42	60	+18
-1.50	0.00	3.50	98	95	-3
-0.95	0.00	3.50	83	75	-8
-0.69	0.27	3.50	71	67	-4
-0.69	0.80	3.50	81	92	+11
-0.27	0.00	3.50	41	44	+3
0.00	0.00	3.75	38	48	+10
-1.50	0.00	1.95	93	104	+11
-0.95	0.00	1.95	93	73	-20
-0.69	0.27	1.95	71	68	-3
-0.69	0.80	1.95	81	90	+9
-0.27	0.00	1.95	38	29	-9
0.00	0.00	2.20	31	31	0
0.27	0.00	1.95	33	35	+2
-0.27	1.07	1.95	81	–	–

Table 8: Location of thermocouples relative to the ignition point and the ignition times of the experiment and the numerical simulation for the four tier high cartoned plastic commodity burn. The x coordinate indicates the distance along the ignition flue, with the negative direction being towards the center of the array, the y coordinate indicates the distance down the non-ignition flue, and the z coordinate indicates the height off the floor. All dimensions are in meters.

7.2.3 Cartoned Plastic Commodity Fire Simulations

A very useful application of the numerical model has been to simulate the five cartoned plastic commodity tests discussed in Section 5 in order to explain and evaluate the results of the experiments. The benefit of the numerical model in this application is that it provides a consistent means of varying test parameters. In other words, if two calculations are performed in which only one input parameter is different, then the difference in the results of the two calculations can safely be attributed to the difference in the input parameter. A drawback of large scale testing is that this type of sensitivity analysis usually requires more tests than can be afforded. If a sufficient number of replicates cannot be performed, then the outcomes of the experiments are often subject to debate as to whether differences in test results were due to changes in test parameters or due to random variations.

Consider, for example, the different outcomes of Tests P-1 and P-4 in which the only difference in test parameters was that draft curtains were installed for Test P-4, but not for Test P-1. Twenty sprinklers activated in Test P-1, five in Test P-4. Was this result due to the draft curtains? One would expect that the draft curtains would have increased the number of activations, not decreased them, based on the results of the first heptane spray burner series. To gain some insight, the numerical model was run to simulate the experiments. Test P-1 was run two ways. First, the simulation was run with no manipulation of the sprinkler activation times (Fig. 49). Second, the calculation was repeated, but with the second sprinkler intentionally delayed a minute to mimic what actually occurred during the experiment (Fig. 50). The reason for modifying the sprinkler activation pattern was to see how the delay could have led to the different outcomes observed in the tests. Tests P-4 and P-5 were simulated without any modification of the sprinkler activation times (Figs. 51 and 52). In the simulations of Test P-4 and Test P-1 without any imposed sprinkler delay, 4 sprinklers activated. In the simulation of Test P-1 with the sprinkler delay, 17 sprinklers activated within the first 5 min. In the actual Test P-1, 20 sprinklers activated, but over about 15 min. The model demonstrated the effect of delaying the second sprinkler. The difference in outcomes of Tests P-1 and P-4 of the cartoned plastic test series was not due to the draft curtains, but rather to the sprinkler delay in Test P-1.

Figure 53 presents the heat release rates for the simulations of Test P-1 (with and without sprinkler delay) and Test P-4. The activation times for the first sprinkler in all cases was between 69 and 71 s. In the case where the second sprinkler is delayed from opening for 58 s (Test P-1, delay), the heat release rate is substantially greater than the cases where both sprinklers activate nearly at the same time (Test P-1, no delay and Test P-4).

If the increased number of sprinkler activations of Test P-1 over Test P-4 can be attributed to the delay of the second nearest sprinkler, did the draft curtains have any effect at all? Comparing the simulation of Test P-4 with the ‘no delay’ simulation of Test P-1, there is not much difference in heat release rates. The overall temperatures near the ceiling are slightly higher in Test P-4, most likely due to the containment of the hot gases by the curtains. This was seen in the analysis of the first series of heptane spray burner tests.

Another interesting case to examine with the numerical model is Test P-2, where the ignition point was directly under the vent, but the vent did not open. What if it had? A calculation was performed where the vent was set to open automatically with a fusible link, and another calculation was done with the vent held closed. In the first calculation, the vent opened after 83 s, followed a half second later by the first sprinkler and 3 s later by the second sprinkler. In the calculation with

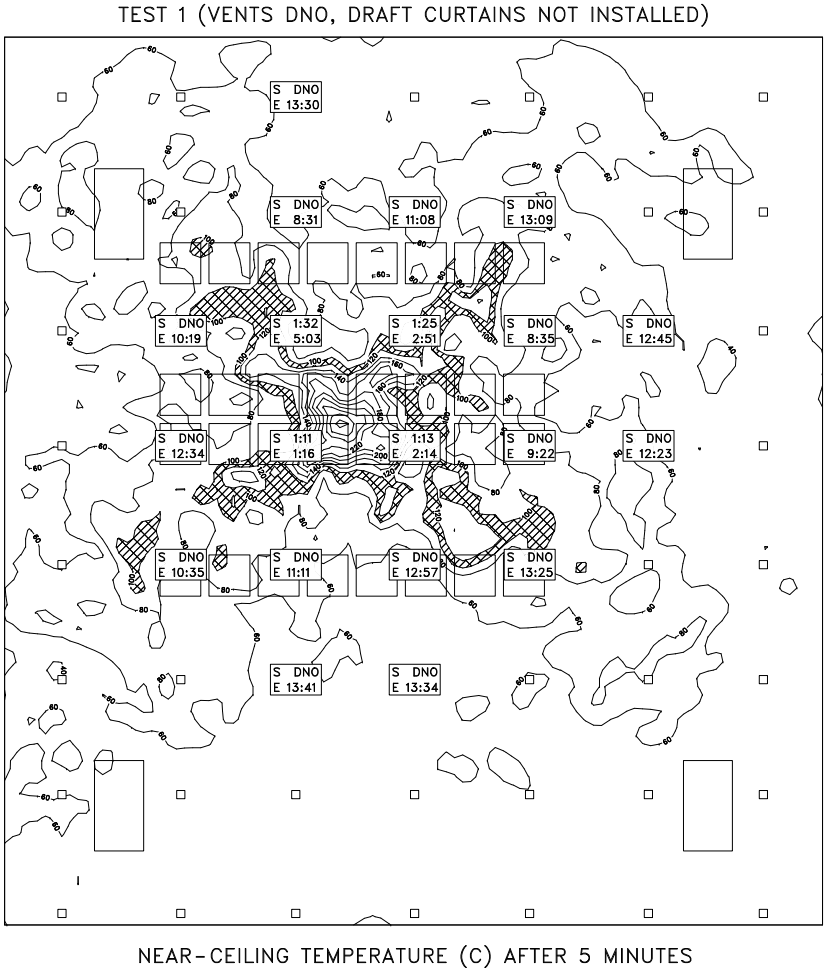

Figure 49: Results of Plastic Test P-1 simulation with no imposed delay in the second sprinkler activation. "S" denotes simulation sprinkler activation time, "E" experiment. The cross-hatched area indicates temperatures between 100 and 120°C.

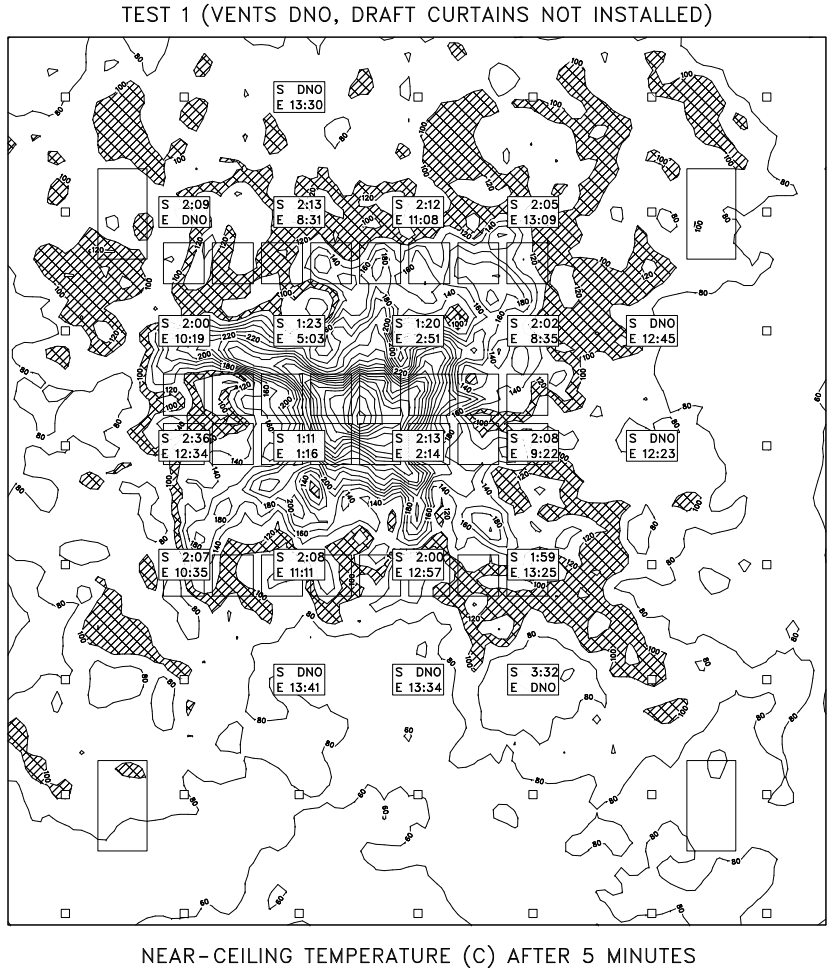

Figure 50: Results of Plastic Test P-1 simulation with the same delay imposed on the second sprinkler activation as was seen in the actual experiment. "S" denotes simulation sprinkler activation time, "E" experiment. The cross-hatched area indicates temperatures between 100 and 120°C.

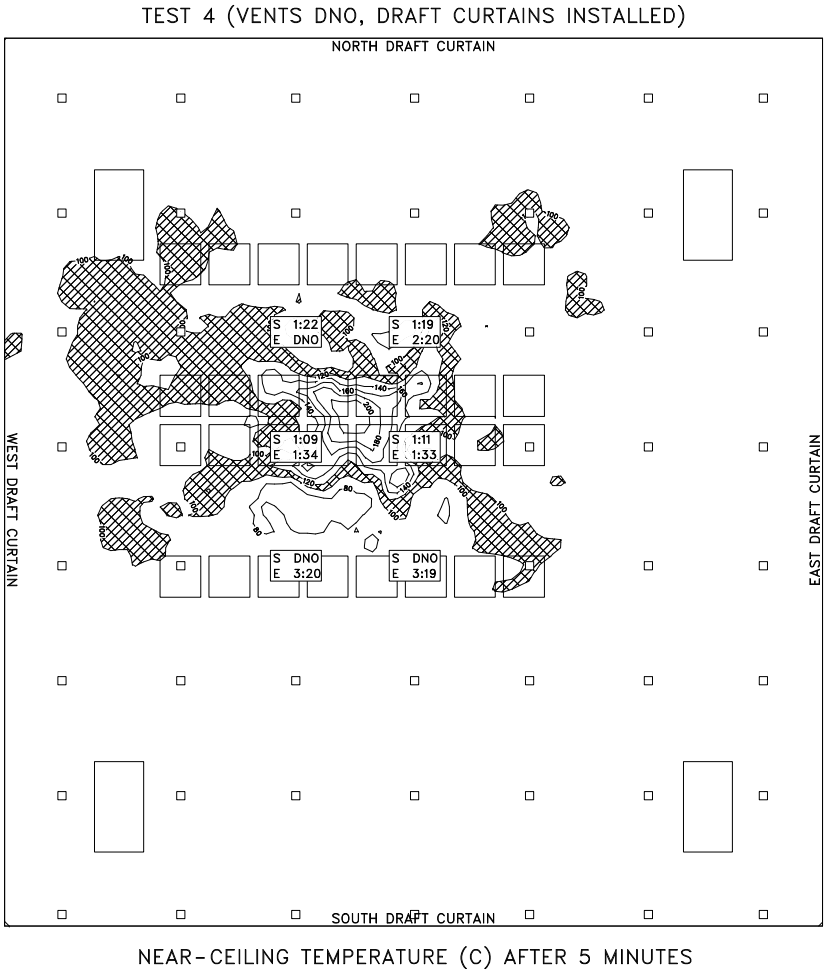

Figure 51: Results of Plastic Test P-4 simulation. "S" denotes simulation sprinkler activation time, "E" experiment. The cross-hatched area indicates temperatures between 100 and 120°C.

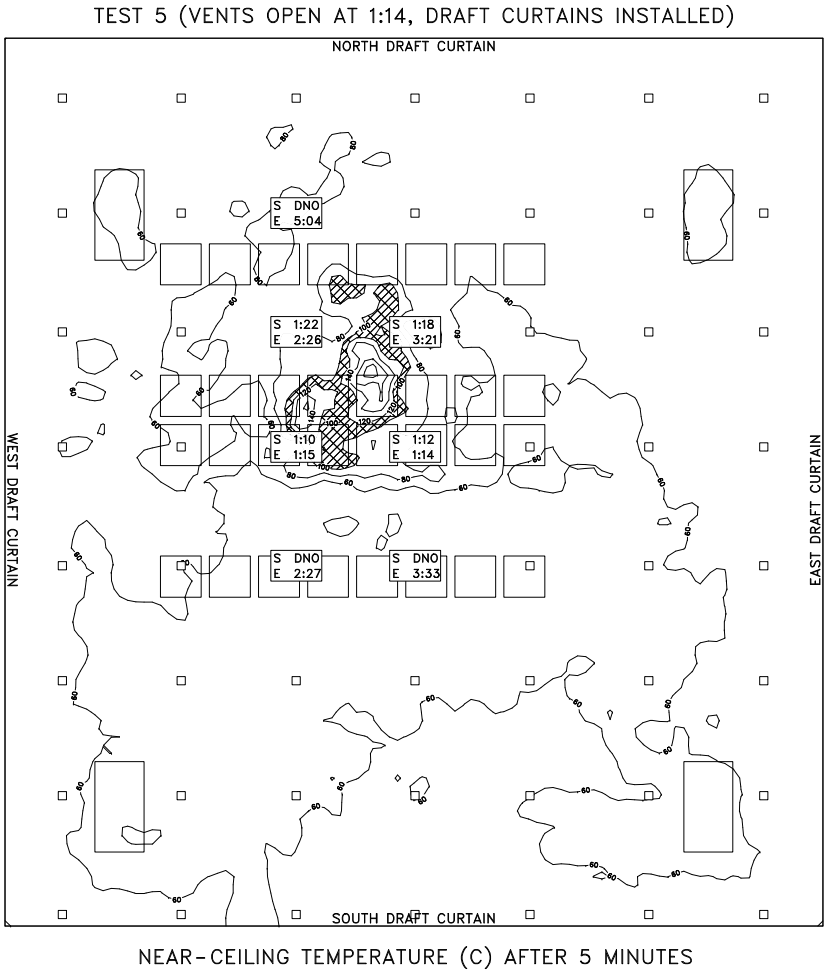

Figure 52: Results of Plastic Test P-5 simulation. "S" denotes simulation sprinkler activation time, "E" experiment. The cross-hatched area indicates temperatures between 100 and 120°C.

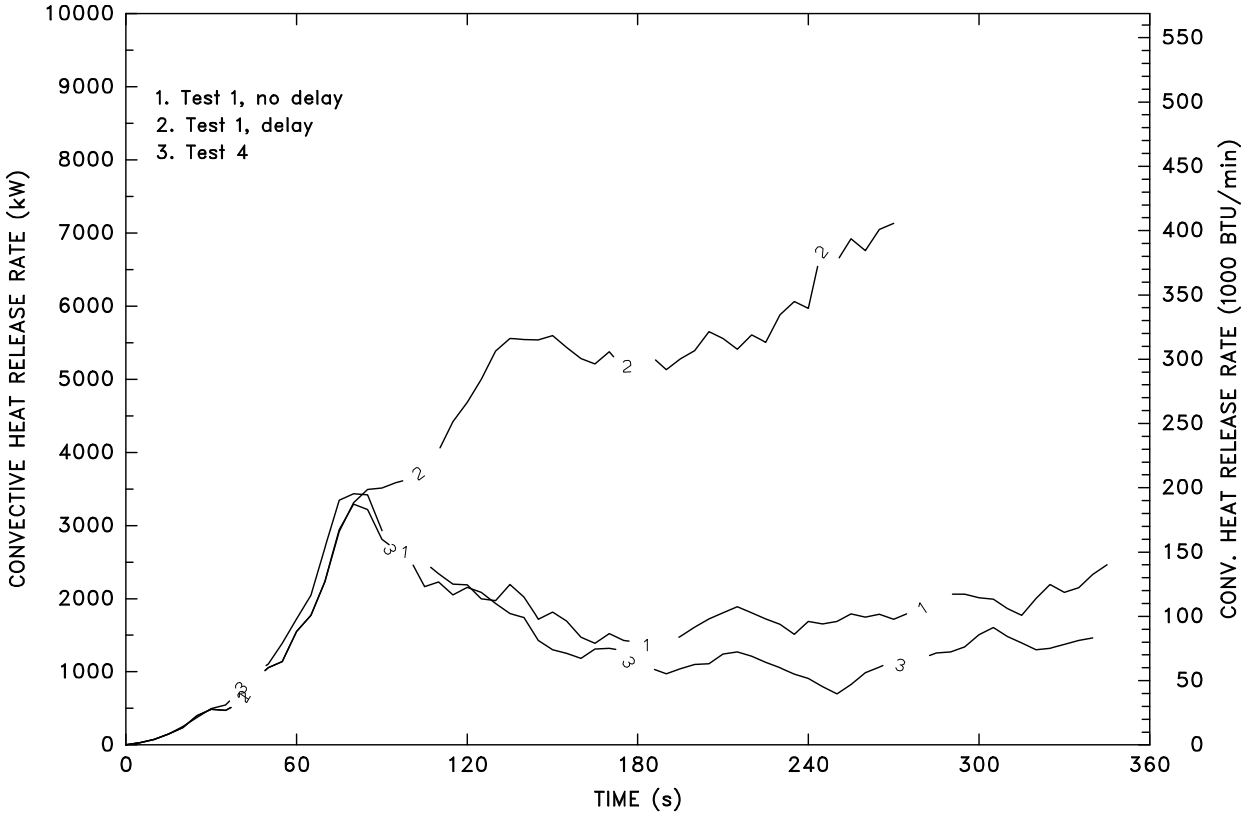

Figure 53: Heat release rates from the numerical simulations of Tests P-1 and P-4 of the Plastic series. The term 'delay' means that the second sprinkler was intentionally opened 58 s after the first in order to mimic the actual experiment.

the vent closed, the first sprinkler opened after 83 s, followed 1.4 s later by the second. Figures 54 and 55 present the results of the simulations. In the simulation where the vent opened, 14 sprinklers activated in the first 7 min following ignition. In the simulation where the vent was not allowed to open, 19 sprinklers activated in the first 7 min. This latter simulation was comparable to the actual experiment where 23 sprinklers opened in the first 6 min. The opening of the vent in the first simulation reduced the number of sprinkler activations by exhausting heat from the fire directly underneath. There is certainly plenty of evidence from the heptane spray burner tests indicating that when the fire was placed directly beneath an opened vent, the number of activations was significantly reduced.

Less clear, however, is why so many sprinklers activated in Test P-2. The simulation of Test P-1 with no manipulation of the sprinkler activation times produced only 4 activations. What was the difference between the simulation of Test P-1 and Test P-2? Only the presence of a 1.2 m by 2.4 m by 0.3 m deep (4 ft by 8 ft by 1 ft deep) cavity in the ceiling formed by the vent in Test P-2. This cavity led to a 14 s delay in the first sprinkler activation in the simulation of Test P-2. The significance of this delay is shown in Fig. 56, in which the heat release rate histories for the simulations of the two versions of Test P-2 are plotted on the same graph as the heat release rate curves for the 2 by 2 by 4 tier cartoned plastic calorimetry experiment and the simulation of Test P-1 with no second sprinkler delay. The growth of the fire during the time period 60 to 100 s after

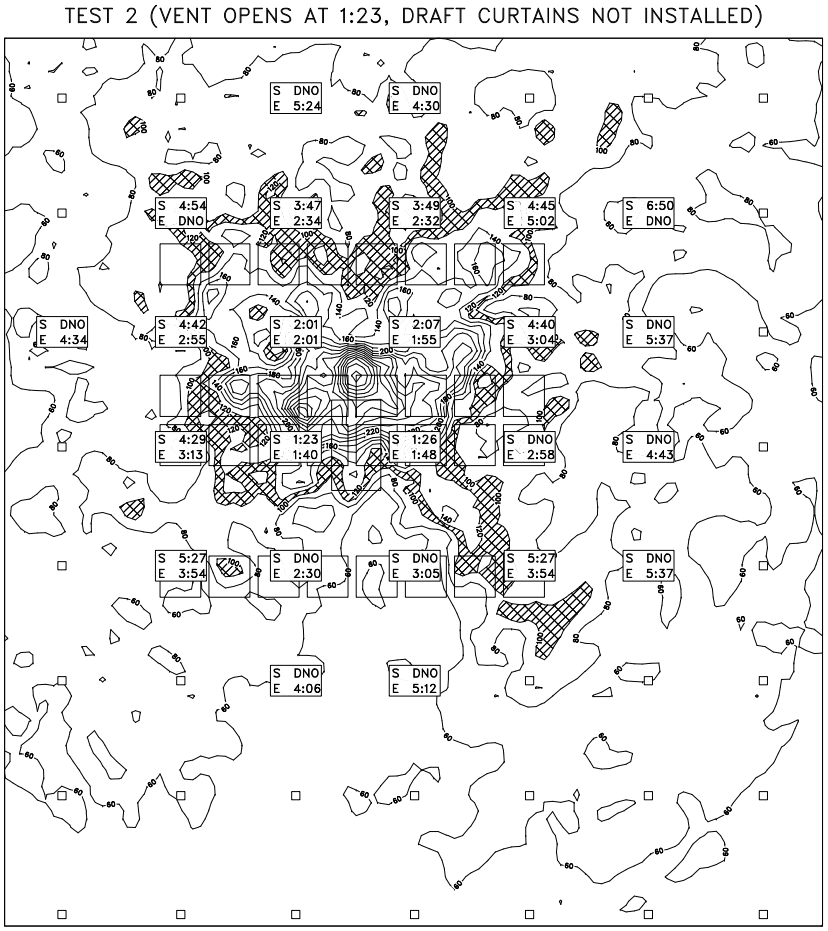

Figure 54: Results of Plastic Test P-2 simulation. “S” denotes simulation sprinkler activation time, “E” experiment. The cross-hatched area indicates temperatures between 100 and 120°C.

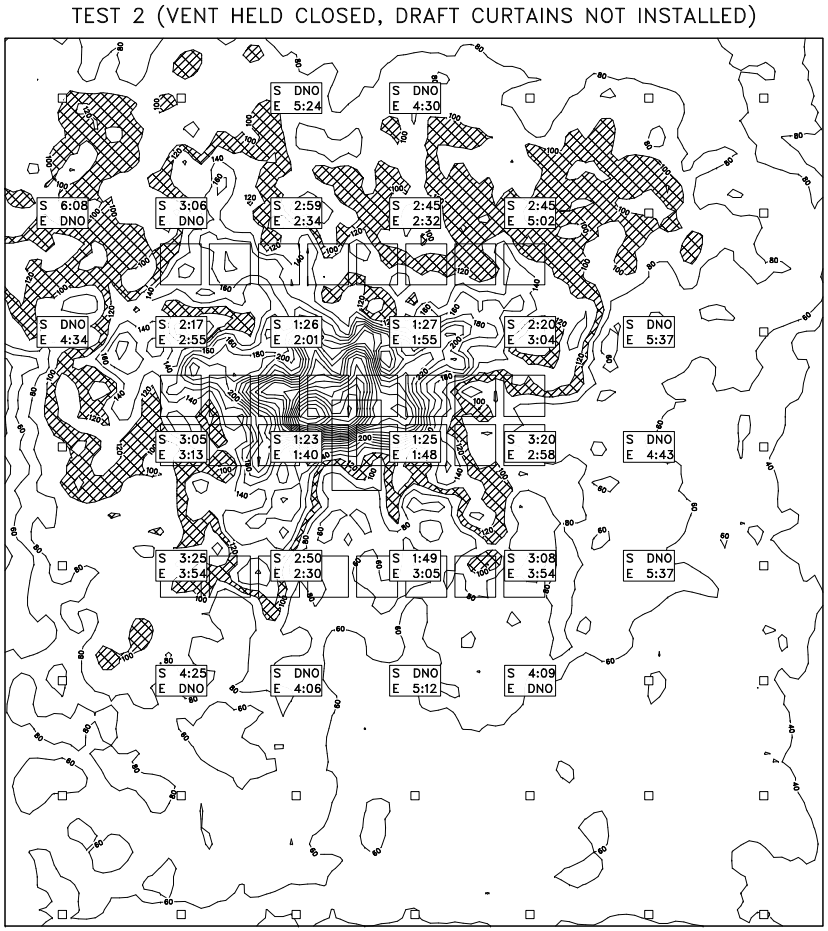

Figure 55: Results of Plastic Test P-2 simulation. “S” denotes simulation sprinkler activation time, “E” experiment. The cross-hatched area indicates temperatures between 100 and 120°C.

ignition was very fast, and it was demonstrated that even a 14 s delay in sprinkler activation could significantly alter the number of sprinkler activations.

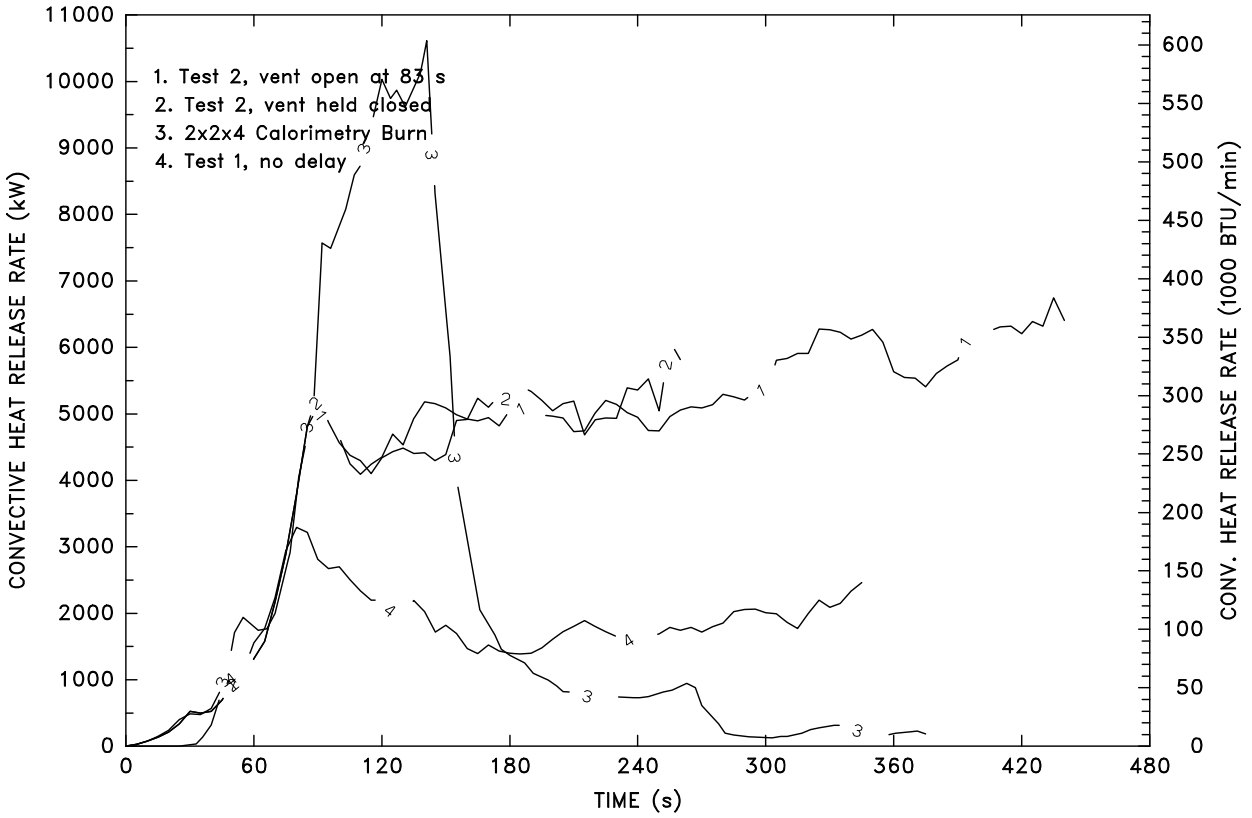

Figure 56: Heat release rates from the numerical simulations of Test P-2 of the Plastic series, plus the 2 by 2 by 4 tier calorimetry burn of cartoned plastic commodity and the simulation of Test P-1 with no second sprinkler delay.

The cartoned plastic burn that caused the most fire damage was Test P-3. In this test, the ignition point was placed close to the intersection of two draft curtains (Fig. 29). An estimated 184 boxes were consumed during the test, compared to 103 and 81 in Tests P-4 and P-5, the other two Plastic tests conducted with draft curtains in place. Figures 57 and 58 present the results of the simulations of Tests P-3 and P-4. The vent nearest the ignition point in Test P-3 opened at 4:11, and no vents opened in Test P-4, thus venting did not have any impact on the results in either case, at least for the first 4 min. Figure 59 shows the convective heat release rates for the two simulations. Clearly, the draft curtains had an effect on the performance of the sprinkler system. The draft curtains delayed the opening of the two sprinklers directly north of the first two sprinklers to activate. Less obvious, the draft curtains changed the near-ceiling flow pattern of both the sprinkler spray and the fire plume. Regardless of the sub-model used to simulate the burning of the cartoned plastic commodity, the calculation showed that less water reached the north side of the central array when the draft curtains were installed. Figure 60 shows a snapshot of the two simulations after 5 min. In Test P-3, the fire has spread to the north face of the array, whereas in Test P-4 the sprinklers in the north aisle prevent the spread to the north face.

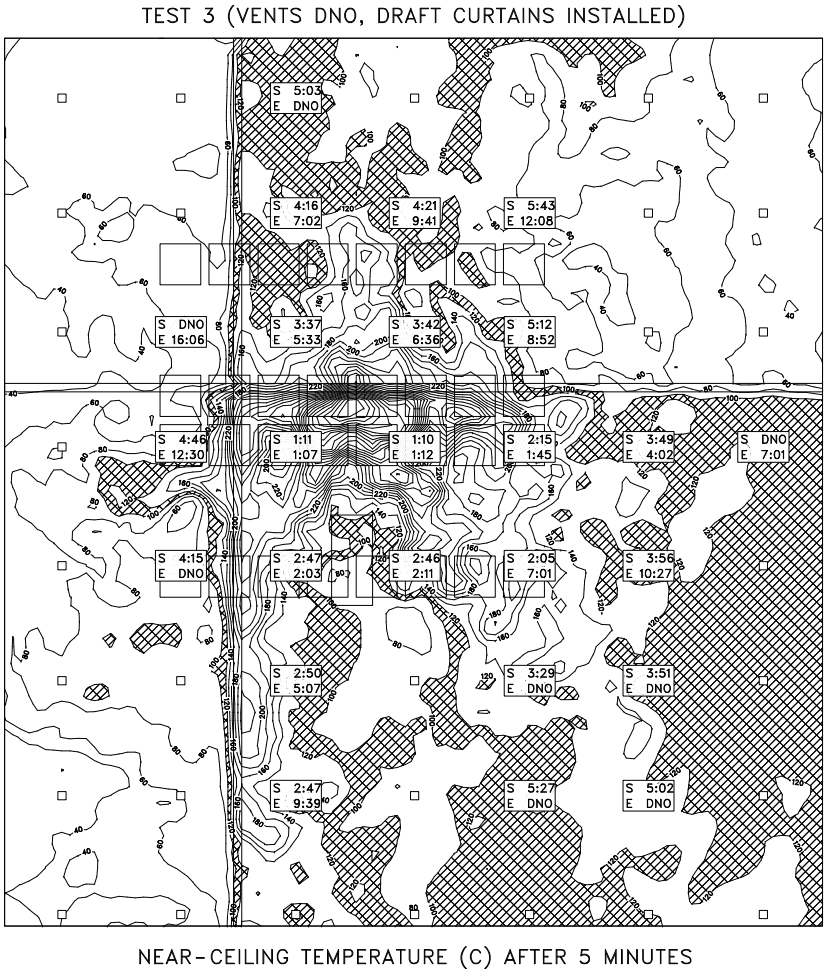

Figure 57: Results of Plastic Test P-3 simulation. "S" denotes simulation sprinkler activation time, "E" experiment. The cross-hatched area indicates temperatures between 100 and 120°C.

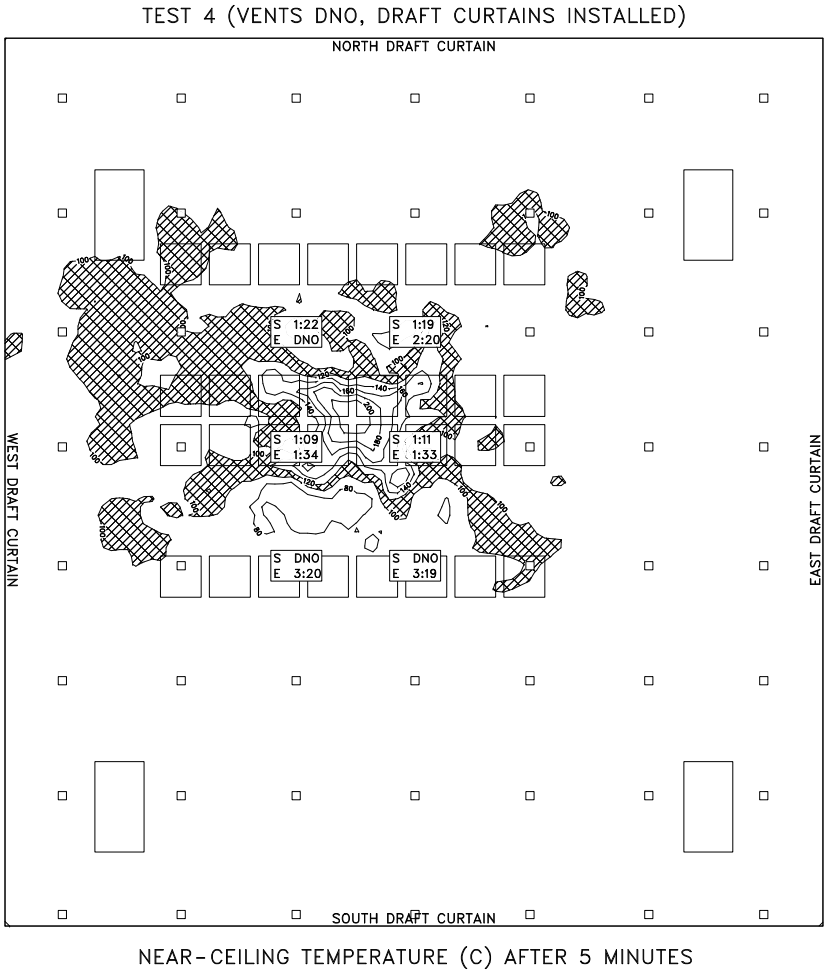

Figure 58: Results of Plastic Test P-4 simulation. "S" denotes simulation sprinkler activation time, "E" experiment. The cross-hatched area indicates temperatures between 100 and 120°C.

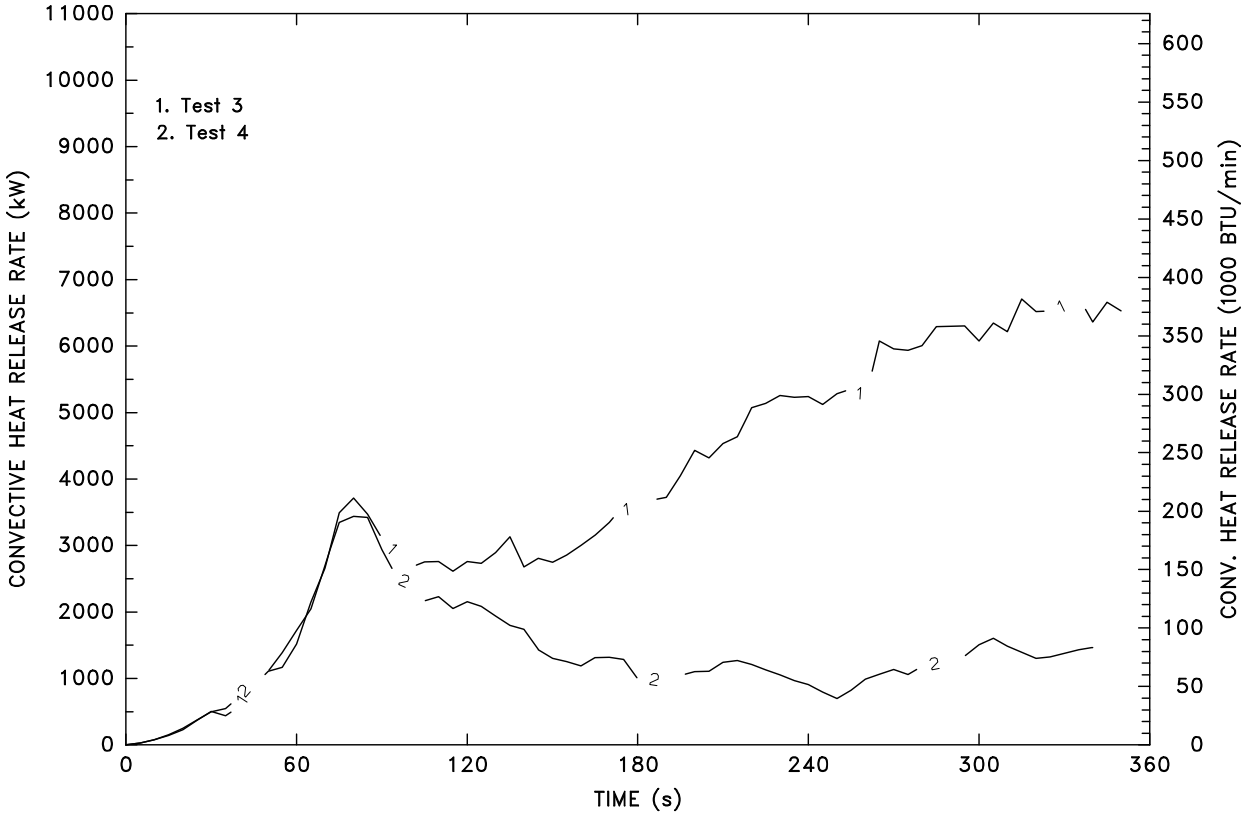

Figure 59: Heat release rates from the numerical simulations of Tests P-3 and P-4 of the cartoned plastic series.

7.2.4 Mass Flow Rates through Vents

One final use of the model was to simulate certain experiments in which important measurements could not be made. Attempts were made to measure the velocity through an opened vent to determine the mass flow rate, but the bi-directional probes produced erroneous results. These measurements of mass flow rate would have been important because the opened vents did not have a significant effect on the number of activated sprinklers or the near-ceiling gas temperatures during the second series of heptane spray burner tests (except in cases where the fire was directly underneath a vent). The heptane test data seems at odds with some experiments performed in the past, notably the Ghent experiments of 1989 [14]. The discrepancy is most likely due to different vent to floor ratios and sprinkler flow rates. These parameters would directly affect the near-ceiling temperatures and the mass flow rates through the vents. Hinkley points out in the SFPE Handbook [50] that for temperature rises less than about 75°C (167°F) there is a serious decrease in the mass flow rate through a vent. This assessment is based on the expression for mass flow rate through a vent due to buoyancy

$$\dot{m} = \frac{C\, A_v\, \rho_\infty \sqrt{2\, g\, d \Delta T\, T_\infty}}{T_\infty + \Delta T} \tag{47}$$

where C is an orifice coefficient equal to about 0.6, A_v is the area of the vent, ρ_∞ is the density of air, g is the acceleration of gravity, d is the depth of the layer of hot gases, ΔT is the average temperature rise in the layer, and T_∞ is the (absolute) ambient temperature. Figure 61 displays

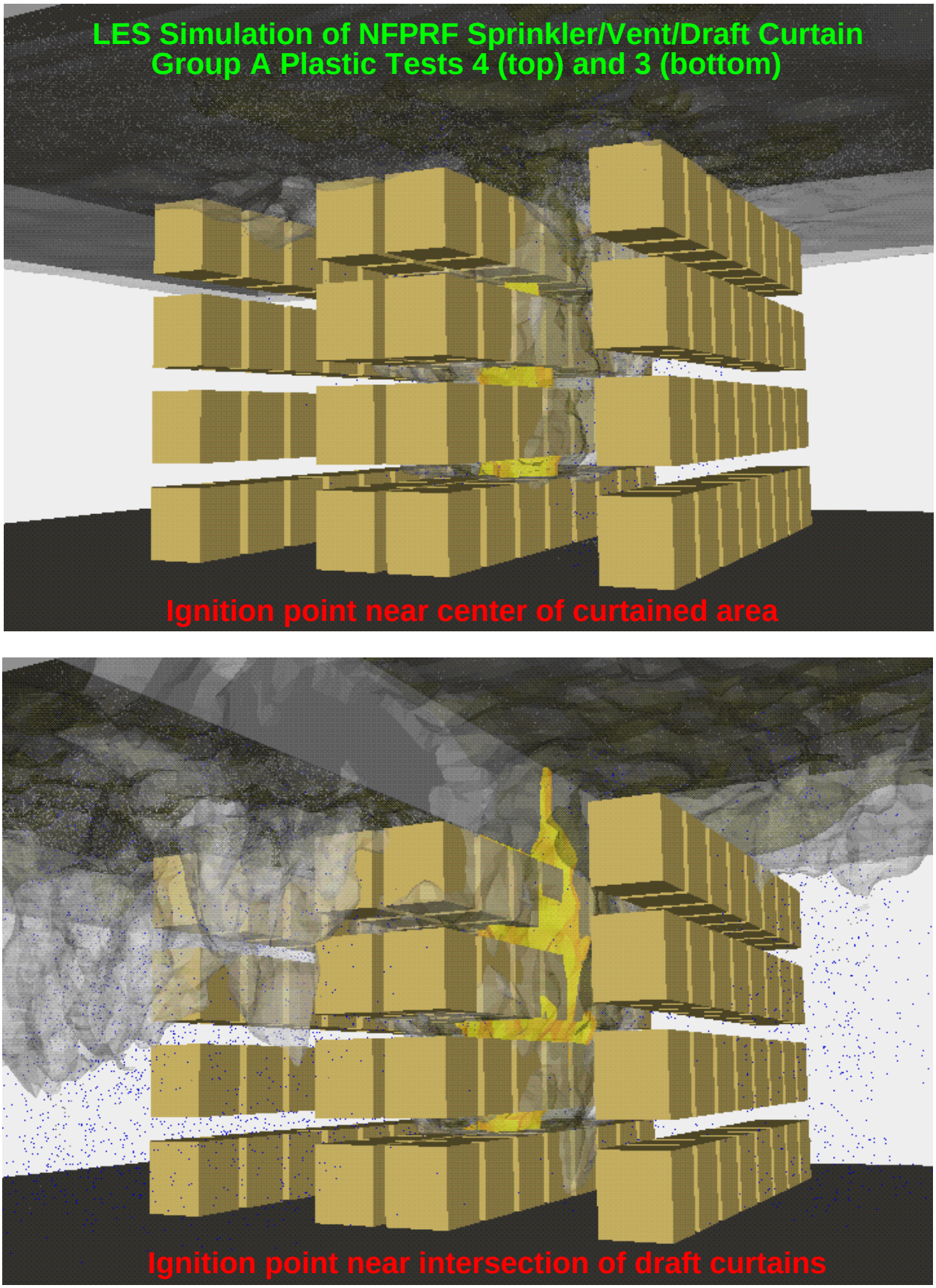

Figure 60: Snapshots of the simulations of Plastic Tests P-3 and P-4 after 5 min.

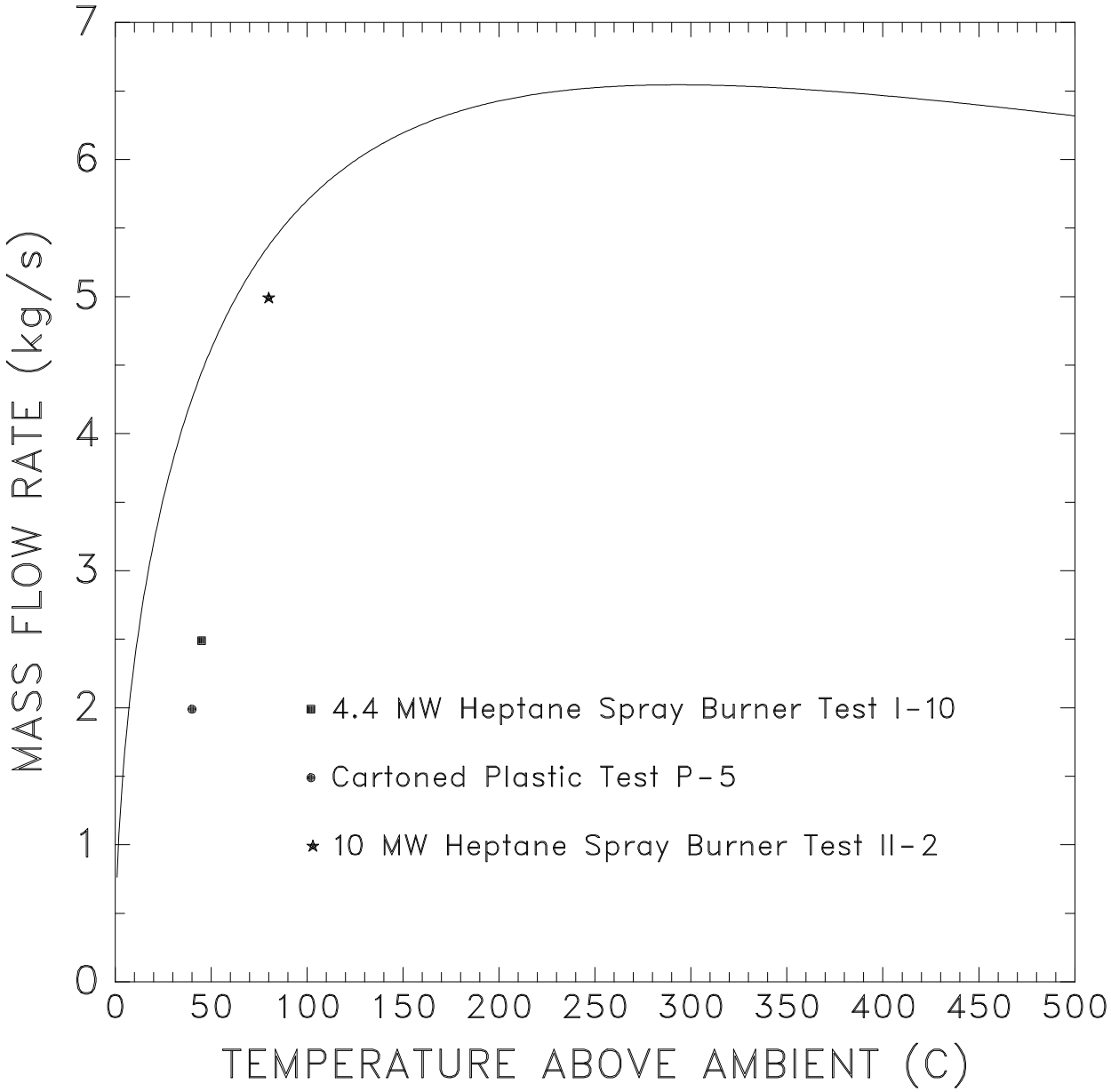

Figure 61: Mass flow rate through a single vent as a function of ceiling layer temperature. The solid line represents the mass flow predicted by Eq. 47 for a 1.2 m by 2.4 m (4 ft by 8 ft) vent and a ceiling layer depth of 1.8 m (6 ft). The points represent the average mass flow through the vent nearest the fire over the time period between 2 and 5 min for three numerical simulations.

the idealized mass flow rate as a function of temperature rise (solid curve). In Appendix A of the 1991 edition of NFPA 204M, Guide for Smoke and Heat Venting, the derivation of the venting relationships contained in that document is explained [5]. Equation 47 is used to estimate the mass flow through a vent, and the vent to floor ratios recommended in the document are based on equating the mass flow of the air entrained into the fire plume with that exhausted through the vents. An important assumption made is that the temperature rise ΔT in Eq. 47 is equal to the

ambient temperature on the Kelvin (Rankine) scale. Thus, if the ambient temperature were 20°C (68°F), then the temperature rise ΔT near the vent would be assumed to be 293°C (559°F). At this temperature, the mass flow through the vent would be very near its theoretical maximum. Of course, this analysis does not take into account the effect of sprinkler sprays because it is stated in Chapter 6-1 of the 1991 edition of 204M that the document "...represents the state of technology of vent design in the absence of sprinklers." Indeed, the test data and the model predictions reported here indicate that the temperature increase over ambient in the vicinity of an opened vent in a sprinklered facility would be far less than 293°C.

The numerical model was used to estimate the mass flow rates through the vent nearest the fire. Figure 61 presents the rates of three typical calculations compared to the rate predicted by Eq. 47. The mass flow rates for Test I-10 and P-5 are relatively low compared with the theoretical maximum because the near-ceiling gas temperatures are greatly reduced by the sprinklers. The flow rate for Test II-2 is much higher because the ceiling layer temperatures are significantly higher for the 10 MW fire. The simulation of Test II-2 was rerun with the draft curtains removed. The computed mass flow from the numerical simulation dropped into a range of 1.5 kg/s to 2.0 kg/s. In terms of Eq. (47), this reduction in mass flow rate is due to the decrease in the smoke layer depth, d, but another contribution is the change in ceiling jet dynamics caused by the draft curtain removal. This latter effect is not accounted for in Eq. (47), but it is in the numerical model.

8 Conclusions

Thirty-nine large scale fire tests were conducted at the Underwriters Laboratories Large Scale Fire Test Facility in Northbrook, Illinois, to investigate what effect roof vents and draft curtains have on the time, number and location of sprinkler activations; and what effect sprinklers and draft curtains have on the time, number and discharge rates of roof vents in a warehouse or warehouse-like retail store. In addition, a computational fluid dynamics model was used as a planning and analysis tool. The test site and experimental test parameters were chosen by an industry-led Technical Advisory Committee to address relatively large, open-area buildings with smooth, unobstructed (except for draft curtains) horizontal ceilings, adequate sprinkler systems and independently-controlled (*i.e.* not grouped) automatic roof vents. Because the smoke was vented into a large plenum space and not the atmosphere, wind effects were not considered and the effect of venting on smoke obscuration could not be quantified.

The major findings relative to the interaction of sprinklers, draft curtains and vents based on the experiments and model simulations in this study were:

- The tests and model simulations showed that when the fire was not ignited directly under a roof vent, venting had no significant effect on the sprinkler activation times, the number of activated sprinklers, the near-ceiling gas temperatures, or the quantity of combustibles consumed.

- The tests and model simulations showed that when the fire was ignited directly under a roof vent, automatic vent activation usually occurred at about the same time as the first sprinkler activation, but the average activation time of the first ring of sprinklers was delayed. The length of the delay depended on the difference in activation times between the vent and the first sprinkler.

- The tests and model simulations showed that when the fire was ignited directly under a roof vent that activated either before or at about the same time as the first sprinkler, the number of sprinkler activations decreased by as much as 50% compared to tests performed with the vent closed.

- The tests and model simulations showed that when draft curtains were installed, up to twice as many sprinklers activated compared to tests performed without curtains.

- In one rack storage test where the ignition of the fire took place near a draft curtain and the fuel array extended underneath the curtain, disruption of the sprinkler spray and delay in sprinkler operation caused by the draft curtain led to a fire that consumed more commodity compared to the other tests where the fires were ignited away from the draft curtains. This result was demonstrated by the model simulation, as well.

- The significant cooling effect of sprinkler sprays on the near-ceiling gas flow often prevented the automatic operation of vents. This conclusion is based on thermocouple measurements within the vent cavity, the presence of drips of solder on the fusible links recovered from unopened vents, and several tests where vents remote from the fire and the sprinkler spray activated. In one cartoned plastic commodity experiment, a vent did not open when the fire was ignited directly beneath it. The model simulations could not predict this phenomenon.

- Model simulations indicated that the cooling effect of sprinkler sprays reduced the total vent discharge rate from that assumed in design calculations for unsprinklered buildings.

- Model simulations showed how the activation times of the the first and second sprinklers had a substantial impact on the overall number of activations in the plastic commodity tests. In the simulation of one test, it was shown that a delay of approximately one minute in the activation of the second sprinkler led to the activation of four times as many sprinklers as in a simulation of a test with no delay. It had been suggested that these different outcomes were due to the presence of draft curtains in the tests with the sprinkler delay, but the simulations showed that the curtains had no effect because they were over 9 m (30 ft) away from the ignition point.

The Industrial Fire Simulator (IFS) developed in conjunction with the test program was shown to be in good *quantitative* agreement with the heptane spray burner tests in terms of both predicting sprinkler activation times and near-ceiling gas temperatures. The sprinkler activation times were predicted to within about 15% of the experiments for the first ring, 25% for the second. The gas temperatures near the ceiling were predicted to within about 15%. Simulations were performed and compared with unsprinklered calorimetry burns of the cartoned plastic commodity. The heat release rates of the growing fires were predicted to within about 20%.Simulations of the 5 cartoned plastic commodity fire tests were then performed. The goal of these simulations was to be able to differentiate between those experiments that activated a large number of sprinklers, and those that activated a small number. This goal has been met. The model also provided valuable insight into what occurred in the experiments, and also what would have occurred in the event of various changes of test parameters. There are plans to continue the development of the IFS model beyond publication of this report.

References

[1] D.T. Sheppard and D.R. Steppan. Sprinkler, Heat & Smoke Vent, Draft Curtain Project – Phase 1 Scoping Tests. Technical report, Underwriters Laboratories, Inc., Northbrook, Illinois, May 1997.

[2] D.T. Sheppard. International Fire Sprinkler, Heat & Smoke Vent, Draft Curtain Fire Test Project – Test Report. Technical report, Underwriters Laboratories, Inc., Northbrook, Illinois, 1998. NC987-96NK37863.

[3] H.R. Baum, O.A. Ezekoye, K.B. McGrattan, and R.G. Rehm. Mathematical Modeling and Computer Simulation of Fire Phenomenon. *Theoretical and Computational Fluid Dynamics*, 6:125–139, 1994.

[4] K.B. McGrattan, H.R. Baum, and R.G. Rehm. Large Eddy Simulations of Smoke Movement. *Fire Safety Journal*, 30:161–178, 1998.

[5] National Fire Protection Association, Quincy, Massachusetts. *Guide for Smoke and Heat Venting*, 1991. NFPA 204M.

[6] National Fire Protection Association, Quincy, Massachusetts. *Standard for Rack Storage of Materials*, 1995. NFPA 231C.

[7] A.L. Busby and G.L. Pigman. Roof Ventilation Requirements for Industrial Plants. Technical report, Armour Research Foundation (now IIT Research), Chicago, 1955. Final Report Project Number L-565.

[8] M.R. Suchomel. A Preliminary Study of Factors Influencing the Use of Vents with Ordinary-Degree Sprinklers. Technical report, Underwriters' Laboratories for the National Board of Fire Underwriters, File NC449, Assignment 63K4340, July 1964.

[9] P.H. Thomas and P.L. Hinkley. The Design of Roof Venting Systems for Single-Storey Buildings. Technical Report No. 10, HMSO, London, Fire Research Station, 1964.

[10] Portsmouth Fire Test. Colt Heating and Ventilation Ltd. Internal Report, 1966.

[11] Factory Mutual Research Corporation, Norwood, Massachusetts. *Fire Tests of Palletized and Racked Tire Storage*, July 1970. Serial No. 19037.

[12] G. Heskestad. Model Study of Automatic Smoke and Heat Vent Performance in Sprinklered Fires. Technical Report FMRC Serial No. 21933 RC74-T-29, Factory Mutual Research Corporation, September 1974.

[13] T.E. Waterman, C.E. Foxx, K.R. Mniszewski, and D.L. Eacret. Fire Venting of Sprinklered Buildings. Technical Report IITRI Project J08385, IIT Research Institute, 10 West 35th Street, Chicago, Illinois 60616, July 1982. Prepared for the Fire Venting Research Committee.

[14] P.L. Hinkley, G.O. Hansell, N.R. Marshall, and R. Harrison. Experiments at the Multifunctioneel Trainingcentrum, Ghent, on the interaction between sprinklers and smoke venting. Technical report, Building Research Establishment, Fire Research Station, Borehamwood, Herts, WD6 2BL, UK, 1992.

[15] H. Ingason and S. Olsson. Interaction between Sprinklers and Fire Vents. Technical report, Swedish National Testing and Research Institute (SP), 1992. SP Report 1992:11.

[16] B. Persson and H. Ingason. Modelling of Interaction between Sprinklers and Fire Vents – Present knowledge. Technical report, Swedish National Testing and Research Institute (SP), 1996. SP Report 1996:32.

[17] P.L. Hinkley, G.O. Hansell, N.R. Marshall, and R. Harrison. Sprinklers and Vents Interaction – Experiments at Ghent. *Fire Surveyor*, pages 18–23, October 1992.

[18] P.L. Hinkley. The Effect of Vents on the Opening of the First Sprinklers. *Fire Safety Journal*, 11:211–225, 1986.

[19] N.E. Gustafsson. A Sprinkler Specialist's View. Position paper presented at the Smoke Ventilation and Sprinklers Seminar, Fire Research Station, Borehamwood, UK, November 1992.

[20] T.E. Waterman. Fire Venting of Sprinklered Buildings. *Fire Journal*, 78(2), March 1984.

[21] J.M.A Troup. Large-Scale Fire Tests of Rack Stored Group A Plastics in Retail Operation Scenarios Protected by Extra Large Orifice (ELO) Sprinklers. Technical Report FMRC J.I. 0X1R0.RR, Factory Mutual Research Corporation, Norwood, Massachusetts, November 1994. Prepared for Group A Plastics Committee, Lansdale, Pennsylvania.

[22] L.Y. Cooper. Simulating the Opening of Thermally-Actuated Fire Vents. Technical Report NIST Internal Report (in preparation), National Institute of Standards and Technology, Gaithersburg, Maryland 20899, 1998.

[23] D.D. Evans and D. Madrzykowski. Characterizing the Thermal Response of Fusible-Link Sprinklers. Technical Report NBSIR 81-2329, National Institute of Standards and Technology, Gaithersburg, Maryland, August 1981.

[24] International Conference of Building Officials, Whittier, California. *Uniform Fire Code*, 1994.

[25] Factory Mutual Research Corporation, Norwood, Massachusetts. *Factory Mutual Engineering Corporation Loss Prevention Data Sheet 8-0*, March 1977.

[26] Factory Mutual Research Corporation, Norwood, Massachusetts. *Factory Mutual Engineering Corporation Loss Prevention Data Sheet 8-0S*, January 1994.

[27] Factory Mutual Research Corporation, Norwood, Massachusetts. *Factory Mutual Engineering Corporation Loss Prevention Data Sheet 8-9*, September 1993.

[28] J.M.A. Troup. Large-Scale Fire Tests of Rack Storage of Plastics Protected by Central Model ELO-231 Sprinklers. Technical Report FMRC J.I. 0X0R4.RR, Factory Mutual Research Corporation, Norwood, Massachusetts, June 1993. Prepared for Central Sprinkler Corporation, Lansdale, Pennsylvania.

[29] R.K. Dean. Stored Plastics Test Program. Technical Report FMRC J.I. 202069, Factory Mutual Research Corporation, Norwood, Massachusetts, June 1975.

[30] R.G. Rehm and H.R. Baum. The Equations of Motion for Thermally Driven, Buoyant Flows. *Journal of Research of the NBS*, 83:297–308, 1978.

[31] J. Smagorinsky. General Circulation Experiments with the Primitive Equations. I. The Basic Experiment. *Monthly Weather Review*, 91:99–164, 1963.

[32] J.W. Deardorff. Numerical Investigation of Neutral and Unstable Planetary Boundary Layers. *Journal of Atmospheric Sciences*, 29:91–115, 1972.

[33] M. Germano, U. Piomelli, P. Moin, and W.H. Cabot. A Dynamic Subgrid-Scale Eddy Viscosity Model. *Physics of Fluids A*, 3:1760–1765, 1991.

[34] D.K. Lilly. A Proposed Modification of the Germano Subgrid-Scale Closure Method. *Physics of Fluids A*, 4:633–635, 1992.

[35] H.R. Baum, K.B. McGrattan, and R.G. Rehm. Large Eddy Simulations of Smoke Movement in Three Dimensions. In *Proceedings of the Seventh International Interflam Conference*, pages 189–198. Interscience Communications, London, 1996.

[36] American National Standards Institute. *ASTM E-1321, Lateral Ignition and Flame Spread Test*, 1994.

[37] T.J. Ohlemiller and K.M. Villa. Material Flammability Test Assessment for Space Station Freedom. Technical Report NISTIR 4591, National Institute of Standards and Technology, Gaithersburg, Maryland, June 1991.

[38] J.P. Holman. *Heat Transfer*. McGraw-Hill, New York, 5th edition, 1989.

[39] American National Standards Institute. *ASTM E-1354, Standard Test Method for Heat and Visible Smoke Release Rates for Materials and Products Using an Oxygen Combustion Calorimeter*, 1994.

[40] S.J. DiGiovanni. An Investigation of the Effect of Water Spray Suppression on the Heat Release Rate of the FMRC Standard Plastic Warehouse Commodity. Technical report, University of Maryland, 1998.

[41] H.R. Baum and B.J. McCaffrey. Fire Induced Flow Field – Theory and Experiment. In *Fire Safety Science – Proceedings of the Second International Symposium*, pages 129–148. International Association for Fire Safety Science, 1989.

[42] G. Heskestad and R.G. Bill. Conduction Heat Loss Effects on Thermal Response of Automatic Sprinklers. Technical report, Factory Mutual Research Corporation, September 1987.

[43] G. Heskestad and R.G. Bill. Quantification of Thermal Responsiveness of Automatic Sprinklers Including Conduction Effects. *Fire Safety Journal*, 14:113–125, 1988.

[44] International Organization for Standardization (ISO), Geneva, Switzerland. *Fire Protection – Automatic Sprinkler Systems – Part 1: Requirements and test methods for sprinklers, ISO 6182-1*, 1993.

[45] S. Kumar, G.M. Heywood, S.K. Liew, and W.S. Atkins. JASMINE Sprinkler Model - Some Validation Studies. In *Proceedings of the First European Symposium on Fire Safety Science*, 1995. ETH, Zurich.

[46] T.S. Chan. Measurements of Water Density and Droplet Size Distributions of Selected ESFR Sprinklers. *Journal of Fire Protection Engineering*, 6(2):79–87, 1994.

[47] F.P. Incropera and D.P. De Witt. *Fundamentals of Heat and Mass Transfer*. John Wiley and Sons, New York, 3rd edition, 1990.

[48] H.Z. Yu, J.L. Lee, and H.C. Kung. Suppression of Rack-Storage Fires by Water. In *Fire Safety Science – Proceedings of the Fourth International Symposium, International Association For Fire Safety Science*, pages 901–912, 1994.

[49] K.B. McGrattan, R.G. Rehm, and H.R. Baum. Fire-Driven Flows in Enclosures. *Journal of Computational Physics*, 110(2):285–292, 1994.

[50] P.L. Hinkley. *SFPE Handbook*, chapter Smoke and Heat Venting. National Fire Protection Association, Quincy, Massachusetts, 2nd edition, 1995.

A Heptane Spray Burner Test Results (Series I)

The experimental data and numerical model results presented in this section represent a subset of both the actual data collected by UL and the results of the model.

A.1 Sprinkler Activation History

The figures on the following pages present the sprinkler activation history of the 22 heptane burner tests (Series I), plus the model predictions. In each figure, the sprinkler activation times from the simulation ("S") and the experiment ("E") are listed at the location of the activated sprinkler. The temperature contours are instantaneous snapshots from the simulation, showing the predicted temperatures near the ceiling at some arbitrary time during the simulation. Highlighted with a cross-hatched filling is the contour interval from 75°C to 100°C. Contours are spaced at intervals of 25°C. The activation temperature for the Central ELO-231 upright sprinklers used in the tests is 74°C. The highlighted contour interval separates the area of almost certain activation from the area of almost no activation. It was observed during the tests that following the activation of the 4 sprinklers nearest the fire after about 65 s, the sprinklers in the next ring would activate if the surrounding gas temperature was at least 100°C. Thus, the 75–100°C interval represents an area of less than likely activation. The contours also show the effect of opening a vent. Thermocouple data along with that of the simulations is included in Appendix A.2.

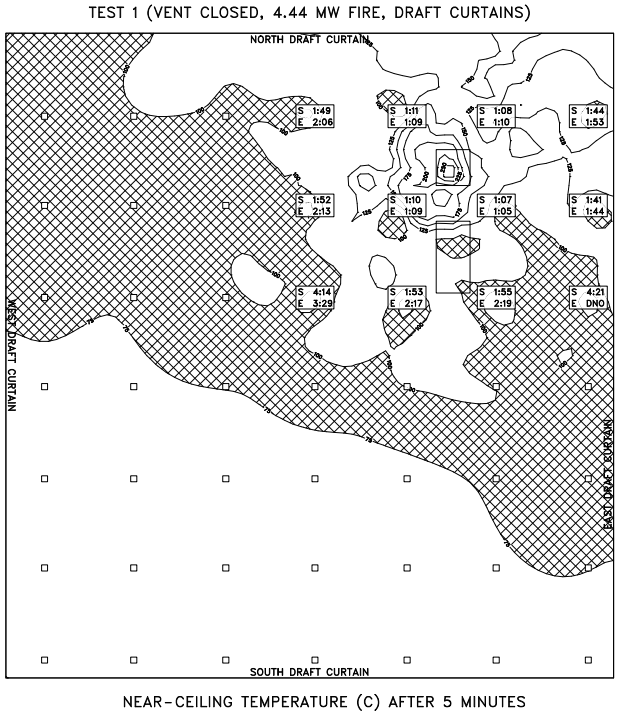

Figure 62: Sprinkler activations for Test I-1.

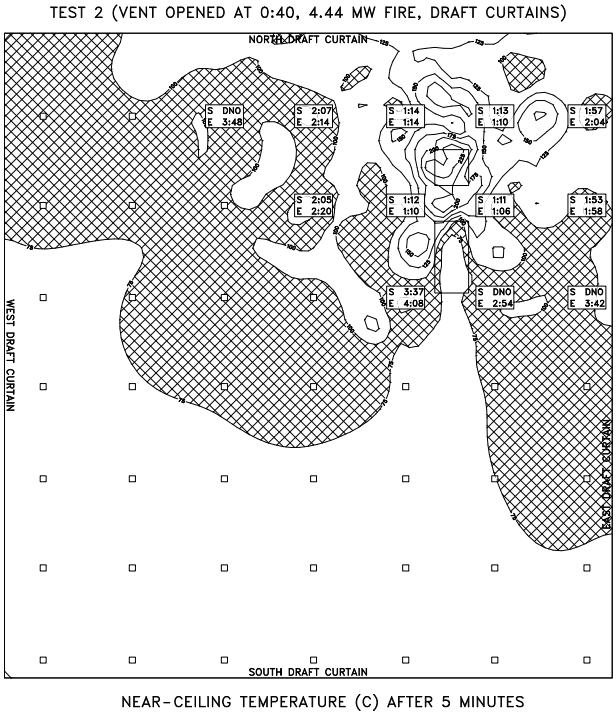

Figure 63: Sprinkler activations for Test I-2.

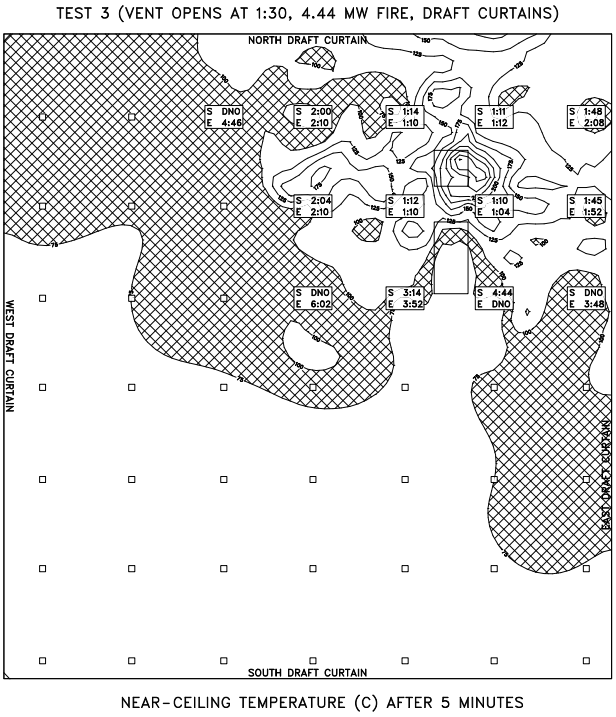

Figure 64: Sprinkler activations for Test I-3.

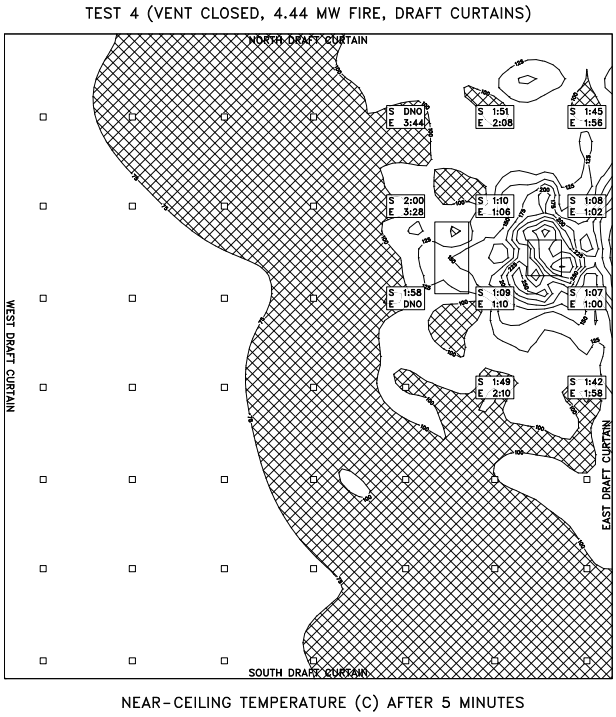

Figure 65: Sprinkler activations for Test I-4.

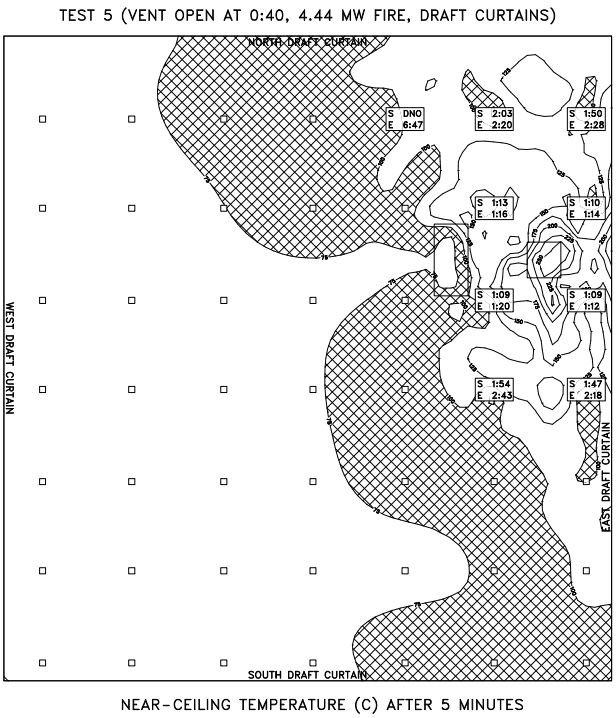

Figure 66: Sprinkler activations for Test I-5.

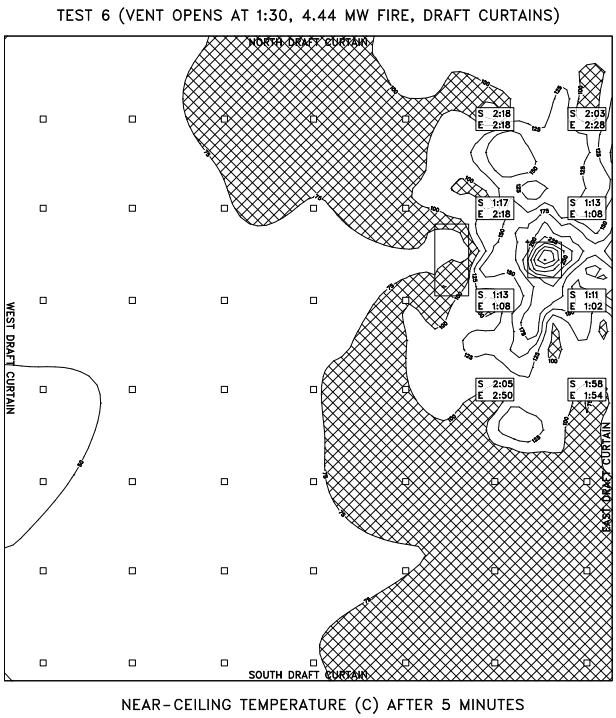

Figure 67: Sprinkler activations for Test I-6.

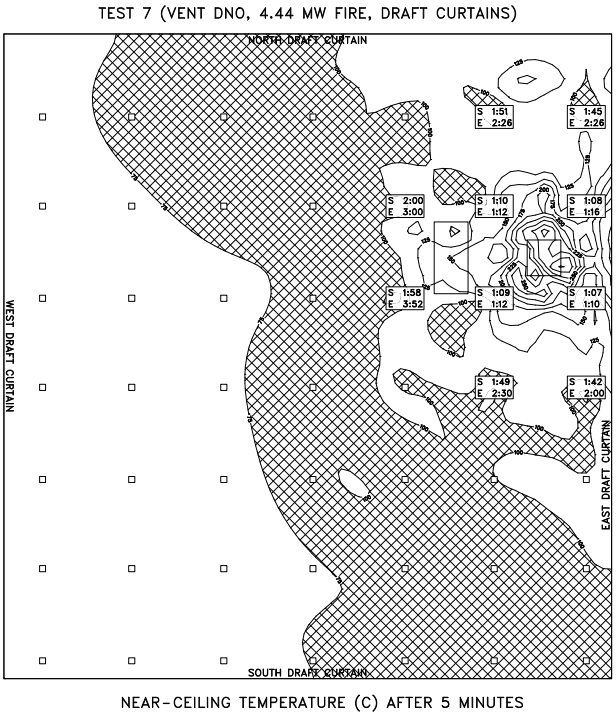

Figure 68: Sprinkler activations for Test I-7.

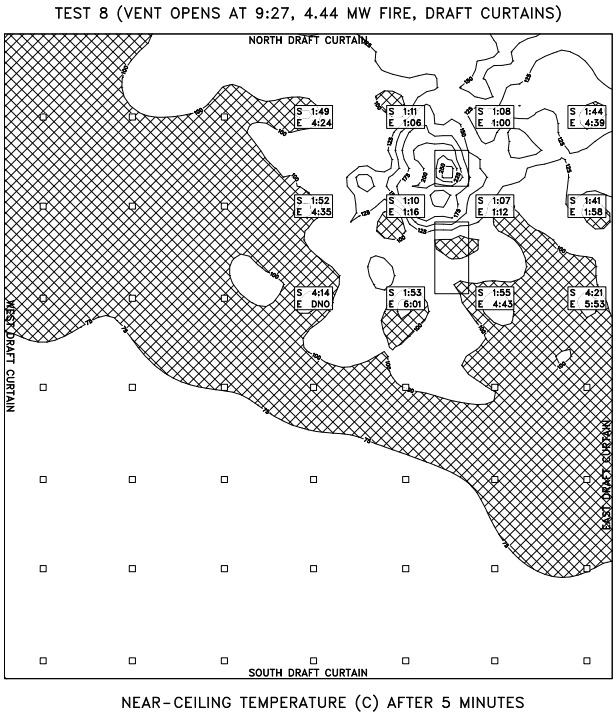

Figure 69: Sprinkler activations for Test I-8.

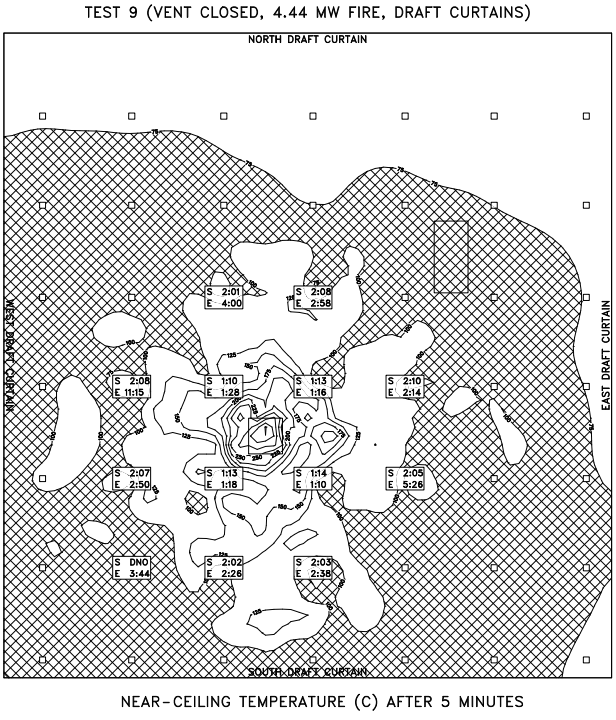

Figure 70: Sprinkler activations for Test I-9.

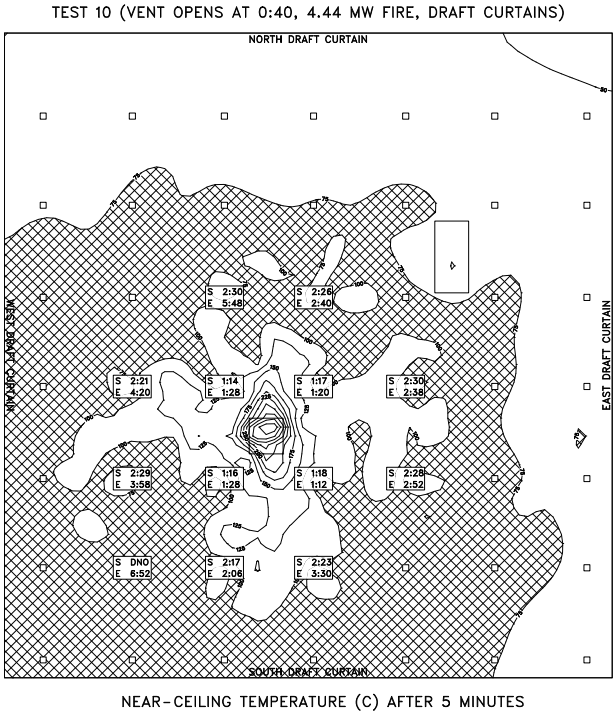

Figure 71: Sprinkler activations for Test I-10.

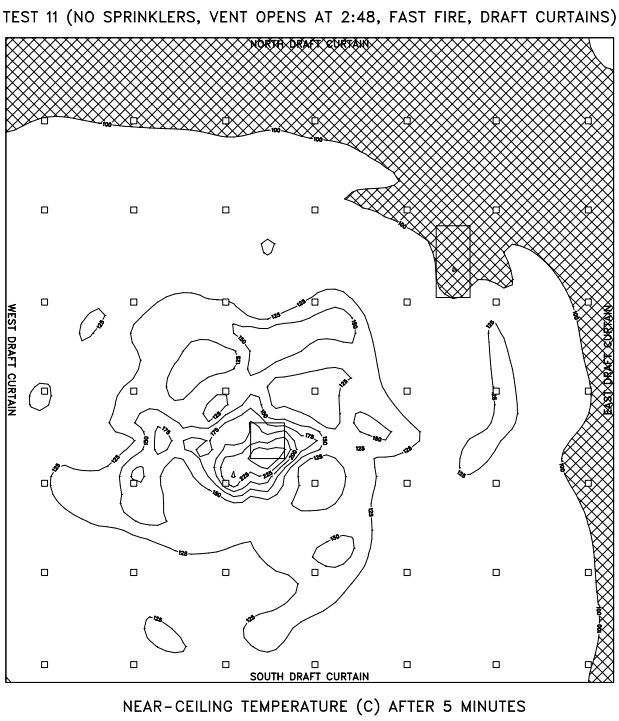

Figure 72: Near-ceiling gas temperatures from the simulation of Test I-11. There were no sprinklers deployed in the experiment.

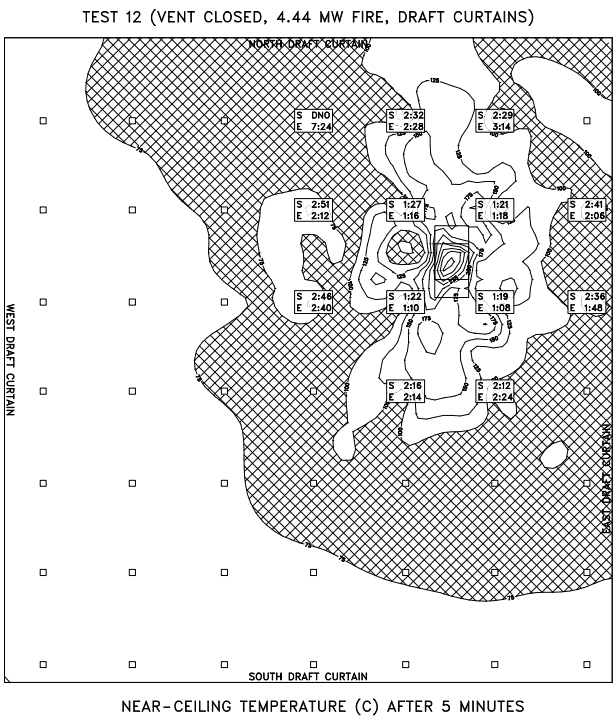

Figure 73: Sprinkler activations for Test I-12.

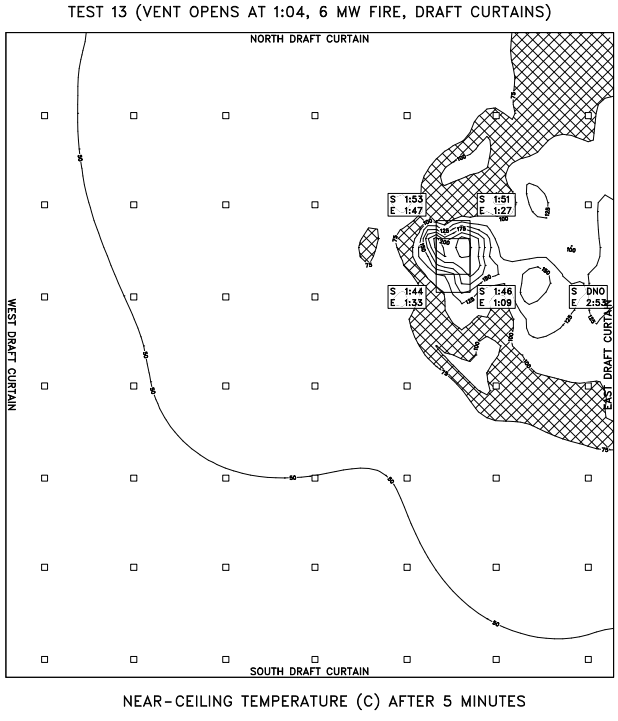

Figure 74: Sprinkler activations for Test I-13.

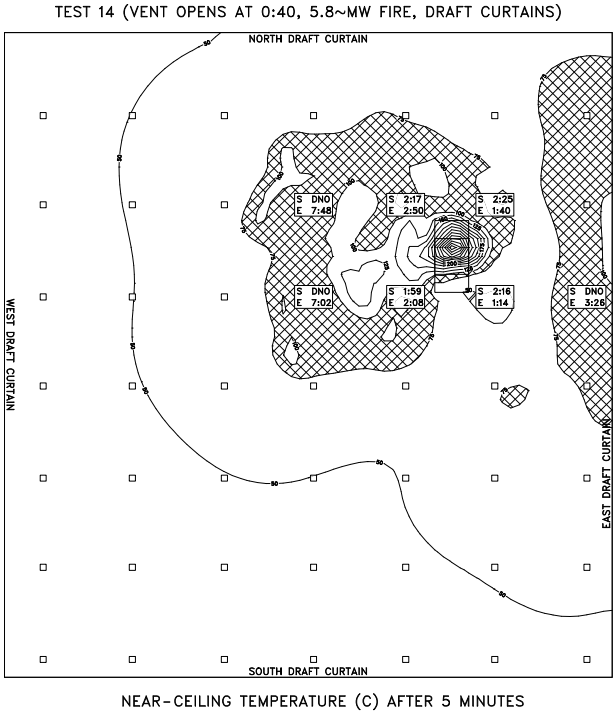

Figure 75: Sprinkler activations for Test I-14.

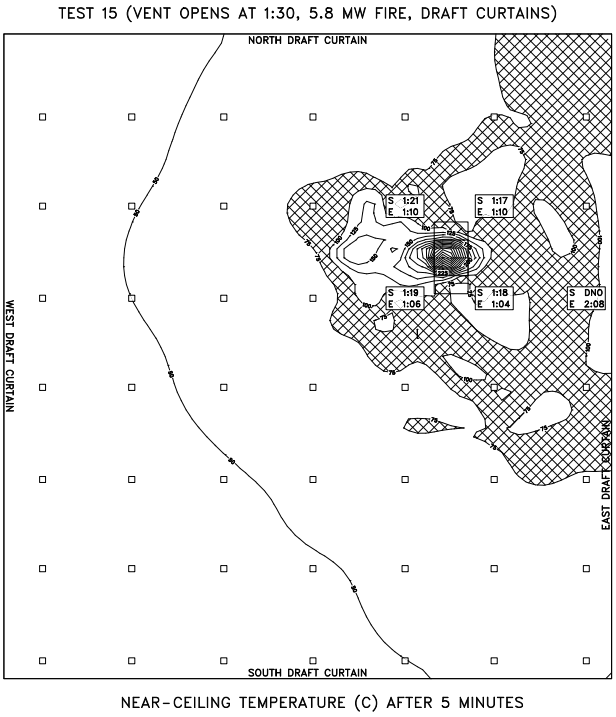

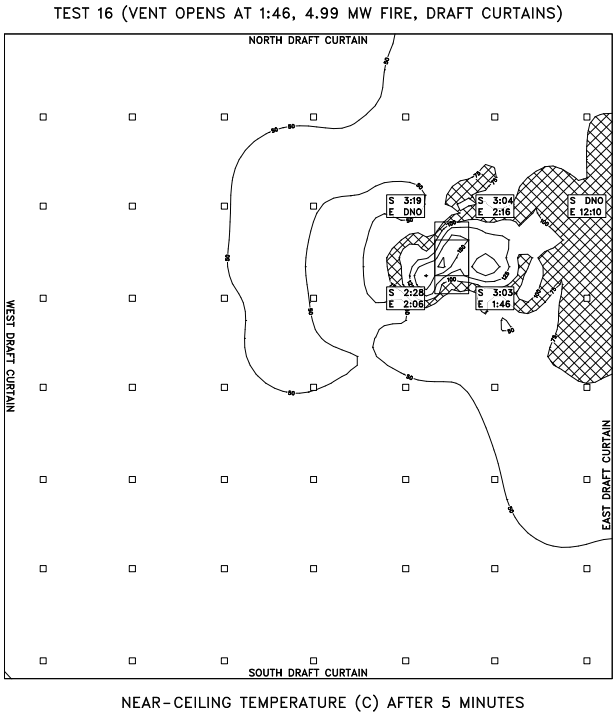

Figure 76: Sprinkler activations for Test I-15. **Figure 77: Sprinkler activations for Test I-16.**

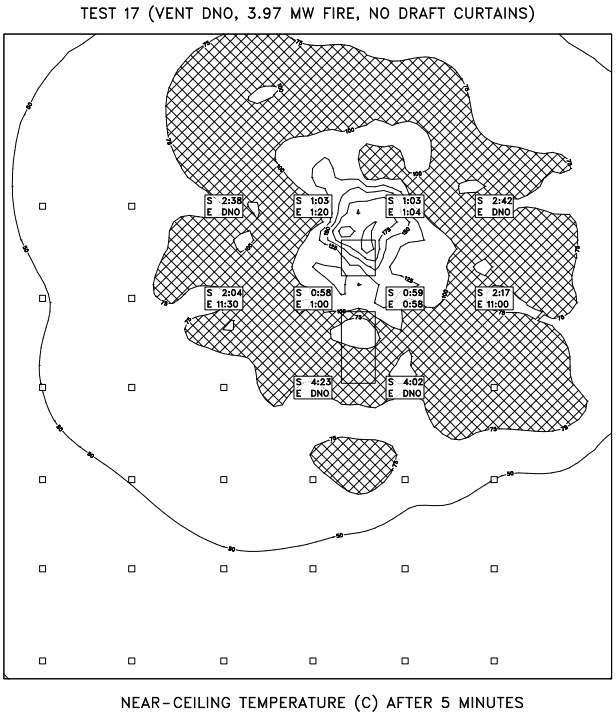

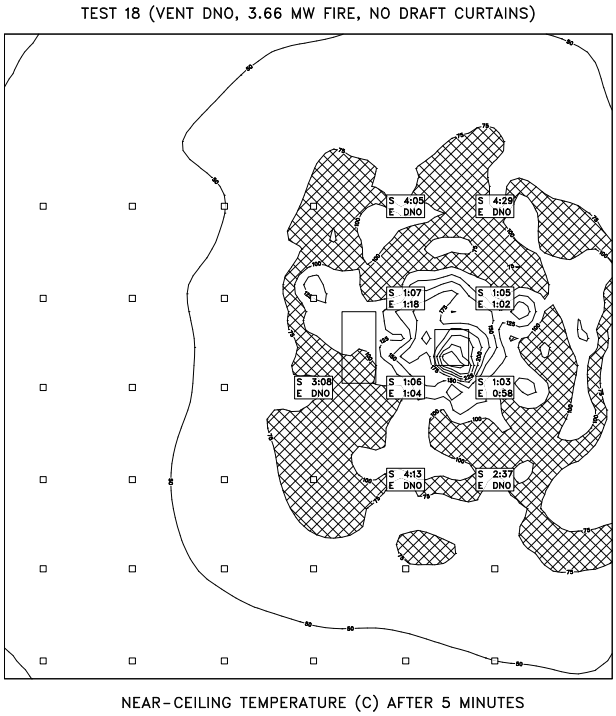

Figure 78: Sprinkler activations for Test I-17. **Figure 79: Sprinkler activations for Test I-18.**

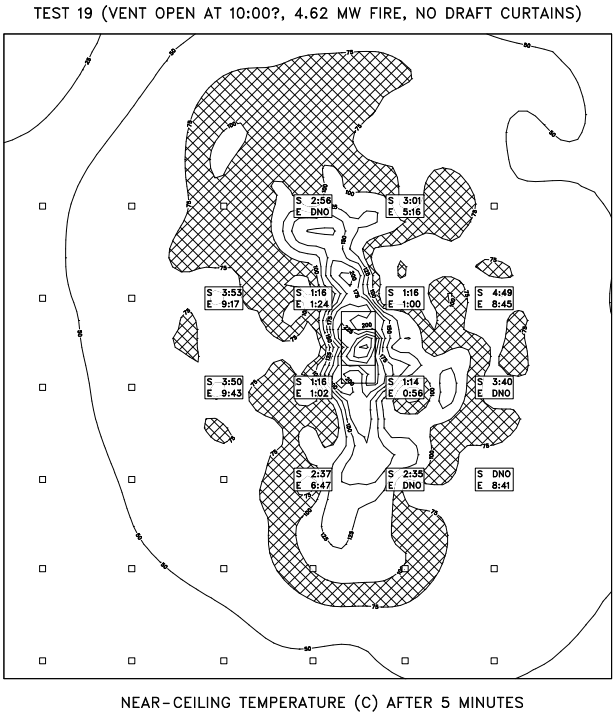

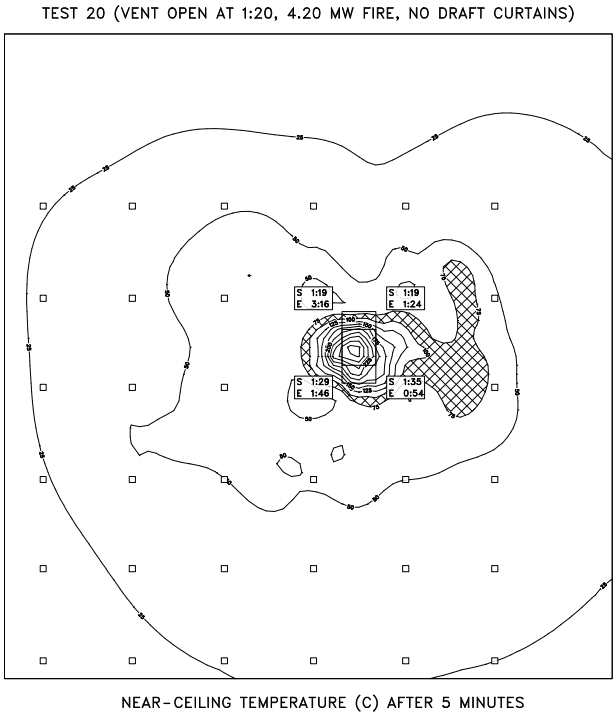

Figure 80: Sprinkler activations for Test I-19.

Figure 81: Sprinkler activations for Test I-20.

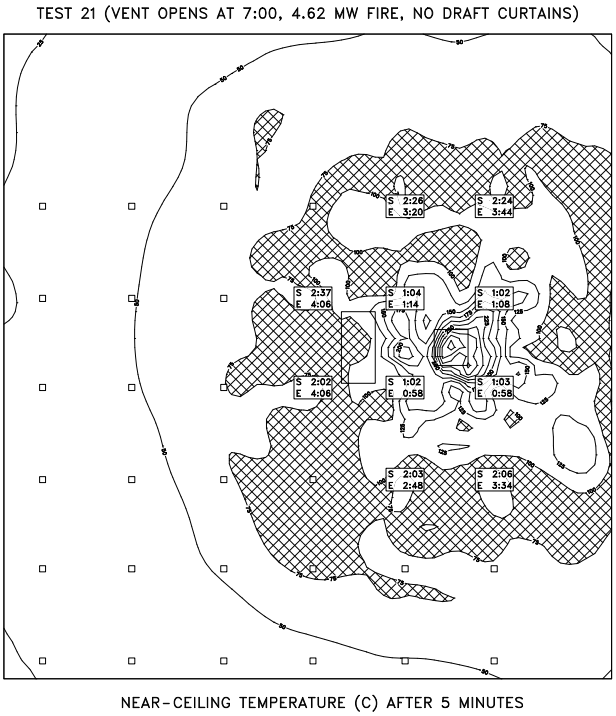

Figure 82: Sprinkler activations for Test I-21.

Figure 83: Sprinkler activations for Test I-22.

A.2 Experimental and Simulated Temperatures

The plots in Figs. 85–106 on the following pages compare the experimental thermocouple temperatures with those of the model. For each of the 22 tests, 104 thermocouples were placed near the ceiling. Their locations are shown in Figure 84. Only the 16 thermocouples nearest the fire are shown for each test on the following pages. For fire locations A, B and C, these thermocouples (channels 50–65) were positioned very close to the sprinkler. For fire location D, 4 of the 16 thermocouples (58, 59, 62, 63) were positioned next to the sprinkler, the rest were placed 2 in below the ceiling directly above the sprinkler deflector. Following sprinkler activation, the temperature of the corresponding thermocouple decreases sharply. The experimental and simulated temperatures are not expected to agree following activation because the actual thermocouple is wet, whereas the simulated thermocouple continues to record the gas temperature.

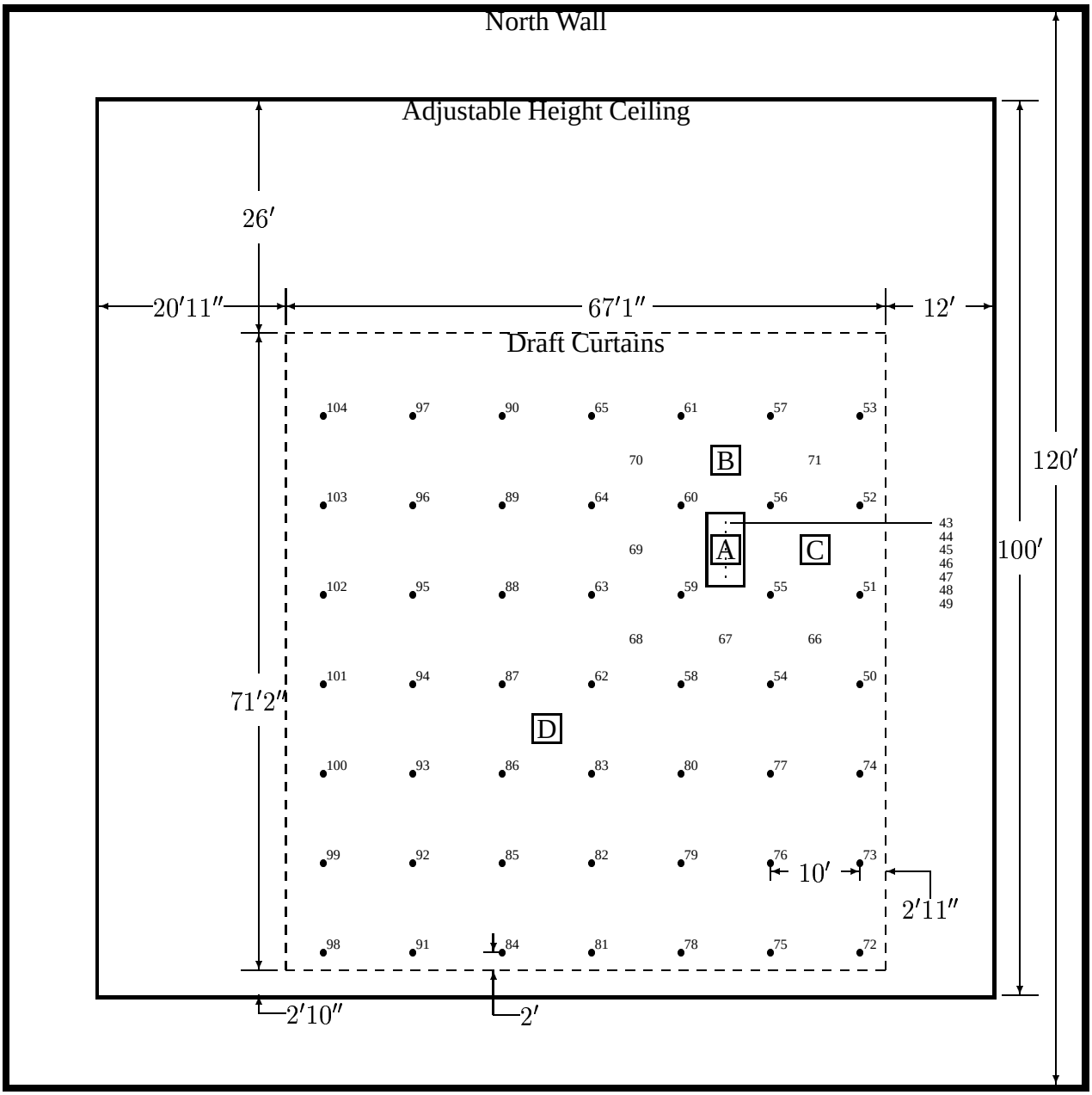

Figure 84: Plan view of heptane spray burner configuration, Series I. The sprinklers are indicated by the solid circles and are spaced 10 ft apart. The number beside each sprinkler location indicates the channel number of the nearest thermocouple. The vent dimensions are 4 ft by 8 ft. The boxed letters A, B, C and D indicate burner positions. Corresponding to each burner position is a vertical array of thermocouples. Thermocouples 1–9 hang 7, 22, 36, 50, 64, 78, 92, 106 and 120 in from the ceiling, respectively, above Position A. Thermocouples 10 and 11 are positioned above and below the tile directly above Position B, followed by 12–20 that hang at the same levels below the ceiling as 1–9. The same pattern is followed at Positions C and D, with thermocouples 21–31 at C and 32–42 at D.

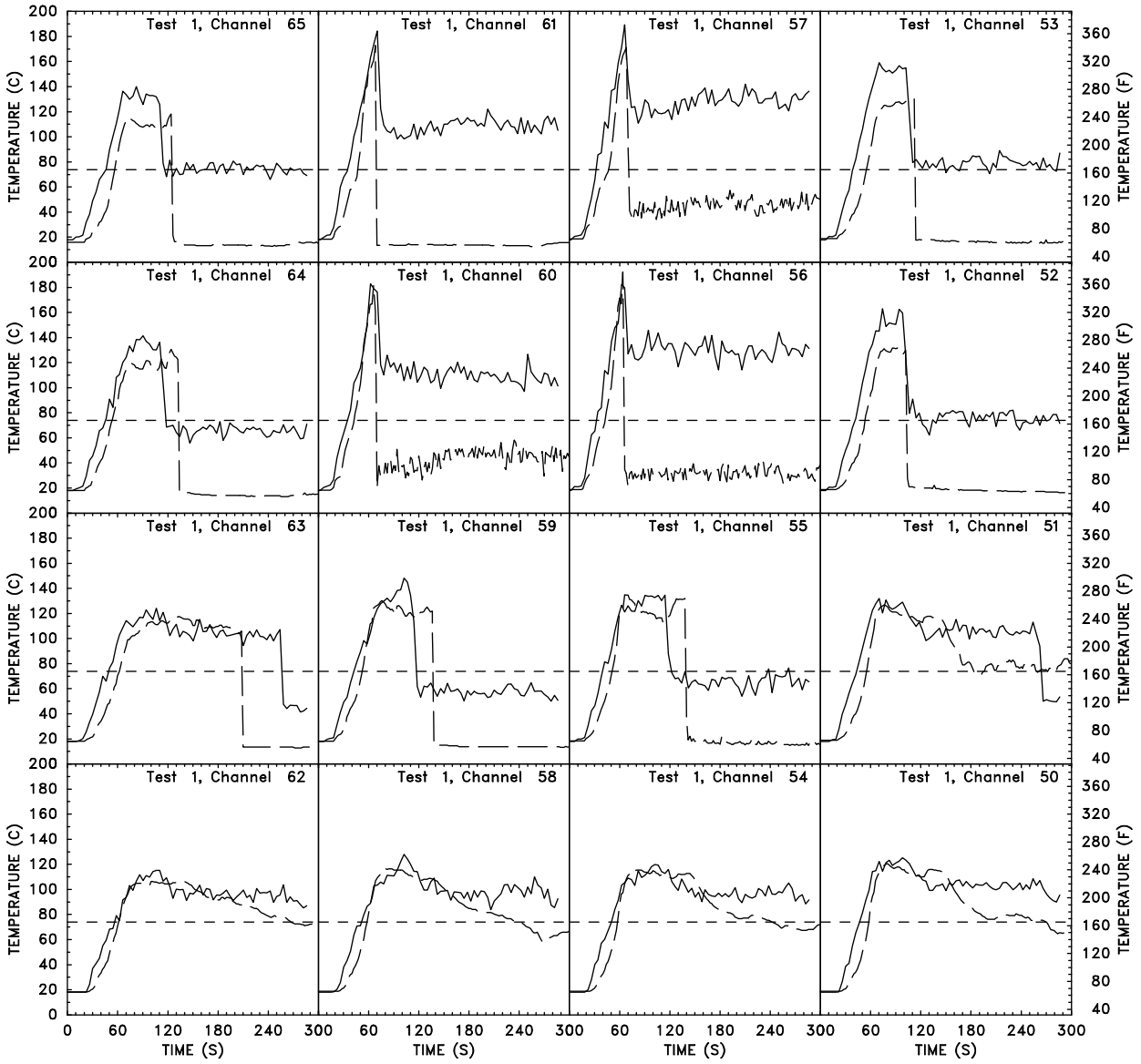

Figure 85: Comparison of experimental (dashed curve) and simulated (solid curve) temperatures of the near-sprinkler thermocouples for Test I-1 of the first series of heptane spray burner tests. The activation temperature of the sprinkler (74°C, 165°F) is denoted with a short dashed line. See Fig. 1 for the location of the sprinklers.

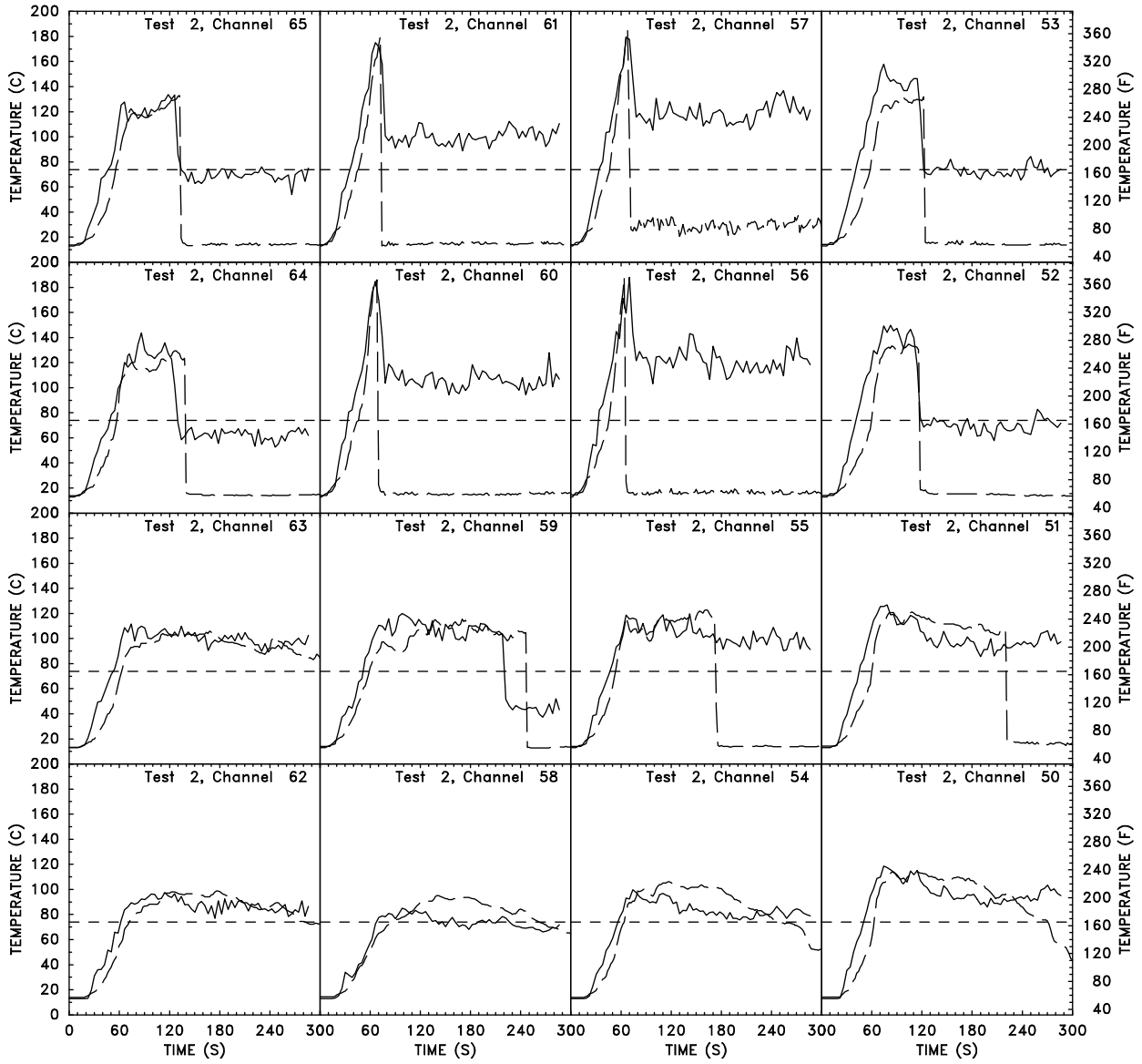

Figure 86: Comparison of experimental (dashed curve) and simulated (solid curve) temperatures of the near-sprinkler thermocouples for Test I-2 of the first series of heptane spray burner tests. The activation temperature of the sprinkler (74°C, 165°F) is denoted with a short dashed line. See Fig. 1 for the location of the sprinklers.

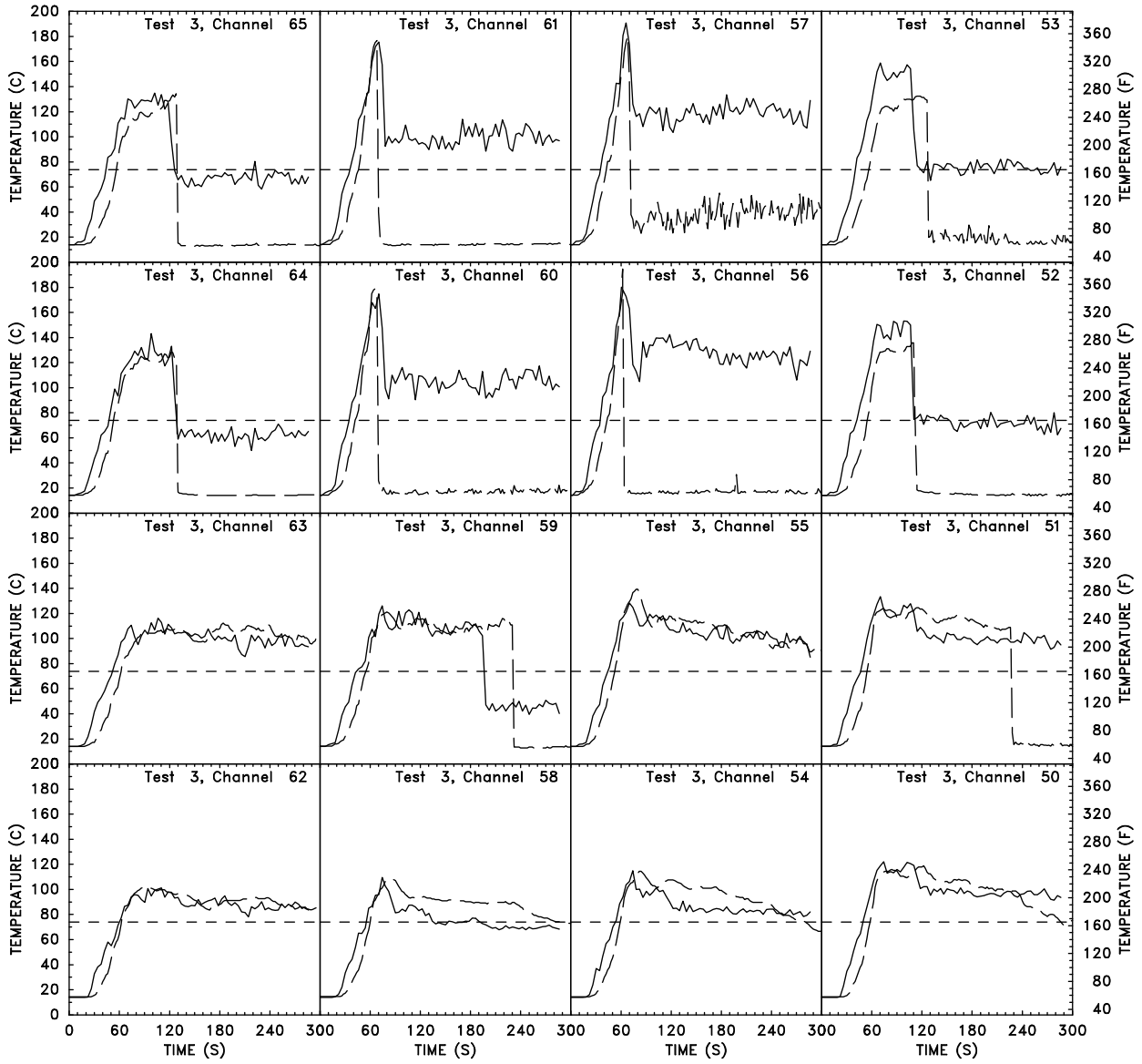

Figure 87: Comparison of experimental (dashed curve) and simulated (solid curve) temperatures of the near-sprinkler thermocouples for Test I-3 of the first series of heptane spray burner tests. The activation temperature of the sprinkler (74°C, 165°F) is denoted with a short dashed line. See Fig. 1 for the location of the sprinklers.

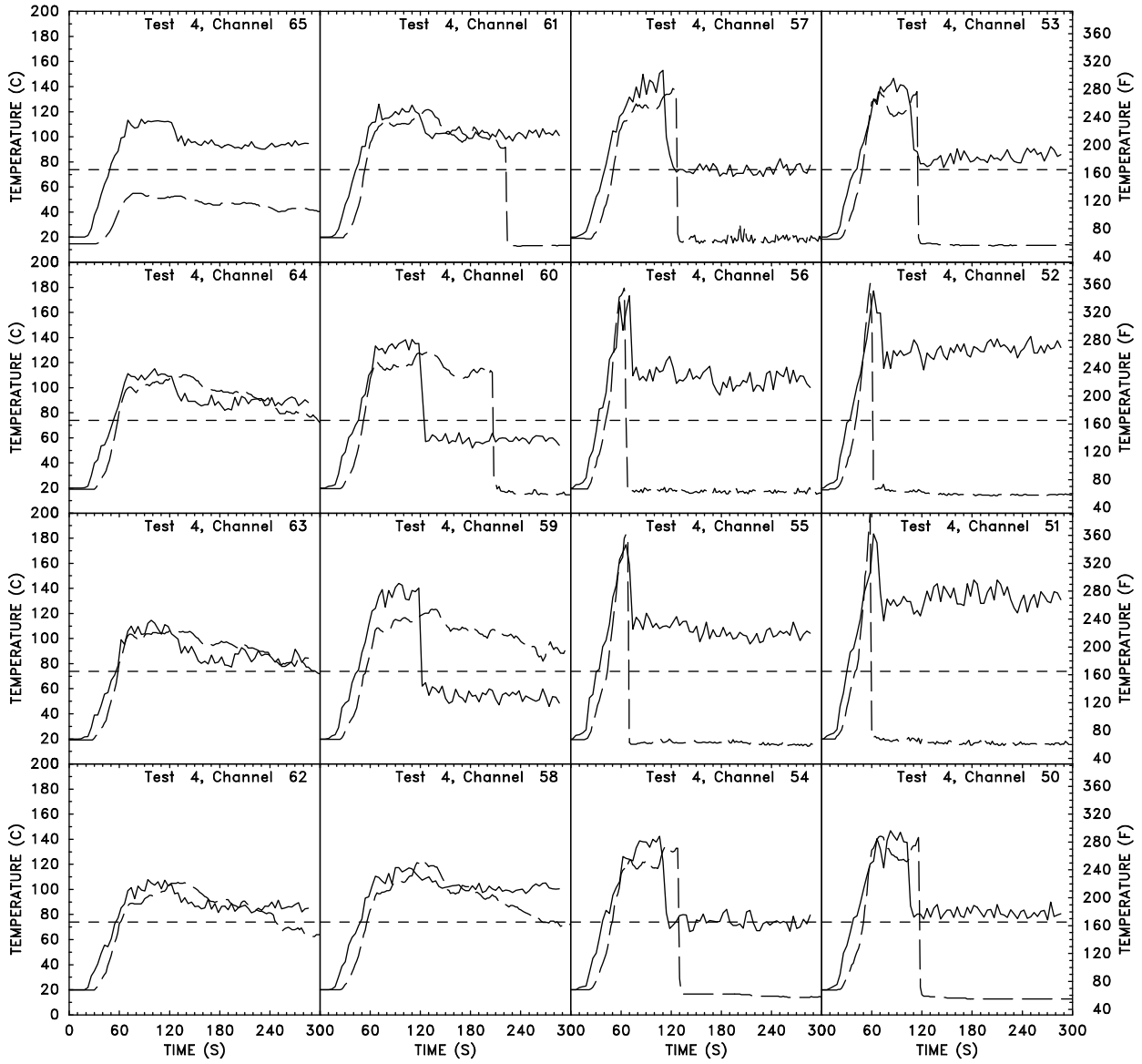

Figure 88: Comparison of experimental (dashed curve) and simulated (solid curve) temperatures of the near-sprinkler thermocouples for Test I-4 of the first series of heptane spray burner tests. The activation temperature of the sprinkler (74°C, 165°F) is denoted with a short dashed line. See Fig. 1 for the location of the sprinklers.

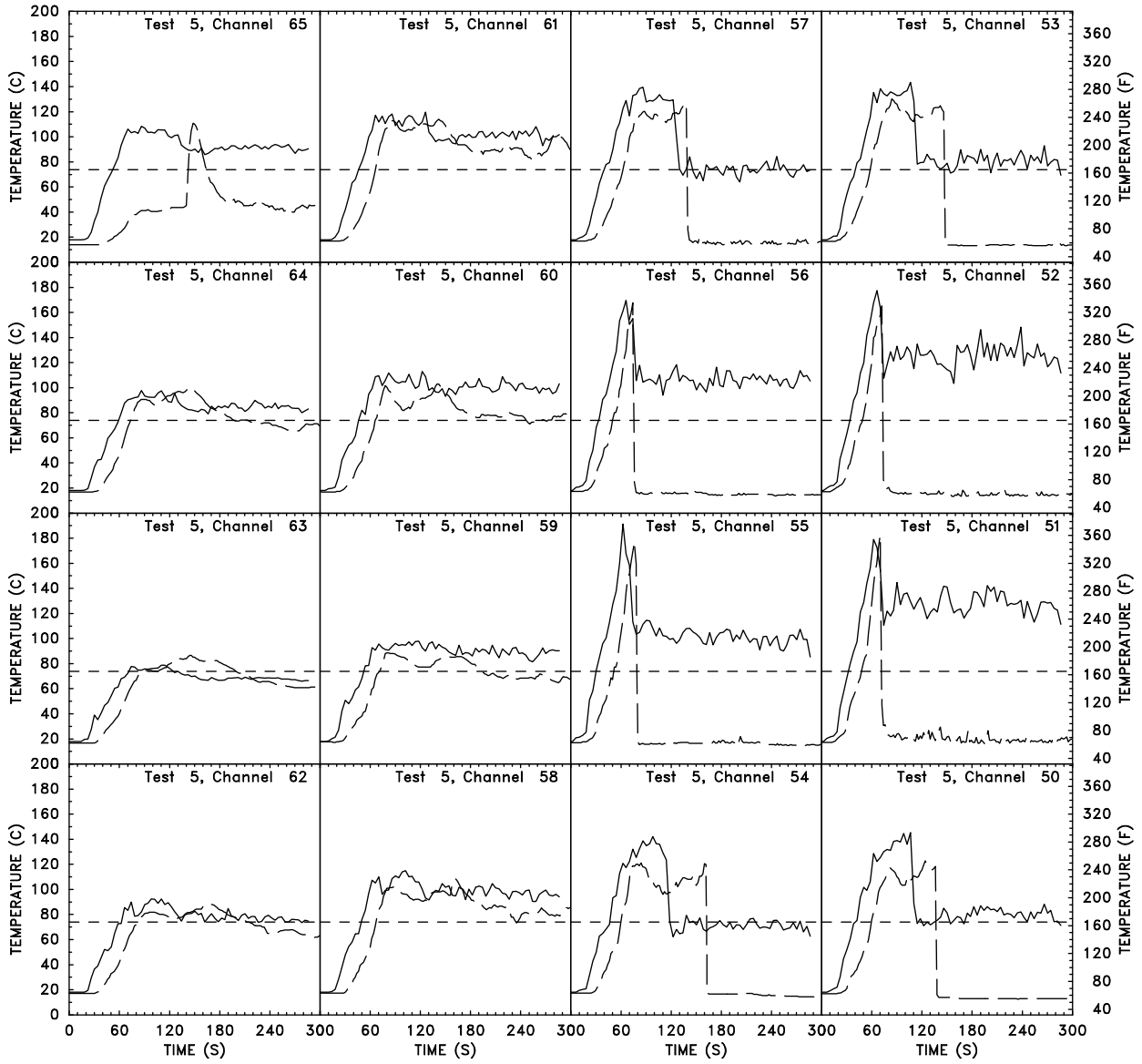

Figure 89: Comparison of experimental (dashed curve) and simulated (solid curve) temperatures of the near-sprinkler thermocouples for Test I-5 of the first series of heptane spray burner tests. The activation temperature of the sprinkler (74°C, 165°F) is denoted with a short dashed line. See Fig. 1 for the location of the sprinklers.

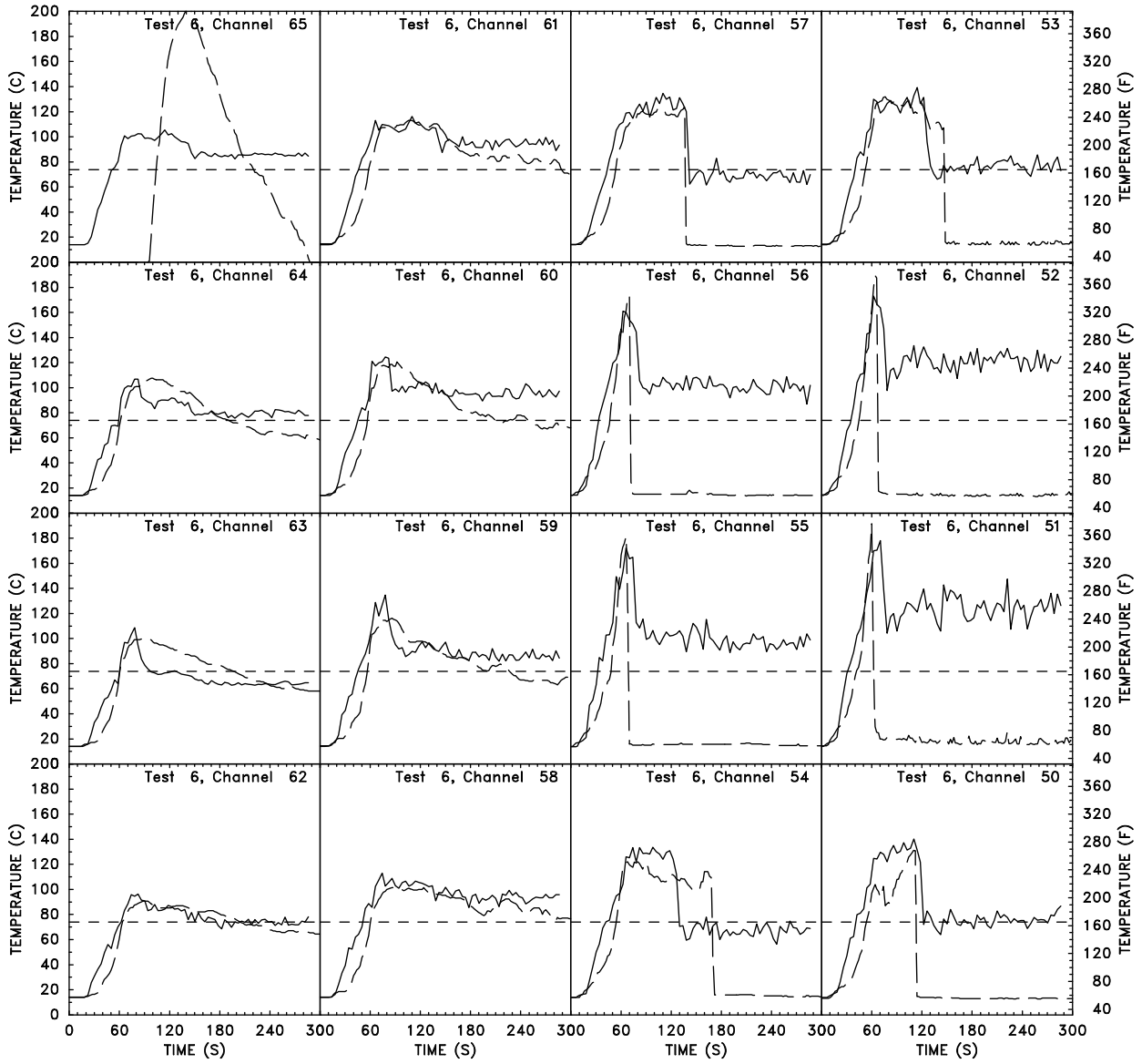

Figure 90: Comparison of experimental (dashed curve) and simulated (solid curve) temperatures of the near-sprinkler thermocouples for Test I-6 of the first series of heptane spray burner tests. The activation temperature of the sprinkler (74°C, 165°F) is denoted with a short dashed line. See Fig. 1 for the location of the sprinklers.

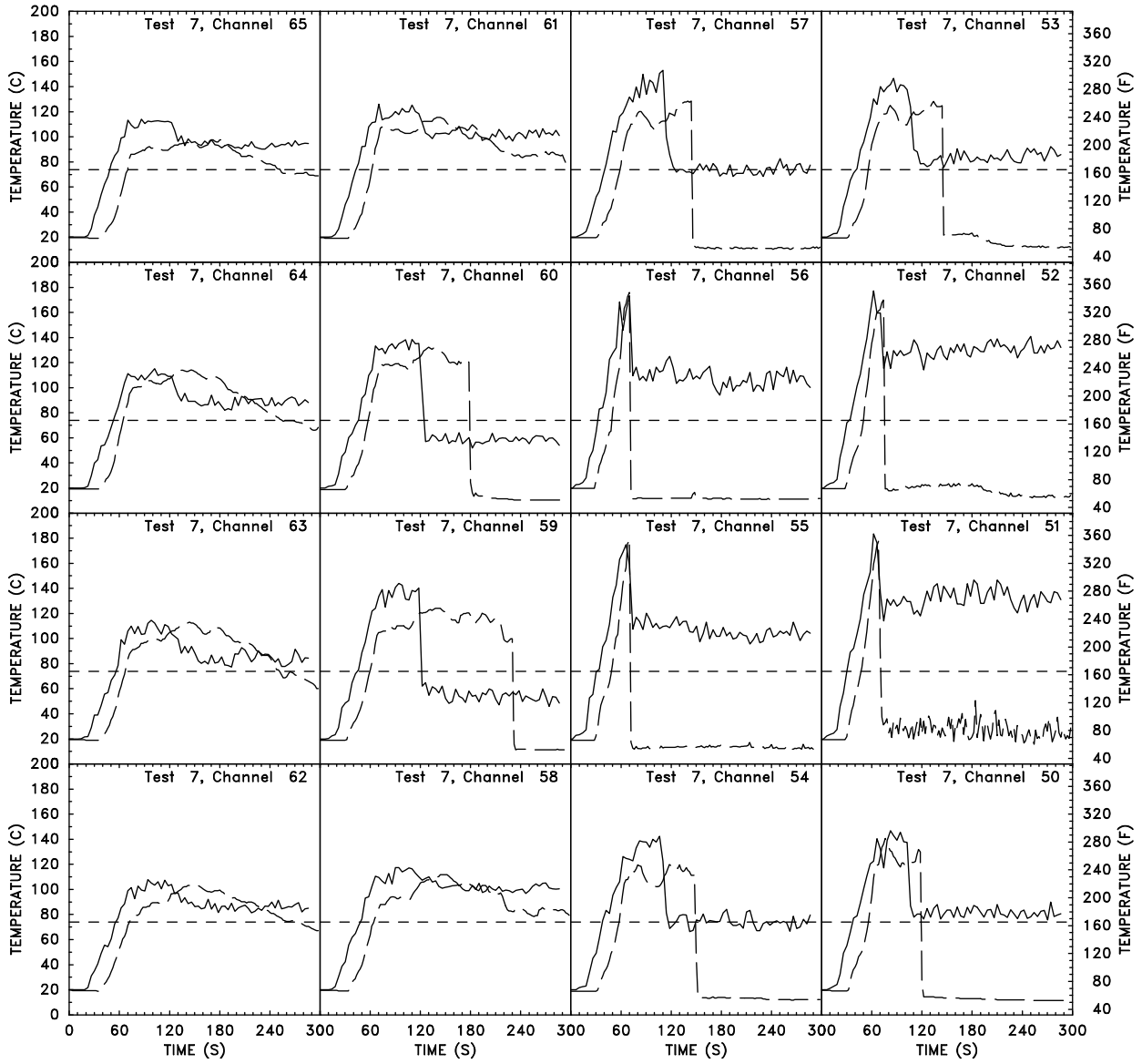

Figure 91: Comparison of experimental (dashed curve) and simulated (solid curve) temperatures of the near-sprinkler thermocouples for Test I-7 of the first series of heptane spray burner tests. The activation temperature of the sprinkler (74°C, 165°F) is denoted with a short dashed line. See Fig. 1 for the location of the sprinklers.

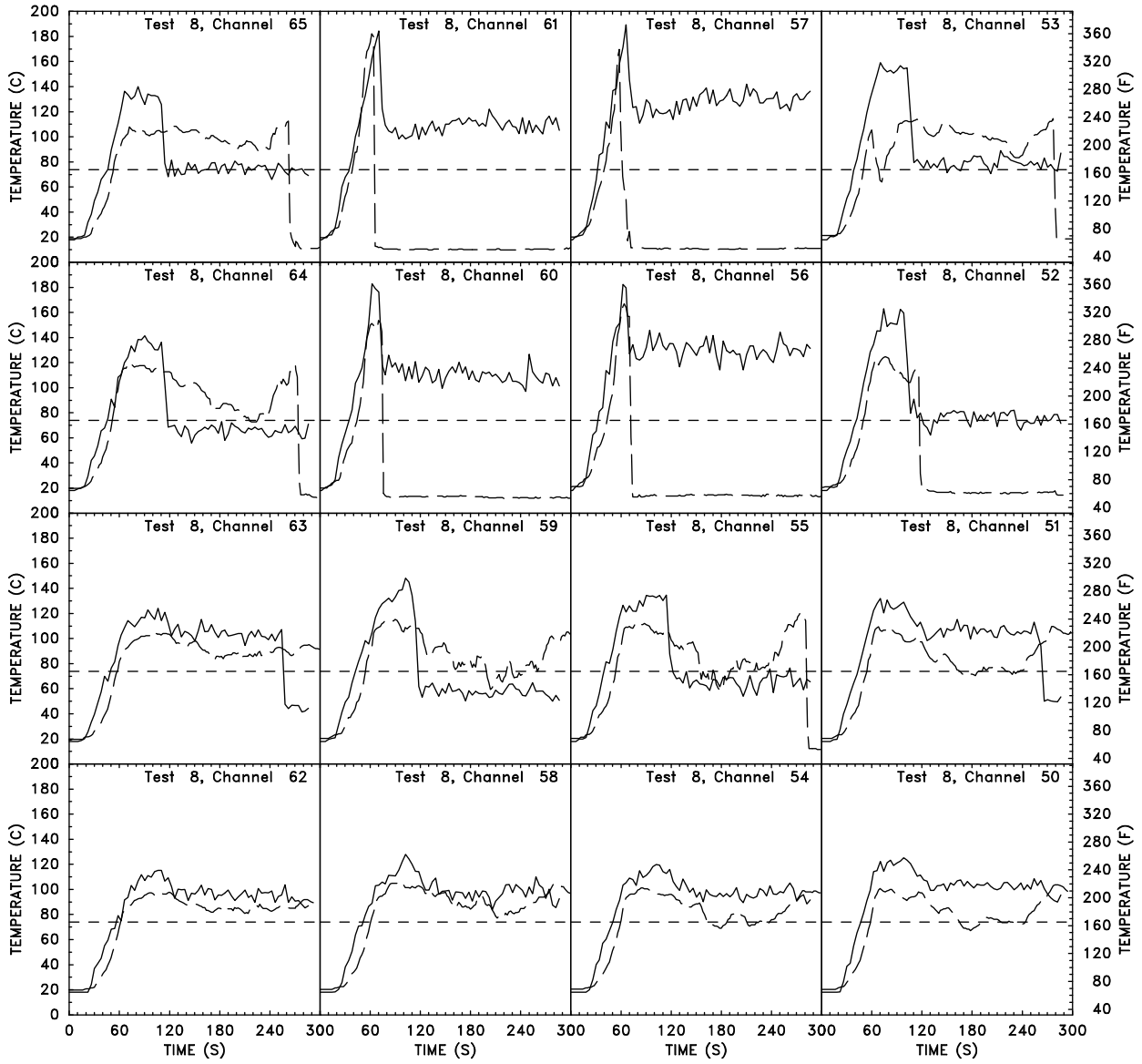

Figure 92: Comparison of experimental (dashed curve) and simulated (solid curve) temperatures of the near-sprinkler thermocouples for Test I-8 of the first series of heptane spray burner tests. The activation temperature of the sprinkler (74°C, 165°F) is denoted with a short dashed line. See Fig. 1 for the location of the sprinklers.

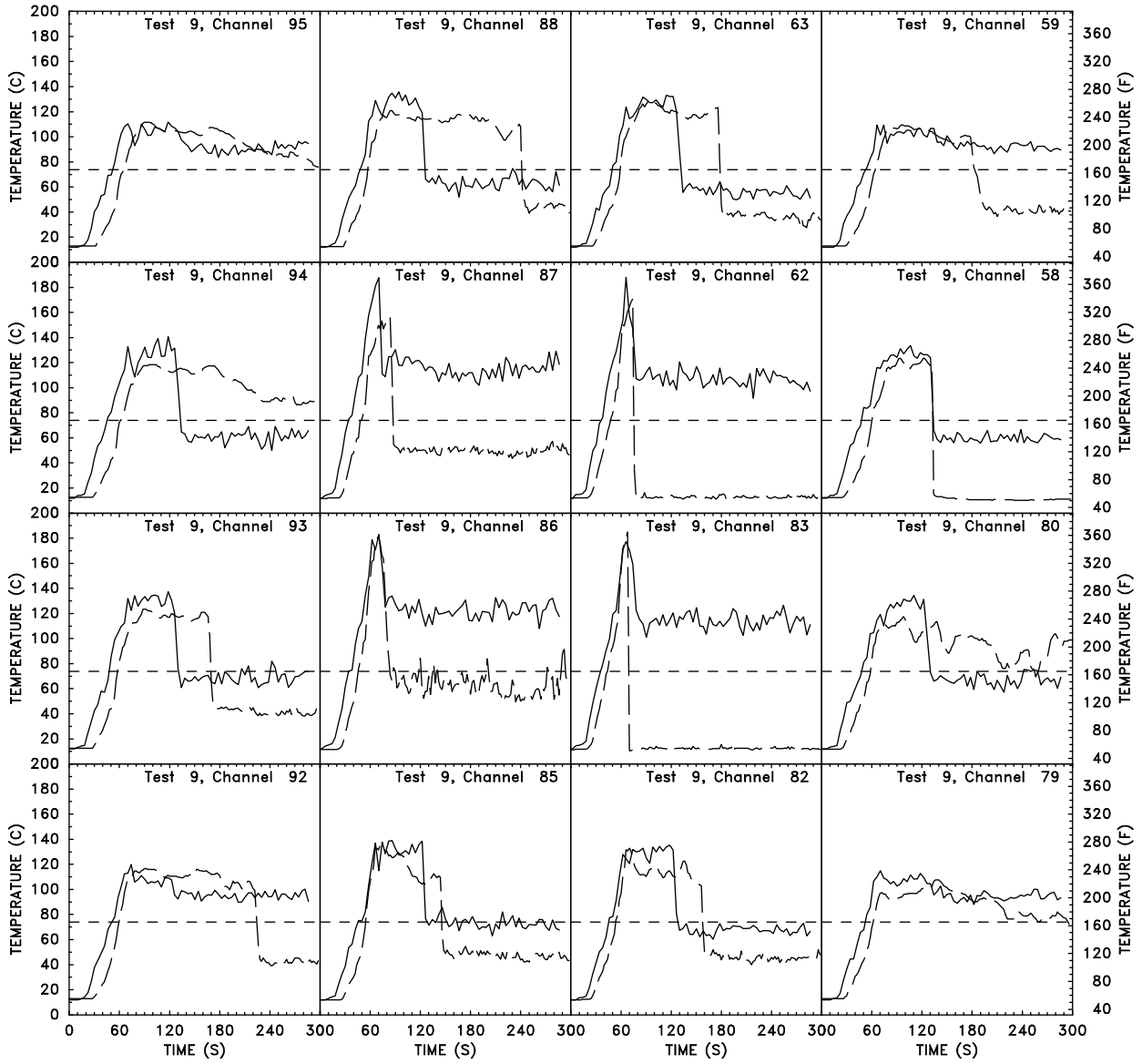

Figure 93: Comparison of experimental (dashed curve) and simulated (solid curve) temperatures of the near-sprinkler thermocouples for Test I-9 of the first series of heptane spray burner tests. The activation temperature of the sprinkler (74°C, 165°F) is denoted with a short dashed line. See Fig. 1 for the location of the sprinklers.

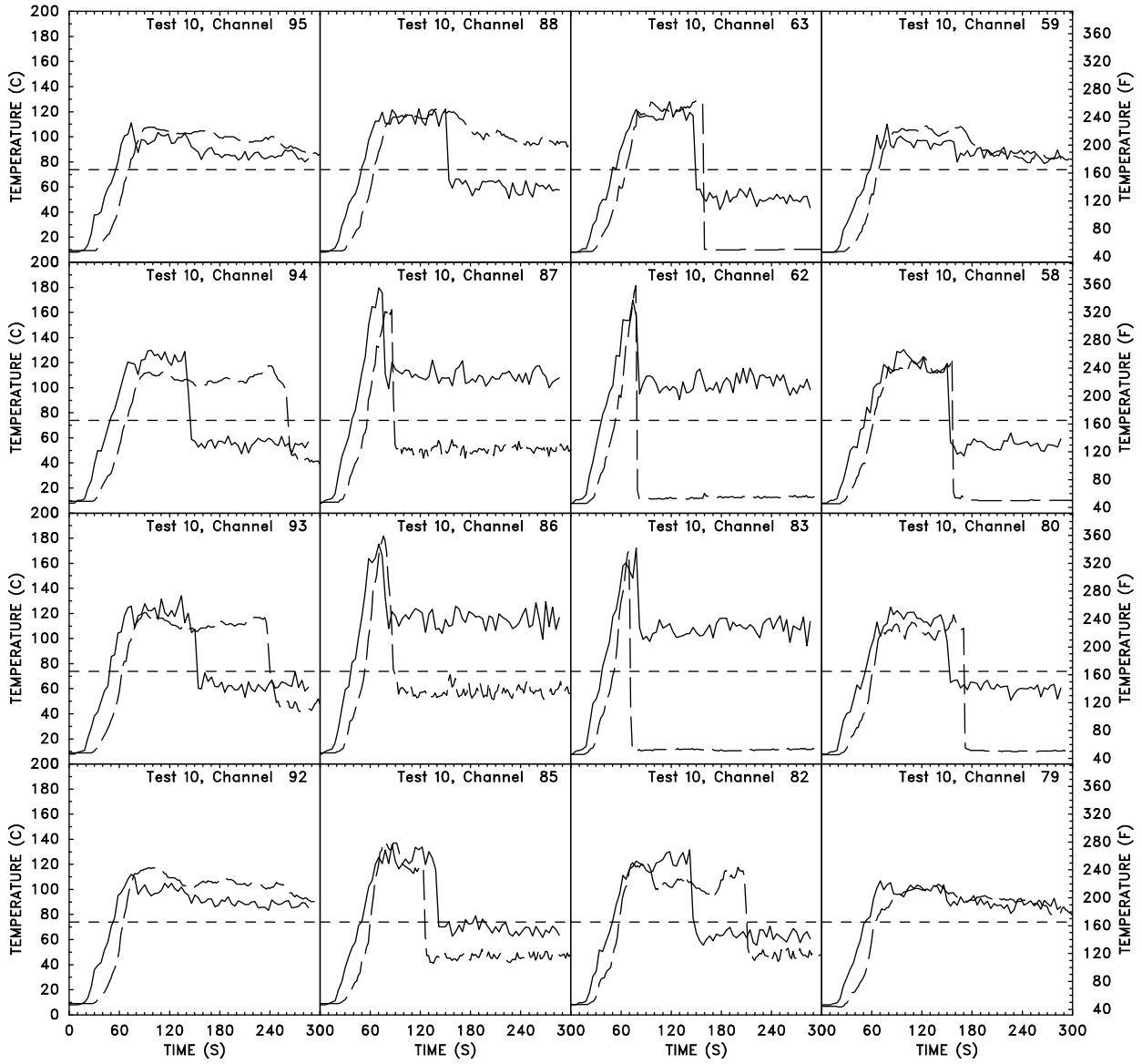

Figure 94: Comparison of experimental (dashed curve) and simulated (solid curve) temperatures of the near-sprinkler thermocouples for Test I-10 of the first series of heptane spray burner tests. The activation temperature of the sprinkler (74°C, 165°F) is denoted with a short dashed line. See Fig. 1 for the location of the sprinklers.

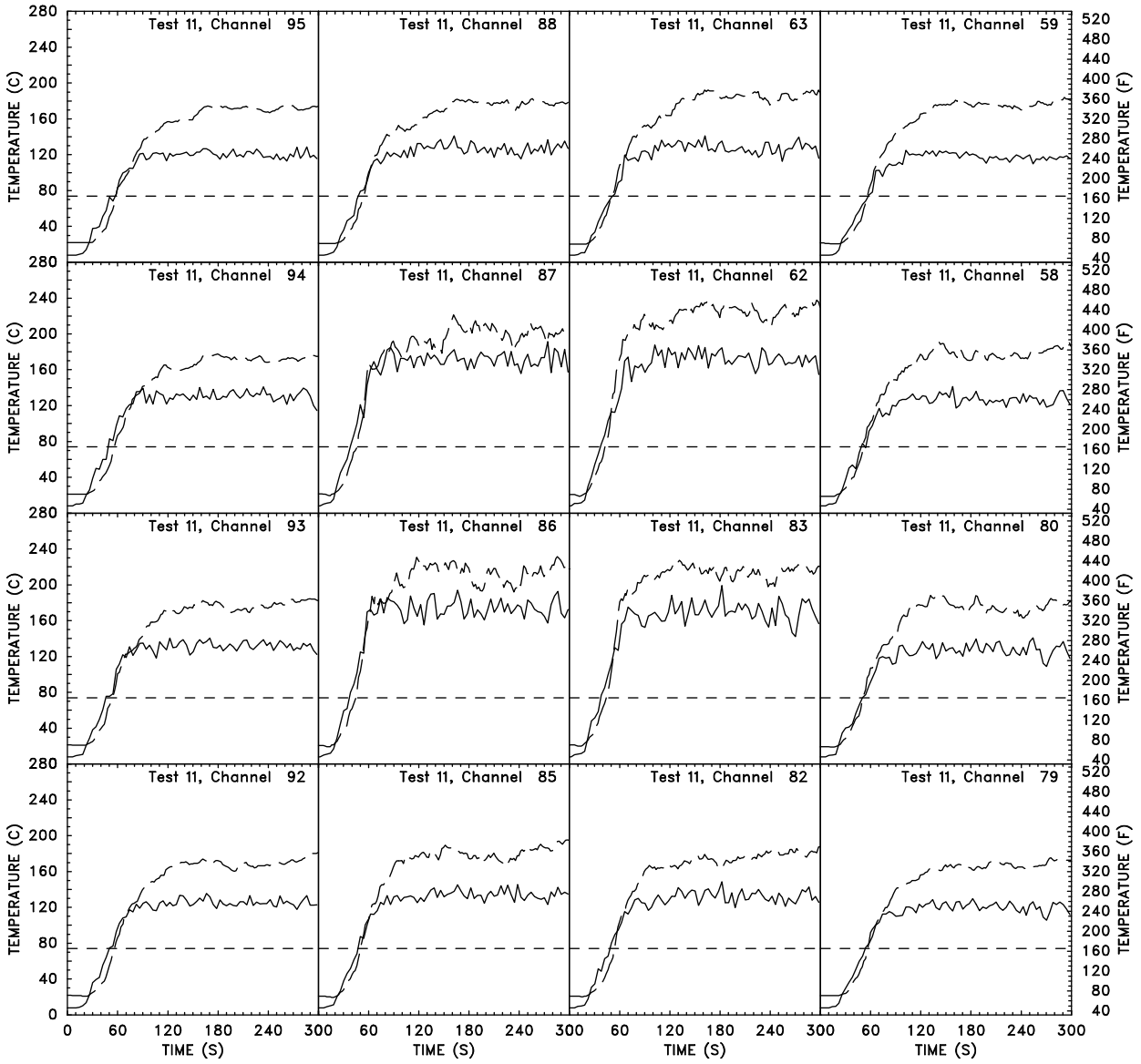

Figure 95: Comparison of experimental (dashed curve) and simulated (solid curve) temperatures of the near-sprinkler thermocouples for Test I-11 of the first series of heptane spray burner tests. The activation temperature of the sprinkler (74°C, 165°F) is denoted with a short dashed line. See Fig. 1 for the location of the sprinklers.

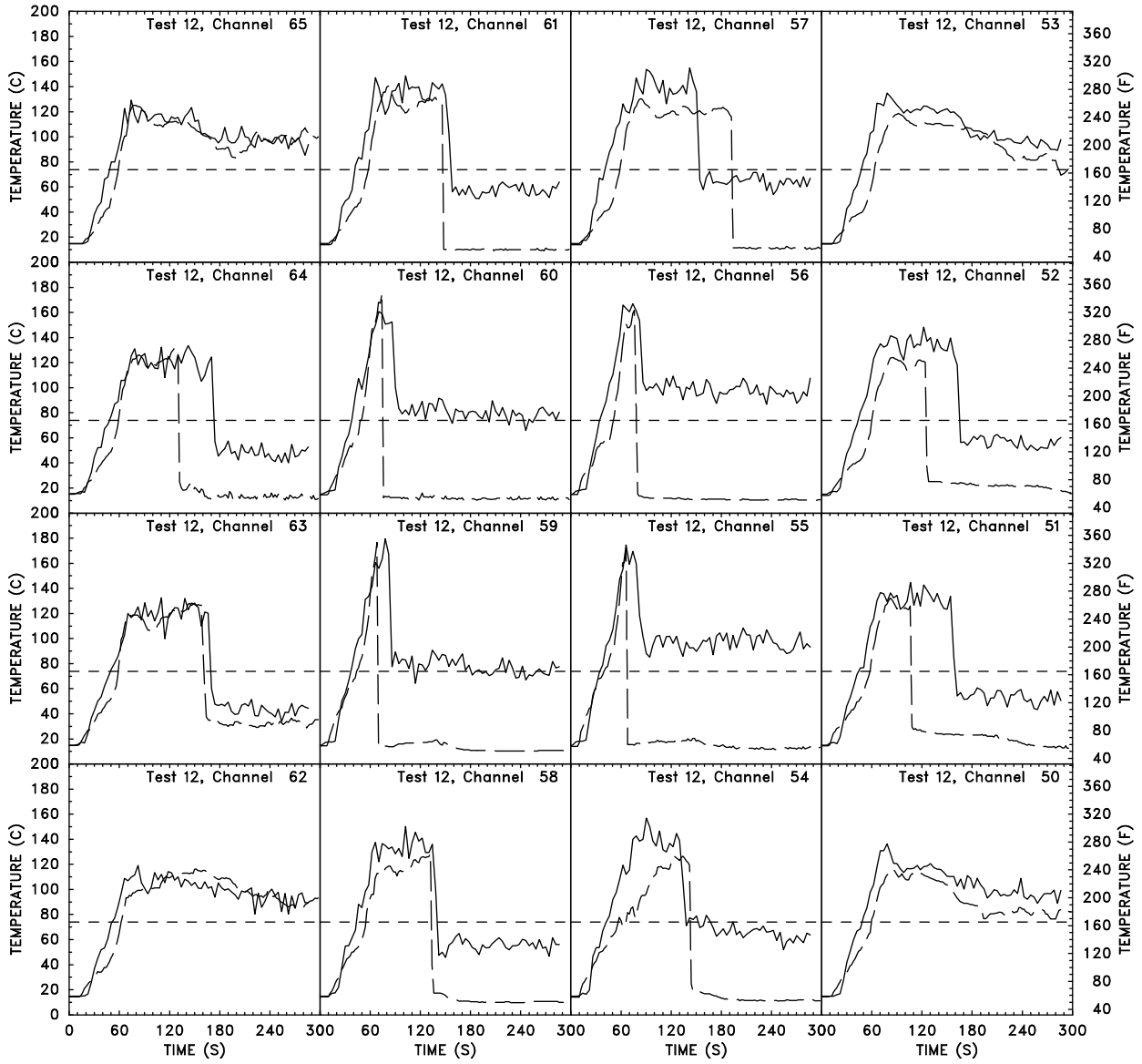

Figure 96: Comparison of experimental (dashed curve) and simulated (solid curve) temperatures of the near-sprinkler thermocouples for Test I-12 of the first series of heptane spray burner tests. The activation temperature of the sprinkler (74°C, 165°F) is denoted with a short dashed line. See Fig. 1 for the location of the sprinklers.

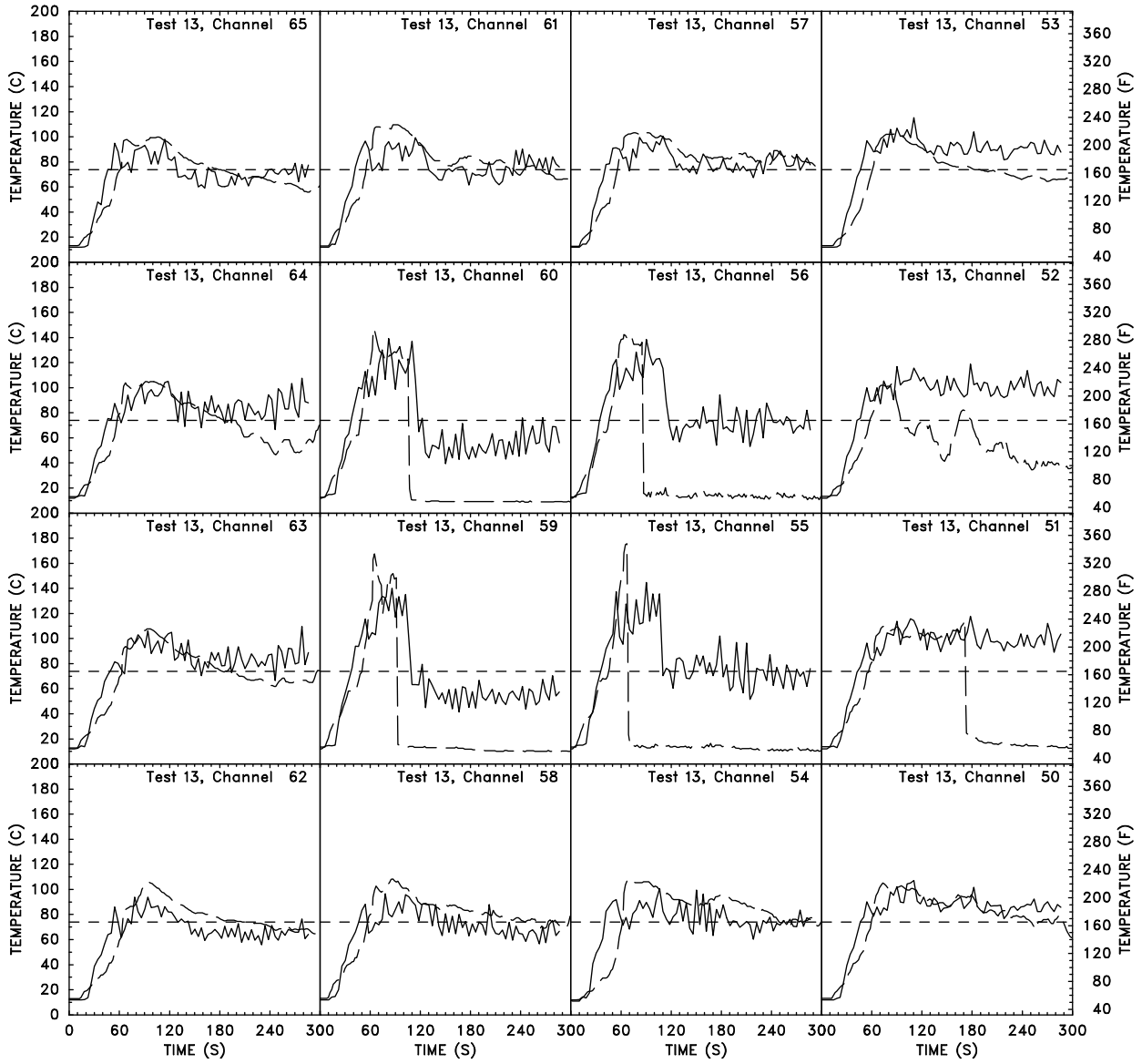

Figure 97: Comparison of experimental (dashed curve) and simulated (solid curve) temperatures of the near-sprinkler thermocouples for Test I-13 of the first series of heptane spray burner tests. The activation temperature of the sprinkler (74°C, 165°F) is denoted with a short dashed line. See Fig. 1 for the location of the sprinklers.

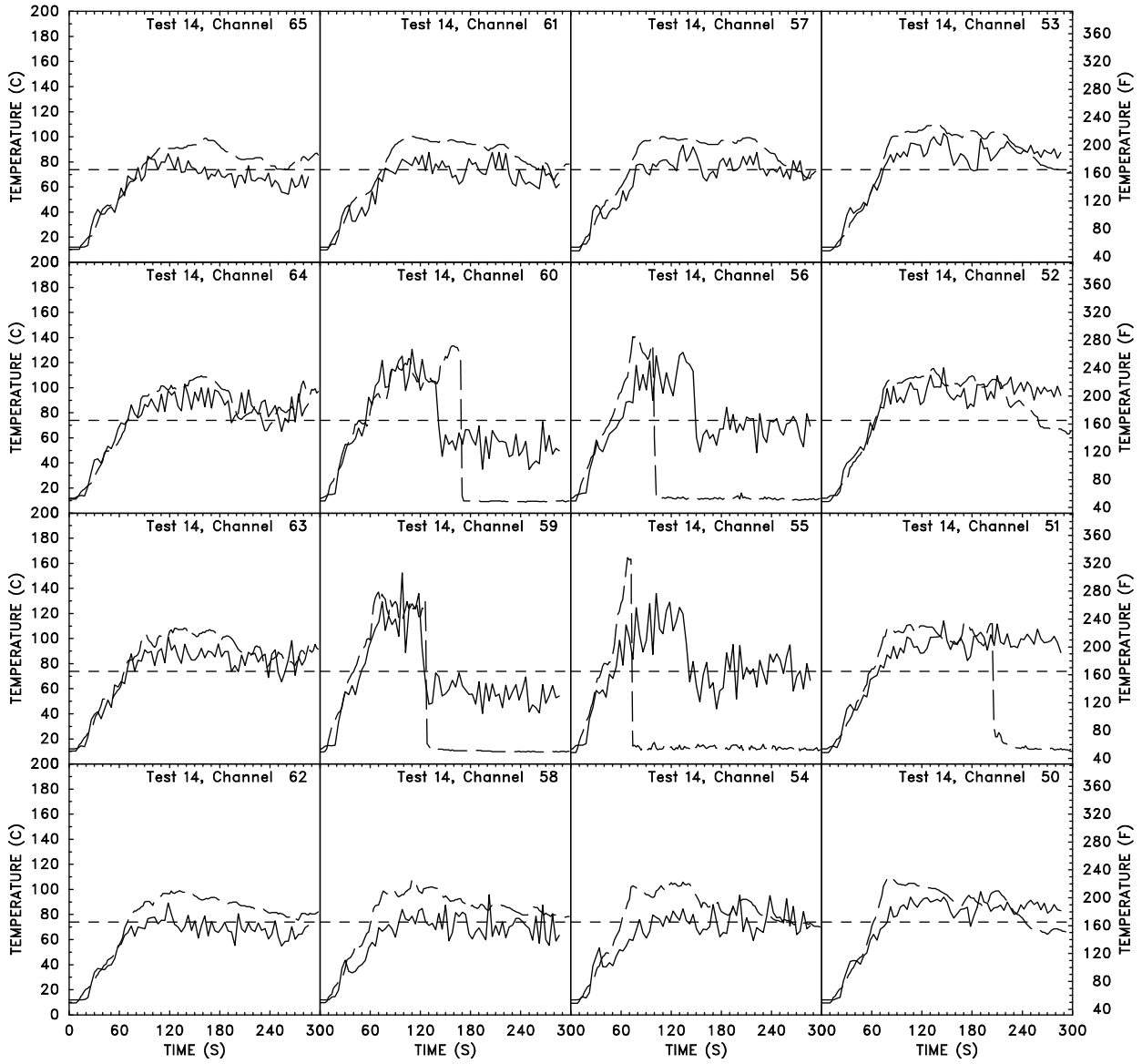

Figure 98: Comparison of experimental (dashed curve) and simulated (solid curve) temperatures of the near-sprinkler thermocouples for Test I-14 of the first series of heptane spray burner tests. The activation temperature of the sprinkler (74°C, 165°F) is denoted with a short dashed line. See Fig. 1 for the location of the sprinklers.

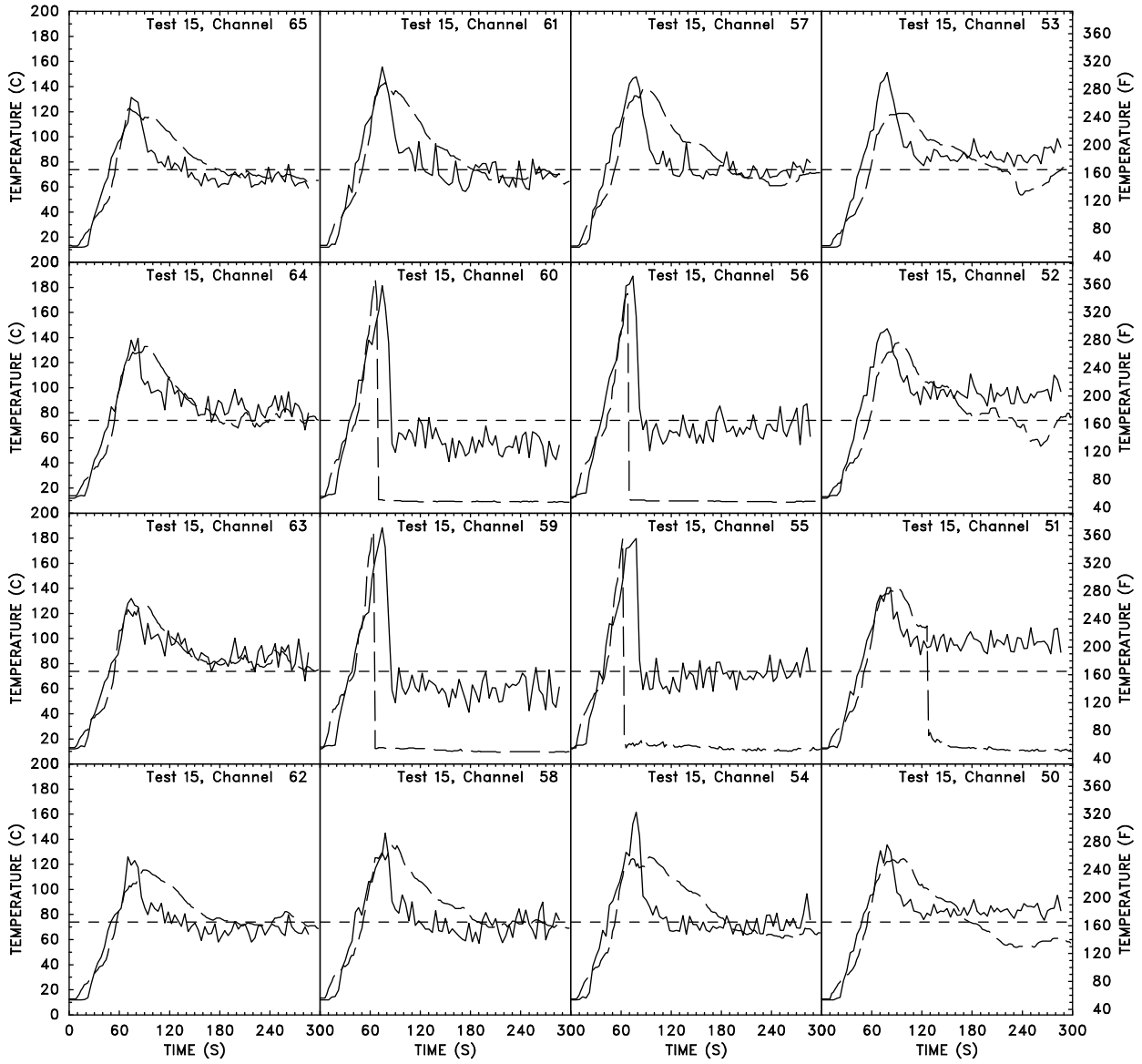

Figure 99: Comparison of experimental (dashed curve) and simulated (solid curve) temperatures of the near-sprinkler thermocouples for Test I-15 of the first series of heptane spray burner tests. The activation temperature of the sprinkler (74°C, 165°F) is denoted with a short dashed line. See Fig. 1 for the location of the sprinklers.

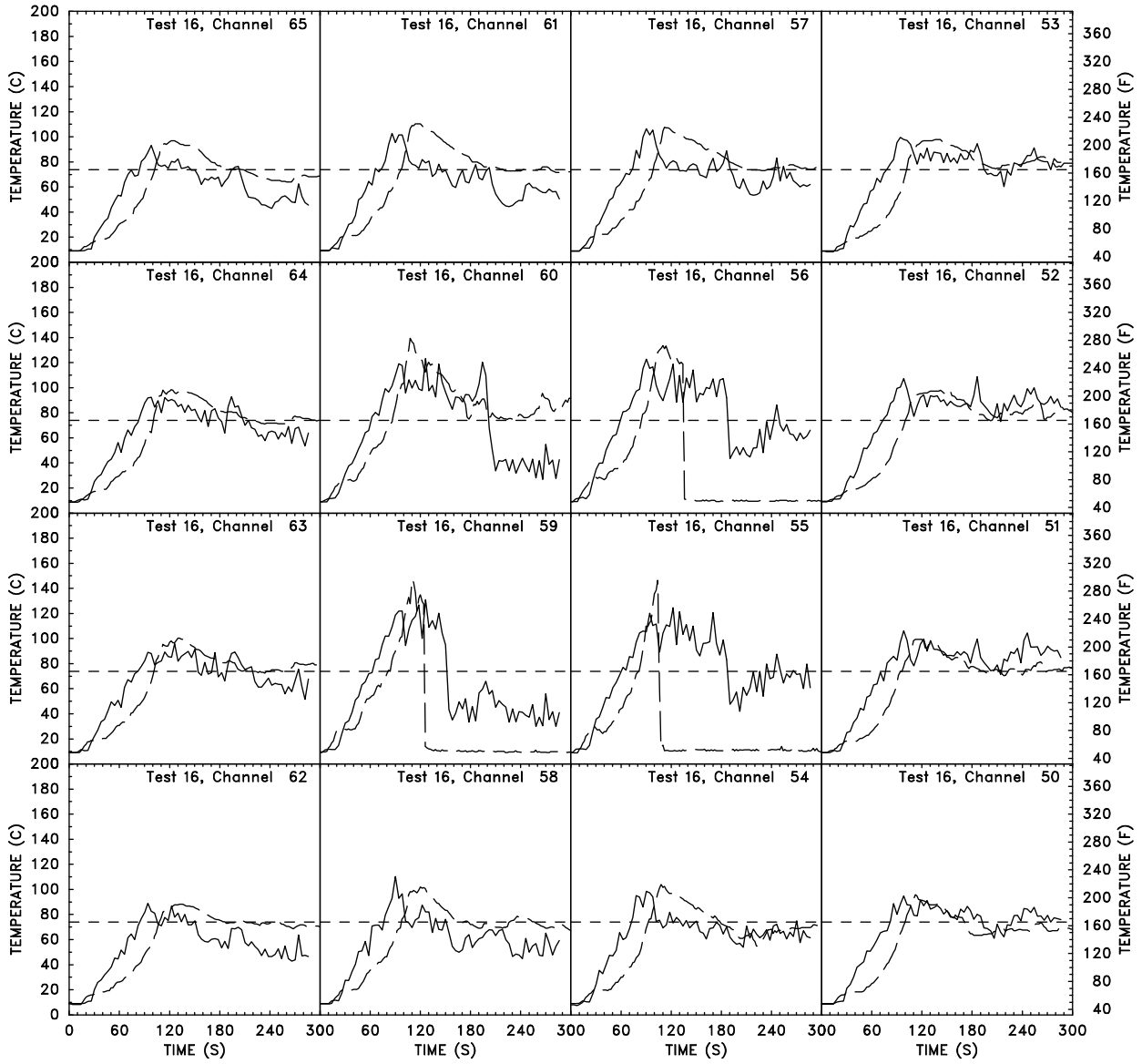

Figure 100: Comparison of experimental (dashed curve) and simulated (solid curve) temperatures of the near-sprinkler thermocouples for Test I-16 of the first series of heptane spray burner tests. The activation temperature of the sprinkler (74°C, 165°F) is denoted with a short dashed line. See Fig. 1 for the location of the sprinklers.

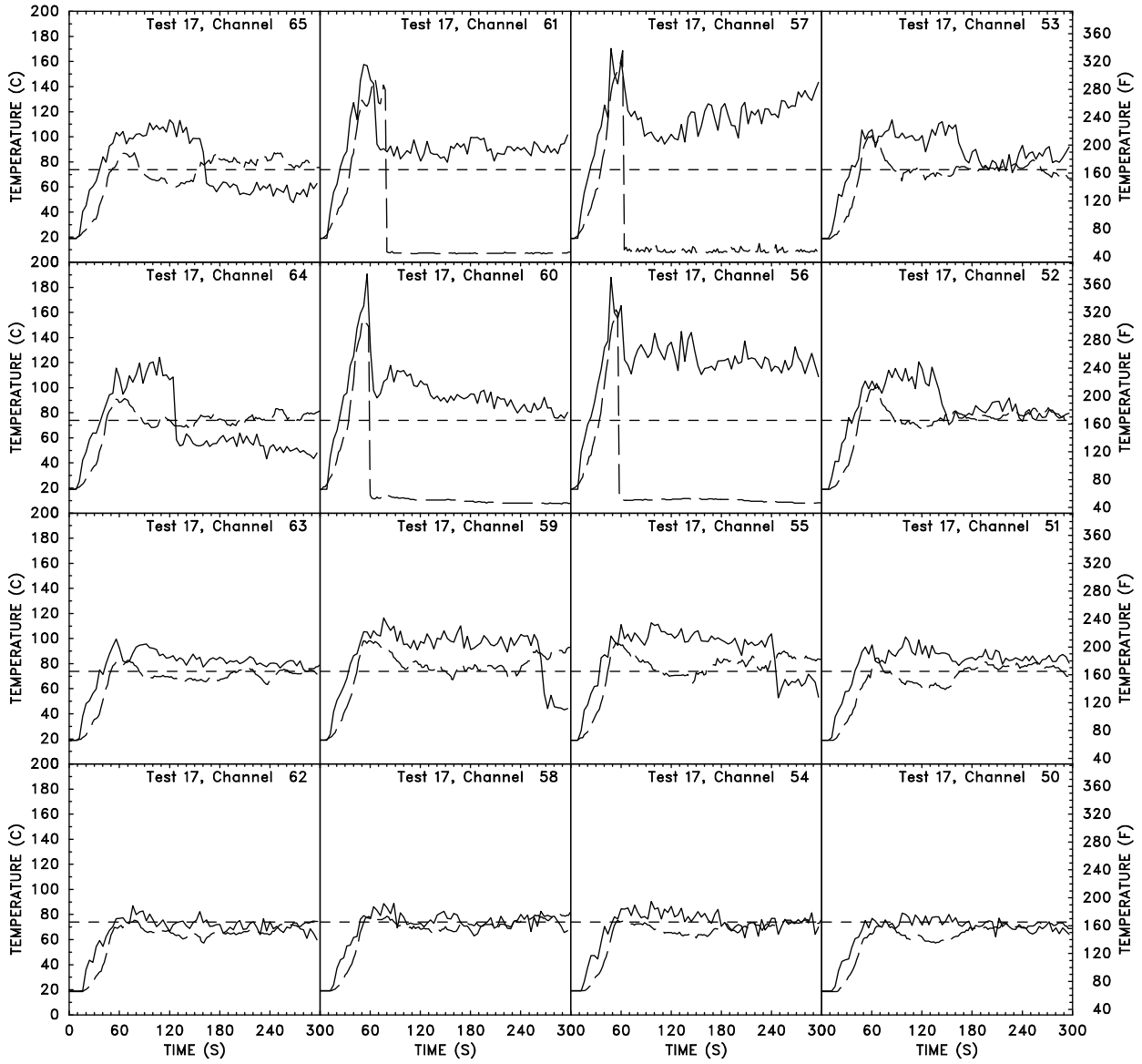

Figure 101: Comparison of experimental (dashed curve) and simulated (solid curve) temperatures of the near-sprinkler thermocouples for Test I-17 of the first series of heptane spray burner tests. The activation temperature of the sprinkler (74°C, 165°F) is denoted with a short dashed line. See Fig. 1 for the location of the sprinklers.

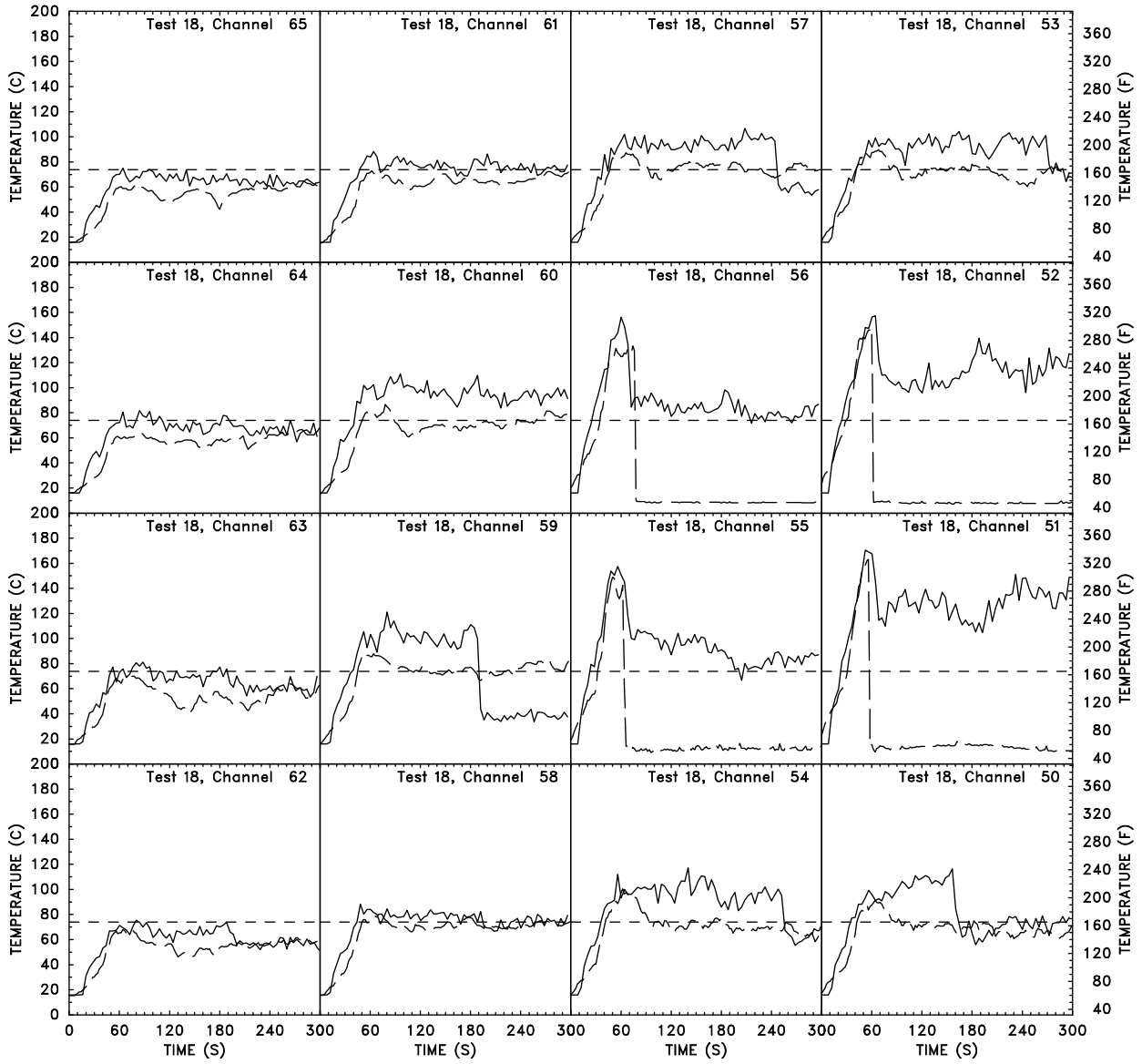

Figure 102: Comparison of experimental (dashed curve) and simulated (solid curve) temperatures of the near-sprinkler thermocouples for Test I-18 of the first series of heptane spray burner tests. The activation temperature of the sprinkler (74°C, 165°F) is denoted with a short dashed line. See Fig. 1 for the location of the sprinklers.

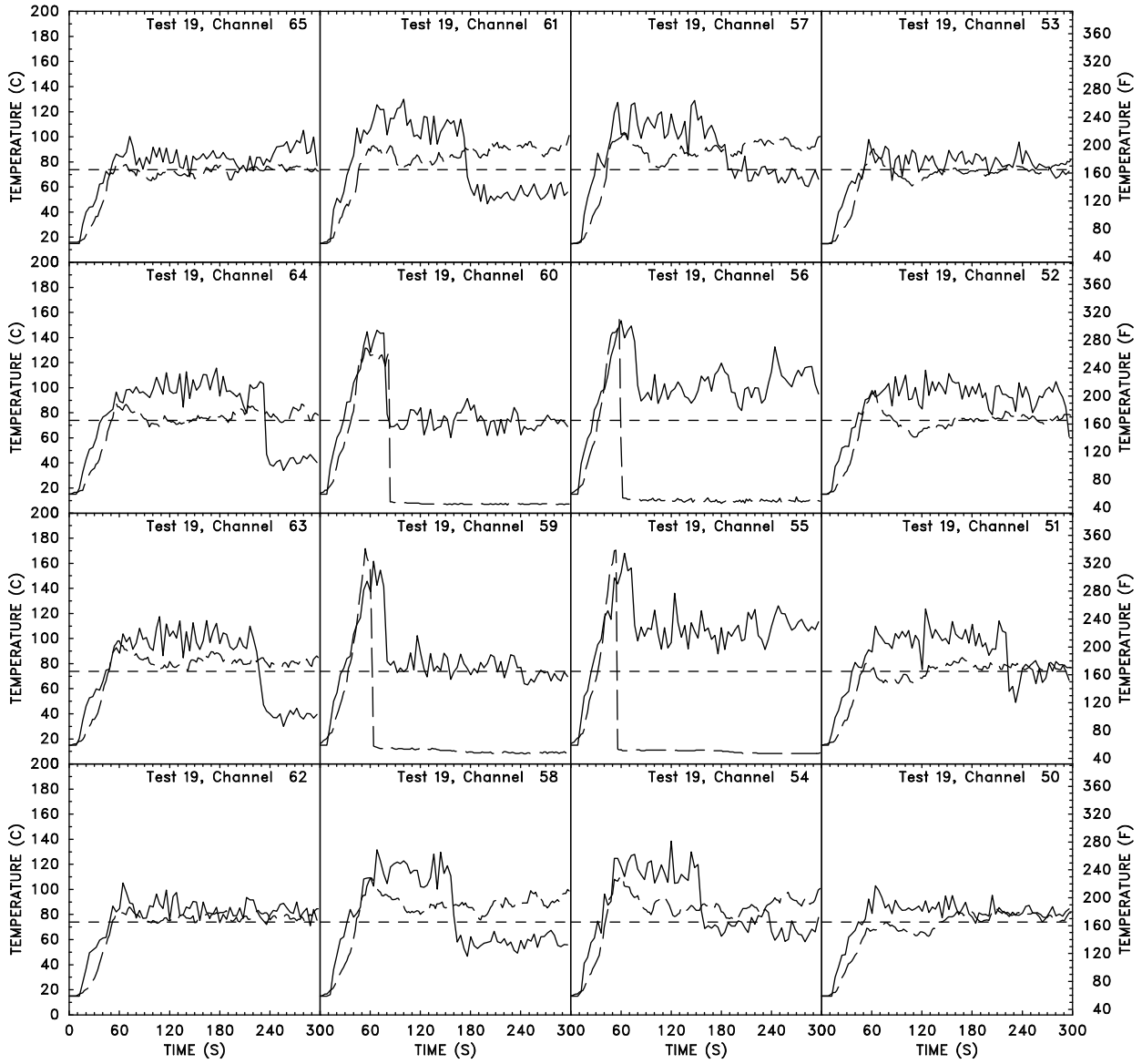

Figure 103: Comparison of experimental (dashed curve) and simulated (solid curve) temperatures of the near-sprinkler thermocouples for Test I-19 of the first series of heptane spray burner tests. The activation temperature of the sprinkler (74°C, 165°F) is denoted with a short dashed line. See Fig. 1 for the location of the sprinklers.

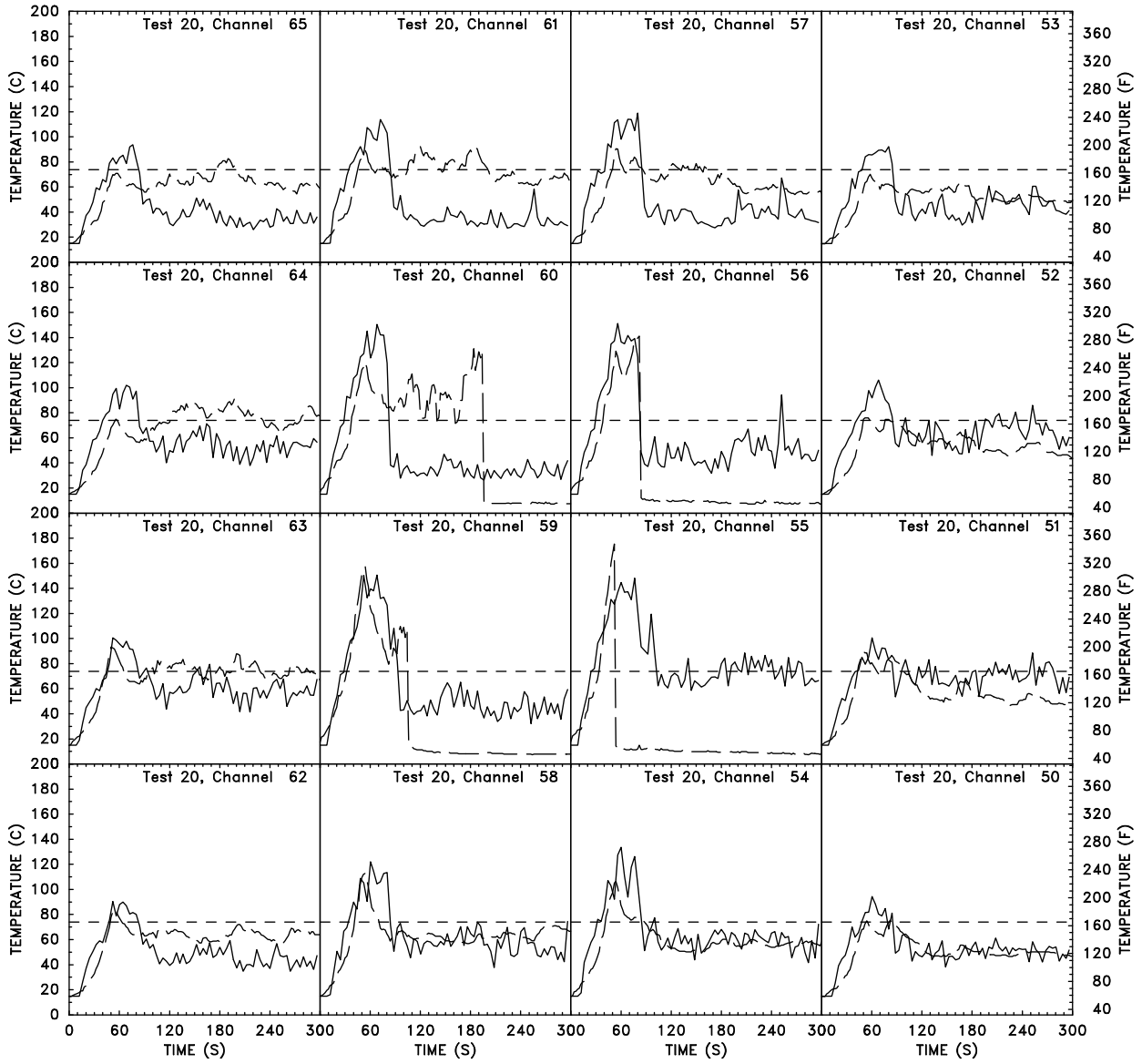

Figure 104: Comparison of experimental (dashed curve) and simulated (solid curve) temperatures of the near-sprinkler thermocouples for Test I-20 of the first series of heptane spray burner tests. The activation temperature of the sprinkler (74°C, 165°F) is denoted with a short dashed line. See Fig. 1 for the location of the sprinklers.

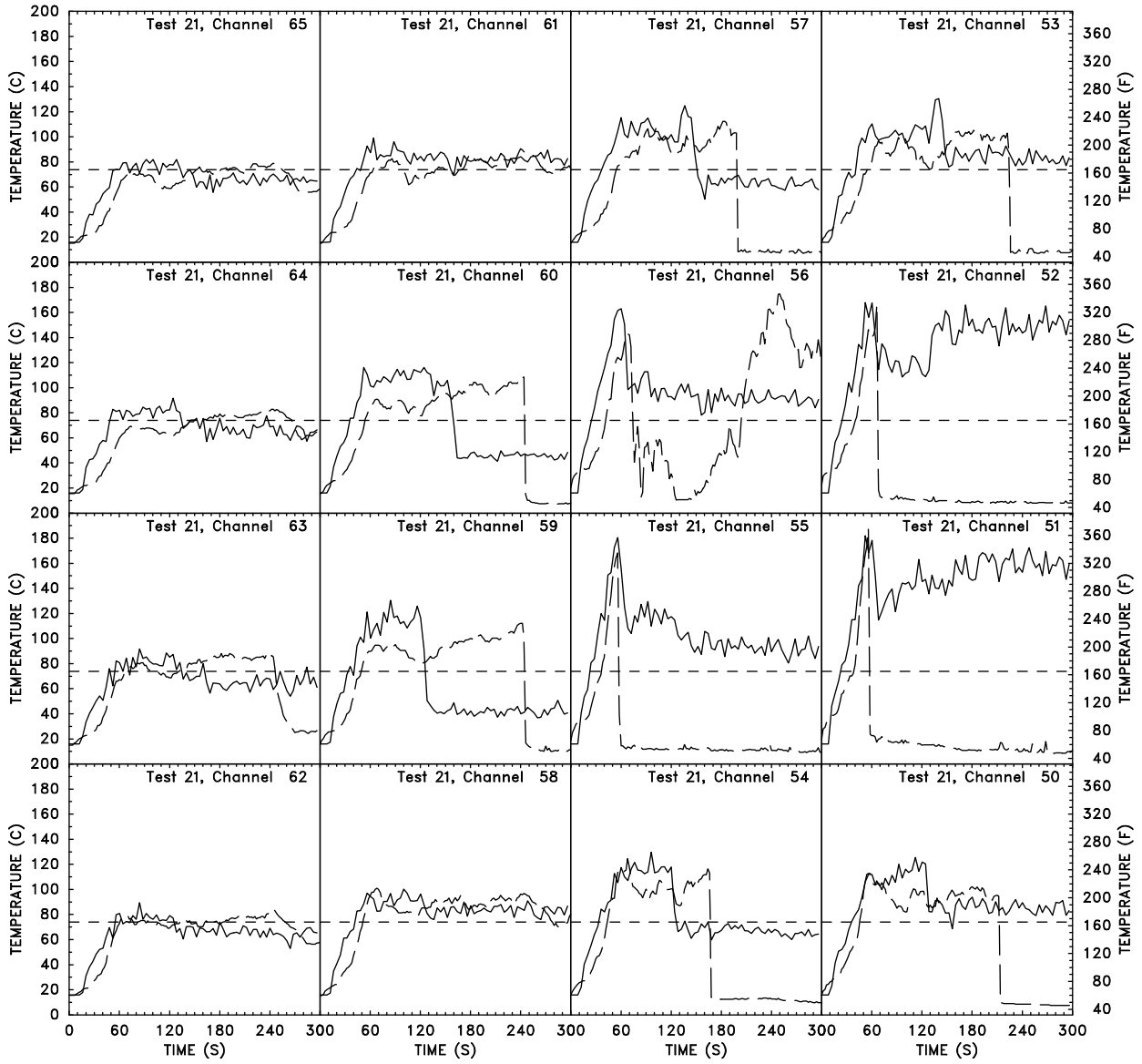

Figure 105: Comparison of experimental (dashed curve) and simulated (solid curve) temperatures of the near-sprinkler thermocouples for Test I-21 of the first series of heptane spray burner tests. The activation temperature of the sprinkler (74°C, 165°F) is denoted with a short dashed line. See Fig. 1 for the location of the sprinklers.

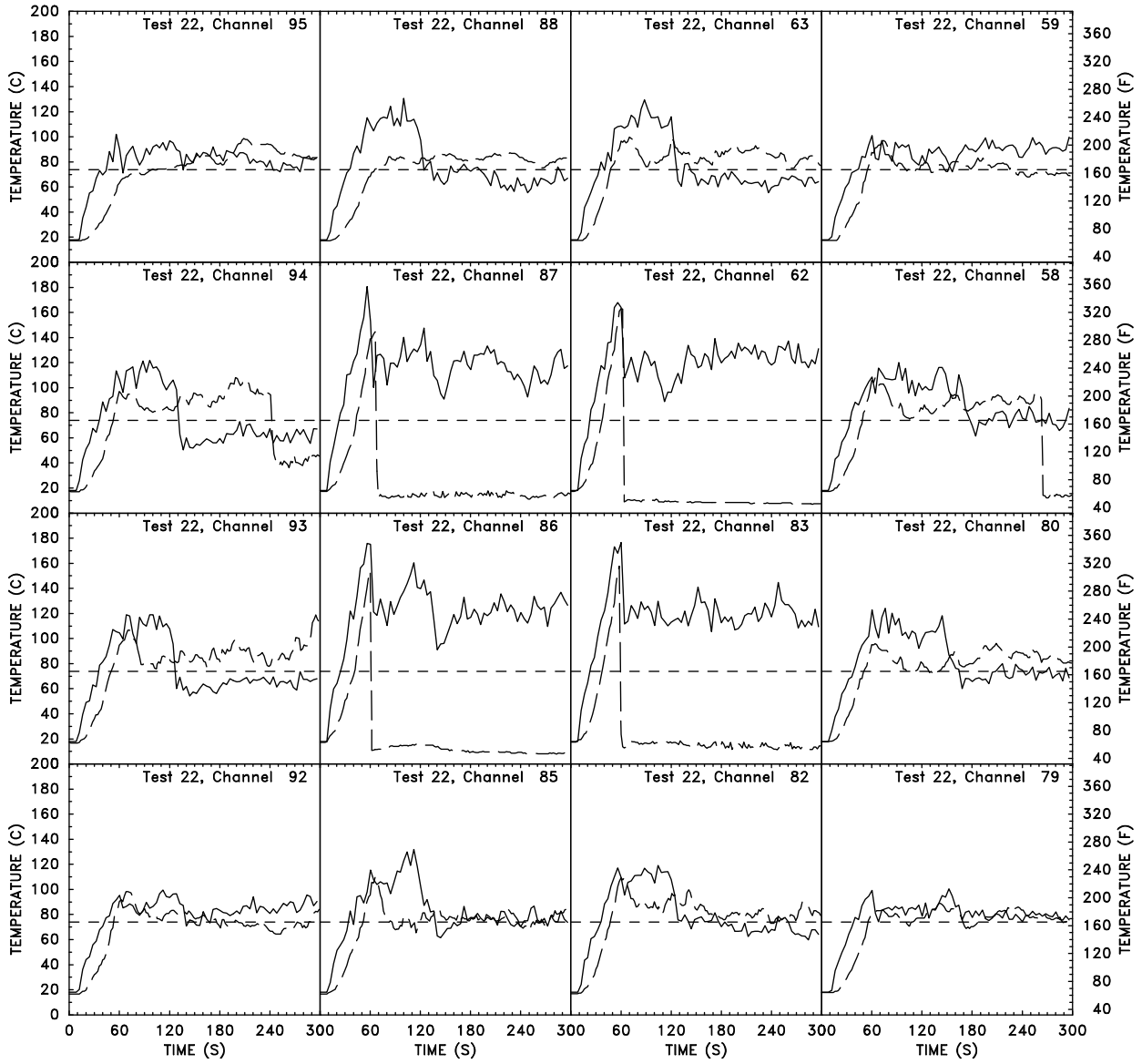

Figure 106: Comparison of experimental (dashed curve) and simulated (solid curve) temperatures of the near-sprinkler thermocouples for Test I-22 of the first series of heptane spray burner tests. The activation temperature of the sprinkler (74°C, 165°F) is denoted with a short dashed line. See Fig. 1 for the location of the sprinklers.

B Heptane Spray Burner Test Results, Series II

Figures 107–118 on the following pages are the temperatures for each of the 12 tests of the second heptane spray burner series.

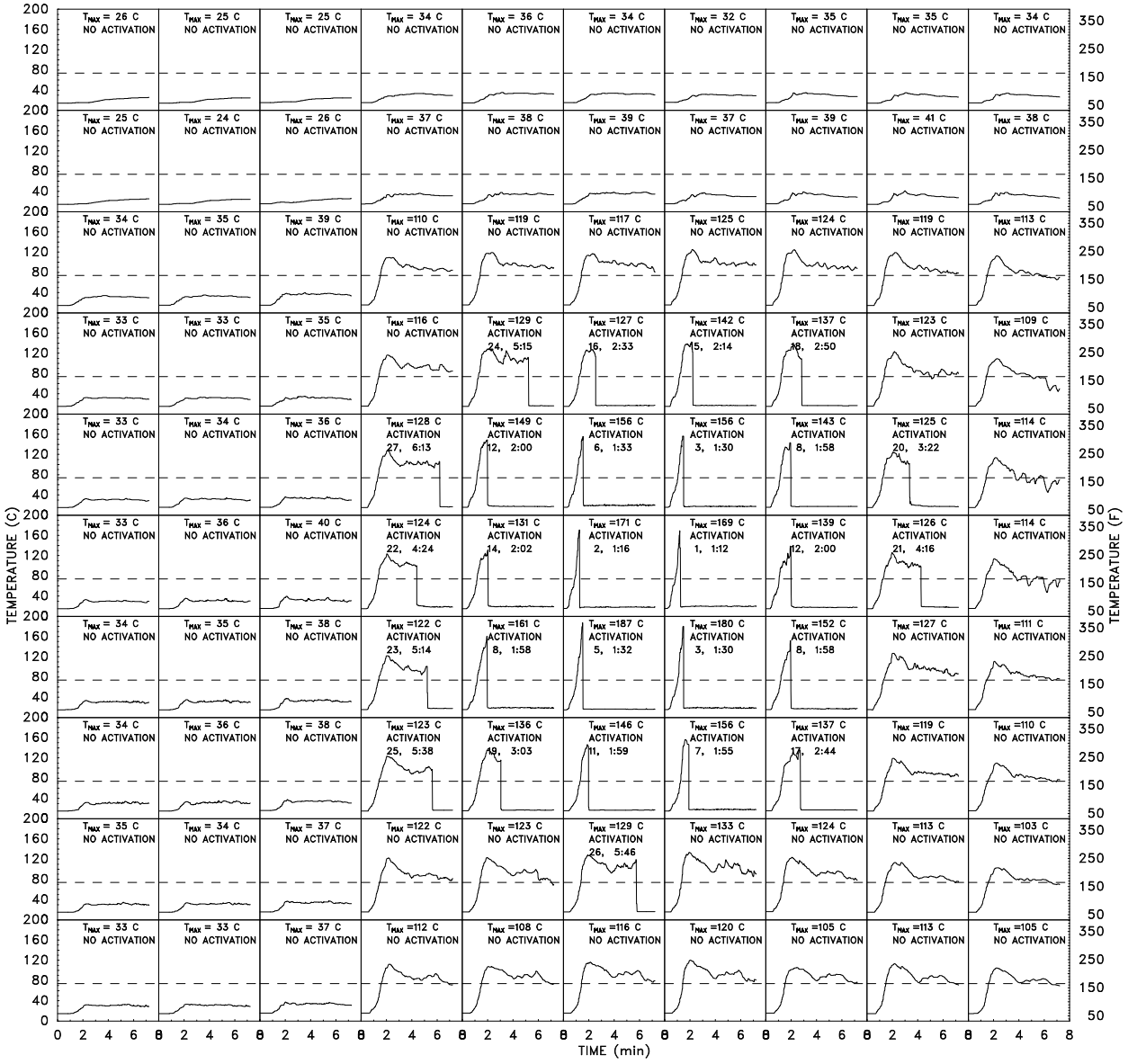

Figure 107: Temperature histories for the 100 near-sprinkler thermocouples for Test II-1, Heptane Series II.

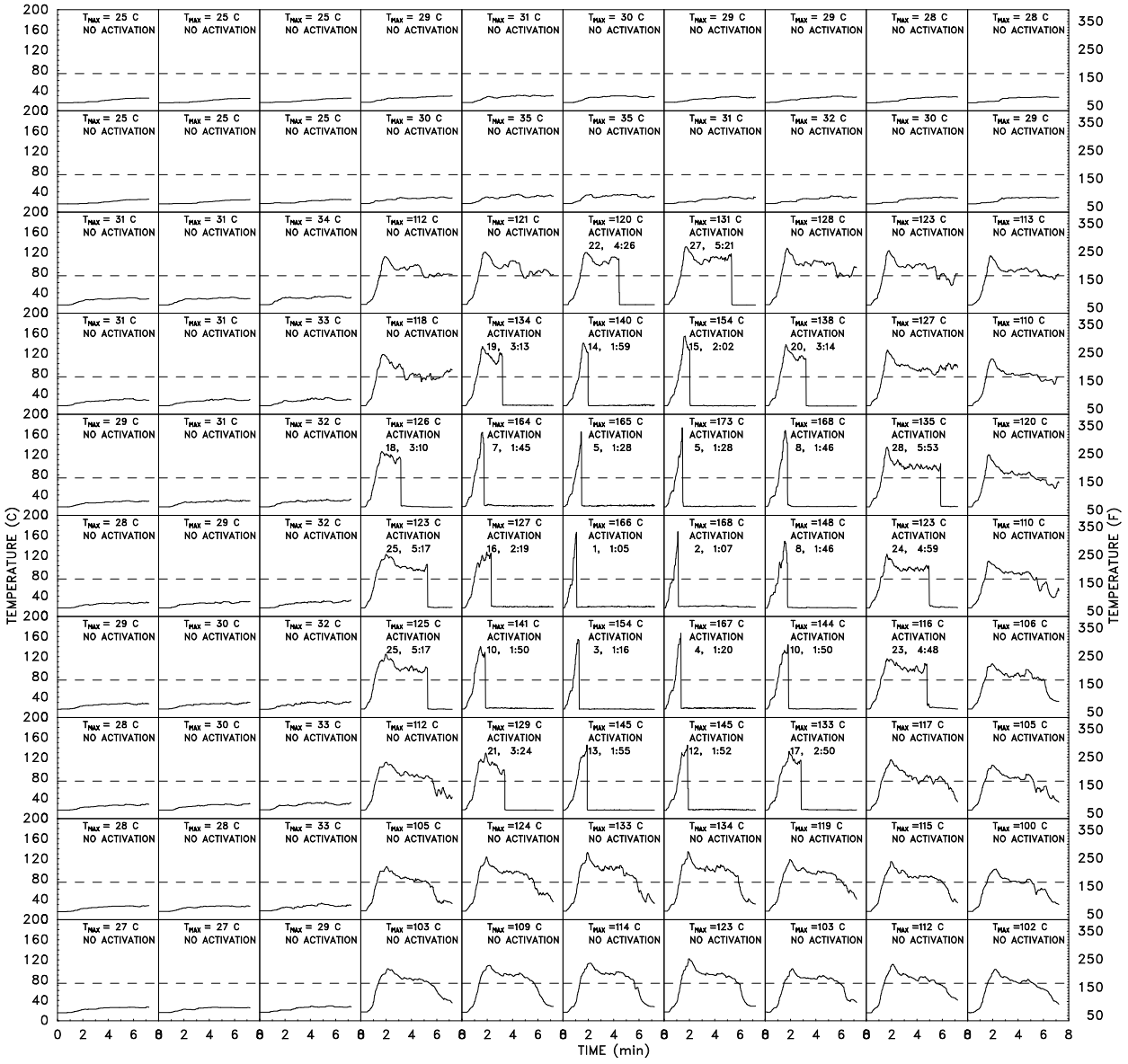

Figure 108: Temperature histories for the 100 near-sprinkler thermocouples for Test II-2, Heptane Series II.

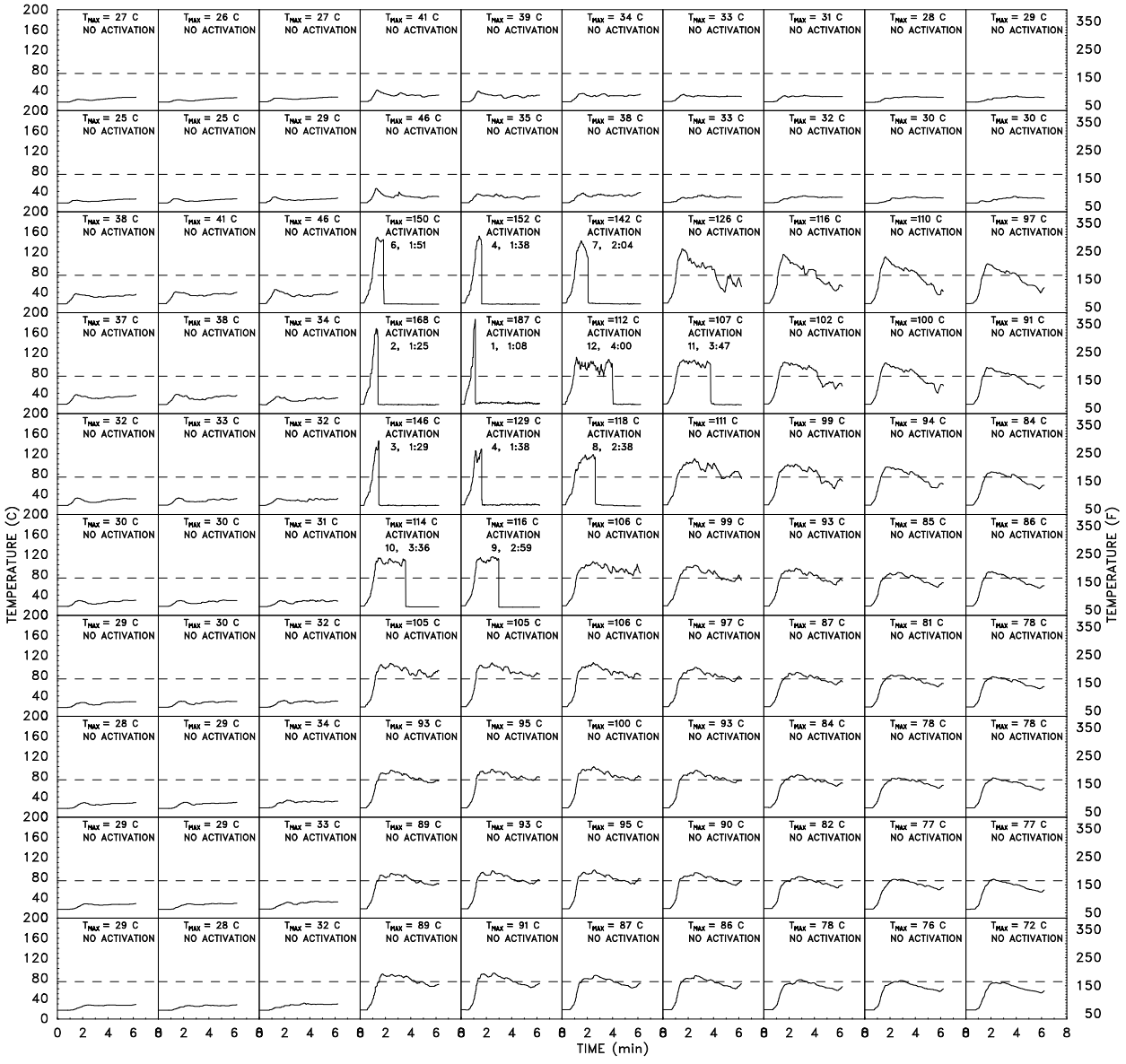

Figure 109: Temperature histories for the 100 near-sprinkler thermocouples for Test II-3, Heptane Series II.

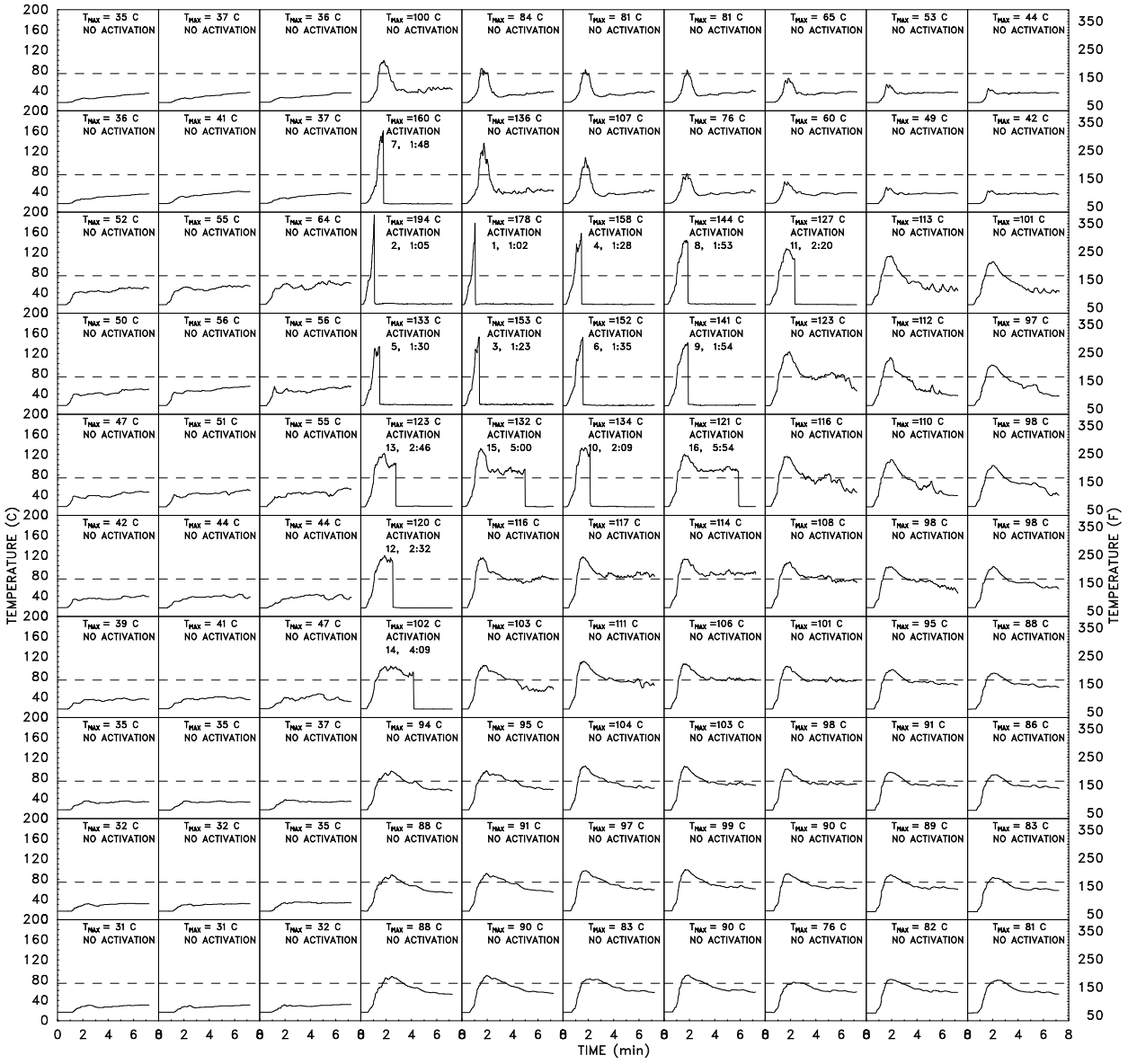

Figure 110: Temperature histories for the 100 near-sprinkler thermocouples for Test II-4, Heptane Series II.

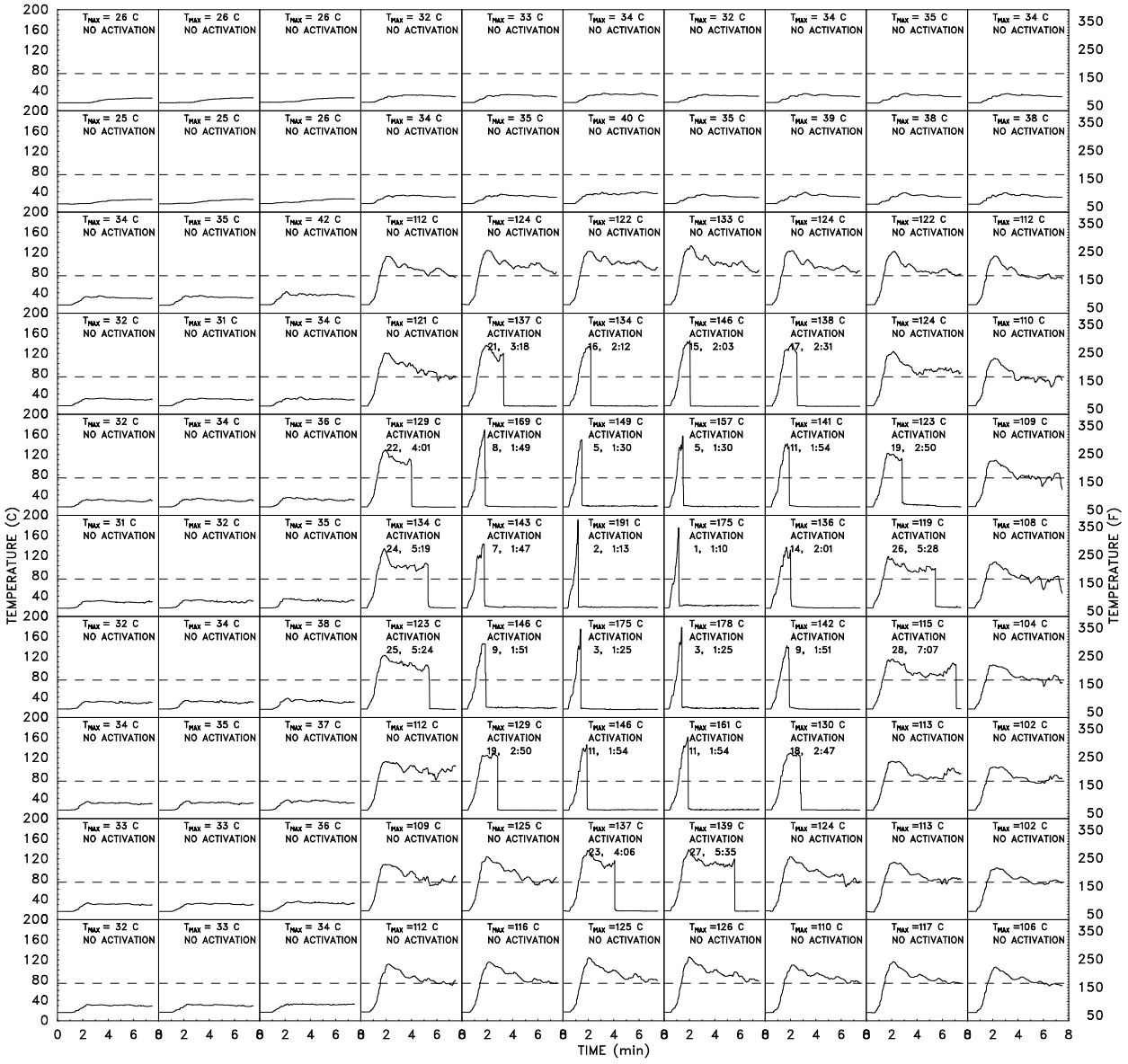

Figure 111: Temperature histories for the 100 near-sprinkler thermocouples for Test II-5, Heptane Series II.

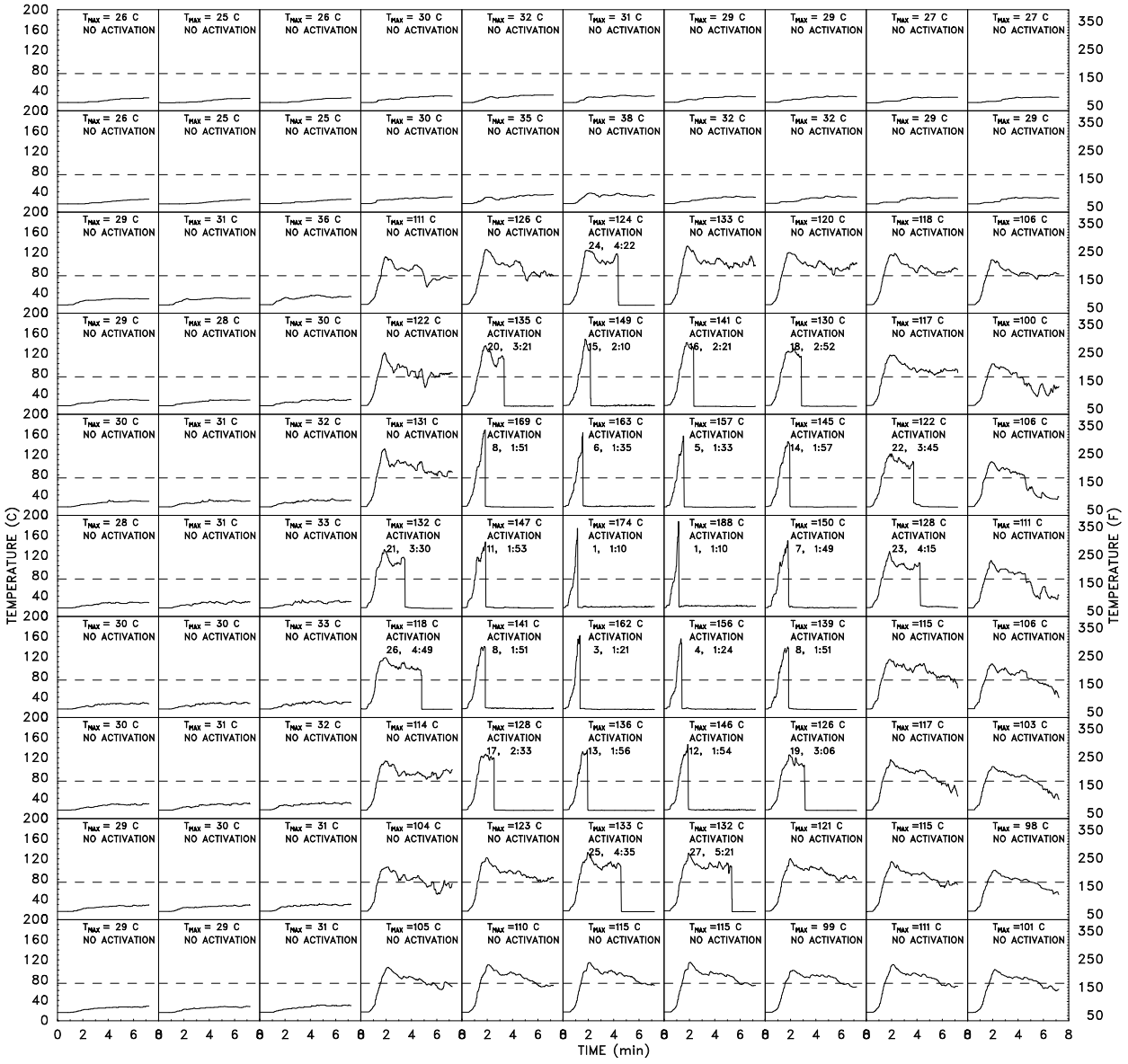

Figure 112: Temperature histories for the 100 near-sprinkler thermocouples for Test II-6, Heptane Series II.

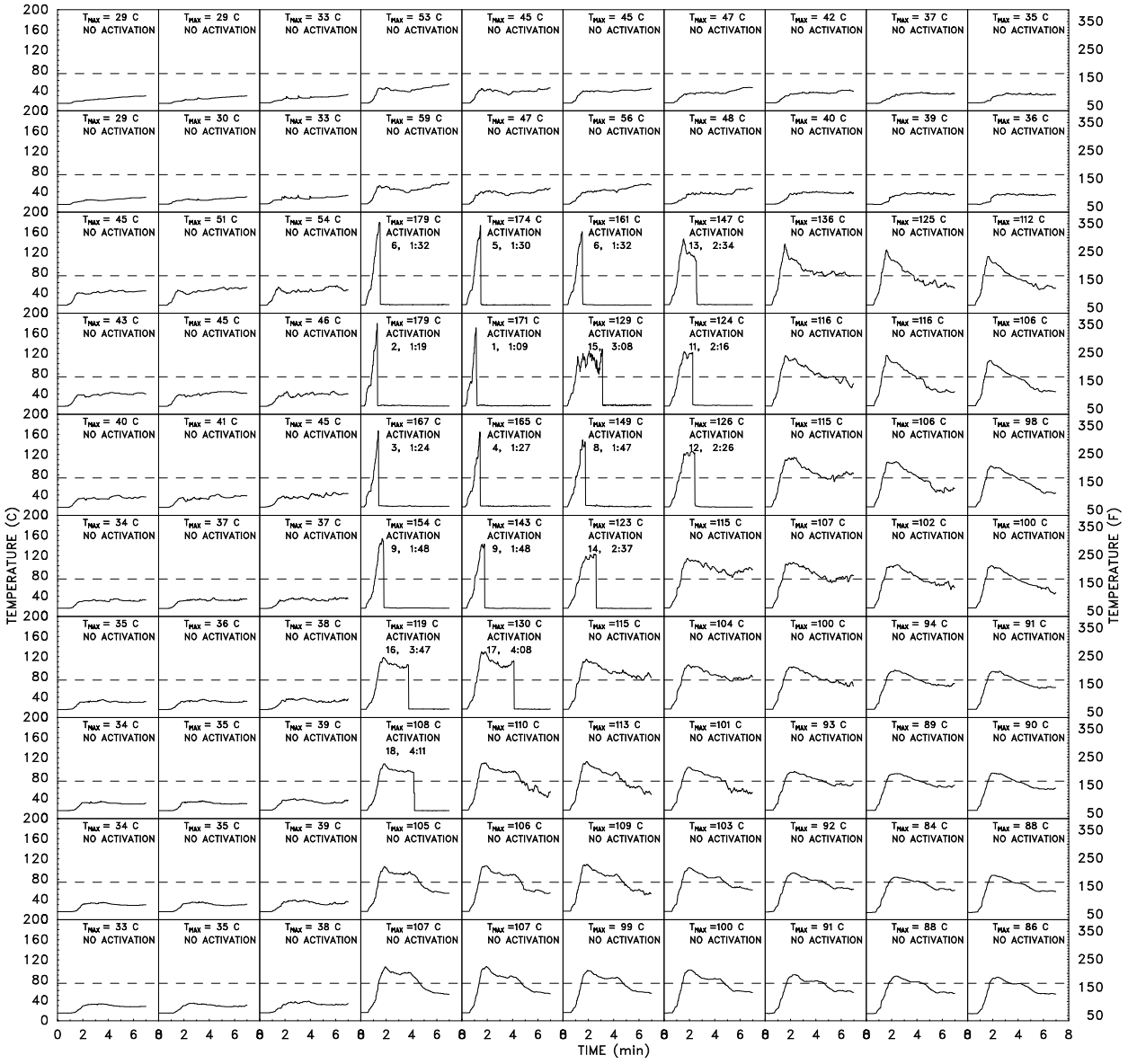

Figure 113: Temperature histories for the 100 near-sprinkler thermocouples for Test II-7, Heptane Series II.

Figure 114: Temperature histories for the 100 near-sprinkler thermocouples for Test II-8, Heptane Series II.

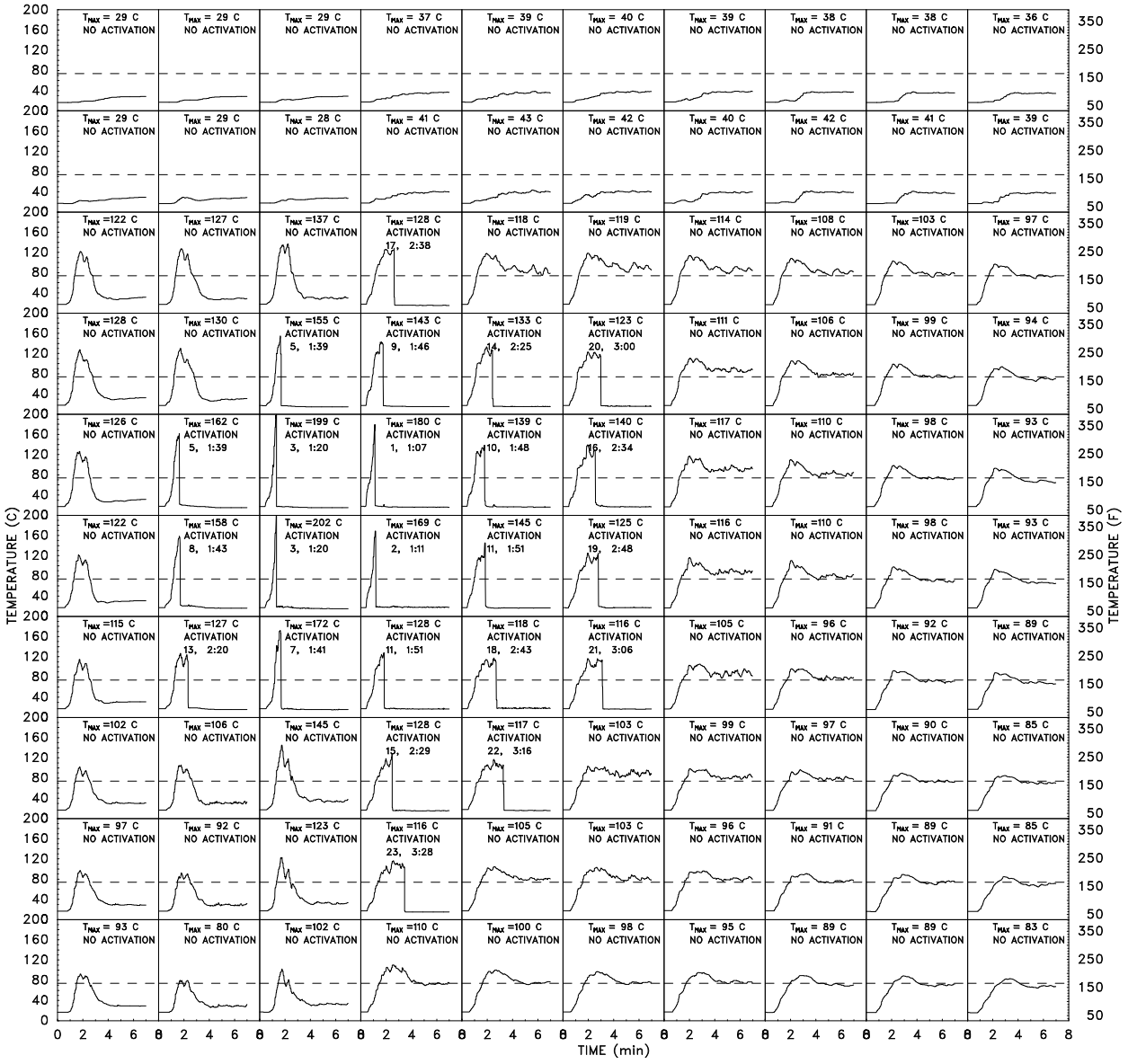

Figure 115: Temperature histories for the 100 near-sprinkler thermocouples for Test II-9, Heptane Series II.

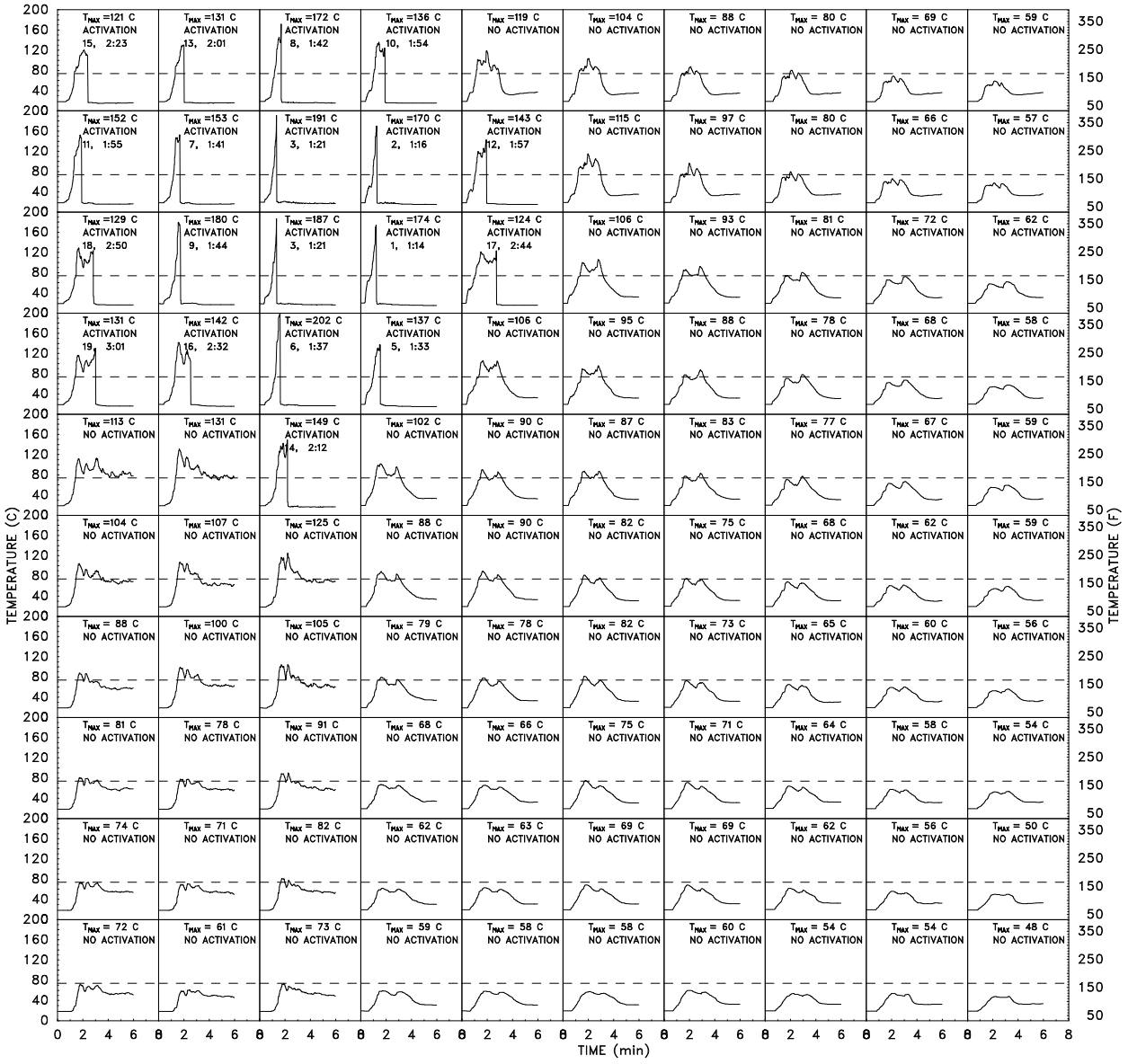

Figure 116: Temperature histories for the 100 near-sprinkler thermocouples for Test II-10, Heptane Series II.

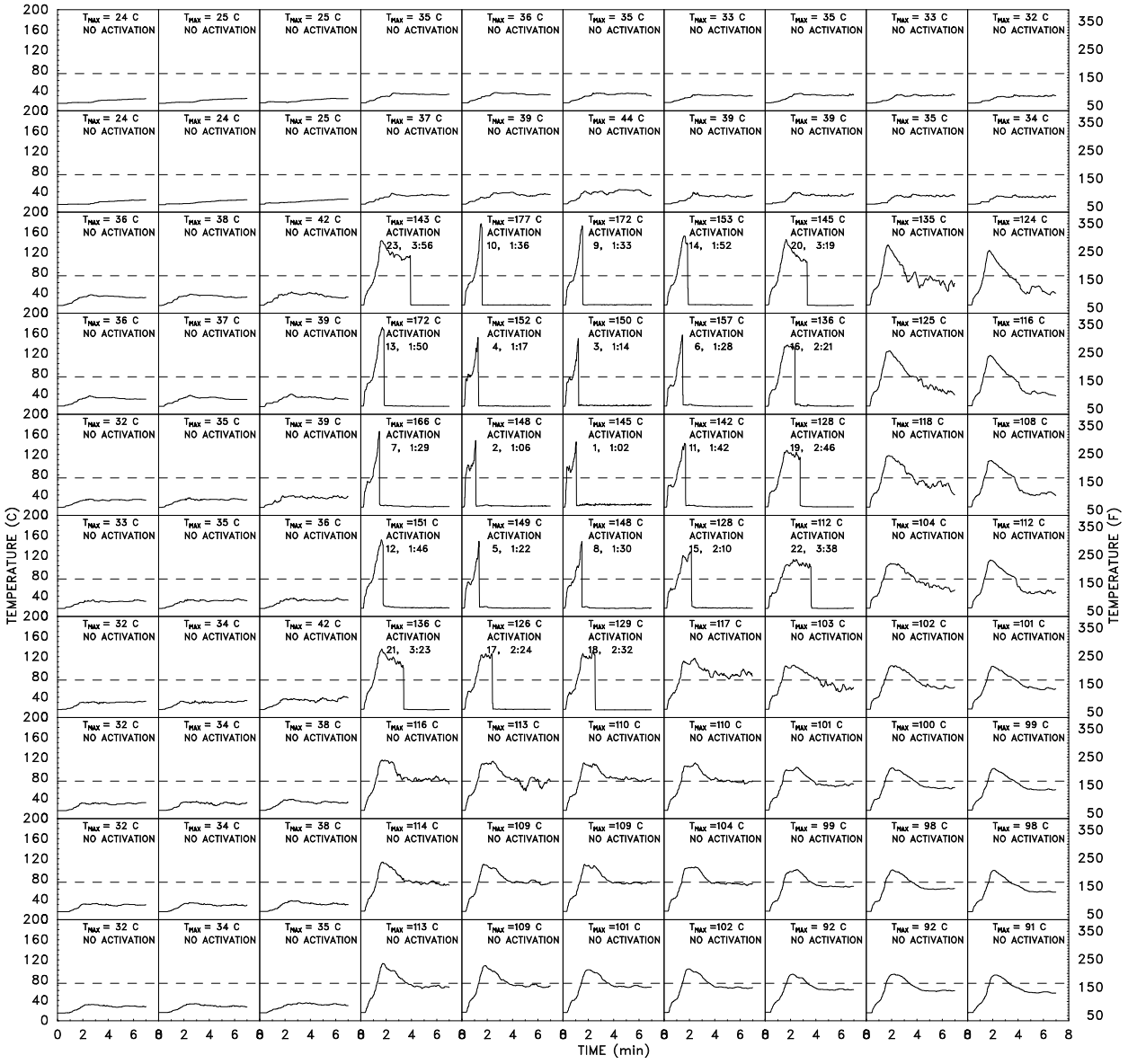

Figure 117: Temperature histories for the 100 near-sprinkler thermocouples for Test II-11, Heptane Series II.

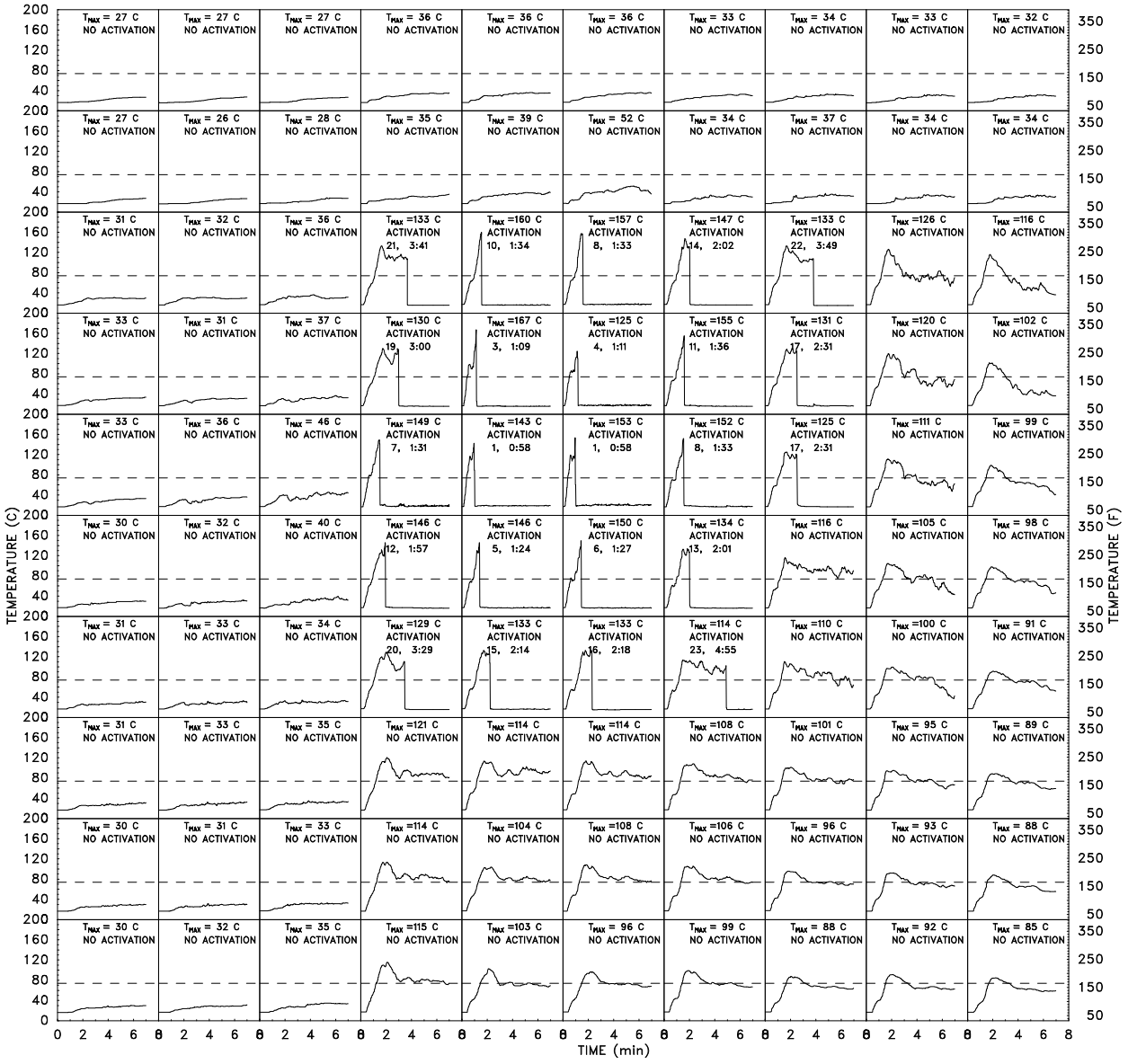

Figure 118: Temperature histories for the 100 near-sprinkler thermocouples for Test II-12, Heptane Series II.